THE PHARMACOKINETICS OF TARGETED ANTICANCER DRUGS AND FOOD TOXINS

Jing Wang

THE PHARMACOKINETICS OF TARGETED ANTICANCER DRUGS AND FOOD TOXINS

Jing Wang

The pharmacokinetics of targeted anticancer drugs and food toxins

© Jing Wang, Utrecht 2022

ISBN: 9789464237252

Cover design: Lei Li
Print: ProefschriftMaken

The research in this thesis was performed at the Department of Pharmacology of The Netherlands Cancer Institute-Antoni van Leeuwenhoek, Amsterdam, The Netherlands, in collaboration with other institutes.

Printing of this thesis was financially supported by the Onderzoekschool Oncologie Amsterdam and the Netherlands Cancer Institute.

The pharmacokinetics of targeted anticancer drugs and food toxins

Roles of ABC efflux and OATP uptake transporters

De farmacokinetiek van gerichte geneesmiddelen tegen kanker en voedseltoxines
Rollen van ABC-efflux en OATP-opnametransporteurs
(met een samenvatting in het Nederlands)

Proefschrift

ter verkrijging van de graad van doctor aan de
Universiteit Utrecht
op gezag van de
rector magnificus, prof.dr. H.R.B.M. Kummeling,
ingevolge het besluit van het college voor promoties
in het openbaar te verdedigen op

maandag 21 maart 2022 des ochtends te 10.15 uur

door

Jing Wang

geboren op 18 mei 1987
te Sichuan, China

Promotor:
Prof. dr. J.H. Beijnen

Copromotor:
Dr. A.H. Schinkel

“It is the time you have wasted for your rose that makes your rose so important.”

- Antoine de Saint-Exupéry, The Little Prince.

TABLE OF CONTENTS

Chapter 1. Introduction

Part I. Introduction to ATP-Binding Cassette (ABC) transporters 13

Part II. Introduction to Organic Anion Transporting Polypeptides of the OATP/SLCO family 23

Part III. Introduction to Cytochrome P450 (CYP) enzymes 29

Part IV. Four generations of EGFR tyrosine kinase inhibitors in treatment of EGFR-mutant non-small cell lung cancer 33
To be submitted

Part V. The blood-brain barrier and EGFR inhibitors: Implications for patients with NSCLC brain metastases 49

Chapter 2. P-glycoprotein (MDR1/ABCB1) and Breast Cancer Resistance Protein (BCRP/ABCG2) affect brain accumulation and intestinal disposition of encorafenib in mice 55
Pharmacological Research, 2018

Chapter 3. P-glycoprotein (MDR1/ABCB1) and Breast Cancer Resistance Protein (BCRP/ABCG2) limit brain accumulation of the FLT3 inhibitor quizartinib in mice 85
International Journal of Pharmaceutics, 2019

Chapter 4. Brain accumulation of tivozanib is restricted by ABCB1 (P-glycoprotein) and ABCG2 (breast cancer resistance protein) in mice 111
International Journal of Pharmaceutics, 2020

Chapter 5. P-glycoprotein (MDR1/ABCB1) restricts brain accumulation of the novel EGFR inhibitor EAI045 and oral elacridar coadministration enhances its brain accumulation and oral exposure 139
To be submitted

Chapter 6. Human organic anion transporting polypeptide (OATP) 1B3 and mouse Oatp1a/1b affect liver accumulation of Ochratoxin A in mice 175
Toxicology and Applied Pharmacology, 2020

Conclusion and future perspective 203

Summary 207

Nederlandse samenvatting 215

Appendices

- Chemical structures discussed in this thesis 224
- Author affiliations 225
- List of publications 226
- Curriculum vitae 228
- Acknowledgements 229

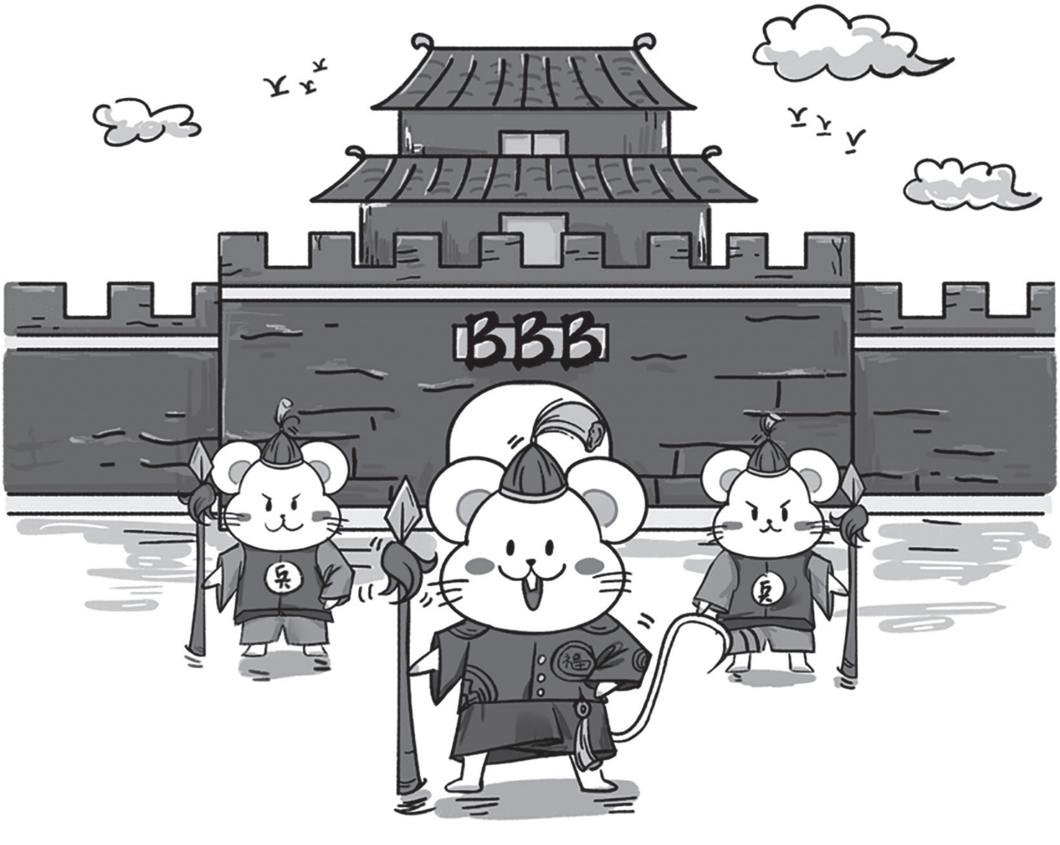
BBB
兵
福
兵

Chapter 1

INTRODUCTION

Part I. Introduction to ATP-Binding Cassette (ABC) transporters

ATP-Binding Cassette (ABC) transporters form a special family of membrane proteins, characterized by conserved ATP-binding, and large, multi-spanning transmembrane domains. ABC transporters can utilize the energy derived from ATP hydrolysis to perform a directed transmembrane movement of their substrates (primary active transporters), or, more rarely, open or close a specific membrane channel (e.g. ion channels), or regulate the permeability of multi-protein channel complexes (receptors) [1]. The ABC domain has to function as a dimer, so two copies of it must be present to form a functional protein. In many cases, especially in mammals, this is achieved by internal duplication of both the ABC sequence and the transmembrane domain in the same polypeptide chain, but in some cases functional proteins are formed by homo- or heterodimers of so-called "half" ABC transporters. It has become clear that several ABC transporters can play an important role in preventing the uptake of toxic compounds, including many drugs and food components, from the gut into the body, and in protecting vital structures in the body, such as the brain, the cerebrospinal fluid, the testis, and the fetus, against natural toxins entering the body [2]. In mammals, especially the well-studied rodents and man, typical substrates of ABC transporters include amino acids, vitamins, lipids, sterols, bile salts, peptides, nucleotides, ions, toxins and (anti-cancer) drugs [3-11]. In this review, we place a special emphasis on the three major groups of ABC transporters involved in cancer multidrug resistance (MDR), which they confer by exporting a large number of cytotoxic drugs from cells: P-glycoprotein (P-gp, ABCB1, MDR1), multidrug resistance-associated protein 2 (ABCC2, MRP2), and breast cancer resistance protein (BCRP, ABCG2). These proteins are also potentially important in the overall pharmacokinetics of a wide range of substrate drugs, including chemotherapeutics. The tissue distribution of these three major multidrug resistance proteins is largely overlapping but not identical.

ABCB1 (P-gp, MDR1) was first detected and isolated by Juliano and Ling in 1976 as a surface phosphoglycoprotein from MDR Chinese hamster ovary cells, and called 'P-glycoprotein' for "permeability glycoprotein" because its expression was associated with apparently reduced drug permeability in resistant cells [12]. ABCB1 is glycosylated and localized in the plasma membrane, and especially in the apical/luminal membrane in polarized cells. It is present in the brush border membrane of intestinal epithelial cells, the biliary canalicular membrane of hepatocytes, the luminal membrane of proximal tubule epithelial cells of the kidney, and also in the endothelial cells constituting blood-tissue interfaces (such as the blood-brain, blood-testis, blood-ovarian, and blood-retinal barriers) [13-20]. This expression profile suggests that a central role of ABCB1 is to prevent the entry of toxins or drugs into sensitive tissues or organs and to facilitate their elimination through hepatobiliary and renal excretory pathways [19-23].

ABCC2 (MRP2) was discovered as an organic anion transporter in the canalicular membrane of hepatocytes, and it was found to be mutated in patients with Dubin-Johnson syndrome [24, 25]. This protein is present in the liver, kidney and gut epithelium apical membranes, where it can mediate the efflux of bilirubin glucuronides and other organic anions, playing a role in the detoxification for many endogenous and xenobiotic compounds. In Dubin-Johnson syndrome the inherited mutations of ABCC2 cause a defect in the hepatobiliary secretion of amphiphilic anionic conjugates, resulting in pronounced conjugated hyperbilirubinemia [1]. ABCC2 has been detected in renal, lung, gastric, colorectal, and hepatocellular carcinomas [2], and it has been documented that ABCC2 may also cause multidrug resistance in tumor cells [1].

ABCG2 (BCRP), a half-transporter causing mitoxantrone resistance and multidrug resistance in breast cancer cell lines, was first found in multidrug-resistant tumor cells not expressing either ABCB1 or ABCC1 (MRP1) [26, 27]. ABCG2 localizes principally to the apical membranes of polarized cells in several healthy tissues, including placental syncytiotrophoblasts, hepatocytes, and intestinal mucosal cells, where it likely shields specific body compartments by secreting potentially damaging toxins into the maternal circulation, bile ducts, and intestinal lumen, respectively. ABCG2 confers multidrug resistance in an analogous way as ABCB1, by keeping the intracellular accumulation of cytotoxic compounds low [28].

The substrate specificity of MDR-ABC proteins exhibits as wide a variety as their tissue distribution and they share the ability to transport a wide range of compounds out of cells, with considerable substrate overlap. As a consequence, the absence or decreased activity of one of these transporters is often compensated for by the activity of one or more other members [4, 6, 29]. Still, each transporter can handle unique compounds as well.

Because of the ability of these ABC transporters to confer multidrug resistance to tumor cells, there has been a lot of interest in using pharmacological blockers of these proteins to enhance the response of tumors to chemotherapy. To predict the biological and pharmacological consequences of the blocking of these drug transporters *in vivo*, mice with a genetic disruption of the encoding genes were generated. Especially knockout mouse models lacking ABCB1 and/or ABCG2 have been widely used as tools to experimentally assess the contribution of these ABC transporters to (limiting) oral availability of drug substrates [30-34]. Indeed, many studies have clearly shown the *in vivo* impact of apical ABC efflux transporters on the oral uptake of many anti-cancer drugs including cytotoxic drugs such as paclitaxel, docetaxel, topotecan and etoposide and new-generation targeted anti-cancer drugs such as the multikinase inhibitor sorafenib [35], multi-targeted RTK inhibitor sunitinib [36], BRAF inhibitor vemurafenib [37], PARP inhibitor rucaparib [38], EGFR inhibitors afatinib and osimertinib [39, 40], CDK4/6 inhibitor ribociclib [41], and countless other drugs. Most of the targeted tyrosine kinase inhibitor (TKI) drugs were found to be transported substrates of Abcb1a/1b and/or Abcg2 and often their oral availability was limited by either Abcb1a/1b and/or Abcg2. In the clinic, several studies have assessed polymorphisms in the genes encoding ABC transporters and tried to correlate these with drug pharmacokinetics and sometimes with the outcomes of anti-cancer drug treatments. These studies are useful to understand the clinical use of ABC transporters as predictive markers for therapy response [42-44]; however, assessment of the overall role of these transporters in anticancer drug disposition in patients remains challenging.

1.1. ABC transporters at the blood-brain-barrier

Neural signaling within the central nervous system (CNS) requires a highly controlled microenvironment. Cells at three key interfaces form barriers between the blood and the CNS: the blood-brain barrier (BBB), the blood-cerebrospinal fluid barrier (BCSFB) and the arachnoid barrier. The BBB at the level of the brain microvessel endothelium is the major site where blood-CNS exchange of compounds occurs [45]. The BBB is formed by brain capillary endothelial cells, pericytes, a basal membrane, and astrocyte foot processes [45-47]. These endothelial cells are connected by very tight junctions, providing the BBB with a very strong, continuous physical barrier. In addition, active mechanisms support this barrier function, namely selective transport systems mediating permeation into and out of the brain, including membrane transport proteins as well as receptors undergoing endocytosis and transcytosis. ABC transporters play a particular role therein by pumping their substrates across the luminal side of the endothelial cells into the blood circulation [47-49]. We limit ourselves here to the ABC transporters ABCB1 (P-gp, MDR1) and ABCG2 (BCRP), which are abundantly expressed in the luminal membrane of the BBB [50-52] (Figure 1a).

The relevance of ABC transporters at the BBB and particularly of ABCB1 was first shown by Schinkel et al., who had generated mice genetically deficient in the *Abcb1a* gene [Abcb1a(-/-) mice], *Abcb1b* gene [Abcb1b(-/-) mice], and both of the *Abcb1a* and *Abcb1b* genes [Abcb1a/1b(-/-) mice]. Using these animal models, they demonstrated dramatic differences in brain concentrations of P-glycoprotein substrates between wild-type animals and these mutants [53, 54]. Many studies have shown that when either Abcb1 or Abcg2 alone is absent, Abcg2 or Abcb1 can partly or fully take over the function at the BBB for many shared substrate drugs. Therefore, a combined Abcb1a/1b and Abcg2 knockout mouse model (Abcb1a/1b;Abcg2$^{-/-}$) [55] is an indispensable tool to study the overlapping functions of ABCB1 and ABCG2 in restricting brain penetration of dual substrate drugs.

Many studies on anticancer drugs done using Abcb1a/1b;Abcg2 knockout mice showed that loss of Abcb1 and Abcg2 caused a pronounced increase in brain penetration in Abcb1a/1b;Abcg2$^{-/-}$ compared to wild-type mice. Some recent examples include lorlatinib, fisogatinib, larotrectinib, and ribociclib [41, 56-58]. These studies showed that the mouse Abcb1 and Abcg2 transporters could sometimes dramatically restrict the brain penetration, suggesting that coadministering anticancer drugs together with a strong ABCB1 and ABCG2 inhibitor (e.g. elacridar) under some circumstances might increase efficacy against brain lesions and malignancies resistant due to ABCB1 and ABCG2 (over)expression.

1.2. Use of elacridar to enhance brain penetration of ABC transporter substrates

Elacridar was initially developed as a multidrug reversal agent for ABCB1 to restore sensitivity of multidrug-resistant tumor cells to chemotherapeutic agents [59]. It turns out to inhibit both ABCB1 and ABCG2, and has been successfully applied in preclinical studies aiming to improve the brain distribution of many substrate drugs. These include the cardiac drug digoxin [60], but also many anticancer drugs, such as sunitinib [36], vemurafenib [37], ribociclib [41], lorlatinib [56, 61], and brigatinib [62], whose brain penetrations were improved mostly to the knockout levels by administration of elacridar. These studies further confirmed that elacridar in preclinical studies can significantly increase the brain penetration of anti-cancer drugs that are dual ABCB1 and ABCG2 substrates.

1.3. Toxicity

Interfering with the activity of ABC transporters transporting various drugs may cause toxicity by several different mechanisms. Inhibition of the efflux function may modulate distribution of co-administered drugs or environmental toxicants, thus changing their toxicity profile. Schinkel et al. accidentally found out that the Abcb1 knockout mice displayed an increased sensitivity to the centrally neurotoxic pesticide ivermectin (100-fold). This compound is normally kept out of the brain by Abcb1a. They also found increased sensitivity to the carcinostatic drug vinblastine (3-fold) [63]. Their findings explain some of the side effects in patients treated with a combination of carcinostatics and ABCB1 inhibitors and indicate that these inhibitors might be useful in selectively enhancing the access of a range of drugs to the brain [63].

In 2020, Baudou et al. reported a case of a 13-year-old boy who is completely deficient for ABCB1 (MDR1) P-glycoprotein, leading to severe adverse drug reactions after administration of a usual therapeutic dose of ivermectin [64]. As far as we know, this is the first case ever reported of a human completely deficient for ABCB1 P-glycoprotein. Although the compound heterozygous deficiency status for ABCB1 is expected to be extremely rare in humans, this clinical case raises a very legitimate question about the conditions of use of ivermectin, and other potentially toxic ABCB1 substrates, in humans.

A recent preclinical study found out that, after oral administration of the same dose of brigatinib, Abcb1a/1b;Abcg2 knockout mice showed severe toxicity signs, whereas in contrast no toxicity signs were observed in wild-type mice [62]. This study further indicate a pronounced protective role of ABCB1 and ABCG2 transporters. In fact, if humans would respond similarly to mice in developing toxicity when blocking ABCB1 and/or ABCG2 function, it may be impossible to safely apply this principle in patients.

Conclusion

ABC transporters such as ABCB1 and ABCG2, expressed in many tissues, certainly have key roles in the disposition of a broad range of anti-cancer drugs to the plasma (oral availability) and tissues (especially brain), and thus are important players in clinical efficacy. Located at the blood-CNS interface they act as double-edged swords: on the one hand they limit penetration of potentially curative CNS-targeted drugs, on the other hand they protect against potential central toxicity of non-CNS-targeted drugs. The interaction of compounds with ABC transporters in the brain may limit the overall drug exposure and efficacy against tumor (micro-)metastases situated behind a functionally intact BBB. The coadministration of anticancer drugs with a strong ABCB1 and ABCG2 inhibitor (e.g. elacridar) under some circumstances might increase the efficacy against brain lesions and resistant malignancies. However, the highly increased CNS distribution of targeted drugs could also lead to lethal toxicity. Therefore, in order to implement a personalized treatment targeting a specific ABC transporter, we need reliable and clinically validated assays to detect the expression of relevant ABC transporters at the protein level. In addition, we would need more specific (less promiscuous) inhibitors that efficiently target a specific transporter, possibly resulting in reduced risk of toxic effects.

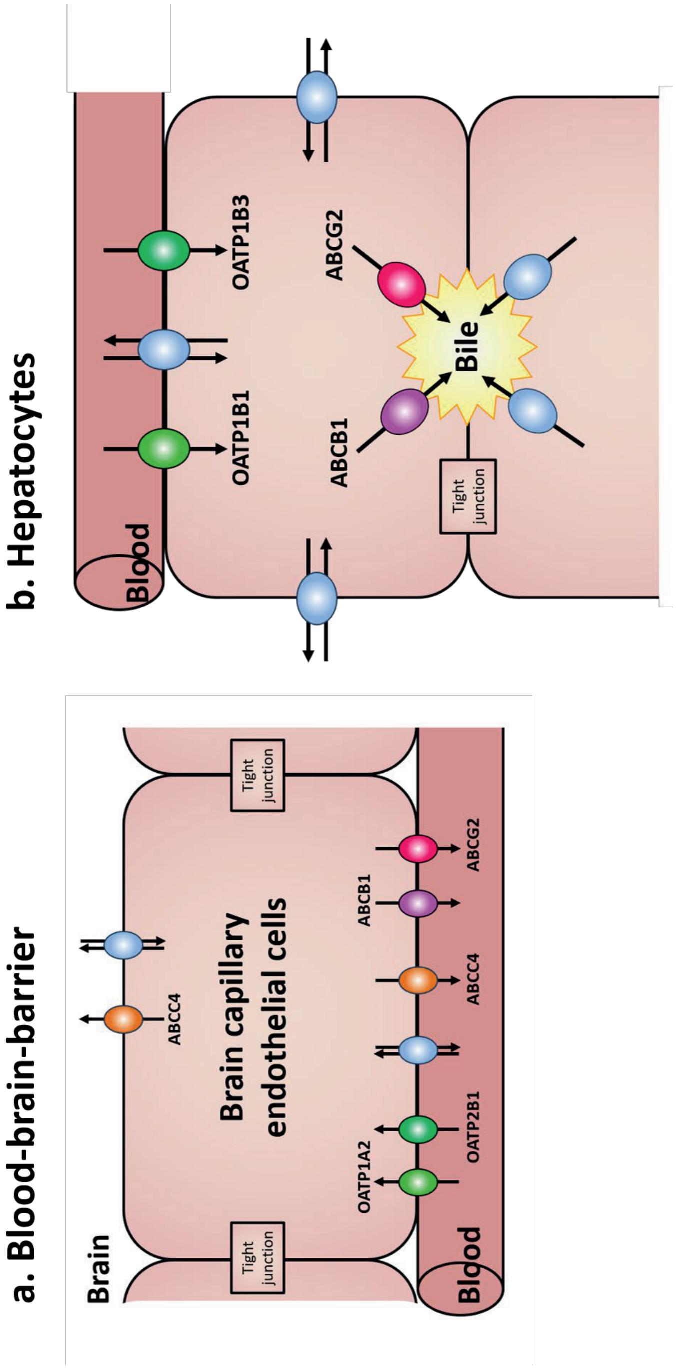
a. Blood-brain-barrier
Brain
Tight junction
Tight junction
ABCC4
Brain capillary endothelial cells
OATP1A2
OATP2B1
ABCC4
ABCB1
ABCG2
Blood
b. Hepatocytes
Blood
OATP1B1
OATP1B3
ABCB1
ABCG2
Bile
Tight junction

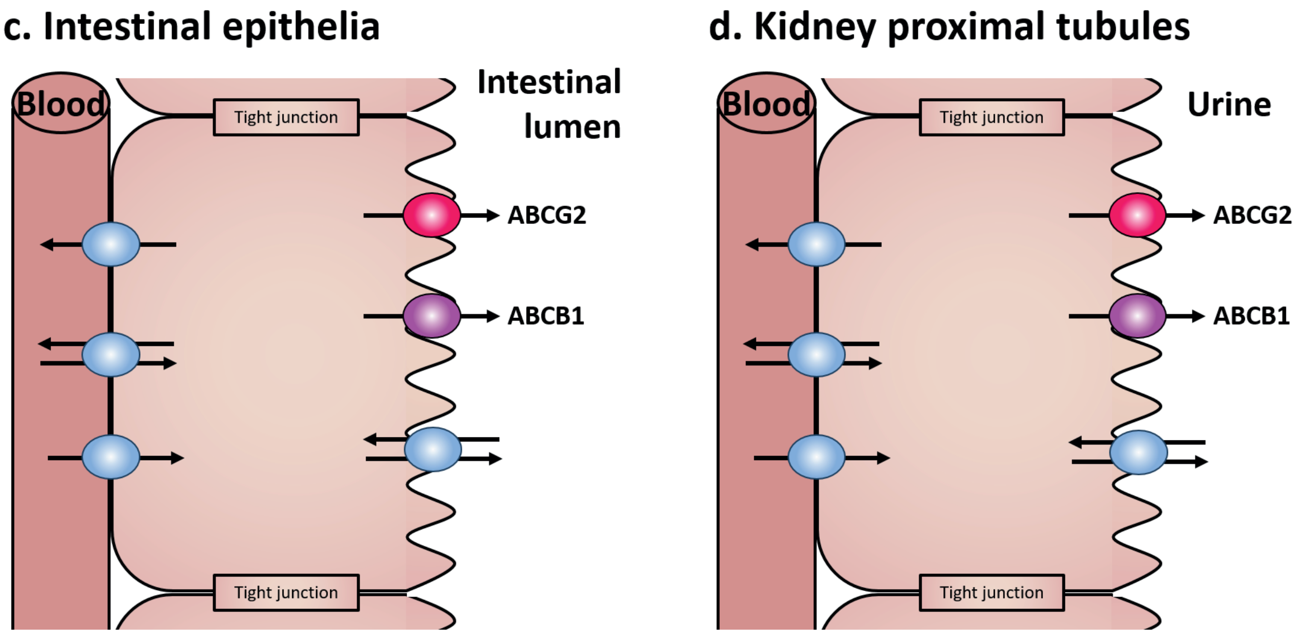
c. Intestinal epithelia
Blood
Tight junction
Tight junction
Intestinal lumen
ABCG2
ABCB1
d. Kidney proximal tubules
Blood
Tight junction
Tight junction
Urine
ABCG2
ABCB1

Figure 1. Tissue localization of human efflux and/or uptake transporters in plasma membrane domains of brain capillary endothelial cells (a), hepatocytes (b), intestinal epithelia (c), and kidney proximal tubules (d). ABCB1 and ABCG2 are the selected transporters described in detail in this chapter. a: Apical (luminal) transport proteins of brain capillary endothelial cells contributing to the function of the blood-brain barrier, including the efflux transporters ABCB1 (P-gp; MDR1), ABCG2 (BCRP), and ABCC4 (MRP4); and the uptake transporters OATP1A2 and OATP2B1. b. Human hepatocyte uptake transporters in the basolateral (sinusoidal) membrane, including OATP1B1 and OATP1B3; and the apical (canalicular) efflux pumps of the hepatocyte including ABCB1, ABCG2. c-d: The efflux transporters ABCB1and ABCG2 located at the apical (luminal) membrane of intestinal epithelia (c) and kidney proximal tubules (d).

References

1. Glavinas, H., et al., The role of ABC transporters in drug resistance, metabolism and toxicity. Current drug delivery, 2004. 1(1): p. 27-42.
2. Borst, P. and R.O. Elferink, Mammalian ABC transporters in health and disease. Annual review of biochemistry, 2002. 71(1): p. 537-592.
3. Borst, P. and R.O. Elferink, Mammalian ABC transporters in health and disease. Annu.Rev.Biochem., 2002. 71: p. 537-592.
4. Lagas, J.S., M.L. Vlaming, and A.H. Schinkel, Pharmacokinetic assessment of multiple ATP-binding cassette transporters: the power of combination knockout mice. Mol.Interv., 2009. 9(3): p. 136-145.
5. Vlaming, M.L., J.S. Lagas, and A.H. Schinkel, Physiological and pharmacological roles of ABCG2 (BCRP): recent findings in Abcg2 knockout mice. Adv.Drug Deliv.Rev., 2009. 61(1): p. 14-25.
6. Klaassen, C.D. and L.M. Aleksunes, Xenobiotic, bile acid, and cholesterol transporters: function and regulation. Pharmacol.Rev., 2010. 62(1): p. 1-96.
7. Franke, R.M., E.R. Gardner, and A. Sparreboom, Pharmacogenetics of drug transporters. Curr Pharm Des, 2010. 16(2): p. 220-230.
8. Tamaki, A., et al., The controversial role of ABC transporters in clinical oncology. Essays Biochem, 2011. 50(1): p. 209-232.
9. Pluchino, K.M., et al., Collateral sensitivity as a strategy against cancer multidrug resistance. Drug Resist Updat, 2012. 15(1-2): p. 98-105.
10. Hayashi, H. and Y. Sugiyama, Bile salt export pump (BSEP/ABCB11): trafficking and sorting disturbances. Curr Mol Pharmacol, 2013. 6(2): p. 95-103.
11. Borst, P. and A.H. Schinkel, P-glycoprotein ABCB1: a major player in drug handling by mammals. J Clin Invest, 2013. 123(10): p. 4131-4133.
12. Juliano, R.L. and V. Ling, A surface glycoprotein modulating drug permeability in Chinese hamster ovary cell mutants. Biochimica et Biophysica Acta (BBA)-Biomembranes, 1976. 455(1): p. 152-162.
13. Endicott, J.A. and V. Ling, The biochemistry of P-glycoprotein-mediated multidrug resistance. Annual review of biochemistry, 1989. 58(1): p. 137-171.
14. Gottesman, M.M. and I. Pastan, Biochemistry of multidrug resistance mediated by the multidrug transporter. Annual review of biochemistry, 1993. 62(1): p. 385-427.
15. Gottesman, M.M., T. Fojo, and S.E. Bates, Multidrug resistance in cancer: role of ATP–dependent transporters. Nature Reviews Cancer, 2002. 2(1): p. 48-58.
16. Thiebaut, F., et al., Cellular localization of the multidrug-resistance gene product P-glycoprotein in normal human tissues. Proceedings of the National Academy of Sciences, 1987. 84(21): p. 7735-7738.
17. Sugawara, I., et al., Tissue distribution of P-glycoprotein encoded by a multidrug-resistant gene as revealed by a monoclonal antibody, MRK 16. Cancer research, 1988. 48(7): p. 1926-1929.
18. Cordon-Cardo, C., et al., Multidrug-resistance gene (P-glycoprotein) is expressed by endothelial cells at blood-brain barrier sites. Proceedings of the National Academy of Sciences, 1989. 86(2): p. 695-698.
19. Kennedy, B.G. and N.J. Mangini, P-glycoprotein expression in human retinal pigment epithelium. Mol Vis, 2002. 8: p. 422-430.
20. Constable, P.A., et al., P-Glycoprotein expression in human retinal pigment epithelium cell lines. Experimental eye research, 2006. 83(1): p. 24-30.
21. Schinkel, A.H. The physiological function of drug-transporting P-glycoproteins. in Seminars in cancer biology. 1997. Elsevier.
22. Schinkel, A.H. and J.W. Jonker, Mammalian drug efflux transporters of the ATP binding cassette (ABC) family: an overview. Advanced drug delivery reviews, 2003. 55(1): p. 3-29.
23. Fromm, M.F., Importance of P-glycoprotein at blood–tissue barriers. Trends in pharmacological sciences, 2004. 25(8): p. 423-429.
24. Kartenbeck, J., et al., Absence of the canalicular isoform of the MRP gene–encoded conjugate export pump from the hepatocytes in Dubin-Johnson syndrome. Hepatology, 1996. 23(5): p. 1061-1066.
25. Paulusma, C.C., et al., A mutation in the human canalicular multispecific organic anion transporter gene causes the Dubin-Johnson syndrome. Hepatology, 1997. 25(6): p. 1539-1542.

26. Doyle, L.A., et al., A multidrug resistance transporter from human MCF-7 breast cancer cells. Proceedings of the National Academy of Sciences, 1998. 95(26): p. 15665-15670.
27. Miyake, H., A. Tolcher, and M.E. Gleave, Antisense Bcl-2 oligodeoxynucleotides inhibit progression to androgen-independence after castration in the Shionogi tumor model. Cancer Research, 1999. 59(16): p. 4030-4034.
28. Sarkadi, B., et al., Human multidrug resistance ABCB and ABCG transporters: participation in a chemoimmunity defense system. Physiological reviews, 2006. 86(4): p. 1179-1236.
29. Polli, J.W., et al., An unexpected synergist role of P-glycoprotein and breast cancer resistance protein on the central nervous system penetration of the tyrosine kinase inhibitor lapatinib (N-{3-chloro-4-[(3-fluorobenzyl)oxy]phenyl}-6-[5-({[2-(methylsulfonyl)ethyl]amino }methyl)-2-furyl]-4-quinazolinamine; GW572016). Drug Metab Dispos., 2009. 37(2): p. 439-442.
30. Schinkel, A., et al., Multidrug resistance and the role of P-glycoprotein knockout mice. European Journal of Cancer, 1995. 31(7-8): p. 1295-1298.
31. van Herwaarden, A.E. and A.H. Schinkel, The function of breast cancer resistance protein in epithelial barriers, stem cells and milk secretion of drugs and xenotoxins. Trends in pharmacological sciences, 2006. 27(1): p. 10-16.
32. Vlaming, M.L., J.S. Lagas, and A.H. Schinkel, Physiological and pharmacological roles of ABCG2 (BCRP): recent findings in Abcg2 knockout mice. Advanced drug delivery reviews, 2009. 61(1): p. 14-25.
33. Lagas, J.S., M.L. Vlaming, and A.H. Schinkel, Pharmacokinetic assessment of multiple ATP-binding cassette transporters: the power of combination knockout mice. Molecular interventions, 2009. 9(3): p. 136.
34. Tang, S.C., et al., Genetically modified mouse models for oral drug absorption and disposition. Current opinion in pharmacology, 2013. 13(6): p. 853-858.
35. Lagas, J.S., et al., Breast cancer resistance protein and P-glycoprotein limit sorafenib brain accumulation. Molecular cancer therapeutics, 2010. 9(2): p. 319-326.
36. Tang, S.C., et al., Brain accumulation of sunitinib is restricted by P-glycoprotein (ABCB1) and breast cancer resistance protein (ABCG2) and can be enhanced by oral elacridar and sunitinib coadministration. International journal of cancer, 2012. 130(1): p. 223-233.
37. Durmus, S., et al., Oral availability and brain penetration of the B-RAFV600E inhibitor vemurafenib can be enhanced by the P-GLYCOprotein (ABCB1) and breast cancer resistance protein (ABCG2) inhibitor elacridar. Molecular pharmaceutics, 2012. 9(11): p. 3236-3245.
38. Durmus, S., et al., Breast cancer resistance protein (BCRP/ABCG2) and P-glycoprotein (P-GP/ABCB1) restrict oral availability and brain accumulation of the PARP inhibitor rucaparib (AG-014699). Pharmaceutical research, 2015. 32(1): p. 37-46.
39. van Hoppe, S., et al., Breast cancer resistance protein (BCRP/ABCG2) and P-glycoprotein (P-gp/ABCB1) transport afatinib and restrict its oral availability and brain accumulation. Pharmacological research, 2017. 120: p. 43-50.
40. van Hoppe, S., et al., Brain accumulation of osimertinib and its active metabolite AZ5104 is restricted by ABCB1 (P-glycoprotein) and ABCG2 (breast cancer resistance protein). Pharmacological research, 2019. 146: p. 104297.
41. Martinez-Chavez, A., et al., P-glycoprotein limits ribociclib brain exposure and CYP3A4 restricts its oral bioavailability. Molecular pharmaceutics, 2019. 16(9): p. 3842-3852.
42. Pander, J., H.J. Guchelaar, and H. Gelderblom, Pharmacogenetics of small-molecule tyrosine kinase inhibitors: Optimizing the magic bullet. Curr.Opin.Mol.Ther., 2010. 12(6): p. 654-661.
43. Erdem, L., et al., Polymorphisms to predict outcome to the tyrosine kinase inhibitors gefitinib, erlotinib, sorafenib and sunitinib. Curr.Top.Med.Chem., 2012. 12(15): p. 1649-1659.
44. Tang, S.C., et al., Genetically modified mouse models for oral drug absorption and disposition. Curr.Opin.Pharmacol., 2013. 13(6): p. 853-858.
45. Abbott, N.J., et al., Structure and function of the blood–brain barrier. Neurobiology of disease, 2010. 37(1): p. 13-25.
46. Quaegebeur, A., C. Lange, and P. Carmeliet, The neurovascular link in health and disease: molecular mechanisms and therapeutic implications. Neuron, 2011. 71(3): p. 406-424.
47. Mahringer, A. and G. Fricker, ABC transporters at the blood–brain barrier. Expert opinion on drug metabolism & toxicology, 2016. 12(5): p. 499-508.
48. Daood, M.J., et al., Abc transporter (P-Gp/Abcb1, Mrp1/Abcc1, Bcrp/Abcg2) expression in the developing human Cns. Neuropediatrics, 2008. 39(4): p. 211.
49. Ghersi-Egea, J., S. Gazzin, and N. Strazielle, Blood-brain interfaces and bilirubin-induced neurological diseases. Current pharmaceutical design, 2009. 15(25): p. 2893-2907.

50. Miller, D.S., et al., Xenobiotic efflux pumps in isolated fish brain capillaries. American Journal of Physiology-Regulatory, Integrative and Comparative Physiology, 2002. 282(1): p. R191-R198.
51. Bauer, B., et al., Modulation of p-glycoprotein transport function at the blood-brain barrier. Experimental Biology and Medicine, 2005. 230(2): p. 118-127.
52. Cooray, H.C., et al., Localisation of breast cancer resistance protein in microvessel endothelium of human brain. Neuroreport, 2002. 13(16): p. 2059-2063.
53. Schinkel, A.H., et al., Normal viability and altered pharmacokinetics in mice lacking mdr1-type (drug-transporting) P-glycoproteins. Proceedings of the National Academy of Sciences, 1997. 94(8): p. 4028-4033.
54. Schinkel, A.H., P-Glycoprotein, a gatekeeper in the blood–brain barrier. Advanced drug delivery reviews, 1999. 36(2-3): p. 179-194.
55. Kodaira, H., et al., Kinetic analysis of the cooperation of P-glycoprotein (P-gp/Abcb1) and breast cancer resistance protein (Bcrp/Abcg2) in limiting the brain and testis penetration of erlotinib, flavopiridol, and mitoxantrone. Journal of Pharmacology and Experimental Therapeutics, 2010. 333(3): p. 788-796.
56. Li, W., et al., P-glycoprotein (MDR1/ABCB1) restricts brain accumulation and cytochrome P450-3A (CYP3A) limits oral availability of the novel ALK/ROS1 inhibitor lorlatinib. International journal of cancer, 2018. 143(8): p. 2029-2038.
57. Li, W., et al., P-glycoprotein (ABCB1/MDR1) limits brain accumulation and Cytochrome P450-3A (CYP3A) restricts oral availability of the novel FGFR4 inhibitor fisogatinib (BLU-554). International Journal of Pharmaceutics, 2020. 573: p. 118842.
58. Wang, Y., et al., OATP1A/1B, CYP3A, ABCB1, and ABCG2 limit oral availability of the NTRK inhibitor larotrectinib, while ABCB1 and ABCG2 also restrict its brain accumulation. British Journal of Pharmacology, 2020. 177(13): p. 3060-3074.
59. Hyafil, F., et al., In vitro and in vivo reversal of multidrug resistance by GF120918, an acridonecarboxamide derivative. Cancer research, 1993. 53(19): p. 4595-4602.
60. Mayer, U., et al., Full blockade of intestinal P-glycoprotein and extensive inhibition of blood-brain barrier P-glycoprotein by oral treatment of mice with PSC833. J Clin Invest, 1997. 100(10): p. 2430-2436.
61. Li, W., et al., Oral coadministration of elacridar and ritonavir enhances brain accumulation and oral availability of the novel ALK/ROS1 inhibitor lorlatinib. European Journal of Pharmaceutics and Biopharmaceutics, 2019. 136: p. 120-130.
62. Li, W., et al., P-glycoprotein and breast cancer resistance protein restrict brigatinib brain accumulation and toxicity, and, alongside CYP3A, limit its oral availability. Pharmacological research, 2018. 137: p. 47-55.
63. Schinkel, A., et al., Disruption of the mouse mdr1a P-glycoprotein gene leads to a deficiency in the blood-brain barrier and to increased sensitivity to drugs. Cell, 1994. 77(4): p. 491-502.
64. Baudou, E., et al., Serious ivermectin toxicity and human ABCB1 nonsense mutations. New England Journal of Medicine, 2020. 383(8): p. 787-789.

Part II. Introduction to Organic Anion Transporting Polypeptides of the OATP/SLCO family

Organic anion transporting polypeptides (rodents: Oatps, human: OATPs; gene names: Slco/SLCO, formerly SLC21) are sodium-independent transport systems [1-4]. They are important transmembrane proteins that can mediate transport (usually uptake) of a wide range of endogenous and exogenous compounds, including bile salts, steroid conjugates, thyroid hormones, anionic oligopeptides, numerous drugs as well as other xenobiotic substances [5]. Eleven OATPs have been identified in humans and can be further subdivided into families and subfamilies in close analogy to the classification of drug-metabolizing enzymes [6, 7]. Hence, Oatps/OATPs within the same family share at least 40% amino acid sequence identities and are designated by arabic numbering and classified into six families (OATP1-6). Individual subfamilies include Oatps/OATPs with amino acid sequence identities of at least 60% and are designated by letters, e.g. subfamilies OATP1A, OATP1B, OATP1C, OATP2A, OATP2B, OATP3A, etc. [5]. Based on the sequence homology and tissue localization, there are not always straightforward orthologs of the OATPs between human and mouse. For example, the OATP1 family contains OATP1A2, OATP1B1, OATP1B3 and OATP1C1 in humans [8], whereas in mice it contains Oatp1a1, Oatp1a4, Oatp1a5, Oatp1a6, Oatp1b2, and Oatp1c1 [5].

Within the six OATP families, members of the OATP1 and OATP2 subfamilies are thought to have profound roles in drug disposition and in drug-drug and drug-food interactions, because they are mainly expressed in pharmacokinetically important organs (e.g. liver, small intestine and kidney) and exhibit wide substrate specificities encompassing many drugs [9, 10].

The OATP1A subfamily contains a single human member, OATP1A2, which is a glycoprotein of 670 amino acids [2] and shares between 66 and 77% amino acid sequence identity with the rodent Oatp1a subfamily members [11]. OATP1A2 was originally cloned from a human liver cDNA library, but its highest expression is in brain [2]. It is expressed at the luminal membrane of the endothelial cells of brain capillaries [12] and is thought to be part of the blood-brain barrier, suggesting a possible role for OATP1A2 in (1) the delivery of drugs and neuroactive peptides to the brain, and/or (2) the removal of organic metabolites from the brain. In addition, OATP1A2 is quite widely distributed throughout the body, with high mRNA expression in the liver, lung, kidney and testes [2, 13], and also in colon cancer cells as well as in the human hepatoma cell line HepG2 [14]. Within the liver, OATP1A2 is exclusively expressed in cholangiocytes [15] and may be involved in the reabsorption of endo- and xenobiotics excreted into the bile. In kidney, OATP1A2 is expressed at the apical membrane of the distal nephron [15], where it could be responsible for either the reabsorption from, or the secretion of xenobiotics into urine. One publication suggested that OATP1A2 protein is localized to the brush border membrane of enterocytes in the duodenum [16], where it might mediate the absorption of xenobiotics. However, subsequent studies have failed to confirm substantial OATP1A2 expression in the small intestine. Considering the initially postulated tissue distribution, it was thought that OATP1A2 could play a critical role in the absorption, distribution and excretion of xenobiotics. It is also thought that human OATP1A2 transports the largest variety of amphipathic substrates of all human OATPs [17]. Unlike the single human OATP1A2, the rodent Oatp1a subfamily has five rat (Oatp1a1, 1a3, 1a4, 1a5, and 1a6) and four mouse members (Oatp1a1, 1a4, 1a5, and 1a6) [5].

The OATP1B subfamily has two human members, OATP1B1 (previously called OATP-C/SLC21A6), and OATP1B3. OATP1B1 shares 80% amino acid identity with OATP1B3, but only 64/65% identity with its rat/mouse ortholog Oatp1b2 [11]. Accordingly, OATP1B1 appears to have a similar broad substrate specificity as OATP1B3. Moreover, OATP1B1 exhibits a similar wide substrate spectrum as the OATP1A subfamily members. OATP1B1 and OATP1B3 are both selectively expressed in the human liver [18-22], where they are localized to the basolateral membrane of hepatocytes [17, 19, 21-23]. OATP1B1 is expressed in hepatocytes throughout the liver lobule, and it appears to be restricted to the basolateral (sinusoidal) plasma membrane of hepatocytes [14, 18, 20, 22]. Its apparently exclusive expression in human liver suggests that OATP1B1 plays a crucial role in the hepatic clearance of, often albumin-bound, amphipathic organic compounds. OATP1B3 is primarily expressed around the central vein in the liver lobule, and likewise in the basolateral membrane of hepatocytes [21]. Consistent with this pattern, expression levels of OATP1B1 mRNA in liver homogenate are higher overall than are levels of OATP1B3 [24, 25]. In rat and mouse the single ortholog Oatp1b2 has been identified for the two human OATP1B-subfamily members [5]. Although Oatp1b2 is also mainly expressed in the liver and is functionally similar to human OATP1B1 and OATP1B3 [11], preliminary studies indicate that Oatp1b2 is expressed additionally in the ciliary body epithelium of the eye [5].

The OATP2B subfamily contains human OATP2B1 as a main drug-transporting protein. It was originally isolated from human brain as a 709 amino acid protein [26], and it shows 77% amino acid sequence identity with its rat ortholog Oatp2b1 [11]. Although human OATP2B1 was originally cloned from a brain library, its strongest expression is in the liver, where the protein is located at the basolateral membrane of hepatocytes [17]. OATP2B1 is also expressed in spleen, placenta, lung, kidney, heart, ovary, small intestine, and at the luminal membrane of the endothelial cells of the blood-brain barrier [12, 14, 17].

The precise mechanism of transport by OATPs has not been completely resolved, and may possibly even diverge between individual OATPs. Oatp/OATP-mediated organic anion exchange is often observed and seems to be pH-dependent and electroneutral [27]. For instance, our in vitro experiments in HEK293 cell lines show that OATP1A2- and OATP2B1-mediated uptake of the fungal toxin Ochratoxin A at pH 6.4 was about twice as high as at pH 7.4. In contrast, OATP1B1 no longer mediated a detectable increase in Ochratoxin A uptake at pH 6.4. Finally, also at pH 6.4, OATP1B3 did not show significant uptake of Ochratoxin A [28]. Most drug-transporting Oatps/OATPs transport a wide range of amphipathic organic compounds. This broad substrate specificity was demonstrated first for rat Oatp1a1 [29]. The broad substrate specificity of many Oatps/OATPs raises the question as to the common chemical and/or structural denominators of Oatp/OATP substrates. As even large, hydrophobic drugs such as paclitaxel and docetaxel are now known to be transported substrates, it may be difficult to come to simple straightforward rules on this [30, 31].

For studying the roles in physiology and drug disposition, several mouse models lacking functional expression of one or more OATPs have been generated. The first reported Oatp knockout models were Oatp1b2 knockout strains in 2008 [32, 33]. Next, Oatp1a1 and Oatp1a4 single knockout mice models were generated and characterized [34, 35]. Then, in 2010, mice deficient for all Oatp1a and Oatp1b genes (Oatp1a/1b knockout mouse) were also generated to avoid the risk of compensatory restoration of function by other OATP1A or 1B proteins [36], since the OATP1A and OATP1B transporters display a large overlap in tissue distribution and substrate specificity. All of these strains were fertile, viable and developed normally. Initial characterization of the models revealed comparatively minor changes in the mRNA expression levels of some other transporters, making it unlikely that subsequent functional studies would be dramatically affected [32-36].

Pharmacokinetic studies in Oatp knockout mouse models indicate that the OATP1A and 1B transporters have a crucial role in the liver uptake and thus systemic clearance of anticancer drugs, organic dyes, estrogen derivates, antibiotics, statins and toxins. For instance, Durmus et al. found that absence of the Oatp1a/1b transporters led to a substantial increase in the systemic exposure and a corresponding decrease in hepatic and small intestinal exposure of doxorubicin in mice [37]. Interestingly, doxorubicin is not a typical organic anion, as it is a weakly basic anthracycline chemotherapy agent used to treat several types of cancers, including leukemias, Hodgkin’s lymphoma, and breast, ovarian, lung, and thyroid cancers [38]. This further illustrates how wide the spectrum of transported Oatp1a/1b substrates can be.

In conclusion, the drug-transporting members of the OATP/SLCO superfamily consist of multi- and oligo specific membrane transport systems that mediate sodium-independent transmembrane solute transport. The multispecific transporters accept a broad range of amphipathic endo- and xenobiotics. Therefore, genetic variation in OATP-encoding genes and inhibition of OATP function may have clinically significant consequences for drug therapy.

References

1. Jacquemin, E., et al., Expression cloning of a rat liver Na (+)-independent organic anion transporter. Proceedings of the National Academy of Sciences, 1994. 91(1): p. 133-137.
2. Kullak-Ublick, G.A., et al., Molecular and functional characterization of an organic anion transporting polypeptide cloned from human liver. Gastroenterology, 1995. 109(4): p. 1274-1282.
3. Noé, B., et al., Isolation of a multispecific organic anion and cardiac glycoside transporter from rat brain. Proceedings of the National Academy of Sciences, 1997. 94(19): p. 10346-10350.
4. Walters, H.C., et al., Expression, transport properties, and chromosomal location of organic anion transporter subtype 3. American Journal of Physiology-Gastrointestinal and Liver Physiology, 2000. 279(6): p. G1188-G1200.
5. Hagenbuch, B. and P.J. Meier, Organic anion transporting polypeptides of the OATP/SLC21 family: phylogenetic classification as OATP/SLCO superfamily, new nomenclature and molecular/functional properties. Pflügers Archiv, 2004. 447(5): p. 653-665.
6. Nelson, D.R., et al., P450 superfamily: update on new sequences, gene mapping, accession numbers and nomenclature. Pharmacogenetics, 1996. 6(1): p. 1-42.
7. Mackenzie, P.I., et al., The UDP glycosyltransferase gene superfamily: recommended nomenclature update based on evolutionary divergence. Pharmacogenetics, 1997. 7(4): p. 255-269.
8. Roth, M., A. Obaidat, and B. Hagenbuch, OATPs, OATs and OCTs: the organic anion and cation transporters of the SLCO and SLC22A gene superfamilies. British journal of pharmacology, 2012. 165(5): p. 1260-1287.
9. Cheng, X., et al., Tissue distribution and ontogeny of mouse organic anion transporting polypeptides (Oatps). Drug metabolism and Disposition, 2005. 33(7): p. 1062-1073.
10. Cheng, X. and C.D. Klaassen, Tissue distribution, ontogeny, and hormonal regulation of xenobiotic transporters in mouse kidneys. Drug Metabolism and Disposition, 2009. 37(11): p. 2178-2185.
11. Hagenbuch, B. and P.J. Meier, The superfamily of organic anion transporting polypeptides. Biochimica et Biophysica Acta (BBA)-Biomembranes, 2003. 1609(1): p. 1-18.
12. Bronger, H., et al., ABCC drug efflux pumps and organic anion uptake transporters in human gliomas and the blood-tumor barrier. Cancer research, 2005. 65(24): p. 11419-11428.
13. Steckelbroeck, S., et al., Steroid sulfatase (STS) expression in the human temporal lobe: enzyme activity, mRNA expression and immunohistochemistry study. Journal of neurochemistry, 2004. 89(2): p. 403-417.
14. Tamai, I., et al., Molecular identification and characterization of novel members of the human organic anion transporter (OATP) family. Biochemical and biophysical research communications, 2000. 273(1): p. 251-260.
15. Lee W., et al. Polymorphisms in human organic anion-transporting polypeptide 1A2 (OATP1A2): implications for altered drug disposition and central nervous system drug entry. Journal of Biological Chemistry, 2005, 280(10): 9610-9617.
16. Glaeser, H., et al., Intestinal drug transporter expression and the impact of grapefruit juice in humans. Clinical Pharmacology & Therapeutics, 2007. 81(3): p. 362-370.
17. Kullak-Ublick, G.A., et al., Organic anion-transporting polypeptide B (OATP-B) and its functional comparison with three other OATPs of human liver. Gastroenterology, 2001. 120(2): p. 525-533.
18. Abe, T., et al., Identification of a novel gene family encoding human liver-specific organic anion transporter LST-1. Journal of Biological Chemistry, 1999. 274(24): p. 17159-17163.
19. Abe, T., et al., LST-2, a human liver-specific organic anion transporter, determines methotrexate sensitivity in gastrointestinal cancers. Gastroenterology, 2001. 120(7): p. 1689-1699.
20. Hsiang, B., et al., A novel human hepatic organic anion transporting polypeptide (OATP2) Identification of a liver-specific human organic anion transporting polypeptide and identification of rat and human hydroxymethylglutaryl-CoA reductase inhibitor transporters. Journal of Biological Chemistry, 1999. 274(52): p. 37161-37168.
21. König, J., et al., Localization and genomic organization of a new hepatocellular organic anion transporting polypeptide. Journal of Biological Chemistry, 2000. 275(30): p. 23161-23168.

22. König, J.r., et al., A novel human organic anion transporting polypeptide localized to the basolateral hepatocyte membrane. American Journal of Physiology-Gastrointestinal and Liver Physiology, 2000. 278(1): p. G156-G164.
23. Cui, Y., et al., Detection of the human organic anion transporters SLC21A6 (OATP2) and SLC21A8 (OATP8) in liver and hepatocellular carcinoma. Laboratory investigation, 2003. 83(4): p. 527.
24. Michalski, C., et al., A Naturally Occurring Mutation in the SLC21A6Gene Causing Impaired Membrane Localization of the Hepatocyte Uptake Transporter. Journal of Biological Chemistry, 2002. 277(45): p. 43058-43063.
25. Briz, O., et al., Oatp8/1B3-mediated cotransport of bile acids and glutathione. An export pathway for organic anions from hepatocytes? Journal of Biological Chemistry, 2006.
26. Nagase, T., et al., Prediction of the coding sequences of unidentified human genes. XII. The complete sequences of 100 new cDNA clones from brain which code for large proteins in vitro. DNA Research, 1998. 5(6): p. 355-364.
27. Satlin, L.M., V. Amin, and A.W. Wolkoff, Organic anion transporting polypeptide mediates organic anion/HCO3− exchange. Journal of Biological Chemistry, 1997. 272(42): p. 26340-26345.
28. Qi, X., et al., Ochratoxin A transport by the human breast cancer resistance protein (BCRP), multidrug resistance protein 2 (MRP2), and organic anion-transporting polypeptides 1A2, 1B1 and 2B1. Toxicology and Applied Pharmacology, 2017. 329: p. 18-25.
29. Bossuyt, X., et al., Polyspecific drug and steroid clearance by an organic anion transporter of mammalian liver. Journal of Pharmacology and Experimental Therapeutics, 1996. 276(3): p. 891-896.
30. Smith, N.F., et al., Identification of OATP1B3 as a high-affinity hepatocellular transporter of paclitaxel. Cancer biology & therapy, 2005. 4(8): p. 815-818.
31. Iusuf, D., et al., Human OATP1B1, OATP1B3 and OATP1A2 can mediate the in vivo uptake and clearance of docetaxel. International journal of cancer, 2015. 136(1): p. 225-233.
32. Lu, H., et al., Characterization of organic anion transporting polypeptide 1b2-null mice: essential role in hepatic uptake/toxicity of phalloidin and microcystin-LR. Toxicological sciences, 2008. 103(1): p. 35-45.
33. Zaher, H., et al., Targeted disruption of murine organic anion-transporting polypeptide 1b2 (Oatp1b2/Slco1b2) significantly alters disposition of prototypical drug substrates pravastatin and rifampin. Molecular pharmacology, 2008. 74(2): p. 320-329.
34. Gong, L., et al., Characterization of organic anion-transporting polypeptide (Oatp) 1a1 and 1a4 null mice reveals altered transport function and urinary metabolomic profiles. Toxicological Sciences, 2011. 122(2): p. 587-597.
35. Ose, A., et al., Functional characterization of mouse Oatp1a4 in the uptake and efflux of drugs across the blood–brain barrier. Drug Metabolism and Disposition, 2009. 38(1): p. 168-176.
36. van de Steeg, E., et al., Organic anion transporting polypeptide 1a/1b–knockout mice provide insights into hepatic handling of bilirubin, bile acids, and drugs. The Journal of clinical investigation, 2010. 120(8): p. 2942-2952.
37. Durmus, S., et al., In vivo disposition of doxorubicin is affected by mouse Oatp1a/1b and human OATP1A/1B transporters. International Journal of Cancer Prevention, 2014. 135(7): p. 1700-1710.
38. Weiss, R.B., et al., Anthracycline analogs the past, present, and future. Cancer chemotherapy and pharmacology, 1986. 18(3): p. 185-197.

Part III. Introduction to Cytochrome P450 (CYP) enzymes

Drug metabolism by multispecific drug-metabolizing enzymes of the cytochrome P450 (CYP) superfamily, can also have major pharmacokinetic effects. The CYP enzymes are important in the oxidative, peroxidative and reductive metabolism of endogenous compounds such as steroids, bile acids, fatty acids, prostaglandins, biogenic amines and retinoids [1-3]. They are of particular relevance because they are also responsible for the majority of phase-I-dependent drug metabolism and for the metabolism of a huge variety of dietary constituents and exogenous chemicals [4, 5]. Although the liver is the major site of CYP-mediated drug metabolism, the enterocytes in the epithelium of the small intestine are also a potentially important site of drug metabolism and may considerably influence the general metabolism, activity and carcinogenicity of xenobiotics. Furthermore, there are also variable levels of CYP expression in extrahepatic tissues and organs, which includes brain, kidney and lung [1, 6-8]. Collectively, approximately 80% of oxidative metabolism of commonly used drugs can be attributed to the CYP enzymes [2, 5, 9, 10].

Structurally, the CYP isoenzymes are classified into families and subfamilies based on their amino acid sequence similarity [3, 11]. In humans 57 putatively functional genes and at least 58 pseudogenes are divided into 18 families of CYP genes and 44 subfamilies (in comparison to 108 functional and 88 pseudogenes in mouse [12]). However, only a relatively small number of the encoded proteins significantly contribute to the metabolism of drugs [9, 13, 14]. It appears that in humans, 15 CYP enzymes are primarily involved in xenobiotic metabolism, virtually all of them being from three main P450 families: CYP1, CYP2 and CYP3 [2, 3, 15]. Indeed, approximately 80% of all clinical drugs are primarily metabolized by the CYP1-3 families, and 50% are exclusively metabolized by members of the CYP3A subfamily [16]. The human *CYP3* family consists only of one subfamily, *CYP3A*, which is located on chromosome 7q22.1 and has a size of 231 kb, it is the predominant CYP subfamily expressed in the small intestine, accounting for 70-80% of total intestinal CYP content [17-22]. This suggests that intestinal metabolism can contribute significantly to the first-pass metabolism of orally administered CYP3A substrates [23-25].

The human CYP3A subfamily contains four members, CYP3A4, 3A5, 3A7 and 3A43 [14]. CYP3A4 is the most studied isoform in the CYP3A subfamily, it is predominant in the small intestines and adult liver, and is responsible for the bulk of the metabolic activities ascribed to this subfamily [26]. CYP3A4 plays a significant role in the metabolism of approximately half the drugs in use recently [16, 27, 28]. CYP3A5, another important member of CYP3A subfamily, is the most abundant isoform expressed in the kidney and lungs [26, 29]. CYP3A5 is also polymorphically expressed in adult liver and intestine, but the expression level is highly dependent on the individual's genotype [26, 30]. A comparison of the primary sequence of members of the CYP3A subfamily shows that they are more than 70% identical, and the homology is as high as 84% between CYP3A4 and CYP3A5 [26]. The high sequence similarity between the CYP3A isozymes leads to highly similar substrate selectivity between the isoforms [16, 31]. CYP3A7 was isolated from fetal liver tissue and characterized by Kitada & Kamataki [32]. The protein appears to be expressed mainly only in fetal liver [33] but also in adult endometrium and placenta [34]. CYP3A4 mRNA is not detectable in fetal liver, which is dominated by CYP3A7 [33, 35, 36]. The least important CYP3A appears to be CYP3A43, which expression was detected in liver, kidney, pancreas, and prostate. The amino acid sequence is 75% identical to that of CYP3A4 and CYP3A5 and 71% identical to CYP3A7 [37].

Subfamilies can differ substantially between mouse and human. In comparison to the four human CYP3A genes, the mouse *Cyp3a* cluster contains 7 full-length genes but there are no obvious orthologous pairs between mouse and human. This suggests that a single *CYP3A* gene present in a common evolutionary ancestor existed, which independently expanded during the last 75 million years [13, 16]. The Cyp3a cluster in mouse has twice as many P450 genes as in human [13].

To investigate the physiological and pharmacological roles of CYP3A, van Herwaarden et al. [38] generated Cyp3a-knockout (Cyp3a$^{-/-}$) mice lacking all functional Cyp3a genes. Cyp3a$^{-/-}$ mice were viable, fertile, and without marked physiological abnormalities. To determine the relative importance of intestinal versus hepatic Cyp3a in first-pass metabolism, they further generated transgenic Cyp3a$^{-/-}$ mice expressing human CYP3A4 in either the intestine (Cyp3a$^{-/-}$V) or the liver (Cyp3a$^{-/-}$A). Finally, homozygous CYP3A4 humanized transgenic mice (Cyp3aXAV) were generated by cross-breeding of transgenic mice with stable human CYP3A4 expression in liver or intestine, respectively, in a Cyp3a$^{-/-}$ background [38]. The genetic models generated and used in that study provide powerful tools to further study CYP3A-mediated xenobiotic metabolism, as well as interactions between CYP3A and other detoxification systems.

References

1. Thelen, K. and J.B. Dressman, Cytochrome P450-mediated metabolism in the human gut wall. Journal of pharmacy and pharmacology, 2009. 61(5): p. 541-558.
2. Testa, B. and S.D. Krämer, The biochemistry of drug metabolism–an introduction: part 2. Redox reactions and their enzymes. Chemistry & biodiversity, 2007. 4(3): p. 257-405.
3. Nelson, D.R., et al., P450 superfamily: update on new sequences, gene mapping, accession numbers and nomenclature. Pharmacogenetics, 1996. 6(1): p. 1-42.
4. Evans, W.E. and M.V. Relling, Pharmacogenomics: translating functional genomics into rational therapeutics. science, 1999. 286(5439): p. 487-491.
5. Wienkers, L.C. and T.G. Heath, Predicting in vivo drug interactions from in vitro drug discovery data. Nature reviews Drug discovery, 2005. 4(10): p. 825-833.
6. Kim, J.H., et al., Expression of cytochromes P450 1A1 and 1B1 in human lung from smokers, non-smokers, and ex-smokers. Toxicology and applied pharmacology, 2004. 199(3): p. 210-219.
7. Ghosh, C., et al., Cellular localization and functional significance of CYP3A4 in the human epileptic brain. Epilepsia, 2011. 52(3): p. 562-571.
8. Knops, N., et al., The functional implications of common genetic variation in CYP3A5 and ABCB1 in human proximal tubule cells. Molecular pharmaceutics, 2015. 12(3): p. 758-768.
9. Wilkinson, G.R., Drug metabolism and variability among patients in drug response. New England Journal of Medicine, 2005. 352(21): p. 2211-2221.
10. Rendic, S. and F.J.D. Carlo, Human cytochrome P450 enzymes: a status report summarizing their reactions, substrates, inducers, and inhibitors. Drug metabolism reviews, 1997. 29(1-2): p. 413-580.
11. Nebert, D.W. and F.J. Gonzalez, P450 genes: structure, evolution, and regulation. Annual review of biochemistry, 1987. 56(1): p. 945-993.
12. Nelson, D.R., Cytochrome P450 Nomenclature, 2004, in Cytochrome P450 protocols. 2006, Springer. p. 1-10.
13. Nelson, D.R., et al., Comparison of cytochrome P450 (CYP) genes from the mouse and human genomes, including nomenclature recommendations for genes, pseudogenes and alternative-splice variants. Pharmacogenetics and Genomics, 2004. 14(1): p. 1-18.
14. Pavek, P. and Z. Dvorak, Xenobiotic-induced transcriptional regulation of xenobiotic metabolizing enzymes of the cytochrome P450 superfamily in human extrahepatic tissues. Current drug metabolism, 2008. 9(2): p. 129-143.
15. Seliskar, M. and D. Rozman, Mammalian cytochromes P450—importance of tissue specificity. Biochimica et Biophysica Acta (BBA)-General Subjects, 2007. 1770(3): p. 458-466.
16. Zanger, U.M. and M. Schwab, Cytochrome P450 enzymes in drug metabolism: regulation of gene expression, enzyme activities, and impact of genetic variation. Pharmacology & therapeutics, 2013. 138(1): p. 103-141.
17. De Waziers, I., et al., Cytochrome P 450 isoenzymes, epoxide hydrolase and glutathione transferases in rat and human hepatic and extrahepatic tissues. Journal of Pharmacology and Experimental Therapeutics, 1990. 253(1): p. 387-394.
18. Paine, M.F., et al., The human intestinal cytochrome P450" pie". Drug metabolism and disposition, 2006. 34(5): p. 880-886.
19. Watkins, P.B., et al., Identification of glucocorticoid-inducible cytochromes P-450 in the intestinal mucosa of rats and man. The Journal of clinical investigation, 1987. 80(4): p. 1029-1036.
20. Paine, M.F., et al., Characterization of interintestinal and intraintestinal variations in human CYP3A-dependent metabolism. Journal of Pharmacology and Experimental Therapeutics, 1997. 283(3): p. 1552-1562.
21. Lown, K.S., et al., Interpatient heterogeneity in expression of CYP3A4 and CYP3A5 in small bowel. Lack of prediction by the erythromycin breath test. Drug Metabolism and Disposition, 1994. 22(6): p. 947-955.
22. Bieche, I., et al., Reverse transcriptase-PCR quantification of mRNA levels from cytochrome (CYP) 1, CYP2 and CYP3 families in 22 different human tissues. Pharmacogenetics and genomics, 2007. 17(9): p. 731-742.
23. Ding, X. and L.S. Kaminsky, Human extrahepatic cytochromes P450: function in xenobiotic metabolism and tissue-selective chemical toxicity in the respiratory and gastrointestinal tracts. Annual review of pharmacology and toxicology, 2003. 43(1): p. 149-173.

24. von Richter, O., et al., Cytochrome P450 3A4 and P-glycoprotein expression in human small intestinal enterocytes and hepatocytes: a comparative analysis in paired tissue specimens. Clin Pharmacol Ther, 2004. 75(3): p. 172-83.
25. Daly, A.K., Significance of the Minor Cytochrome P450 3A Isoforms. Clinical Pharmacokinetics, 2006. 45(1): p. 13-31.
26. Lolodi, O., et al., Differential regulation of CYP3A4 and CYP3A5 and its implication in drug discovery. Current drug metabolism, 2017. 18(12): p. 1095-1105.
27. Guengerich, F.P., Human cytochrome P450 enzymes, in Cytochrome P450. 1995, Springer. p. 473-535.
28. Guengerich, F.P., Human Cytochrome P450 Enzymes, in Cytochrome P450: Structure, Mechanism, and Biochemistry, P.R.O. de Montellano, Editor. 1995, Springer US: Boston, MA. p. 473-535.
29. Krusekopf, S., I. Roots, and U. Kleeberg, Differential drug-induced mRNA expression of human CYP3A4 compared to CYP3A5, CYP3A7 and CYP3A43. European journal of pharmacology, 2003. 466(1-2): p. 7-12.
30. Kuehl, P., et al., Sequence diversity in CYP3A promoters and characterization of the genetic basis of polymorphic CYP3A5 expression. Nature genetics, 2001. 27(4): p. 383-391.
31. Williams, J.A., et al., Comparative metabolic capabilities of CYP3A4, CYP3A5, and CYP3A7. Drug Metabolism and Disposition, 2002. 30(8): p. 883-891.
32. Kitada, M., et al., Purification and properties of cytochrome P-450 from homogenates of human fetal livers. Archives of biochemistry and biophysics, 1985. 241(1): p. 275-280.
33. Komori, M., et al., Fetus-specific expression of a form of cytochrome P-450 in human livers. Biochemistry, 1990. 29(18): p. 4430-4433.
34. Schuetz, J.D., S. Kauma, and P.S. Guzelian, Identification of the fetal liver cytochrome CYP3A7 in human endometrium and placenta. The Journal of clinical investigation, 1993. 92(2): p. 1018-1024.
35. Schuetz, J.D., D.L. Beach, and P.S. Guzelian, Selective expression of cytochrome P450 CYP3A mRNAs in embryonic and adult human liver. Pharmacogenetics, 1994. 4(1): p. 11-20.
36. Guengerich, F.P., Cytochrome P-450 3A4: regulation and role in drug metabolism. Annual review of pharmacology and toxicology, 1999. 39(1): p. 1-17.
37. Domanski, T.L., et al., cDNA cloning and initial characterization of CYP3A43, a novel human cytochrome P450. Molecular Pharmacology, 2001. 59(2): p. 386-392.
38. van Herwaarden, A.E., et al., Knockout of cytochrome P450 3A yields new mouse models for understanding xenobiotic metabolism. The Journal of clinical investigation, 2007. 117(11): p. 3583-3592.

Part IV. Four generations of EGFR tyrosine kinase inhibitors in treatment of EGFR-mutant non-small cell lung cancer

(To be submitted)

Abstract

Non-small cell lung cancer (NSCLC) accounts for about 80% to 85% of all lung cancer. The development of targeted therapies have tremendous progress in the understanding of the biology and management of NSCLC over the past 20 years. The development of the epidermal growth factor receptor (EGFR) tyrosine kinase inhibitors (TKIs) represented a significant breakthrough in the treatment of patients with EGFR mutant. Currently, targeted drugs are most often used for advanced lung cancers, either with or without chemotherapy. In this review, we discussed the latest treatments in patients with advanced or metastatic NSCLC with specific mutations of the EGFR that are highly sensitive to EGFR-TKIs (e.g., exon 19 deletions or L858R point mutations), from the first to fourth generation, including the median progression-free survival, overall survival, median duration of response, and so on. And the potential challenges and perspectives that current researchers were also addressed. An understanding of the mechanisms of acquired resistance to the four generation EGFR TKIs will greatly aid in the development of the next generation of EGFR TKIs.

Keywords: Non-small cell lung cancer; epidermal growth factor receptor; tyrosine kinase inhibitor; targeted therapy

Abbreviations: median progression-free survival (PFS), overall survival (OS), median duration of response (DOR), objective response (ORR), median time to treatment (TTF), disease control rate (DCR), adverse events (AEs), confidence interval (CI), complete remission (CR), partial remission (PR), not reached (NR), not assessable (NA), twice-daily (BID), once daily (QD)

1. Introduction

Lung cancer is the leading cause of cancer death among men and women in the United States. In fact, almost one-quarter of all cancer deaths is due to lung cancer. For 2020, 228,820 new cases were expected and 135,720 persons were projected to die from the disease in the United States alone [1]. There are two main types of lung cancers: small cell lung cancer (SCLC) and non-SCLC (NSCLC); NSCLC accounts for about 80% to 85% of all cases of lung cancer [2-5]. Chemotherapy, the mainstay of treatment in advanced NSCLC, slightly prolongs survival among patients [6, 7], associated with a response rate of 20-35% and a median survival time of 10-12 months [6, 8]. The outcomes have been poor, and associated with clinically significant adverse effects [6]. Patients with a good performance status and stage III NSCLC have been treated with chemoradiotherapy (chemotherapy combined with radiation therapy) [9]. However, the outcomes did not improve significantly after chemoradiotherapy, with a median survival of no more than 28 months [9, 10], and a 5-year survival rate of 15-30%. After patients had disease control with chemoradiotherapy, a few studies have tested the administration of systemic therapy with curative intent. However, these therapies have proved ineffective, with a median survival after consolidation treatment ranging from 18 to 23 months [11-16]. Overall, the 5-year relative survival rate of lung cancer is low, ranging from 5%-19% [1, 17]. The low lung cancer survival rates reflect the large proportion of patients (57%) diagnosed with metastatic disease. In patients diagnosed with NSCLC, the distant NSCLC metastases were most commonly found in the brain (47%), followed by bone (36%), liver (22%), adrenal glands (15%), body wall (13%), lung (11%), spleen (6%), (non-osseous) spinal canal (3%), and pancreas (1%) [18]. One phase II study showed that metastatic disease to the brain is common for lung cancer and occurs in approximately 31.6% [19]. Another study showed that 18% of patients with advanced NSCLC had brain metastases [20]. NSCLC is also the most common tumor metastasizing to the brain, accounting for 40% to 60% of all detected brain metastases [21, 22].

2. Treatment targets

Targeted drugs have been specifically designed for a certain molecular target, and often work differently from standard chemotherapy drugs. They sometimes work when chemotherapy drugs don’t, and they often have different side effects. Currently, targeted drugs are most often used for advanced lung cancers, either with or without chemotherapy [23]. In patients with advanced or metastatic NSCLC with specific mutations of the epidermal growth factor receptor (EGFR) that are highly sensitive to EGFR tyrosine kinase inhibitors (TKIs) (e.g., exon 19 deletions or L858R point mutations), guidelines recommend treatment with an EGFR-TKI [24-26]. In 40% to 80% of patients with NSCLC, EGFR is overexpressed, and its overexpression is associated with poor prognosis [5, 27] and disease progression, providing a strong rationale for assessing EGFR inhibitors in NSCLC (as well as various other solid tumors) [28-30]. There are several possible approaches to targeting EGFR, including monoclonal antibodies directed against the extracellular ligand-binding domain and small-molecule inhibitors of the intracellular tyrosine kinase domain [30, 31]. At present, tyrosine kinase inhibitors still remain the first choice for patients with the most advanced NSCLC.

2.1. First-generation EGFR TKIs

During the past twenty years, several EGFR inhibitors have been developed that are either binding the receptor tyrosine kinase domain or are monoclonal antibodies. Gefitinib (Iressa, ZD183) was the first targeted therapy to be registered and later approved by the Food and Drug Administration (FDA) for use in lung cancer [32]. It is a small molecule that competes with the binding of ATP to the intracellular tyrosine kinase domain of EGFR, thereby inhibiting receptor autophosphorylation and thus blocking downstream signal transduction [30, 33, 34]. In a phase III randomized trial, gefitinib (250 mg orally per day) or gefitinib plus chemotherapy (Gef+C) were given to patients with advanced NSCLC harboring an EGFR-sensitizing mutation. Radiologic response rates were 75% and 63% in the Gef+C and gefitinib group. Estimated median PFS was significantly longer with Gef+C than gefitinib (16 months (95% CI, 13.5-18.5) vs 8 months (95% CI, 7.0-9.0), respectively. Estimated median OS was significantly longer with Gef+C than gefitinib (not reached vs 17 months). However, adding pemetrexed and carboplatin chemotherapy to gefitinib significantly prolonged PFS and OS but also increased toxicity. Clinically relevant serious toxicities occurred more commonly in the Gef+C group (50.6%) than in the gefitinib group (25.3%;) [20].

2.2. Second-generation EGFR TKIs

One of the most common mechanisms of resistance to the first EGFR TKIs was the development of the gatekeeper mutation T790M. In a phase II study of olmutinib in patients with EGFR-mutated NSCLC, 96.1% of study populations were T790M mutation activated; in the same study in total phase I and II, the populations for T790M mutation activation were 50.7% [19]. And sixty percent of mutations that confer resistance to first- and second-generation EGFR TKIs are T790M [35, 36]. The second generation of EGFR TKIs, afatinib and dacomitinib, are irreversible EGFR inhibitors designed to overcome T790M resistance, but they were found not to work very well in overcoming this resistance.

2.2.1 Afatinib

Afatinib is approved in first-line treatment for advanced NSCLC patients harboring sensitizing EGFR mutations. In the international phase 2B trial (LUX-Lung 7), patients with stage IIIB or IV NSCLC and a common EGFR mutation (exon 19 deletion or L858R) were randomly treated with afatinib (40 mg/day) or gefitinib (250 mg/day). Afatinib showed a significantly longer PFS compared to gefitinib, although the improvement was modest, with the median PFS 11.0 months (95% CI, 10.6-12.9) in the afatinib group, and 10.9 months (95% CI, 9.1-11.5) in the gefitinib group. In patients with exon 19 deletions, median PFS was 12.7 (95% CI, 10.6-14.7) and 11.0 (95% CI, 9.1-12.7) months for afatinib and gefitinib, respectively. In patients with the L858R mutation, median PFS was 10.9 (95% CI,8.1-12.9) and 10.8 (95% CI, 7.2-12.8) months, respectively [37] (Table 1).

There was no significant difference in OS with afatinib versus gefitinib, with a total OS of 24.5 (21.2-26.4), and 27.9 (25-30.7) months for afatinib and gefitinib, respectively. Median OS in patients with exon 19 deletions (30.7 versus 26.4 months) and patients with the L858R mutation (25.0 versus 21.2 months) was generally consistent with the overall EGFR mutation-positive study population. Updated ORR was significantly higher with afatinib (72.5%) than with gefitinib (56.0%), and TTF (median 13.7 versus 11.5 months) were significantly improved with afatinib versus gefitinib [38] (Table 1).

Although afatinib and gefitinib were well tolerated, adverse event (AE) profiles with both drugs were also detected. Diarrhea (13.1% versus 1.3%) and rash (9.4% versus 3.1%) were more frequent with afatinib; interstitial lung disease (1.9% versus 0%) and elevated liver enzymes were associated with gefitinib, for instance, elevated alanine transaminase and aspartate aminotransferase were 8.2% and 2.5% for gefitinib, but 0% and 0% for afatinib [37, 38].

In this LUX-Lung 7 study, the findings were generally consistent across EGFR mutation types (exon 19 deletion versus L858R) [38]. A previous study suggested that first- and second-generation EGFR-TKIs may be particularly active in NSCLC with exon 19 deletions compared to the L858R mutation, but there they used chemotherapy-to-TKI comparisons rather than TKI-to-TKI comparisons [39].

2.2.2. Dacomitinib

In the phase III ARCHER 1050 trial, dacomitinib (45 mg/day) was compared to gefitinib (250 mg/day) as first-line treatment for patients with EGFR-mutation-positive NSCLC [40-42]. This trail showed that OS was significantly longer in the dacomitinib group than in the gefitinib group; the median OS was 34.1 months (95% CI, 29.5-37.7) with dacomitinib and 26.8 months (95% CI, 23.7-32.1) with gefitinib [41]; or with median OS of 34.1 months (95% CI, 29.5-39.8) versus 27.0 months (95% CI, 24.4-31.6), respectively, after a median follow-up of 47.9 months [42]. The median PFS was 14.7 months (11.1-16.6) with dacomitinib versus 9.2 months (11.1-16.6) with gefitinib [40]. The ORR was similar between the dacomitinib and the gefitinib groups (74.9% versus 71.6%, respectively) [40] (Table 2). In the ARCHER 1050 trial, the most frequently reported AEs of any grade in patients who received dacomitinib were diarrhea (87.7%), paronychia (61.7%), dermatitis acneiform (49.3%), and stomatitis (43.6%) [42]. In patients who received gefitinib these AEs were diarrhea (55.8%), increased alanine aminotransferase (ALT) (40.2%) and increased aspartate aminotransferase (37.5%) [42].

In this ARCHER 1050 study, the improvement in PFS with dacomitinib versus gefitinib (14.7 versus 9.2 months) was greater than that with afatinib versus gefitinib (11.0 versus 10.9 months) in LUX-Lung 7. The estimated PFS at 24 months with dacomitinib (30.6%) was higher than that with afatinib (17.6%) in LUX-Lung 7 [40]. One of the limitations of this study is that brain metastases were excluded from the patient population, as this criterion may enrich the population for patients with better overall prognosis.

2.3. Third-generation EGFR TKIs

Even when the first- or second-generation EGFR inhibitors were tested against T790M tumors, the result was that they were not active in overcoming T790M resistance, due to a narrow therapeutic window resulting in gastrointestinal (diarrhea, mucositis) and dermatologic toxicity resulting from wild-type (WT) EGFR inhibition [43, 44]. The development of third-generation EGFR TKIs was therefore aimed at compounds that were mutant selective and EGFR wild-type sparing, primarily targeting sensitizing EGFR mutations as well as T790M EGFR.

2.3.1. Osimertinib (AZD9291)

Osimertinib (AZD9291) is a third-generation, irreversible tyrosine kinase inhibitor of the EGFR that selectively inhibits both EGFR-TKI-sensitizing and EGFR T790M resistance mutations. It is a mono-anilino-pyrimidine compound that is structurally distinct from other third-generation EGFR TKIs and offers a pharmacologically differentiated profile from earlier generation EGFR TKIs [45]. Treatment with osimertinib is primarily associated with a loss of EGFR T790M and the subsequent emergence of EGFR-independent resistance mechanisms [46].

In a phase III trial, osimertinib was compared to two other EGFR-TKIs, gefitinib or erlotinib with previously untreated advanced NSCLC with an *EGFR* mutation (exon 19 deletion or L858R allele) (the FLAURA study (NCT02296125)) [47, 48]. Those who received osimertinib had longer OS than those who received a comparator EGFR-TKI (either gefitinib or erlotinib). The median OS was 38.6 months (95% CI, 34.5 to 41.8) in the osimertinib group, and 31.8 months (95% CI, 26.6 to 36.0) in the comparator group [47]. In this trial, the median PFS was significantly longer for the osimertinib group than for the comparator group, namely 18.9 months (95% CI, 15.2 to 21.4) versus 10.2 months (95% CI, 9.6 to 11.1), respectively. The ORR (with response assessed by the investigator) was 80% (95% CI, 75 to 85) in the osimertinib group, and 76% (95% CI, 70 to 81) in the comparator EGFR-TKI group. The median duration of response was 17.2 months (95% CI, 13.8 to 22.0) with osimertinib, and 8.5 months (95% CI, 7.3 to 9.8) with comparator EGFR-TKIs [48] (Table 2).

A phase II study in Korea showed that osimertinib demonstrated favorable activity with manageable toxicity in patients with NSCLC harboring uncommon EGFR mutations, with ORR 50% (18 of 36 patients; 95% CI, 33% to 67%). Median PFS was 8.2 months (95% CI, 5.9-10.5), and median OS was not reached. Median DOR was 11.2 months (95% CI, 7.7-14.7) [49] (Table 2). In one phase I study, osimertinib (160 mg once daily) was evaluated in patients with leptomeningeal metastases (LMs) from EGFR-mutated (EGFRm) advanced NSCLC whose disease had progressed on previous EGFR-TKI therapy. Overall, median investigator-assessed PFS was 8.6 months (95% CI, 5.4-13.7) with 78% maturity; median OS was 11.0 months (95% CI, 8.0-18.0) with 68% maturity. ORR by investigator was 41% (95% CI, 26%-58%), and median DOR was 8.3 months (95% CI, 5.6-16.5) [50]. The safety data in this study indicated that osimertinib 160 mg was generally well tolerated [50] (Table 2).

In the FLAURA study, AEs of grade 3 or higher were reported in fewer patients in the osimertinib group than in the standard EGFR-TKI group (34% vs 45%). The most commonly reported AEs were rash or acne (58% in the osimertinib group and 78% in the comparator EGFR-TKI group) and diarrhea (58% and 57%, respectively) [48]. Although there was PFS benefit with osimertinib compared to gefitinib or erlotinib, OS data were only at 25% maturity at the time of interim analysis [48]. Osimertinib showed efficacy better than that of standard EGFR-TKIs in the first-line treatment of EGFR mutation-positive advanced NSCLC. However, a significant proportion of patients did not receive any subsequent therapy beyond their initial treatment.

2.3.2. Rociletinib (CO-1686)

Rociletinib (CO-1686) is also a novel third-generation EGFR-TKI. A phase III study of rociletinib with chemotherapy showed that the rociletinib group had a more favorable median PFS than the chemotherapy group, with a PFS of 4.1 months (95% CI, 2.6-5.4) in the rociletinib 500-mg group and 5.5 months (95% CI, 1.8-8.1) in the 625-mg group, and 2.5 months (95% CI, 1.4-2.9) in the chemotherapy group. And there was a trend (albeit not significant) toward improved PFS with rociletinib versus second-line chemotherapy in the T790M-positive and T790M-negative patient populations. In the T790M-positive group, median PFS was 6.8 months (95% CI, 3.8-12.2) versus 2.7 months (95% CI, 1.3-7.0) for rociletinib and chemotherapy, respectively. In the T790M-negative population, median PFS was 4.1 months (95% CI, 2.5-4.6) versus 1.4 months (95% CI, 1.3-2.7), respectively. A confirmed ORR of 17.3% (95% CI, 9.6-27.8) was observed in the combined rociletinib group (500-mg plus 625-mg doses) versus 8.2% (95% CI, 3.1-17.0) in the chemotherapy group. Data of ORR and DOR are shown in Table 3 [51].

In patients who received rociletinib, 20% (n = 15) received treatment for more than 12 months. Nevertheless, rociletinib had unacceptable toxicities [51]. In the rociletinib group, there were 7 (9.3%) deaths due to disease progression (n = 2 (2.7%) in chemotherapy group), and grade 3 diarrhea and vomiting occurred at a higher rate. 8/75 (10.7%) was reported to have cataract in rociletinib-treated patients (vs 1/73 (1.4%) in chemotherapy patients). Four patients (5.3%) had pneumonitis (n = 0 in the chemotherapy group), which was higher than the rate of 1.3%-2.6% in patients treated with gefitinib or afatinib [52, 53].

2.3.3. Olmutinib

Olmutinib was approved in South Korea for the second-line treatment of patients with EGFR T790M-mutation-positive NSCLC [54]. It shows promising inhibitory activity against T790M and L858R mutant and exon 19 deleted lung cancer cells [55]. It showed a good safety profile and promising anti-tumor activity in patients with EGFR-mutated NSCLC that progressed after EGFR-TKIs, especially in those with T790M mutation.

In part of the phase I trial, 83 EGFR T790M mutation-positive patients received olmutinib 300 mg once daily and 18.1% (n = 15) had a confirmed PR. Median PFS was 2.8 (95% CI, 2.6-5.4) months; ORR was 18.1 (95% CI, 10.5-28.0) months; median DOR was 11.2 (95% CI, 5.6-13.6) months [19]. In patients who received olmutinib 500 mg twice daily (n = 19), median PFS was 5.3 (95% CI, 2.0-11.0) months; the confirmed ORR was 26.3% (95% CI, 9.1-51.2; n = 5) months; the DOR was not reached [19] (Table 4). In the phase II study, patients received olmutinib 800 mg once daily. In this study, 31.6% patients had brain metastases, 96.1% were T790M mutation activated; in phase I and II combined, T790M mutation activation represented 50.7%; overall ORR was 55.1% (95% CI, 42.6-67.1); estimated median PFS was 6.9 (95% CI, 5.6-9.7) months; The DOR was 8.4 (95% CI, 5.7-14.2) months; estimated median OS was not reached [19] (Table 4). In patients with brain metastases (n = 22), the median PFS was 6.2 (95% CI, 2.8-9.5) months, and the confirmed ORR was 45.5% (95% CI, 24.4-67.8). In patients without brain metastases (n = 47), median PFS was 7.6 (95% CI, 5.4-11.1) months, and ORR was 59.6% (95% CI, 44.3-73.6). In the phase II trial, the most frequent treatment-related AEs were diarrhea (59.2% of patients), pruritus (42.1%), rash (40.8%), and nausea (39.5%) [19].

Considering all patients in this study, 91.2% (248 patients) had treatment-related AEs, 26.8% (73 patients) had grade≥3 events. The most frequent treatment-related AEs were diarrhea (37.1%), rash (35.3%), and nausea (28.3%) [19]. For a pooled phase II trial, the most frequent treatment-related AEs were diarrhea (59.2% of patients), pruritus (42.1%), rash (40.8%), nausea (39.5%), palmar-plantar erythrodysesthesia syndrome (31.6%), decreased appetite (31.6%), dry skin (27.6%), and skin exfoliation (26.3%) (N = 76). The high dose of olmutinib (500 mg twice daily) in part IIB was not tolerable, supported by a high proportion of severe AEs (52.4%) and treatment discontinuations (19.0%). In the 800 mg once daily or higher dose, abdominal pain was reported and was considered to be related to the HCl salt form of olmutinib [19]. However, the company decided to terminate the study programs with the conclusion of not pursuing further olmutinib development in April 2018, on consideration of the competitive landscape of evolving EGFR-mutant NSCLC treatment options [19].

3. Fourth-generation EGFR TKIs

The C797S mutation in the tyrosine kinase domain of EGFR is a leading mechanism of resistance to the third generation of irreversible EGFR inhibitors targeting the T790M mutation [56-59]. To overcome the commonly-acquired C797S mutation, Jia et al. screened a library of approximately 2.5 million compounds against the L858R/T790M EGFR mutant kinase peptide. Among the compounds, EGFR allosteric inhibitor-1 (EAI001) was discovered. However, it only had modest potency against individual L858R and T790M mutants. With further characterization and optimization, EAI045 was found to be the most selective inhibitor, with the highest selective inhibition of the EFGR mutant over the wild-type EGFR [60]. The combination of EAI045 and cetuximab in a mouse model carrying the EGFR mutant with L858R/T790M/C797S caused a marked tumor shrinkage. Thus, EAI045 represents the first fourth-generation EGFR-TKI compound which targets the T790M and C797S mutations [60].

BLU-945 is another fourth-generation EGFR TKI designed to target the triple-mutant $\mathrm{EGFR}^{\mathrm{ex19del/T790M/C797S}}$, $\mathrm{EGFR}^{\mathrm{L858R/T790M/C797S}}$, $\mathrm{EGFR}^{\mathrm{ex19del/T790M}}$, and $\mathrm{EGFR}^{\mathrm{L858R/T790M}}$ mutants with sub-nanomolar IC_{50} values in an enzyme assay with a >1000-fold window over wild-type EGFR enzyme activity [61]. In a virtual poster presentation during the 2020 ESMO Virtual Congress, Schalm et al. reported that BLU-945 only inhibits 1% of the kinome at more than 90% at a concentration of 3 μM, and the selectivity profile enables combinations to cover a wide spectrum of resistant mechanisms. Moreover, BLU-945, but not osimertinib, inhibits the EGFR pathway in ex19del/T790M/C797S and L858R/T790M/C797S mutation-driven Ba/F3 cell lines. BLU-945 showed significant tumor regression in combination with gefitinib or osimertinib. BLU-945 was examined in combination with gefitinib or osimertinib, leading to an enhanced antitumor activity compared with single agent treatment in an EGFR+/T790M/C797S-driven PDX model. After oral administration, BLU-945 induced significant tumor regression in a NCI-H1975 NSCLC CDX (L858R/T790M) tumor model similar to the covalently binding drug osimertinib. Based on these findings, testing of BLU-945 is planned in combination with other TKIs across multiple treatment settings, and clinical development of BLU-945 monotherapy is expected to begin with an international phase 1 dose-escalation trial in patients with EGFR-driven NSCLC in the first half of 2021 [62].

4. Discussion and future perspectives

Over the past 20 years, the development of targeted therapies has seen enormous progress in the understanding of the biology and management of NSCLC. Early phase clinical trials suggested that almost all the EGFR-TKIs are highly efficacious and well tolerated. And combining EGFR-TKIs with other non-EGFR targeted agents (e.g. apatinib (NCT03811054)), or combining EGFR-TKIs with chemotherapy appears to be a promising treatment strategy. Previous clinical trials of combined therapy appear to improve PFS by 3 to 4 months compared to TKI therapy alone [63-65]. In addition, adding pemetrexed and carboplatin chemotherapy to gefitinib significantly prolonged PFS and OS, which represents a new standard first-line therapy for EGFR-mutant NSCLC [20]. Combining TKIs with chemotherapy is therefore a promising treatment strategy, although it does come with a higher risk for toxicity.

Although the efficacy of third-generation EGFR TKIs looks highly promising, responses are not durable and disease progression still occurs. Acquired drug resistance to EGFR TKIs during NSCLC treatment has become a main research focus in recent years. It generally occurs about one year after treatment begins for first- or second-generation EGFR TKIs. The resistance mechanisms evoked by third-generation EGFR TKIs are quite different. For instance, the resistance to rociletinib is largely due to EGFR amplification or histological transformation, while that for osimertinib is mainly caused by the C797S mutation. [66].The C797S mutation is detected in 50.7% of patients with NSCLC with T790M-mutant EGFR [19], and it is the most commonly-acquired mutation that confers resistance to third-generation EGFR TKIs.

The data discussed here have shown that osimertinib extends the PFS and OS of NSCLC patients compared to other EGFR TKIs. We should notice that osimertinib was approved by the FDA for patients with metastatic EGFR T790M mutation-positive NSCLC. However, the resistance to osimertinib is mainly caused by the C797S mutation, leading to EGFR T790M/C797S double-resistant mutants. Currently, there are no approved targeted therapies for NSCLC patients with T790M/C797S mutations. Therefore, the paramount requirement to find new agents is to overcome EGFR T790M/C797S-associated resistance. Recently, Su et al. designed and prepared a series of indole derivatives to increase additional interaction with the Asp855 in the conservative DFG site, to overcome the resistance mutation 19D/T790M/C797S [67].

In summary, tyrosine kinase inhibitors still remain the first choice of treatment for patients with the most advanced NSCLC. At present, challenges still exist in repeating a biopsy to determine the molecular mechanism of acquired resistance. However, the development of fourth-generation EGFR TKIs targeting C797S/T790M mutants represents a significant breakthrough in the treatment in patients with EGFR-mutant NSCLC. A further understanding of the mechanisms of resistance will be key to developing the next (fourth/fifth) generation of EGFR TKIs. In addition, continuing drug development and combination therapies (such as with chemotherapeutic agents, MET and MEK inhibitors), provide the hope for prolonged survival in an increasing number of patients. Moreover, dynamic real-time monitoring of tumour gene mutations will also be needed in overcoming the challenge of acquired resistance and improving the clinical efficacy of targeted NSCLC treatments.

Table 1. Clinical data of afatinib compared to gefitinib as first-line treatment of patients with EGFR mutation-positive NSCLC (LUX-Lung 7)

EGFR inhibitors	Phase	Dose (mg/day)	PFS (months) (95% CI) [37]			TTF (months) (95% CI) [37]			OS (months) (95% CI) [38]			ORR (95% CI) [38]
			Total	L858R	Del19	Total	L858R	Del19	Total	L858R	Del19	
Afatinib	2B [37, 38]	40	11.0 (10.6-12.9)	10.9 (8.1-12.9)	12.7 (10.6-14.7)	13.7 (11.9-15.0)	12.9 (9.2-14.8)	14.7 (11.7-17.7)	24.5 (21.2-26.4)	25.0	30.7	72.5%
Gefitinib		250	10.9 (9.1-11.5)	10.8 (7.2-12.8)	11.0 (9.1-12.7)	11.5 (10.1-13.1)	9.8 (7.4-12.9)	12.9 (11.0-15.6	27.9 (25-30.7)	21.2	26.4	56%

Table 2. Clinical data of dacomitinib compared to gefitinib, and clinical data for osimertinib

EGFR inhibitors	Phase	Dose	PFS (months) (95% CI)	OS (months) (95% CI)	ORR (%) (95% CI)	DOR (months) (95% CI)
Dacomitinib	III [40-42]	45 (mg/day)	14.7 (11.1-16.6) [40]	34.1 (29.5-39.8) [42] 34.1 (29.5-37.7) [41]	74.9% [40]	15.4 (0.07-60.5) [42]
Gefitinib		250 (mg/day)	9.2 (11.1-16.6) [40]	27.0 (24.4-31.6) [42] 26.8 (23.7-32.1) [41]	71.6% [40]	12.0 (0.07-48.1) [42]
Osimertinib (AZD9291)	III [47, 48]	80 mg QD	18.9 (15.2-21.4) [48]	38.6 (34.5-41.8) [47]	80% (75-85) [48]	17.2 (13.8-22.0) [48]
		comparator ^{a}	10.2 (9.6-11.1) [48]	31.8 (26.6-36.0) [47]	76% (70-81) [48]	8.5 (7.3-9.8) [48]
	II [49]	80 mg QD	8.2 (5.9-10.5)	NR	50% (33-67)	11.2 (7.7-14.7)
	I [50]	160 mg QD	8.6 (5.4-13.7)	11.0 (8.0-18.0)	41% (26-58)	8.3 (5.6-16.5)

^{a}: Gefitinib at a dose of 250 mg once daily or erlotinib at a dose of 150 mg once daily, with patients receiving these drugs combined in a single comparator group.

Table 3. Clinical data of rociletinib compared to chemotherapy in patients with EGFR-mutated NSCLC

EGFR Inhibitors	Phase	Dose	PFS (months) (95% CI)				ORR (%) (95% CI)				DOR (months) (95% CI)			
			Total	T790M+	T790M-	T790M unknown	Total	T790M+	T790M-	T790M unknown	Total	T790M+	T790M-	T790M unknown
Rociletinib (CO-1686)	III [51]	500 mg BID	4.1 (2.6-5.4)	6.8 (3.8-12.2) [a]	4.1 (2.5-4.6) [a]	2.3 (1.2-9.6) [a]	17.3 (9.6-27.8) [a]	36.0 (18.0-57.5) [a]	8.3% (1.8-22.5) [a]	7.1% (0.2-33.9) [a]	11.0 (4.3-13.7) [a]	12.3 (2.5-22.1) [a]	5.5 (2.8-13.1) [a]	4.3 [51] [b]
	III [51]	625 mg BID	5.5 (1.8-8.1)											
	III [51]	Chemotherapy	2.5 (1.4-2.9)	2.7 (1.3-7.0)	1.4 (1.3-2.7)	4.4 (1.4-7.1)	8.2 (3.1-17.0)	15.0 (3.2-37.9)	4.9% (0.6-16.5)	8.3% (0.2-38.5)	6.8 (4.5-NA)	NA (4.5-NA)	NA (5.8-NA)	6.8 [51] [b]

[a]:Rociletinib 500 mg BID and 625 mg BID dosage groups were pooled for this analysis.

[b]:No 95% CI interval as n=1.

Table 4. Clinical data for olmutinib

EGFR inhibitors	Phase	Dose	PFS (months) (95% CI)	ORR (%) (95% CI)	DOR (months) (95% CI)	DCR (%) (95% CI)	TTP (months) (95% CI)
Olmutinib (HM61713) [19]	I-1 (n=83)	300 mg QD	2.8 (2.6-5.4)	18.1 (10.5-28.0)	11.2 (5.6-13.6)	63.9 (52.6-74.1)	2.8 (2.6-5.2)
	I-2B (n=19)	500 mg BID (T790M-)	5.3 (2.0-11.0)	26.3 (9.1-51.2)	NR (4.9-NR)	73.7 (48.8-90.85)	6.1 (2.5-11.0)
	I-3 (n=26)	800 mg QD (T790M-)	3.8 (1.4-8.1)	7.7 (0.9-25.1)	NR	53.9 (33.4-73.4)	3.8 (1.4-8.1)
	II	800 mg QD (T790M+)	6.9 (5.6-9.7)	55.1 (42.6-67.1)	8.4 (5.7-14.2)	88.4 (78.4-94.9)	6.8 (5.4-8.8)

References

1. Siegel, R.L., K.D. Miller, and A. Jemal, Cancer statistics, 2020. CA: a cancer journal for clinicians, 2020. **70**(1): p. 7-30.
2. Zarogoulidis, K., et al., Treatment of non-small cell lung cancer (NSCLC). Journal of thoracic disease, 2013. **5**(Suppl 4): p. S389.
3. Navada, S., et al., Temporal trends in small cell lung cancer: analysis of the national Surveillance, Epidemiology, and End-Results (SEER) database. Journal of Clinical Oncology, 2006. **24**(18_suppl): p. 7082-7082.
4. Sher, T., G.K. Dy, and A.A. Adjei. Small cell lung cancer. in Mayo Clinic Proceedings. 2008. Elsevier.
5. Molina, J.R., et al. Non-small cell lung cancer: epidemiology, risk factors, treatment, and survivorship. in Mayo clinic proceedings. 2008. Elsevier.
6. Schiller, J.H., et al., Comparison of four chemotherapy regimens for advanced non–small-cell lung cancer. New England Journal of Medicine, 2002. **346**(2): p. 92-98.
7. Scagliotti, G.V., et al., Phase III randomized trial comparing three platinum-based doublets in advanced non–small-cell lung cancer. Journal of Clinical Oncology, 2002. **20**(21): p. 4285-4291.
8. Ohe, Y., et al., Randomized phase III study of cisplatin plus irinotecan versus carboplatin plus paclitaxel, cisplatin plus gemcitabine, and cisplatin plus vinorelbine for advanced non-small-cell lung cancer: Four-Arm Cooperative Study in Japan. Annals of oncology, 2007. **18**(2): p. 317-323.
9. Yoon, S.M., T. Shaikh, and M. Hallman, Therapeutic management options for stage III non-small cell lung cancer. World Journal of Clinical Oncology, 2017. **8**(1): p. 1.
10. Bradley, J., et al., Long-term results of RTOG 0617: a randomized phase 3 comparison of standard dose versus high dose conformal chemoradiation therapy+/-cetuximab for stage III NSCLC. International Journal of Radiation Oncology• Biology• Physics, 2017. **99**(2): p. S105.
11. Ahn, J.S., et al., Multinational randomized phase III trial with or without consolidation chemotherapy using docetaxel and cisplatin after concurrent chemoradiation in inoperable stage III non–small-cell lung cancer: KCSG-LU05-04. Journal of Clinical Oncology, 2015. **33**(24): p. 2660-2666.
12. Skrzypski, M. and J. Jassem, Consolidation systemic treatment after radiochemotherapy for unresectable stage III non-small cell lung cancer. Cancer treatment reviews, 2018. **66**: p. 114-121.
13. Tsujino, K., et al., Is consolidation chemotherapy after concurrent chemo-radiotherapy beneficial for patients with locally advanced non–small-cell lung cancer?: A pooled analysis of the literature. Journal of Thoracic Oncology, 2013. **8**(9): p. 1181-1189.
14. Kelly, K., et al., Phase III trial of maintenance gefitinib or placebo after concurrent chemoradiotherapy and docetaxel consolidation in inoperable stage III non–small-cell lung cancer: SWOG S0023. Journal of clinical oncology, 2008. **26**(15): p. 2450-2456.
15. Hanna, N., et al., Phase III study of cisplatin, etoposide, and concurrent chest radiation with or without consolidation docetaxel in patients with inoperable stage III non–small-cell lung cancer: the Hoosier Oncology Group and US Oncology. Journal of clinical oncology, 2008. **26**(35): p. 5755-5760.
16. Antonia, S.J., et al., Overall survival with durvalumab after chemoradiotherapy in stage III NSCLC. New England Journal of Medicine, 2018. **379**(24): p. 2342-2350.
17. Howlader, N., et al., SEER cancer statistics review, 1975–2016. Bethesda, MD: National Cancer Institute, 2019: p. 1423-37.
18. Quint, L.E., et al., Distribution of distant metastases from newly diagnosed non-small cell lung cancer. The Annals of thoracic surgery, 1996. **62**(1): p. 246-250.
19. Kim, D.-W., et al., Safety, tolerability, and anti-tumor activity of olmutinib in non-small cell lung cancer with T790M mutation: A single arm, open label, phase 1/2 trial. Lung Cancer, 2019. **135**: p. 66-72.
20. Noronha, V., et al., Gefitinib versus gefitinib plus pemetrexed and carboplatin chemotherapy in EGFR-mutated lung cancer. Journal of Clinical Oncology, 2020. **38**(2): p. 124-136.
21. Wright, D.C., Surgical treatment of brain metastases. Surgical Treatment of Metastatic Cancer. Philadelphia: JB Lippincott, 1987: p. 165-222.

22. Burt, M., et al., Resection of brain metastases from non-small-cell lung carcinoma: results of therapy. The Journal of thoracic and cardiovascular surgery, 1992. **103**(3): p. 399-411.
23. https://www.cancer.org/cancer/lung-cancer/treating-non-small-cell/targeted-therapies.html
24. Hanna, N., et al., Systemic therapy for stage IV non–small-cell lung cancer: American Society of Clinical Oncology clinical practice guideline update. Journal of Clinical Oncology, 2017.
25. Planchard, D., et al., Metastatic non-small cell lung cancer: ESMO Clinical Practice Guidelines for diagnosis, treatment and follow-up. Annals of Oncology, 2018. **29**(Supplement_4): p. iv192-iv237.
26. Wu, Y.-L., et al., Pan-Asian adapted Clinical Practice Guidelines for the management of patients with metastatic non-small-cell lung cancer: a CSCO–ESMO initiative endorsed by JSMO, KSMO, MOS, SSO and TOS. Annals of Oncology, 2019. **30**(2): p. 171-210.
27. Mendelsohn, J. and J. Baselga, Status of epidermal growth factor receptor antagonists in the biology and treatment of cancer. Journal of clinical oncology, 2003. **21**(14): p. 2787-2799.
28. Salomon, D.S., et al., Epidermal growth factor-related peptides and their receptors in human malignancies. Critical reviews in oncology/hematology, 1995. **19**(3): p. 183-232.
29. Baselga, J., Why the epidermal growth factor receptor? The rationale for cancer therapy. The oncologist, 2002. **7**(90004): p. 2-8.
30. Muhsin, M., J. Graham, and P. Kirkpatrick, Gefitinib. 2003, Nature Publishing Group.
31. Dancey, J. and E.A. Sausville, Issues and progress with protein kinase inhibitors for cancer treatment. Nature reviews Drug discovery, 2003. **2**(4): p. 296-313.
32. Kris, M.G., et al., Efficacy of gefitinib, an inhibitor of the epidermal growth factor receptor tyrosine kinase, in symptomatic patients with non–small cell lung cancer: a randomized trial. Jama, 2003. **290**(16): p. 2149-2158.
33. Wakeling, A.E., et al., ZD1839 (Iressa): an orally active inhibitor of epidermal growth factor signaling with potential for cancer therapy. Cancer research, 2002. **62**(20): p. 5749-5754.
34. Barker, A.J., et al., Studies leading to the identification of ZD1839 (Iressa™): an orally active, selective epidermal growth factor receptor tyrosine kinase inhibitor targeted to the treatment of cancer. Bioorganic & medicinal chemistry letters, 2001. **11**(14): p. 1911-1914.
35. Planchard, D., et al., EGFR-independent mechanisms of acquired resistance to AZD9291 in EGFR T790M-positive NSCLC patients. Annals of Oncology, 2015. **26**(10): p. 2073-2078.
36. Jia, Y., et al., EGF816 exerts anticancer effects in non–small cell lung cancer by irreversibly and selectively targeting primary and acquired activating mutations in the EGF receptor. Cancer research, 2016. **76**(6): p. 1591-1602.
37. Park, K., et al., Afatinib versus gefitinib as first-line treatment of patients with EGFR mutation-positive non-small-cell lung cancer (LUX-Lung 7): a phase 2B, open-label, randomised controlled trial. The Lancet Oncology, 2016. **17**(5): p. 577-589.
38. Paz-Ares, L., et al., Afatinib versus gefitinib in patients with EGFR mutation-positive advanced non-small-cell lung cancer: overall survival data from the phase IIb LUX-Lung 7 trial. Annals of Oncology, 2017. **28**(2): p. 270-277.
39. Lee, C.K., et al., Impact of specific epidermal growth factor receptor (EGFR) mutations and clinical characteristics on outcomes after treatment with EGFR tyrosine kinase inhibitors versus chemotherapy in EGFR-mutant lung cancer: a meta-analysis. Journal of Clinical Oncology, 2015. **33**(17): p. 1958-1965.
40. Wu, Y.-L., et al., Dacomitinib versus gefitinib as first-line treatment for patients with EGFR-mutation-positive non-small-cell lung cancer (ARCHER 1050): a randomised, open-label, phase 3 trial. The Lancet Oncology, 2017. **18**(11): p. 1454-1466.
41. Mok, T.S., et al., Improvement in overall survival in a randomized study that compared dacomitinib with gefitinib in patients with advanced non-small-cell lung cancer and EGFR-activating mutations. J Clin Oncol, 2018. **36**(22): p. 2244-2250.
42. Mok, T.S., et al., Updated Overall Survival in a Randomized Study Comparing Dacomitinib with Gefitinib as First-Line Treatment in Patients with Advanced Non-Small-Cell Lung Cancer and EGFR-Activating Mutations. Drugs, 2020: p. 1-10.
43. Ou, S.-H.I., Second-generation irreversible epidermal growth factor receptor (EGFR) tyrosine kinase inhibitors (TKIs): a better mousetrap? A review of the clinical evidence. Critical reviews in oncology/hematology, 2012. **83**(3): p. 407-421.

44. Tan, C.-S., B.-C. Cho, and R.A. Soo, Next-generation epidermal growth factor receptor tyrosine kinase inhibitors in epidermal growth factor receptor-mutant non-small cell lung cancer. Lung cancer, 2016. **93**: p. 59-68.
45. Cross, D.A., et al., AZD9291, an irreversible EGFR TKI, overcomes T790M-mediated resistance to EGFR inhibitors in lung cancer. Cancer discovery, 2014. **4**(9): p. 1046-1061.
46. Lee, J., et al., Genomic landscape of acquired resistance to third-generation EGFR tyrosine kinase inhibitors in EGFR T790M-mutant non–small cell lung cancer. Cancer, 2020. **126**(11): p. 2704-2712.
47. Ramalingam, S.S., et al., Overall survival with osimertinib in untreated, EGFR-mutated advanced NSCLC. New England Journal of Medicine, 2020. **382**(1): p. 41-50.
48. Soria, J.-C., et al., Osimertinib in untreated EGFR-mutated advanced non–small-cell lung cancer. New England journal of medicine, 2018. **378**(2): p. 113-125.
49. Cho, J.H., et al., Osimertinib for patients with non–small-cell lung cancer harboring uncommon EGFR mutations: a multicenter, open-label, phase II trial (KCSG-LU15-09). Journal of Clinical Oncology, 2020. **38**(5): p. 488.
50. Yang, J.C., et al., Osimertinib in Patients With Epidermal Growth Factor Receptor Mutation–Positive Non–Small-Cell Lung Cancer and Leptomeningeal Metastases: The BLOOM Study. Journal of Clinical Oncology, 2020. **38**(6): p. 538-547.
51. Yang, J.C.-H., et al., Efficacy and Safety of Rociletinib Versus Chemotherapy in Patients With EGFR-Mutated Non–Small Cell Lung Cancer: Results of TIGER-3, a Phase III Randomized Study. JTO Clinical and Research Reports, 2020: p. 100114.
52. Mok, T.S., et al., Gefitinib or carboplatin–paclitaxel in pulmonary adenocarcinoma. New England Journal of Medicine, 2009. **361**(10): p. 947-957.
53. Sequist, L.V., et al., Phase III study of afatinib or cisplatin plus pemetrexed in patients with metastatic lung adenocarcinoma with EGFR mutations. Journal of clinical oncology, 2013. **31**(27): p. 3327-3334.
54. Liao, B.-C., et al., Update on recent preclinical and clinical studies of T790M mutant-specific irreversible epidermal growth factor receptor tyrosine kinase inhibitors. Journal of biomedical science, 2016. **23**(1): p. 86.
55. Kim, E.S., Olmutinib: first global approval. Drugs, 2016. **76**(11): p. 1153-1157.
56. Thress, K.S., et al., Acquired EGFR C797S mutation mediates resistance to AZD9291 in non–small cell lung cancer harboring EGFR T790M. Nature medicine, 2015. **21**(6): p. 560-562.
57. Niederst, M.J., et al., The allelic context of the C797S mutation acquired upon treatment with third-generation EGFR inhibitors impacts sensitivity to subsequent treatment strategies. Clinical Cancer Research, 2015. **21**(17): p. 3924-3933.
58. Helena, A.Y., et al., Acquired resistance of EGFR-mutant lung cancer to a T790M-specific EGFR inhibitor: emergence of a third mutation (C797S) in the EGFR tyrosine kinase domain. JAMA oncology, 2015. **1**(7): p. 982-984.
59. Wang, S., et al., EGFR C797S mutation mediates resistance to third-generation inhibitors in T790M-positive non-small cell lung cancer. Journal of hematology & oncology, 2016. **9**(1): p. 1-5.
60. Jia, Y., et al., Overcoming EGFR (T790M) and EGFR (C797S) resistance with mutant-selective allosteric inhibitors. Nature, 2016. **534**(7605): p. 129-132.
61. Schalm, S., et al., 1296P BLU-945, a highly potent and selective 4th generation EGFR TKI for the treatment of EGFR T790M/C797S resistant NSCLC. Annals of Oncology, 2020. **31**: p. S839.
62. Schalm, S., et al., BLU-945, a highly potent and selective 4 th-generation EGFR TKI for the treatment of EGFR+/T790M/C797S resistant NSCLC.
63. Wang, S., Y. Song, and D. Liu, EAI045: the fourth-generation EGFR inhibitor overcoming T790M and C797S resistance. Cancer Letters, 2017. **385**: p. 51-54.
64. Wu, Y.-L., et al., Intercalated combination of chemotherapy and erlotinib for patients with advanced stage non-small-cell lung cancer (FASTACT-2): a randomised, double-blind trial. The lancet oncology, 2013. **14**(8): p. 777-786.
65. Cheng, Y., et al., Randomized phase II trial of gefitinib with and without pemetrexed as first-line therapy in patients with advanced nonsquamous non–small-cell lung cancer with activating epidermal growth factor receptor mutations. Journal of Clinical Oncology, 2016. **34**(27): p. 3258-3266.

66. Li, R., et al., Four generations of EGFR TKIs associated with different pathogenic mutations in non-small cell lung carcinoma. Journal of Drug Targeting, 2020: p. 1-12.
67. Su, Z., et al., Design, synthesis and biological evaluation of potent EGFR kinase inhibitors against 19D/T790M/C797S mutation. Bioorganic & Medicinal Chemistry Letters, 2020: p. 127327.

Part V. The blood-brain barrier and EGFR inhibitors: Implications for patients with NSCLC brain metastases

The development of brain metastases is one of the most serious consequences of advanced non-small cell lung cancer (NSCLC). In patients diagnosed with NSCLC, distant metastases are most commonly found in the brain (47%), followed by bone (36%), liver (22%), adrenal glands (15%), body wall (13%), lung (11%), spleen (6%), (non-osseous) spinal canal (3%), and pancreas (1%) [1]. One phase II study showed that metastatic disease to the brain is common for lung cancer and occurs in approximately 31.6% of cases [2]. Brain metastases from NSCLC also form the most commonly occurring group, accounting for 40% to 60% of all brain metastases [3, 4].

These days, targeted drugs are very often used for treatment of advanced lung cancer, either with or without chemotherapy (Reference: https://www.cancer.org/cancer/lung-cancer/treating-non-small-cell/targeted-therapies.html). In patients with advanced or metastatic NSCLC containing mutations of the epidermal growth factor receptor (EGFR) conferring high sensitivity to EGFR tyrosine kinase inhibitors (TKIs) (e.g., exon 19 deletions or L858R point mutations), guidelines recommend treatment with an EGFR-TKI [5-7] (Reference: Clinical practice guidelines in oncology: NCCN guidelines for non-small cell lung cancer V.7. Fort Washington, PA: National Comprehensive Cancer Network, 2019 (https://www .nccn .org). In 40% to 80% of patients with NSCLC, EGFR is overexpressed, and it seems that its overexpression is associated with poor prognosis [8, 9] and disease progression, providing a strong rationale for assessing EGFR inhibitors in NSCLC (as well as various other solid tumors) [10-12]. There are several possible approaches to targeting EGFR, including monoclonal antibodies directed against the extracellular ligand-binding domain and small-molecule inhibitors of the intracellular tyrosine kinase domain [12, 13]. At present, TKIs still remain the first choice of treatment for patients with the most advanced NSCLCs. However, the efflux transport of drugs across the blood-brain barrier (BBB) presents a challenge to the use of many TKIs.

The brain is separated from the systemic circulation by two physical barriers, namely the blood-brain barrier (BBB) and the blood-cerebrospinal fluid barrier (BCSFB), which form a very effective barrier to the free diffusion of many polar solutes into the brain. The BBB is formed by brain capillary endothelial cells, pericytes, a basal membrane, and astrocyte foot processes [14-16]. These capillary endothelial cells are closely connected by very tight junctions, and therefore the BBB presents a very strong, continuous physical barrier. In addition, active mechanisms support this barrier function, namely selective transport systems mediating permeation into and out of the brain, including membrane transport proteins as well as specific receptors undergoing endocytosis and transcytosis.

ATP Binding Cassette (ABC) transporters form a special family of membrane proteins, characterized by homologous ATP-binding sites, and large, multi-spanning transmembrane domains. ABC proteins can utilize the energy derived from ATP binding and hydrolysis to perform a directed transmembrane movement of their substrates (primary active transporters), open or close a specific membrane channel (e.g. ion channels), or regulate the permeability of multi-protein channel complexes (receptors) [17]. There are two major groups of ABC transporters involved in cancer multidrug resistance (MDR) that also affect the overall pharmacokinetics of substrate drugs: ABCB1 (P-gp, MDR1) and ABCG2 (BCRP). Both transporters mediate the active cellular extrusion of a structurally very broad range of compounds, including many anticancer drugs. It has become clear that ABCB1 and ABCG2 transporters are localized at the luminal surface of brain capillary endothelial cells, where they can play a particular role by pumping their substrates across the luminal side of the endothelial cells into the blood circulation [18-20]. The central roles of ABCB1 and ABCG2 transporters at the BBB are therefore to prevent the net entry of toxins or drugs into the brain. Of course from a biological point of view, virtually all drugs, given their pharmacodynamic action against various targets in the body, can be considered potential toxins depending on the dose at which they are given. One of the main biological roles of ABCB1 and ABCG2 is therefore to protect the brain from various toxins which can be derived from food, the intestinal microbiome, or some infectious organisms.

Among the EGFR inhibitors, while preclinical studies have addressed the brain uptake of afatinib [21], brigatinib [22], and osimertinib [23], this has never been explored for the experimental drug EAI045. Recently, we studied the single and combined effects of Abcb1 and Abcg2 deficiencies on EAI045 plasma pharmacokinetics and organ accumulation in male wild-type, *Abcg2*$^{-/-}$, *Abcb1a/1b*$^{-/-}$, and *Abcb1a/1b;Abcg2*$^{-/-}$ mice, using oral administration of 20 mg/kg EAI045. EAI045 showed rapid systemic uptake following oral administration, with a t_{max} of 5-10 min, or even before 5 min. Analysis of brain penetration showed the brain-to-plasma drug ratio to be about 10% of plasma EAI045 in wild-type mice. In mice lacking the drug transporter Abcb1a/1b this was 40%, 3.9-fold increased, or lacking both Abcb1a/1b and Abcg2 49%, 4.8-fold increased, whereas these increases were not observed in single Abcg2 knockout mice (9% of plasma level of EAI045). While in the same mouse models, osimertinib showed the greatest level of brain uptake in wild-type mice (brain concentration: 2003 ng/g; brain-to-plasma ratio: 14.5), followed by afatinib (brain concentration: 51 ng/g; brain-to-plasma ratio: 0.43), brigatinib (brain concentration: 41 ng/g; brain-to-plasma ratio: 0.06), and then EAI045 (brain concentration: 23 ng/g; brain-to-plasma ratio: 0.10).

The wild-type mouse data match the preclinical findings from Colclough et al. [24] quite closely, where they compared the brain distribution for 16 EGFR-TKIs (e.g., osimertinib, icotinib, erlotinib, dacomitinib, olmutinib, gefitinib, rociletinib, afatinib, and so on) in normal healthy rat, and found that osimertinib has the highest relative BBB penetrance compared with the other TKIs tested. The work from Chen et al. further showed that osimertinib reverses ABCB1- and ABCG2-mediated MDR via inhibiting ABCB1 and ABCG2 from pumping out chemotherapeutic agents and thus might provide a possibility for cancer combinational therapy with osimertinib in the clinic [25]. However, there are currently limited data on the effectiveness of osimertinib alone for patients with progressing brain metastases.

Our study showed that coadministration of oral EAI045 with elacridar, an ABCB1/ABCG2 inhibitor, could substantially improve the plasma $AUC_{0\text{-}30min}$ by 4-fold and the brain-to-plasma ratios by 5.4-fold in wild-type mice. Li et al. [22] showed that coadministration of oral brigatinib with elacridar could markedly improve the brain-to-plasma ratios of brigatinib in wild-type mice by 36-fold, without substantially altering systemic exposure. If the differences as seen in wild-type and Abcb1a/1b;Abcg2$^{-/-}$ mice apply similarly to humans with respect to brain-to-plasma ratios, it would suggest that hABCB1 and hABCG2 would not have an enormous impact on human EAI045 pharmacokinetics and tissue distribution. Thus, other things being equal, brigatinib could be the best drug of choice for the treatment of brain metastases in NSCLC patients, followed by afatinib (28-fold), osimertinib (6.4-fold), and then EAI045. However, clear toxicities were observed in mice in the brigatinib experiment with genetic knockout or pharmacological inhibition of mAbcb1a/1b and mAbcg2 [22]. If humans would respond similarly to mice in developing toxicity when blocking ABCB1 function during brigatinib treatment, the increased CNS toxicity might be the biggest problem when considering applying brigatinib together with an ABCB1/ABCG2 inhibitor in patients.

All the studies indicate that both ABCB1 and ABCG2 can restrict the net accumulation of afatinib, brigatinib, osimertinib, and EAI045 in the brain. These studies are useful to understand the clinical use of ABC transporters as predictive markers for therapy response for the EGFR inhibitors. Although, for understandable reasons, there are very limited data on the brain accumulation in patients, our findings further suggest that the use of ABCB1 and ABCG2 inhibitors might help to enhance drug exposure for tumors that are positioned in part or in whole behind the BBB, and thus possibly improve therapeutic efficacy.

Overall, the effect of Abcb1 and Abcg2 on brain penetration of EAI045 in mice was relatively modest compared to that for other EGFR inhibitors. If this would also apply to the human brain, this might perhaps mean that the gain from such an inhibitor co-administration approach would be relatively limited. Therefore, our study suggests that EAI045 may not be the optimal choice for the treatment of NSCLC with brain metastases when the BBB is intact. More work is urgently needed to develop novel, more brain permeable, EGFR inhibitors and novel drug combinations to tackle the rising incidence of brain metastases in NSCLC patients.

References

1. Quint, L.E., et al., Distribution of distant metastases from newly diagnosed non-small cell lung cancer. The Annals of thoracic surgery, 1996. 62(1): p. 246-250.
2. Kim, D.-W., et al., Safety, tolerability, and anti-tumor activity of olmutinib in non-small cell lung cancer with T790M mutation: A single arm, open label, phase 1/2 trial. Lung Cancer, 2019. 135: p. 66-72.
3. Wright, D.C., Surgical treatment of brain metastases. Surgical Treatment of Metastatic Cancer. Philadelphia: JB Lippincott, 1987: p. 165-222.
4. Burt, M., et al., Resection of brain metastases from non-small-cell lung carcinoma: results of therapy. The Journal of thoracic and cardiovascular surgery, 1992. 103(3): p. 399-411.
5. Hanna, N., et al., Systemic therapy for stage IV non–small-cell lung cancer: American Society of Clinical Oncology clinical practice guideline update. Journal of Clinical Oncology, 2017.
6. Planchard, D., et al., Metastatic non-small cell lung cancer: ESMO Clinical Practice Guidelines for diagnosis, treatment and follow-up. Annals of Oncology, 2018. 29(Supplement_4): p. iv192-iv237.
7. Wu, Y.-L., et al., Pan-Asian adapted Clinical Practice Guidelines for the management of patients with metastatic non-small-cell lung cancer: a CSCO–ESMO initiative endorsed by JSMO, KSMO, MOS, SSO and TOS. Annals of Oncology, 2019. 30(2): p. 171-210.
8. Mendelsohn, J. and J. Baselga, Status of epidermal growth factor receptor antagonists in the biology and treatment of cancer. Journal of clinical oncology, 2003. 21(14): p. 2787-2799.
9. Molina, J.R., et al. Non-small cell lung cancer: epidemiology, risk factors, treatment, and survivorship. in Mayo clinic proceedings. 2008. Elsevier.
10. Salomon, D.S., et al., Epidermal growth factor-related peptides and their receptors in human malignancies. Critical reviews in oncology/hematology, 1995. 19(3): p. 183-232.
11. Baselga, J., Why the epidermal growth factor receptor? The rationale for cancer therapy. The oncologist, 2002. 7(90004): p. 2-8.
12. Muhsin, M., J. Graham, and P. Kirkpatrick, Gefitinib. 2003, Nature Publishing Group.
13. Dancey, J. and E.A. Sausville, Issues and progress with protein kinase inhibitors for cancer treatment. Nature reviews Drug discovery, 2003. 2(4): p. 296-313.
14. Abbott, N.J., et al., Structure and function of the blood–brain barrier. Neurobiology of disease, 2010. 37(1): p. 13-25.
15. Quaegebeur, A., C. Lange, and P. Carmeliet, The neurovascular link in health and disease: molecular mechanisms and therapeutic implications. Neuron, 2011. 71(3): p. 406-424.
16. Mahringer, A. and G. Fricker, ABC transporters at the blood–brain barrier. Expert opinion on drug metabolism & toxicology, 2016. 12(5): p. 499-508.
17. Glavinas, H., et al., The role of ABC transporters in drug resistance, metabolism and toxicity. Current drug delivery, 2004. 1(1): p. 27-42.
18. Miller, D.S., et al., Xenobiotic efflux pumps in isolated fish brain capillaries. American Journal of Physiology-Regulatory, Integrative and Comparative Physiology, 2002. 282(1): p. R191-R198.
19. Bauer, B., et al., Modulation of p-glycoprotein transport function at the blood-brain barrier. Experimental Biology and Medicine, 2005. 230(2): p. 118-127.
20. Cooray, H.C., et al., Localisation of breast cancer resistance protein in microvessel endothelium of human brain. Neuroreport, 2002. 13(16): p. 2059-2063.
21. van Hoppe, S., et al., Breast cancer resistance protein (BCRP/ABCG2) and P-glycoprotein (P-gp/ABCB1) transport afatinib and restrict its oral availability and brain accumulation. Pharmacological research, 2017. 120: p. 43-50.
22. Li, W., et al., P-glycoprotein and breast cancer resistance protein restrict brigatinib brain accumulation and toxicity, and, alongside CYP3A, limit its oral availability. Pharmacological research, 2018. 137: p. 47-55.
23. van Hoppe, S., et al., Brain accumulation of osimertinib and its active metabolite AZ5104 is restricted by ABCB1 (P-glycoprotein) and ABCG2 (breast cancer resistance protein). Pharmacological research, 2019. 146: p. 104297.
24. Colclough, N., et al., Preclinical Comparison of the Blood–brain barrier Permeability of Osimertinib with Other EGFR TKIs. Clinical Cancer Research, 2021. 27(1): p. 189-201.

25. Chen, Z., et al., Osimertinib (AZD9291) enhanced the efficacy of chemotherapeutic agents in ABCB1-and ABCG2-overexpressing cells in vitro, in vivo, and ex vivo. Molecular cancer therapeutics, 2016. 15(8): p. 1845-1858.

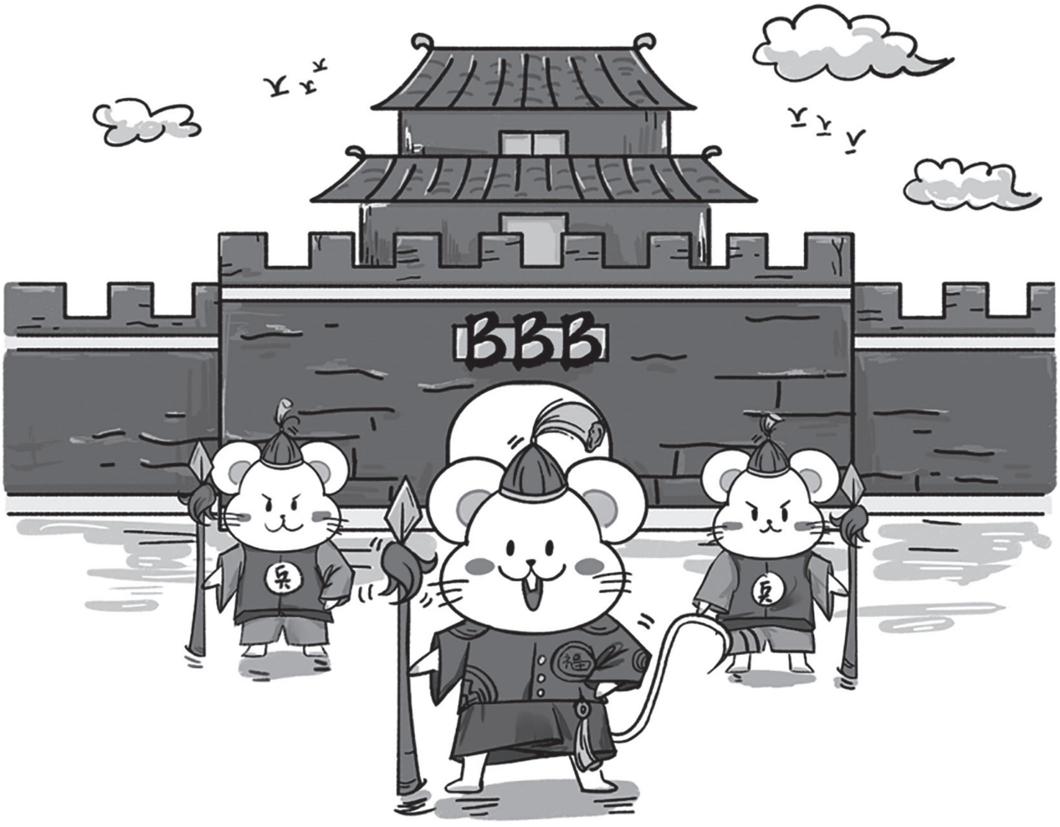
BBB
兵
福
兵

Chapter 2

P-glycoprotein (MDR1/ABCB1) and Breast Cancer Resistance Protein (BCRP/ABCG2) affect brain accumulation and intestinal disposition of encorafenib in mice

Jing Wang
Changpei Gan
Rolf W. Sparidans
Els Wagenaar
Stéphanie van Hoppe
Jos H. Beijnen
Alfred H. Schinkel

Pharmacological Research, 2018, 129: 414-423.

Abstract

Encorafenib (LGX818) is a promising BRAF^{V600E} inhibitor that has efficacy against metastatic melanoma. To better understand its pharmacokinetics, we studied its interactions with the multidrug efflux transporters ABCB1 and ABCG2 and the multidrug metabolizing enzyme CYP3A. In polarized MDCK-II cells, encorafenib was efficiently transported by canine and human ABCB1 and ABCG2 and by mouse Abcg2. Upon oral administration to wild-type, *Abcb1a/1b*$^{-/-}$, *Abcg2*$^{-/-}$, and *Abcb1a/1b;Abcg2*$^{-/-}$ mice, encorafenib was absorbed very quickly and to very high plasma levels, but without clear changes in oral availability between the strains. Upon oral or intravenous administration, encorafenib brain accumulation was markedly increased in *Abcb1a/1b;Abcg2*$^{-/-}$ mice and to a lesser extent in *Abcb1a/1b*$^{-/-}$ mice. However, absolute brain concentrations and brain-to-plasma ratios remained very low in all strains, indicating intrinsically poor brain penetration of encorafenib. Upon intravenous administration, *Abcb1a/1b;Abcg2*$^{-/-}$ mice showed somewhat reduced plasma elimination of encorafenib compared to wild-type mice, and lower accumulation of the drug in the intestinal tract, suggesting a limited role for these transporters in intestinal elimination of the drug. In *Cyp3a*$^{-/-}$ mice plasma levels of encorafenib were not markedly increased, suggesting a limited impact of Cyp3a on encorafenib oral availability. The low brain penetration of encorafenib might limit its efficacy against malignancies positioned behind a functional blood-brain barrier, but its oral bioavailability and distribution to other tested organs (liver, kidney, spleen, testis) was high.

Keywords: ABCB1, ABCG2, CYP3A enzymes, encorafenib, brain penetration

Graphical abstract:

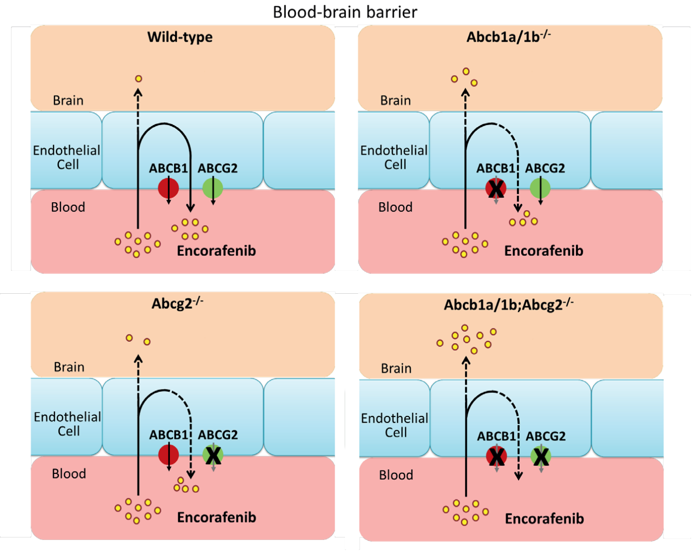

1. Introduction

In 2016, cutaneous melanoma caused 76,380 new cases and 10,103 deaths in the United States alone [1]. Melanoma has a high propensity to metastasize to the brain [2], lung, liver and bone [3], which contributes significantly to overall mortality. At autopsy, cerebral metastases are found in 49% to 73% of patients that die as a result of melanoma [4, 5]. Moreover, from the time of diagnosis of central nervous system (CNS) metastasis, the median overall survival of melanoma patients is often limited to less than 6 months [6]. Efficacy of anticancer drugs against CNS metastases may therefore be an important requisite for effective treatment of melanoma.

The mutant BRAF oncogene, especially BRAF^{V600E}, has turned out to be an important driver of many melanomas, and recent drugs specifically targeting this mutant protein have considerably improved melanoma survival times [7, 8]. Two mutant BRAF inhibitors, vemurafenib and dabrafenib, have been approved by the US Food and Drug Administration (FDA) [9, 10], and they have shown about 50% response rates in BRAF mutant melanoma in the clinic [11]. Although these drugs have demonstrated clinical benefit, they have been associated with various side effects, such as skin rash, photosensitivity, cutaneous squamous cell carcinoma and keratoacanthoma, which can affect the patients' quality of life [12].

Another selective BRAF inhibitor, encorafenib (LGX818), is currently under evaluation in clinical (phase II) trials combined with the MEK inhibitor binimetinib in relapsed/refractory multiple myeloma with BRAF^{V600E} or BRAF^{V600K} mutations (NCT02834364). It is also investigated (phase III) in BRAF^{V600E}-mutated metastatic colon carcinoma patients, where it is given in combination with binimetinib plus EGFR inhibitor cetuximab (NCT02928224). Compared to vemurafenib and dabrafenib, encorafenib has unique biochemical properties with a longer dissociation half-life from its molecular target [13] and greater potency in preclinical models [14]. It can induce sustained activity of the mitogen-activated protein kinase (MAPK) pathway, leading to cell cycle arrest, it exhibits antiproliferative activity, and it induces senescence and autophagy in BRAF^{V600E} melanoma cells [15]. In some clinical trials, encorafenib was well tolerated, and showed signs of promising activity [7, 16, 17].

Membrane transporters can play important roles in pharmacokinetic pathways (drug absorption, distribution, metabolism, and excretion) [18]. Multispecific efflux transporters of the ATP binding cassette (ABC) superfamily can transport many structurally diverse endogenous and exogenous compounds. Especially P-glycoprotein (MDR1/ABCB1) and Breast Cancer Resistance Protein (BCRP/ABCG2) are important ABC efflux transporters [19, 20]. They are localized at apical membranes of liver, kidney and intestine, where they can pump their substrates into bile, urine, and feces, respectively, and at pharmacological sanctuary site barriers such as the blood-brain barrier (BBB) and blood-testis barrier, where they can pump their substrates back into blood. Consequently, they can reduce oral availability, enhance elimination, and limit tissue distribution of substrate drugs. Many anticancer drugs, including vemurafenib and dabrafenib, are transported substrates of ABCB1 and ABCG2 and consequently show a restricted brain penetration [21-23]. Their interaction with ABC transporters may limit the overall drug exposure and efficacy against tumor (micro-)metastases situated behind a functionally intact BBB.

Drug metabolism by multispecific drug-metabolizing enzymes of the cytochrome P450 (CYP) superfamily, can also have major pharmacokinetic effects. CYP3A is the most abundant subfamily expressed in several tissues, metabolizing many structurally diverse drugs, often reducing their oral availability, and sometimes forming active or toxic metabolites. CYP3A4 is highly expressed in human liver and small intestine, and it plays a significant role in the metabolism of approximately half the drugs in use recently [24, 25]. As CYP3A can display a high degree of inter- and intra-individual activity, it is a major player in variable drug exposure [26, 27].

Encorafenib, like vemurafenib and dabrafenib, is administered orally in the clinic. Thus, depending on its interaction with ABC transporters, these might have a significant impact on oral bioavailability and tissue or tumor distribution of encorafenib. In this study, we aimed to assess encorafenib transport by ABCB1 and ABCG2 *in vitro*, and to establish their individual and combined effects *in vivo* on oral availability and tissue distribution of encorafenib using wild-type and transporter knockout mouse strains. Moreover, as some active and main circulating metabolites of encorafenib are formed by Cyp3a enzymes, we also studied this drug in Cyp3a knockout mice.

2. Material and methods

2.1. Chemicals

Encorafenib and zosuquidar were obtained from Sequoia Research Products (Pangbourne, UK). Ko143 was from Tocris Bioscience (Bristol, UK). Bovine Serum Albumin (BSA) Fraction V was obtained from Roche Diagnostics (Mannheim, Germany). Glucose water 5% w/v was from B. Braun Medical Supplies (Melsungen, Germany). Isoflurane was purchased from Pharmachemie (Haarlem, The Netherlands), heparin (5000 IU ml-1) was from Leo Pharma (Breda, The Netherlands). Chemicals used in the encorafenib assay were described before [28]. All other chemicals and reagents were obtained from Sigma-Aldrich (Steinheim, Germany).

2.2. Transport Assays

Polarized Madin-Darby Canine idney (MDCK-II) cells stably transduced with human (h) ABCB1, hABCG2, or murine (m) Abcg2 were used in transport assays. Growth conditions were described previously [21]. Transepithelial transport was tested using 12-well Transwell® plates (Corning Inc., USA), as described previously [21]. Cells were seeded on the same day and at the same density (5 x 10^5 cells per well), and cultured for 3 days to allow formation of an intact monolayer. Monolayer tightness was assessed by measurement of transepithelial electrical resistance (TEER), using reference values that were previously established and well correlated to <1% transepithelial [^{14}C]inulin leakage per hour [21]. Where appropriate 5 μM zosuquidar (ABCB1 inhibitor) and/or 5 μM Ko143 (ABCG2/Abcg2 inhibitor) were used during the transport experiments, after pre-incubation with these inhibitors for 1 h in both compartments. The transport phase was started (t = 0) by replacing the medium in the apical or basolateral compartment with fresh DMEM including 10% FBS and encorafenib at 5 μM, as well as the appropriate inhibitor(s). Cells were kept at 37°C in 5% (v/v) CO_2 during the experiment, and 50 μl aliquots were taken from the acceptor compartment at 1, 2, 4 and 8 h, and stored at -30°C until LC-MS/MS measurement of the concentrations of encorafenib. Active transport was expressed using the transport ratio r, *i.e.*, the amount of apically directed drug transport divided by basolaterally directed drug translocation after 8 hours.

2.3. Animals

Mice were housed and handled according to institutional guidelines complying with Dutch and EU legislation. Animals used were WT, *Cyp3a*$^{-/-}$ [29], *Abcb1a/1b*$^{-/-}$ [30], *Abcg2*$^{-/-}$ [31] and *Abcb1a/1b;Abcg2*$^{-/-}$ [32] mice of a >99% FVB genetic background, between 9 and 14 weeks of age. Animals were kept in a temperature-controlled environment with a 12 h light/12 h dark cycle and received a standard diet (Transbreed, SDS Diets, Technilab − BMI) and acidified water *ad libitum*.

2.4. Drug Solutions

Encorafenib was administered to mice at a dose of 10 mg/kg, using a volume of 10 ml/kg body weight. For oral administration, encorafenib stock solution was prepared in DMSO at a concentration of 100 mg/ml, the working solution was 1 mg/ml. This working solution included 1% (v/v) DMSO, 1% (v/v) Tween 80/ethanol (1:1;v/v) and 98% glucose water (5%;w/v). For intravenous injection, encorafenib was initially dissolved in DMSO at a concentration of 25 mg/ml, whereas the working solution was 2 mg/ml. This i.v. working solution included 8% DMSO, 8% Tween 80/ethanol (1:1;v/v) and 84% glucose water (5%;w/v). All working solutions were prepared freshly on the day of the experiment.

2.5. Plasma pharmacokinetic experiments and tissue distribution

Oral encorafenib (10 mg/kg) was administered to the mice by oral gavage using a blunt-ended needle. In order to minimize the variation in absorption, mice were fasted for about 3 h before encorafenib was administered (n = 4-10). For the 8 h or 2 h experiments, multiple blood samples (about 50 μl) were collected from the tail vein at 15 min, 30 min, 1 h, 2 h and 4 h or 7.5 min, 15 min, 30 min and 1 h, respectively, using heparinized capillary tubes (Sarstedt, Germany). At 8 h or 2 h, mice were anesthetized with isoflurane and blood was collected by cardiac puncture. Mice were sacrificed by cervical dislocation immediately thereafter, and brain and a set of other organs were removed and rapidly frozen at −30˚C. Organs were homogenized on ice in 4% (w/v) BSA in water, and stored further at −30°C until analysis. Blood samples were centrifuged at 9,000 *g* for 6 min at 4°C immediately after collection, and the plasma fraction was collected and stored at −30°C until analysis. Unless indicated otherwise, brain concentration was corrected for the amount of drug still present in the brain vasculature (estimated at 0.8% of the total brain volume after cardiac puncture at the time point of collection).

2.6. LC-MS/MS analysis

Encorafenib concentrations in cell culture medium, plasma samples, and tissue homogenates were determined using a liquid chromatography-tandem mass spectrometric assay based on an existing method [28].

2.7. Pharmacokinetic calculations and statistical analysis

Pharmacokinetic parameters were calculated by non-compartmental methods using the software GraphPad Prism7 (GraphPad Software Inc., La Jolla, CA, USA). The area under the plasma concentration-time curve (AUC) was calculated using the trapezoidal rule with the Microsoft Excel plug in PKsolver [33]. The peak plasma concentration (C_{max}) and the time of the maximum plasma concentration (t_{max}) were estimated from the original data. Relative organ accumulation (P_{organ}) was calculated by dividing organ concentrations (C_{organ}) at either t = 2 h or t = 8 h by the $AUC_{0\text{-}2h}$ or $AUC_{0\text{-}8h}$, respectively. One-way analysis of variance (ANOVA) was used to determine significance of differences between groups, after which post-hoc tests with Tukey correction were performed for comparison between individual groups. When variances were not homogeneously distributed, data were log-transformed before statistical tests were applied. Differences were considered statistically significant when $P < 0.05$. Data are presented as mean ± SD.

3. Results

3.1. In vitro transport of encorafenib by ABCB1 and ABCG2

Encorafenib transport was tested using the polarized Madin-Darby Canine Kidney (MDCK-II) cell line and its subclones transduced with human ABCB1, human ABCG2, or murine Abcg2. In the MDCK-II parental line, the translocation of encorafenib (5 µM) in the apical direction was much higher than that in the basolateral direction, with a transport ratio (r) of 10.3 (Figure 1A). Treatment of these cells with the ABCB1 inhibitor zosuquidar (at 5 µM) resulted in a clear decrease in apically directed transport and a clear increase in basolaterally directed translocation (r = 1.3, Figure 1B). This suggests that encorafenib is a very good transport substrate of the endogenous canine ABCB1, known to be present at modest levels in the MDCK-II cells [21, 34, 35].

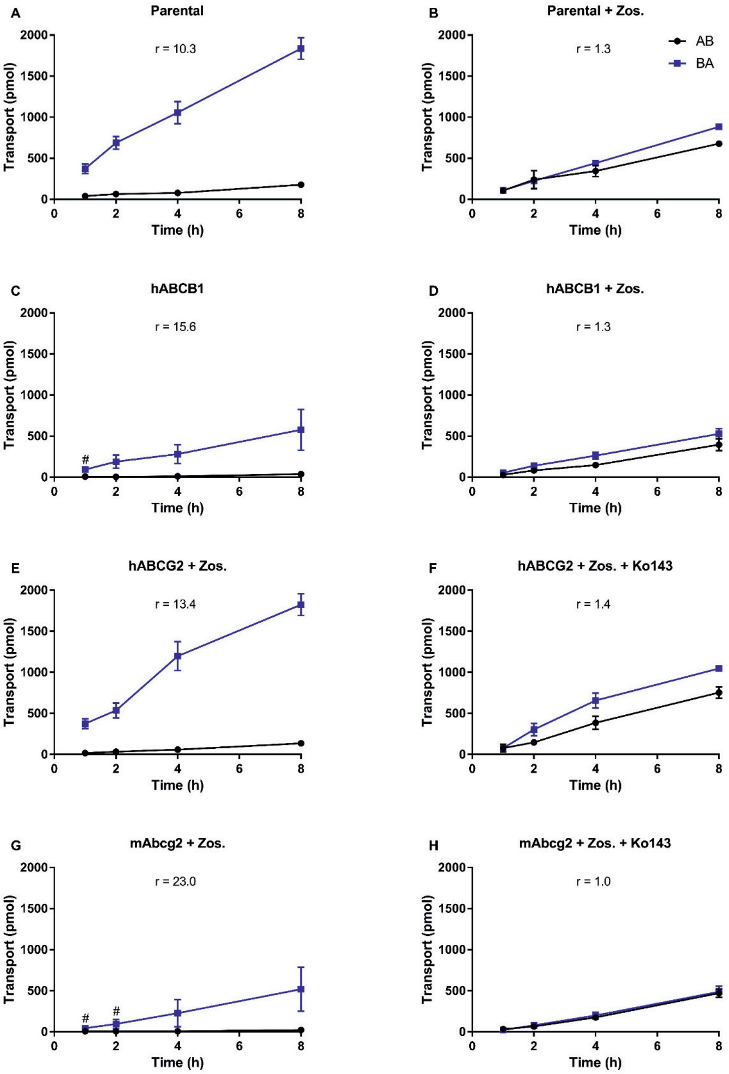

Figure 1. In vitro transport of encorafenib. Transepithelial transport of encorafenib (5 μM) was assessed in MDCK-II cells either nontransduced (A, B) or transduced with hABCB1 (C, D), hABCG2 (E, F) or mAbcg2 (G, H) cDNA. At t = 0 h, encorafenib was applied to the donor compartment and the concentrations in the acceptor compartment at t = 1, 2, 4 and 8 h were measured and plotted as total amount of transport (pmol) in the graphs (n = 3). B, D–H: Zos. (zosuquidar, 5 μM) and/or Ko143 (5 μM) were applied as indicated to inhibit ABCB1 and hABCG2 or mAbcg2, respectively. r, relative transport ratio. BA (■), translocation from the basolateral to the apical compartment; AB (●), translocation from the apical to the basolateral compartment. Points, mean; bars, SD. #: levels of encorafenib in AB translocation direction were < LLQ and therefore replaced with the LLQ value (~7 pmol).

In hABCB1-overexpressing MDCKII cells, there was an even more pronounced apically directed transport with r = 15.6 (Figure 1C), which was reduced to 1.3 (Figure 1D) by zosuquidar co-incubation. The further increase in transport ratio r from 10.3 in the parental MDCK-II cells to 15.6 in the MDCK-II-hABCB1 cells suggests that encorafenib is also a good hABCB1 transport substrate.

To suppress the high background transport of encorafenib by endogenous canine ABCB1, subsequent experiments on ABCG2 were done in the presence of zosuquidar (5 μM). In hABCG2-overexpressing MDCK-II cells, there was extensive apically directed transport of encorafenib with r = 13.4 (Figure 1E) and this could be strongly reduced with 5 μM of the ABCG2 inhibitor Ko143 (r = 1.4, Figure 1F). Net apically directed transport of encorafenib was most efficient in mAbcg2-overexpressing MDCK-II cells (r = 23.0, Figure 1G), and this transport was completely inhibited by Ko143 (r = 1.0, Figure 1H). These data indicate that encorafenib is a good to very good transport substrate of hABCG2 and mAbcg2.

3.2. Plasma exposure and brain accumulation of encorafenib after oral administration

We wanted to assess the *in vivo* impact of Abcb1 and Abcg2, as well as Cyp3a on encorafenib oral availability and tissue distribution. Since this drug is orally administered to patients at a dose of about 200 mg, mice received encorafenib by oral gavage into the stomach at a physiologically roughly equivalent dose of 10 mg/kg. We first performed a pilot study using female wild-type (WT), *Cyp3a*$^{-/-}$ and combination *Abcb1a/1b;Abcg2*$^{-/-}$ mice. Encorafenib was very rapidly absorbed in all strains, with a t_{max} at or before 15 min. Plasma levels were also very high, with a C_{max} of 9-25 μg/ml, among the highest we have seen at comparable oral dose levels for a range of targeted anticancer drugs. Plasma exposure of encorafenib over 8 h (AUC_{0-8}) was not significantly different between WT and *Abcb1a/1b;Abcg2*$^{-/-}$ mice, but *Cyp3a*$^{-/-}$ mice did show a significantly higher AUC_{0-8} than WT mice (Figure 2A; Supplemental Table 1). However, inter-individual variation was high, as we often observe shortly after oral drug administration.

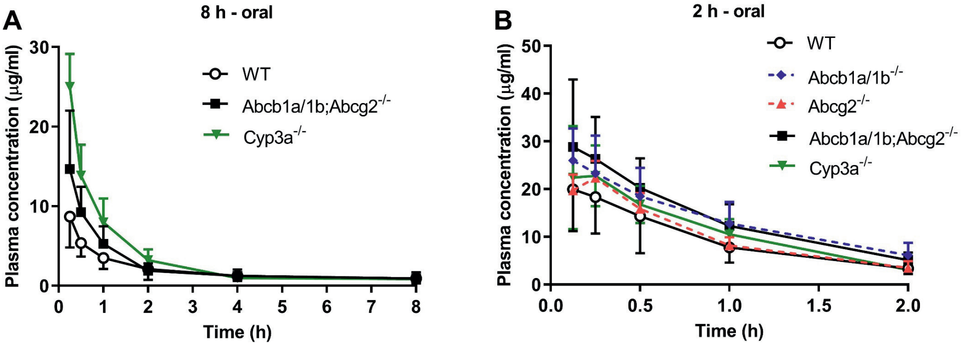

Figure 2. Plasma concentration-time curves of encorafenib in female mice after oral administration of 10 mg/kg encorafenib. Data are given as mean ± S.D. (n = 4-10).

We next measured brain, liver, kidney and spleen concentrations of encorafenib 8 h after oral administration in the WT, *Abcb1a/1b;Abcg2*$^{-/-}$ and *Cyp3a*$^{-/-}$ mice. Encorafenib concentrations in plasma of all strains hardly decreased between 4 and 8 h (Figure 2A, Supplemental Figure 1A), possibly suggesting slow release of this compound from one or more compartments in the body. We observed no significant differences in brain concentration, brain-to-plasma ratio, and brain accumulation of encorafenib between the three strains at 8 h (Supplemental Figures 2A-C). The same applied for encorafenib distribution to the liver, kidney, and spleen of these mouse strains (Supplemental Figure 3). The brain-to-plasma ratio of encorafenib was very low (in the order of 1-2%), indicating very low penetration of encorafenib into the brain at this time point, whereas tissue-to-plasma ratios in spleen, kidney and liver were substantially higher, in the order of 10-50% (Supplemental Figures 2 and 3).

To better assess the plasma concentration and the tissue distribution of encorafenib in a phase where active elimination was still ongoing, we subsequently tested females of the mouse strains over 2 h after oral administration. We also included single Abcb1a/1b and Abcg2 knockout strains to look at possible single and overlapping pharmacokinetic roles of these transporters. In this 2-h experiment, no significant differences were observed in the oral plasma AUC_{0-2} or C_{max} in all strains, even though there was a tendency for the AUC_{0-2} to be higher in the Abcb1a/1b, Abcb1a/1b;Abcg2, and Cyp3a knockout mice (Figure 2B; Table 1). Interindividual variation at these early time points was again high (Figure 2B), probably due to variable stomach emptying rates for this drug.

We next measured the impact of the transporters and Cyp3a on the brain concentration of encorafenib at 2 h after oral administration. Although plasma AUC curves up to 2 hours had revealed no significant differences between the mouse strains, the brain concentration was markedly increased in the combination *Abcb1a/1b;Abcg2*$^{-/-}$ mice compared to WT mice, and similar results were obtained for the brain-to-plasma ratio and brain accumulation ($P < 0.001$, Figures 3A-C; Table 1). No significant differences for these parameters were observed for the single Abcb1a/1b, Abcg2 and Cyp3a knockout strains compared to WT, respectively (Figures 3A-C; Table 1). As previously observed at 8 h, also at 2 h the brain-to-plasma distribution ratio of encorafenib was very low, ranging from about 0.4% to 1.5%, indicating very poor brain penetration of encorafenib. Qualitatively similar results were obtained without correcting for the blood vascular contribution to total brain encorafenib (Supplemental Figure 4).

We further analyzed the liver, kidney and spleen concentrations of encorafenib at 2 h after oral administration (Supplemental Figure 5). In contrast to the brain concentrations, we found no meaningful differences in tissue concentrations, tissue-to-plasma ratios, or tissue accumulation between the strains. Tissue to plasma distribution ratios were about 60%, 25%, and 8% for liver, kidney, and spleen, respectively (Supplemental Figures 5B, E, H), again far higher than observed for the brain.

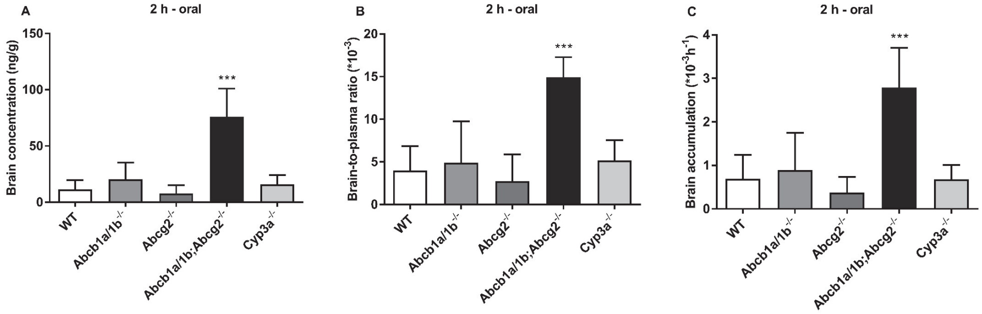

Figure 3. Brain concentration (A), brain-to-plasma ratio (B) and brain accumulation (C) of encorafenib in female WT, *Abcb1a/1b*$^{-/-}$, *Abcg2*$^{-/-}$, *Abcb1a/1b;Abcg2*$^{-/-}$ and *Cyp3a*$^{-/-}$ mice 2 h after oral administration of 10 mg/kg encorafenib (n = 4-8). *, $P < 0.05$; **, $P < 0.01$; ***, $P < 0.001$ compared to WT mice.

Table 1. Plasma pharmacokinetic parameters and brain concentration 2 h after oral administration of 10 mg/kg encorafenib to female WT, *Abcb1a/1b*$^{-/-}$, *Abcg2*$^{-/-}$, *Abcb1a/1b;Abcg2*$^{-/-}$ and *Cyp3a*$^{-/-}$ mice.

Parameter	Genotype				
	WT	*Abcb1a/1b*$^{-/-}$	*Abcg2*$^{-/-}$	*Abcb1a/1b;Abcg2*$^{-/-}$	*Cyp3a*$^{-/-}$
Plasma AUC_{0-2} (h*µg/ml)	18.8 ± 7.5	27.2 ± 7.9	20.5 ± 3.8	27.9 ± 7.6	22.8 ± 5.4
Fold change $AUC_{(0-2)}$	1.0	1.5	1.1	1.5	1.2
C_{max} (µg/ml)	20.5 ± 8.2	26.9 ± 5.6	22.4 ± 3.5	29.8 ± 13.7	24.4 ± 8.5
T_{max} (min)	7.5 - 15	7.5 - 15	15	7.5 - 30	7.5 - 15
C_{brain} (ng/g)	11.5 ± 8.1	20.4 ± 14.9	7.8 ± 7.3	75.9 ± 25.1 ***	15.9 ± 8.2
Fold change C_{brain}	1.0	1.8	0.7	6.6	1.4
Brain-to-plasma ratio (*10^{-3})	4.0 ± 2.9	4.9 ± 4.6	2.7 ± 3.2	14.9 ± 2.4 ***	5.2 ± 2.4
Fold change ratio	1.0	1.2	0.7	3.7	1.3
P_{brain} (*$10^{-3}h^{-1}$)	0.7 ± 0.6	0.9 ± 0.9	0.4 ± 0.4	2.8 ± 0.9 ***	0.7 ± 0.3
Fold change P_{brain}	1.0	1.3	0.6	4.0	1.0

Data are given as mean ± S.D. (n = 4-8). C_{max}, maximum concentration in plasma; T_{max}, time point (h) of maximum plasma concentration; C_{brain}, brain concentration; P_{brain}, brain accumulation. *, $P < 0.05$; **, $P < 0.01$; ***, $P < 0.001$ compared to WT mice.

3.3 Plasma exposure and brain accumulation of encorafenib after intravenous injection

Upon oral administration of encorafenib we observed only very low brain penetration of encorafenib which was enhanced, but still very low, by combined deficiency of Abcb1a/1b and Abcg2. To see whether this could be improved by exposure to initially much higher plasma levels of encorafenib, we also tested intravenous encorafenib pharmacokinetics in male WT, single Abcb1a/1b, single Abcg2, and combination Abcb1a/1b;Abcg2 knockout mice, at a dose of 10 mg/kg. Plasma exposure of encorafenib over 2 h (AUC_{0-2}) was increased by the combined absence of Abcb1a/1b and Abcg2 ($P < 0.001$, 1.5-fold) compared to WT mice, but not by the absence of Abcb1a/1b or Abcg2 alone (Figure 4; Table 2). At t = 2 h, the plasma concentrations in the *Abcb1a/1b;Abcg2$^{-/-}$* mice were also significantly higher than those in the other three strains (Figure 4B). The data suggest that mABCB1 and mABCG2 together may have some impact on the intravenous clearance of encorafenib.

The encorafenib brain concentration 2 h after i.v. injection showed no significant differences between the single *Abcb1a/1b$^{-/-}$* and *Abcg2$^{-/-}$* and WT mice, potentially due to the high variance especially in the *Abcb1a/1b$^{-/-}$* mice. However, in *Abcb1a/1b;Abcg2$^{-/-}$* mice, the brain concentration, brain-to-plasma ratio, and brain accumulation were markedly increased relative to WT mice (7- to 16-fold, $P < 0.001$), as well as relative to single *Abcb1a/1b$^{-/-}$* and *Abcg2$^{-/-}$* mice (Figures 5A-C; Table 2). Upon log transformation of the data in view of the high variance, also the brain concentration, brain-to-plasma ratio, and brain accumulation in the *Abcb1a/1b$^{-/-}$* mice were significantly increased (3- to 4-fold, $P < 0.01$) relative to WT mice (Supplemental Figure 6). Again, qualitatively similar results were obtained without correcting for the blood vascular contribution to total brain encorafenib (Supplemental Figure 7). The data suggest that Abcb1a/b and Abcg2 together restrict the accumulation of encorafenib into the brain, and that Abcb1a/1b can take over the Abcg2 function at the BBB when Abcg2 is absent. Under these higher (i.v.) plasma exposure conditions, deficiency of Abcb1a/1b alone does result in significantly increased brain concentrations of encorafenib. This might indicate that Abcg2 located in the BBB approaches saturation under these conditions. Still, qualitatively the intravenous brain accumulation data (Figure 5) are well in line with the oral data (Figure 3). Although the brain-to-plasma distribution ratios were slightly increased in the intravenous experiment (0.4-2.8%) relative to the oral experiment (0.4-1.5%), the brain concentrations of encorafenib were still very low (~5-100 ng/g), and not substantially higher than in the oral experiment.

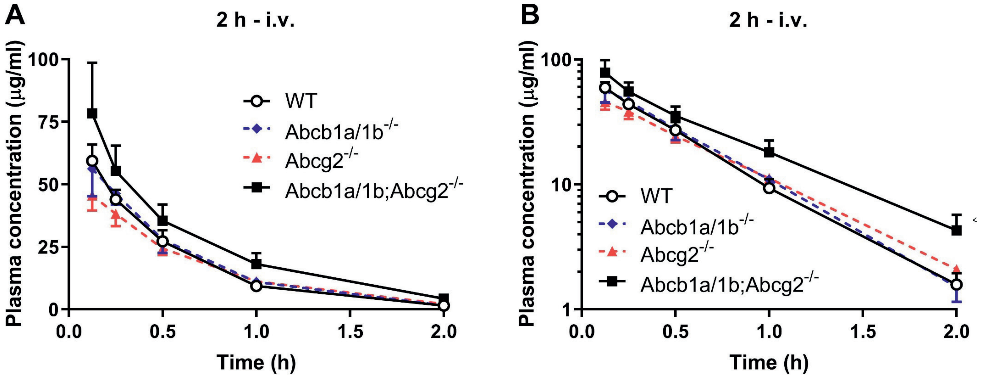

Figure 4. Plasma concentration-time curves of encorafenib in male WT, *Abcb1a/1b$^{-/-}$*, *Abcg2$^{-/-}$* and *Abcb1a/1b;Abcg2$^{-/-}$* mice after intravenous injection of 10 mg/kg encorafenib. Data are given as mean ± S.D. (n = 4-8).

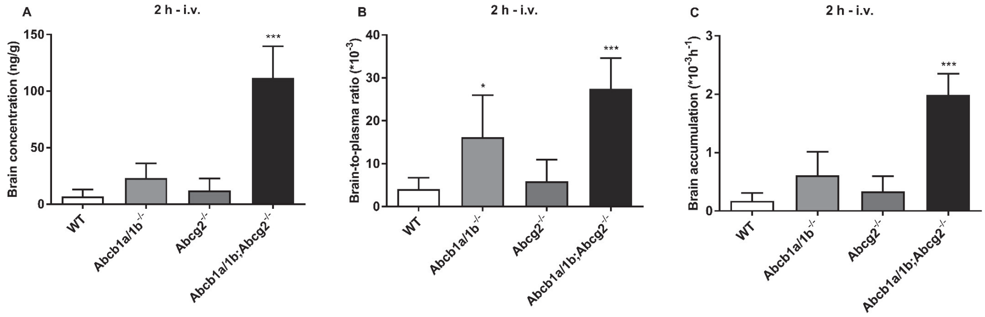

Figure 5. Brain concentration (A), brain-to-plasma ratio (B) and brain accumulation (C) of encorafenib in male WT, *Abcb1a/1b*$^{-/-}$, *Abcg2*$^{-/-}$ and *Abcb1a/1b;Abcg2*$^{-/-}$ mice 2 h after intravenous injection of 10 mg/kg (n = 4-8). *, $P < 0.05$; **, $P < 0.01$; ***, $P < 0.001$ compared to WT mice.

Table 2. Plasma pharmacokinetic parameters and brain and testis concentration 2 h after intravenous injection of 10 mg/kg encorafenib to male WT, *Abcb1a/1b*$^{-/-}$, *Abcg2*$^{-/-}$ and *Abcb1a/1b;Abcg2*$^{-/-}$ mice.

Parameter	Genotype			
	WT	*Abcb1a/1b*$^{-/-}$	*Abcg2*$^{-/-}$	*Abcb1a/1b;Abcg2*$^{-/-}$
Plasma AUC_{0-2} (h*µg/ml)	38.7 ± 3.9	39.6 ± 6.1	34.9 ± 4.2	56.6 ± 11.3 ***
Fold change $AUC_{(0-2)}$	1.0	1.0	0.9	1.5
C_{max} (µg/ml)	59.4 ± 6.4	58.1 ± 7.6	45.6 ± 6.0	78.4 ± 2.0 *
T_{max} (min)	7.5	7.5 - 15	7.5	7.5
C_{brain} (ng/g)	6.9 ± 6.0	23.2 ± 12.9	12.2 ± 10.5	111.7 ± 27.9 ***
Fold change C_{brain}	1.0	3.4	1.8	16.1
Brain-to-plasma ratio ($*10^{-3}$)	4.1 ± 2.7	16.1 ± 9.8 *	5.9 ± 5.0	27.5 ± 7.1 ***
Fold change ratio	1.0	4.0	1.5	6.8
P_{brain} ($*10^{-3}h^{-1}$)	0.2 ± 0.1	0.6 ± 0.4	0.3 ± 0.3	2.0 ± 0.4 ***
Fold change P_{brain}	1.0	3.6	2.0	11.7
C_{testis} (ng/g)	550.8 ± 83.7	701.8 ± 170.8	614.0 ± 124.5	1373.0 ± 267.9 ***
Fold change C_{testis}	1.0	1.3	1.1	2.5
Testis-to-plasma ratio ($*10^{-3}$)	344.9 ± 82.2	468.7 ± 74.3 *	295.0 ± 18.5	399.2 ± 53.5
Fold change ratio	1.0	1.4	0.9	1.2
P_{testis} ($*10^{-3}h^{-1}$)	14.1 ± 0.7	17.6 ± 1.8	17.7 ± 3.0	26.9 ± 8.8 **
Fold change P_{testis}	1.0	1.3	1.3	1.9

Data are given as mean ± S.D. (n = 4-8). C_{max}, maximum concentration in plasma; T_{max} , time point (h) of maximum plasma concentration; C_{brain}, brain concentration; P_{brain}, brain accumulation. *, $P < 0.05$; **, $P < 0.01$; ***, $P < 0.001$ compared to WT mice.

Abcb1 and Abcg2 often play protective roles at the blood-testis barrier (BTB) just as at the BBB, therefore we additionally measured the testis encorafenib concentrations at 2 h after intravenous injection. The testis concentration was significantly increased in *Abcb1a/1b;Abcg2*$^{-/-}$ mice compared to WT mice (~2.5-fold, $P < 0.001$), but after correction for the plasma levels, no significant differences were found (Supplemental Figures 8 A and B; Table 2). Overall, it seems unlikely that these transporters play a marked role in keeping encorafenib out of the testis. Moreover, encorafenib concentrations in testis were far higher than those in brain, with testis-to-plasma distribution ratios of 30% to 47% in the various strains.

Liver, kidney, and spleen appeared to equilibrate fairly efficiently with plasma levels of encorafenib after intravenous administration, with very similar tissue-to-plasma ratios between the different strains (Supplemental Figures 9B, E, H). Tissue-to-plasma distribution ratios were also very similar to those seen after oral encorafenib administration, with 60%, 25%, and 10% for liver, kidney, and spleen, respectively.

3.4. Effect of ABC transporters on encorafenib concentrations in small intestine

The plasma levels of encorafenib in the different strains after intravenous administration (Figure 4A) suggested that Abcb1a/1b and/or Abcg2 might play a role in the plasma elimination of encorafenib. A semi-log plot of the plasma concentrations indeed revealed a somewhat reduced elimination rate of encorafenib in the *Abcb1a/1b;Abcg2*$^{-/-}$ mice relative to the three other tested strains after 0.5 h (Figure 4B). This might in part be explained by active excretion of encorafenib by these transporters from the liver into bile (hepatobiliary excretion), or directly from the blood into the intestinal lumen (direct intestinal excretion). Both processes would increase the amount of drug ending up in the small intestinal lumen. We therefore also examined the amount of encorafenib in the tissue and contents of the small intestine, 2 h after intravenous administration. Although the interindividual variation was high, necessitating log-transformation of the data for proper analysis, the small intestinal tissue concentration, tissue-to-plasma ratio, and tissue accumulation of encorafenib were nearly all significantly lower in the *Abcb1a/1b*$^{-/-}$ and *Abcb1a/1b;Abcg2*$^{-/-}$ mice than in the WT and *Abcg2*$^{-/-}$ mice (Supplemental Figure 10; Supplemental Table 2). Accordingly, when the percentage of dose of encorafenib retrieved from the intestinal contents was measured, it was on average more than 10-fold lower in the *Abcb1a/1b*$^{-/-}$ and *Abcb1a/1b;Abcg2*$^{-/-}$ mice compared to the WT and *Abcg2*$^{-/-}$ mice, whether expressed as percentage of dose, percentage of dose-to-plasma ratio, or percentage of dose accumulation (Figures 6A-C; Supplemental Table 2). These results suggest that Abcb1a/1b plays a significant role in either directly or indirectly excreting encorafenib towards the lumen of the small intestine, or keeping it in the intestinal lumen once it is there, or both. The values for the single *Abcg2*$^{-/-}$ mice were not significantly different from the WT values, suggesting no substantial role for Abcg2 in these processes.

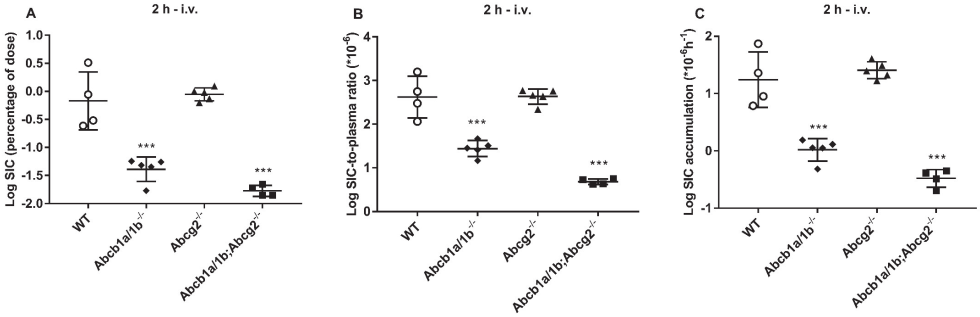

Figure 6. Log-transformed small intestinal contents (SIC) percentage of dose (A), log-transformed percentage of dose-to-plasma ratio (B) and log-transformed percentage of dose accumulation (C) of encorafenib in male WT, *Abcb1a/1b*$^{-/-}$, *Abcg2*$^{-/-}$ and *Abcb1a/1b;Abcg2*$^{-/-}$ mice 2 h after intravenous injection of 10 mg/kg (n = 4-5). A: Drug percentage of dose in SIC, which was expressed as total drug (ng) in SIC divided by total drug administrated to mouse (ng). B, expressed as A divided by last time point plasma concentration. C, expressed as A divided by AUC$_{0\text{-}2\text{ h}}$. *, $P < 0.05$; **, $P < 0.01$; ***, $P < 0.001$ compared to WT mice.

3.5. Oral availability of encorafenib

Because encorafenib was orally and intravenously administered to mice at the same dosage, 10 mg/kg, we used the oral and i.v. AUC$_{0\text{-}2}$ to estimate the oral bioavailability of encorafenib in the different mouse strains (Supplemental Figure 11). Although female mice were analyzed in the oral experiment, and male mice in the i.v. experiment, the data do suggest that the oral bioavailability of encorafenib was high (49-69%), and not markedly different between the analyzed mouse strains.

4. Discussion

We found that encorafenib is efficiently transported *in vitro* by canine and human ABCB1 and by human ABCG2 and mouse Abcg2, and that this transport can be virtually completely inhibited with the ABCB1 or ABCG2 inhibitors zosuquidar and Ko143, respectively. Upon oral administration to mice, encorafenib was very rapidly absorbed, with a t$_{max}$ occurring at or before 7.5-15 min, and yielding very high plasma levels. Variation in initial plasma concentrations was high, yielding significantly increased plasma AUCs in *Cyp3a*$^{-/-}$ mice in an 8 h, but not in a 2 h experiment. Plasma AUCs were not significantly altered after oral administration of encorafenib to Abcb1 or Abcg2 single or combination knockout strains, but upon intravenous administration combination *Abcb1a/1b;Abcg2*$^{-/-}$ mice did show a modestly higher plasma AUC and reduced elimination rate compared to wild-type and single transporter knockout mice. As expected for a well-transported Abcb1 and Abcg2 substrate, brain levels of encorafenib were substantially increased in *Abcb1a/1b;Abcg2*$^{-/-}$ mice, and under some circumstances also *Abcb1a/1b*$^{-/-}$ mice. However, absolute brain concentrations of encorafenib remained extremely low, even in *Abcb1a/1b;Abcg2*$^{-/-}$ mice, also considering the very high plasma concentrations of this drug.

Very little literature is available on the possible interaction of encorafenib with CYP3A. Our pilot experiments on oral encorafenib in *Cyp3a*$^{-/-}$ mice suggest there may be at most a modest limiting effect of mouse Cyp3a on encorafenib oral availability (Figure 2; Supplemental Figure 1), with otherwise no significant effects on relative tissue distribution of the drug (Supplemental Figures 2-5). However, as we cannot exclude that mouse Cyp2c enzymes, which are compensatorily upregulated in *Cyp3a*$^{-/-}$ mice [36], may also metabolize encorafenib, it could still be that there is a more pronounced impact of CYP3A on encorafenib pharmacokinetics than suggested by our pilot experiments.

There is a clear impact of the Abcb1a/1b and Abcg2 transporters on the brain accumulation, and possibly the plasma levels and elimination of encorafenib in mice. After both oral and intravenous administration, effective brain levels of encorafenib are significantly increased in the combination *Abcb1a/1b;Abcg2*$^{-/-}$ mice, and upon intravenous administration also in single *Abcb1a/1b*$^{-/-}$ mice (Figures 3 and 5). Collectively, the data indicate that both Abcb1a/1b and Abcg2 are involved in restricting the net accumulation of encorafenib into the brain, with likely a somewhat more pronounced effect of Abcb1a/1b (Figure 5B; Supplemental Figure 6B). Still, especially after oral administration, both transporters appear to be able to largely take over each other's functions at the BBB. Qualitatively, this ABC transporter-drug interaction behavior at the BBB is similar to that seen for a number of other targeted anticancer drugs, including the BRAF^{V600E} inhibitor vemurafenib [21, 23], and can be readily explained by published pharmacokinetic models [37, 38]. One could therefore consider to try and improve the brain accumulation of encorafenib by co-administration of a strong ABCB1 and ABCG2 inhibitor, such as elacridar, as was previously demonstrated in mice for vemurafenib [21]. Theoretically, this might help to enhance drug exposure for tumors that are positioned in part or in whole behind the BBB, and thus possibly improve therapeutic efficacy. However, the effective brain concentration of encorafenib in mice, even in *Abcb1a/1b;Abcg2*$^{-/-}$ mice, is strikingly low, with brain-to-plasma ratios of only 0.4-2.8% in WT and transporter knockout mice. This compares to 2-40% for vemurafenib [21], and 5-25% for the BRAF^{V600E} inhibitor dabrafenib [22]. This suggests that encorafenib has an intrinsically very low ability to accumulate into the mouse brain. If this would also apply to the human brain, this might perhaps turn out to be a limitation for encorafenib in targeting malignancies positioned behind a functional BBB. Since a substantial fraction of melanoma patients develop brain metastases, this could be a matter of possible concern in the clinical use of encorafenib.

Although somewhat higher, the oral AUC_{0-8} and AUC_{0-2} in *Abcb1a/1b;Abcg2*$^{-/-}$ mice were not significantly different from those in WT mice (Figures 2A and B; Table 1 and Supplemental Table 1). This suggests that there is only a very limited effect of these transporters on restricting the oral availability of encorafenib. Interestingly, there is a striking contrast between the efficiency with which encorafenib is taken up across the intestinal wall (very fast, and to very high plasma concentrations), and its extremely poor uptake into the brain (Figures 2 and 3, Supplemental Figure 2). Although the lipid composition of enterocyte and brain endothelial cell luminal membranes is different, it is hard to see how such profound differences in membrane permeation could be caused merely by differences in passive diffusion characteristics of encorafenib between the two membranes. It therefore seems more likely that there are important differences in transmembrane uptake transporters for encorafenib between the two membranes. For instance, there might be one or more efficient uptake transporters for encorafenib in the enterocytes, which are mostly or completely absent from the BBB. The molecular nature of possible intestinal uptake transporters for encorafenib remains a mystery, as in fact is the case for many rapidly absorbed oral drugs. Some research groups have suggested that OATP2B1 might be a candidate broad-specificity intestinal drug uptake transporter [39], but direct experimental evidence for that is scarce, and often based on inhibition experiments with fruit juices of complex and poorly defined composition. Definitive identification of intestinal drug uptake transporters will obviously be of great interest, but falls outside the scope of this study. In any case, a high uptake capacity for encorafenib across the intestinal wall also helps to explain the low impact of Abcb1a/1b and Abcg2 on encorafenib oral availability: a very high intestinal uptake rate will easily overwhelm any more limited efflux capacity. Conversely, the very low uptake rate of encorafenib into the brain makes it much easier for Abcb1a/1b and Abcg2 to have a substantial impact on the net brain accumulation of encorafenib.

After intravenous administration, the *Abcb1a/1b;Abcg2*$^{-/-}$ mice demonstrated a modestly reduced elimination rate of encorafenib, and an increased AUC_{0-2} compared to WT mice (Figures 4A and B, Table 2). This suggests a modest role of ABCB1 and/or ABCG2 in the elimination of encorafenib, which was supported by markedly decreased levels of the drug recovered from the small intestinal contents of *Abcb1a/1b;Abcg2*$^{-/-}$ as well as *Abcb1a/1b*$^{-/-}$ mice 2 h after drug administration. Although the intestinal contents in *Abcg2*$^{-/-}$ mice were not decreased relative to WT values, the levels recovered in *Abcb1a/1b;Abcg2*$^{-/-}$ mice were consistently lower than those found in the *Abcb1a/1b*$^{-/-}$ mice (Figure 6). Collectively, the data indicate that Abcb1a/1b, and to a smaller extent Abcg2, contribute to the excretion of encorafenib into the intestinal lumen, most likely by mediating hepatobiliary and/or direct intestinal excretion. It is worth noting that at the 2 h time point only about 1% of the encorafenib dose was recovered from the small intestinal contents of the WT mice. These comparatively low values are in line with the modest effect of Abcb1a/1b and Abcg2 on encorafenib plasma elimination (Figure 4B).

For many drugs, Abcb1a/1b and Abcg2 show similar functions at the BBB as at the blood-testis-barrier (BTB) [37]. However, encorafenib accumulation in testis was far higher than that in the brain (tissue-to-plasma ratio of 30-47% instead of 0.4-2.8%), and there was no substantial effect of the ABC transporters on testis accumulation of the drug (Supplemental Figure 8). Possibly, there are also relatively efficient uptake transporters for encorafenib in testis, which would overwhelm any protective efflux effect of the ABC transporters at the BTB.

The encorafenib tissue distribution in other major organs tested (liver, kidney, spleen) generally followed the plasma concentrations of encorafenib, both after oral and i.v. administration among all the strains tested. In fact, tissue-to-plasma ratios in these organs were remarkably similar also under the different circumstances (oral 2 and 8 h, i.v. 2 h), with values for liver around 60%, for kidney around 25%, and for spleen around 8%. This suggests that in these organs Abcb1a/1b and Abcg2, and, for the oral administration, Cyp3a do not have a marked impact on the tissue concentrations of encorafenib, separate from their effect on encorafenib plasma concentrations.

The result that we obtained with the estimation of oral bioavailability of encorafenib in mice suggests that this is quite good, with values around or above 50% (Supplemental figure 11). This specific finding seems also compatible with the highly efficient intestinal uptake of encorafenib. If this result is replicated in humans, this would present a relatively favorable situation for the clinical application of this anticancer drug.

5. Conclusion

Our data indicate that both Abcb1a/1b and Abcg2 are involved in restricting the net accumulation of encorafenib in the brain. The strikingly low brain concentration of encorafenib, even in the absence of Abcb1a/1b and Abcg2, suggests that encorafenib may not have optimal access to malignancies positioned behind a functional blood-brain barrier. It will be important to assess whether this also applies in humans. On the other hand, the high oral bioavailability of encorafenib, if replicated in humans, would present a relatively favorable situation for the clinical application of this anticancer drug.

6. References

1. Siegel, R.L., K.D. Miller, and A. Jemal, Cancer statistics, 2016. CA: a cancer journal for clinicians, 2016. 66(1): p. 7-30.
2. Johnson, J. and B. Young, Demographics of brain metastasis. Neurosurgery clinics of North America, 1996. 7(3): p. 337-344.
3. Lee, S.M., D.C. Betticher, and N. Thatcher, Melanoma: chemotherapy. British medical bulletin, 1995. 51(3): p. 609-630.
4. Patel, J., et al., Metastatic pattern of malignant melanoma: a study of 216 autopsy cases. The American Journal of Surgery, 1978. 135(6): p. 807-810.
5. De la Monte, S., G.W. Moore, and G.M. Hutchins, Patterned distribution of metastases from malignant melanoma in humans. Cancer research, 1983. 43(7): p. 3427-3433.
6. Fife, K., et al., Determinants of outcome in melanoma patients with cerebral metastases. Journal of clinical oncology, 2004. 22(7): p. 1293-1300.
7. Delord, J.-P., et al., Phase I Dose-Escalation and-Expansion Study of the BRAF Inhibitor Encorafenib (LGX818) in Metastatic BRAF-Mutant Melanoma. Clinical Cancer Research, 2017: p. clincanres. 2923.2016.
8. Larkin, J., et al., Combined vemurafenib and cobimetinib in BRAF-mutated melanoma. New England Journal of Medicine, 2014. 371(20): p. 1867-1876.
9. Ascierto, P.A., et al., Phase II trial (BREAK-2) of the BRAF inhibitor dabrafenib (GSK2118436) in patients with metastatic melanoma. Journal of clinical oncology, 2013. 31(26): p. 3205-3211.
10. Chapman, P.B., et al., Improved survival with vemurafenib in melanoma with BRAF V600E mutation. New England Journal of Medicine, 2011. 364(26): p. 2507-2516.
11. Jang, S. and M. Atkins, Treatment of BRAF-mutant melanoma: the role of vemurafenib and other therapies. Clinical Pharmacology & Therapeutics, 2014. 95(1): p. 24-31.
12. Gençler, B. and M. Gönül, Cutaneous side effects of BRAF inhibitors in advanced melanoma: review of the literature. Dermatology research and practice, 2016. 2016.
13. Dummer, R., et al., Initial results from a phase I, open-label, dose escalation study of the oral BRAF inhibitor LGX818 in patients with BRAF V600 mutant advanced or metastatic melanoma. 2013, American Society of Clinical Oncology.
14. Stuart, D.D., et al., Preclinical profile of LGX818: A potent and selective RAF kinase inhibitor. 2012, AACR. p. Abstract 3790.
15. Li, Z., et al., Encorafenib (LGX818), a potent BRAF inhibitor, induces senescence accompanied by autophagy in BRAFV600E melanoma cells. Cancer letters, 2016. 370(2): p. 332-344.
16. Dummer, R., et al. Results of COLUMBUS Part 1: a phase 3 trial of encorafenib (ENCO) plus binimetinib (BINI) versus vemurafenib (VEM) or ENCO in BRAF-mutant melanoma. in Society for Melanoma Research annual meeting. 2016.
17. van Geel, R.M., et al., A phase Ib dose-escalation study of encorafenib and cetuximab with or without alpelisib in metastatic BRAF-mutant colorectal cancer. Cancer Discovery, 2017. 7(6): p. 610-619.
18. Szakacs, G., et al., The role of ABC transporters in drug absorption, distribution, metabolism, excretion and toxicity (ADME–Tox). Drug discovery today, 2008. 13(9): p. 379-393.
19. Borst, P. and R.O. Elferink, Mammalian ABC transporters in health and disease. Annual review of biochemistry, 2002. 71(1): p. 537-592.
20. Schinkel, A.H. and J.W. Jonker, Mammalian drug efflux transporters of the ATP binding cassette (ABC) family: an overview. Advanced drug delivery reviews, 2003. 55(1): p. 3-29.
21. Durmus, S., et al., Oral availability and brain penetration of the B-RAFV600E inhibitor vemurafenib can be enhanced by the P-GLYCOprotein (ABCB1) and breast cancer resistance protein (ABCG2) inhibitor elacridar. Molecular pharmaceutics, 2012. 9(11): p. 3236-3245.
22. Mittapalli, R.K., et al., Mechanisms limiting distribution of the threonine-protein kinase B-RaFV600E inhibitor dabrafenib to the brain: implications for the treatment of melanoma brain metastases. Journal of Pharmacology and Experimental Therapeutics, 2013. 344(3): p. 655-664.
23. Mittapalli, R.K., et al., Impact of P-glycoprotein (ABCB1) and breast cancer resistance protein (ABCG2) on the brain distribution of a novel BRAF inhibitor: vemurafenib (PLX4032). Journal of Pharmacology and Experimental Therapeutics, 2012. 342(1): p. 33-40.

24. Guengerich, F.P., Human cytochrome P450 enzymes, in Cytochrome P450. 1995, Springer. p. 473-535.
25. Zanger, U.M. and M. Schwab, Cytochrome P450 enzymes in drug metabolism: regulation of gene expression, enzyme activities, and impact of genetic variation. Pharmacology & therapeutics, 2013. 138(1): p. 103-141.
26. van Waterschoot, R.A., et al., Intestinal cytochrome P450 3A plays an important role in the regulation of detoxifying systems in the liver. The FASEB Journal, 2009. 23(1): p. 224-231.
27. van Hoppe, S., et al., Breast cancer resistance protein (BCRP/ABCG2) and P-glycoprotein (P-gp/ABCB1) transport afatinib and restrict its oral availability and brain accumulation. Pharmacological research, 2017. 120: p. 43-50.
28. Sparidans, R.W., et al., Liquid chromatography tandem mass spectrometric assay for therapeutic drug monitoring of the B-Raf inhibitor encorafenib, the EGFR inhibitors afatinib, erlotinib and gefitinib and the O desmethyl metabolites of erlotinib and gefitinib in human plasma. Journal of Chromatography B, 2016. 1033: p. 390-398.
29. van Waterschoot, R.A., et al., Absence of both cytochrome P450 3A and P-glycoprotein dramatically increases docetaxel oral bioavailability and risk of intestinal toxicity. Cancer research, 2009. 69(23): p. 8996-9002.
30. Schinkel, A.H., et al., Normal viability and altered pharmacokinetics in mice lacking mdr1-type (drug-transporting) P-glycoproteins. Proceedings of the National Academy of Sciences, 1997. 94(8): p. 4028-4033.
31. Jonker, J.W., et al., The breast cancer resistance protein protects against a major chlorophyll-derived dietary phototoxin and protoporphyria. Proceedings of the National Academy of Sciences, 2002. 99(24): p. 15649-15654.
32. Jonker, J.W., et al., The breast cancer resistance protein BCRP (ABCG2) concentrates drugs and carcinogenic xenotoxins into milk. Nature medicine, 2005. 11(2): p. 127-129.
33. Zhang, Y., et al., PKSolver: An add-in program for pharmacokinetic and pharmacodynamic data analysis in Microsoft Excel. Computer methods and programs in biomedicine, 2010. 99(3): p. 306-314.
34. Durmus, S., et al., P-glycoprotein (MDR1/ABCB1) and breast cancer resistance protein (BCRP/ABCG2) restrict brain accumulation of the JAK1/2 inhibitor, CYT387. Pharmacological research, 2013. 76: p. 9-16.
35. Durmus, S., et al., Breast cancer resistance protein (BCRP/ABCG2) and P-glycoprotein (P-GP/ABCB1) restrict oral availability and brain accumulation of the PARP inhibitor rucaparib (AG-014699). Pharmaceutical research, 2015. 32(1): p. 37-46.
36. van Waterschoot, R.A., et al., Midazolam metabolism in cytochrome P450 3A knockout mice can be attributed to up-regulated CYP2C enzymes. Molecular pharmacology, 2008. 73(3): p. 1029-1036.
37. Kodaira, H., et al., Kinetic analysis of the cooperation of P-glycoprotein (P-gp/Abcb1) and breast cancer resistance protein (Bcrp/Abcg2) in limiting the brain and testis penetration of erlotinib, flavopiridol, and mitoxantrone. Journal of Pharmacology and Experimental Therapeutics, 2010. 333(3): p. 788-796.
38. Kalvass, J.C. and G.M. Pollack, Kinetic considerations for the quantitative assessment of efflux activity and inhibition: implications for understanding and predicting the effects of efflux inhibition. Pharmaceutical research, 2007. 24(2): p. 265-276.
39. Tamai, I. and T. Nakanishi, OATP transporter-mediated drug absorption and interaction. Current opinion in pharmacology, 2013. 13(6): p. 859-863.

7. Supplemental materials

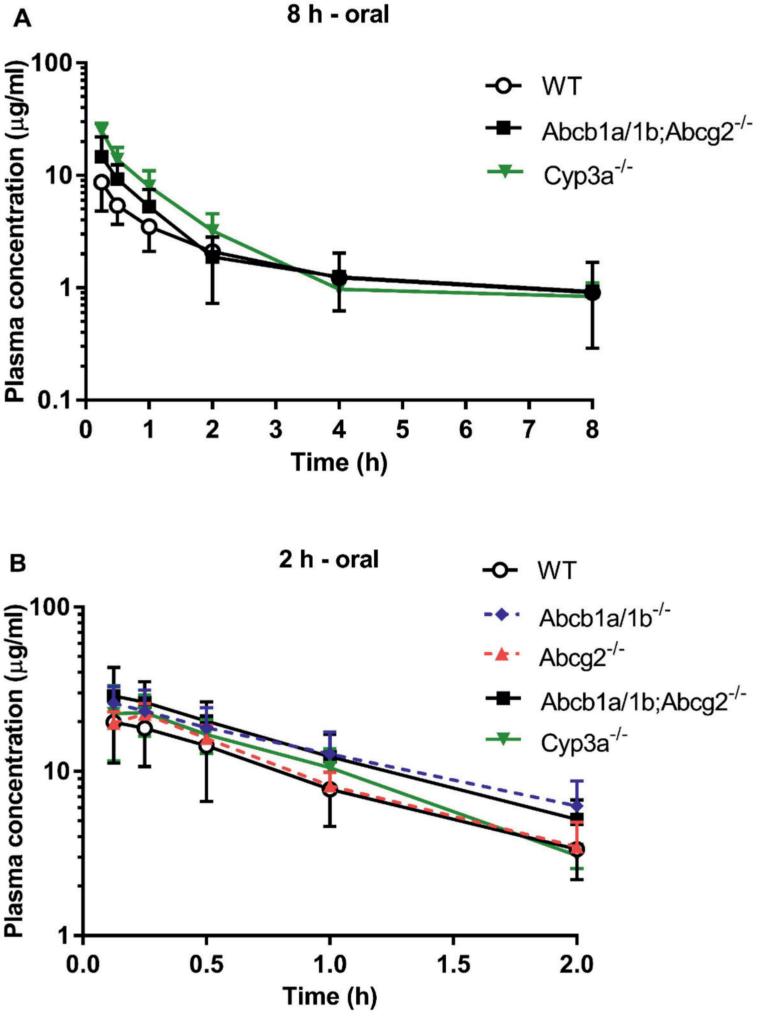

Supplemental Figure 1. Semi-log plots of plasma concentration-time curves of encorafenib in female mice after oral administration of 10 mg/kg encorafenib. A, 8-hour experiment; B, 2-hour experiment. Data are given as mean ± S.D. (n = 4-10).

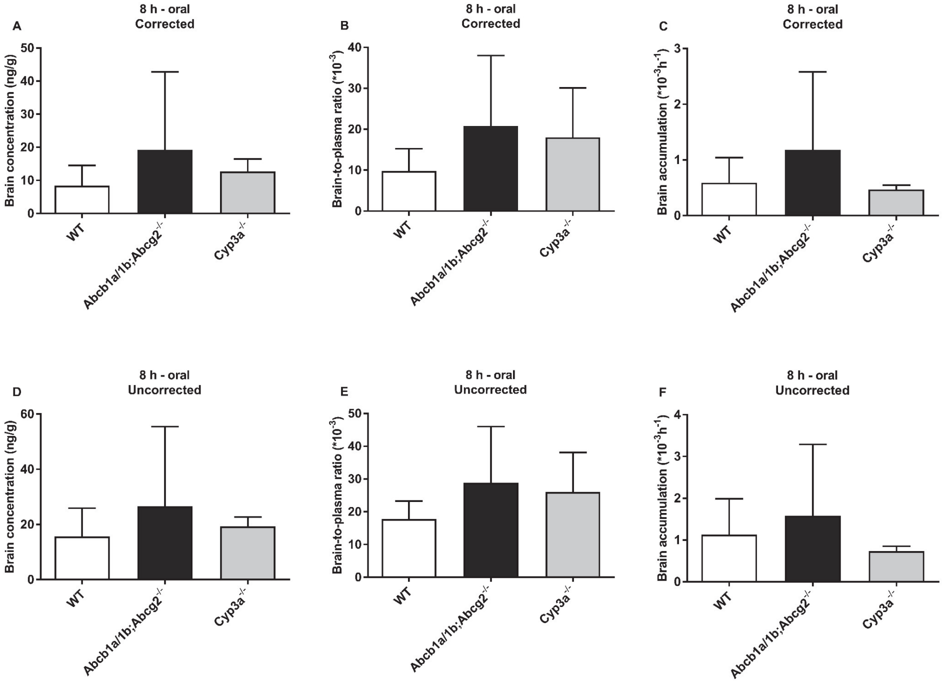

Supplemental Figure 2. Corrected and uncorrected brain concentration (A, D), brain-to-plasma ratio (B, E) and brain accumulation (C, F) of encorafenib in female WT, *Cyp3a*$^{-/-}$ and *Abcb1a/1b;Abcg2*$^{-/-}$ mice 8 h after oral administration of 10 mg/kg encorafenib (n = 4-10). Corrected: brain concentration was corrected for the amount of drug still present in the brain vasculature. Uncorrected: brain concentration was not corrected for the amount of drug still present in the brain vasculature.

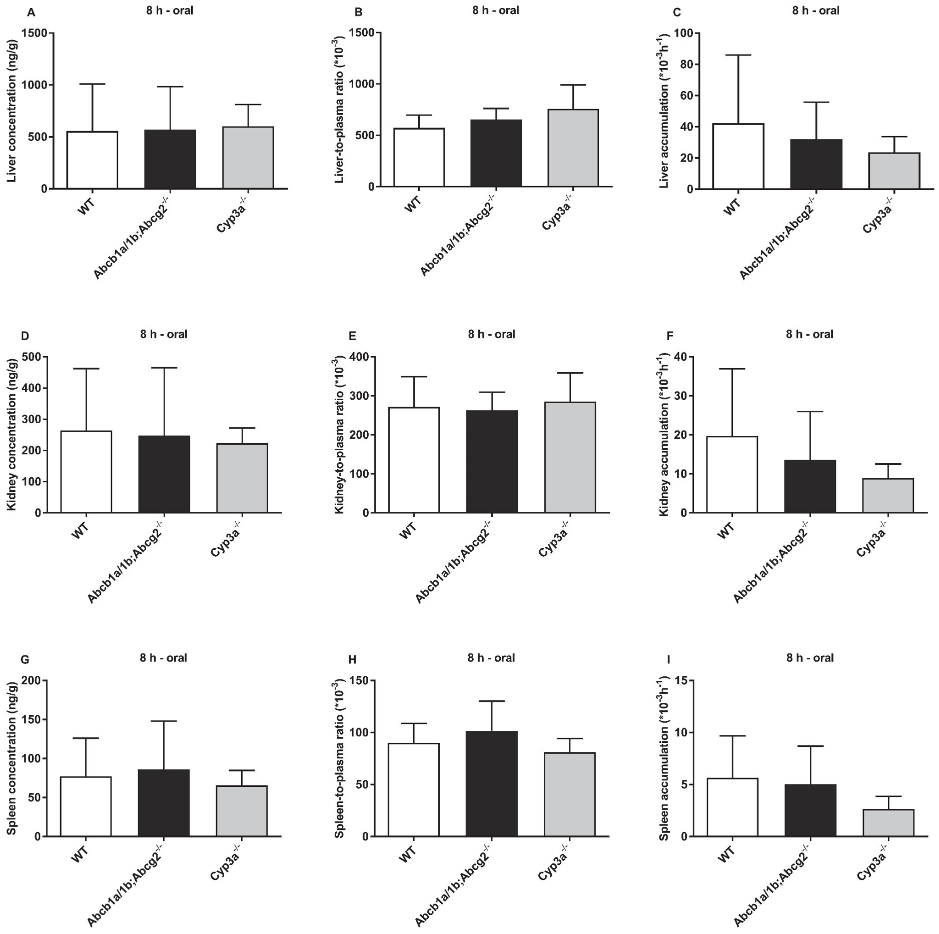

Supplemental Figure 3. Organ concentration (A, D, G), organ-to-plasma ratio (B, E, H) and organ accumulation (C, F, I) of encorafenib in female WT, *Cyp3a*$^{-/-}$ and *Abcb1a/1b;Abcg2*$^{-/-}$ mice 8 h after oral administration of 10 mg/kg encorafenib (n = 4-10). No statistically significant differences compared to WT mice were observed ($P > 0.05$).

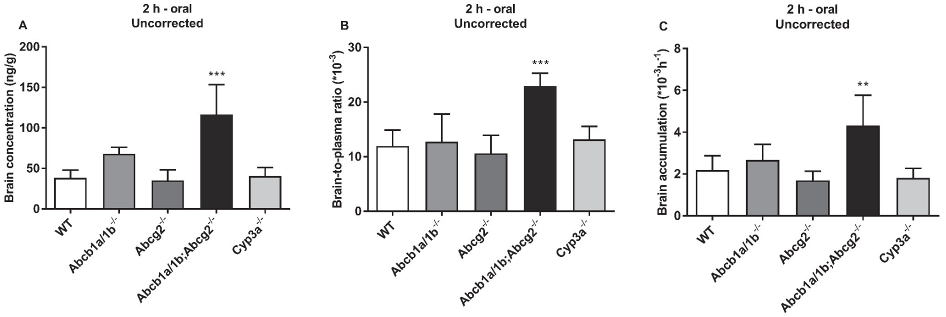

Supplemental Figure 4. Uncorrected brain concentration (A), brain-to-plasma ratio (B) and brain accumulation (C) of encorafenib in female WT, *Abcb1a/1b*$^{-/-}$, *Abcg2*$^{-/-}$, *Abcb1a/1b;Abcg2*$^{-/-}$ and *Cyp3a*$^{-/-}$ mice 2 h after oral administration of 10 mg/kg encorafenib (n = 4-8). *, $P < 0.05$; **, $P < 0.01$; ***, $P < 0.001$ compared to WT mice.

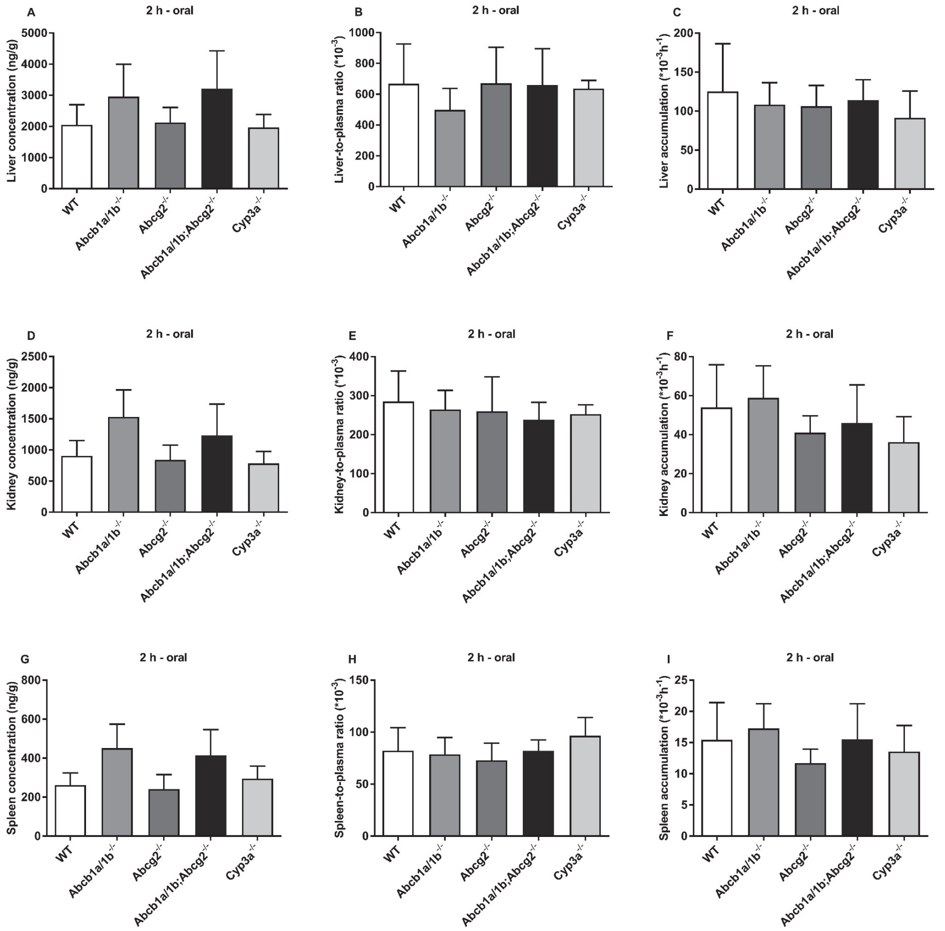

Supplemental Figure 5. Organ concentration (A, D, G), organ-to-plasma ratio (B, E, H) and organ accumulation (C, F, I) of encorafenib in female WT, *Abcb1a/1b*$^{-/-}$, *Abcg2*$^{-/-}$, *Abcb1a/1b;Abcg2*$^{-/-}$ and *Cyp3a*$^{-/-}$ mice 2 h after oral administration of 10 mg/kg encorafenib (n = 4-8). No statistically significant differences compared to WT mice were observed (*P* > 0.05).

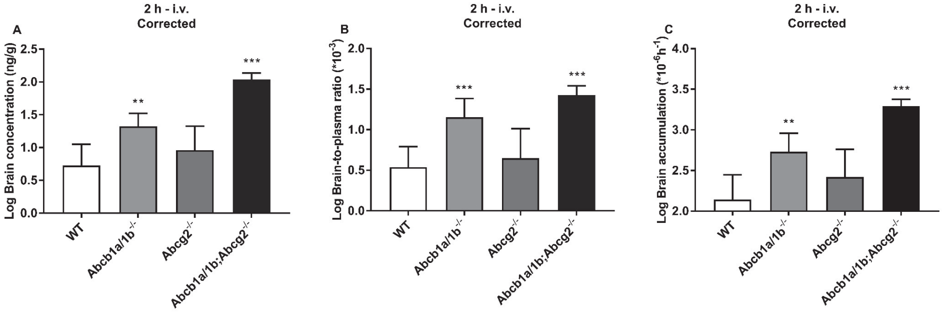

Supplemental Figure 6. Log-transformed brain concentration (A), brain-to-plasma ratio (B) and brain accumulation (C) of encorafenib in male WT, *Abcb1a/1b*$^{-/-}$, *Abcg2*$^{-/-}$ and *Abcb1a/1b;Abcg2*$^{-/-}$ mice 2 h after intravenous injection of 10 mg/kg encorafenib (n = 4-8). *, $P < 0.05$; **, $P < 0.01$; ***, $P < 0.001$ compared to WT mice.

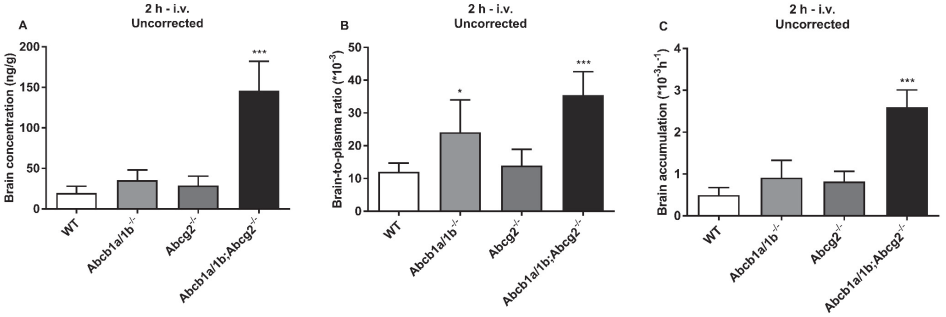

Supplemental Figure 7. Uncorrected brain concentration (A), brain-to-plasma ratio (B) and brain accumulation (C) of encorafenib in male WT, *Abcb1a/1b*$^{-/-}$, *Abcg2*$^{-/-}$ and *Abcb1a/1b;Abcg2*$^{-/-}$ mice 2 h after intravenous injection of 10 mg/kg encorafenib (n = 4-8). *, $P < 0.05$; **, $P < 0.01$; ***, $P < 0.001$ compared to WT mice.

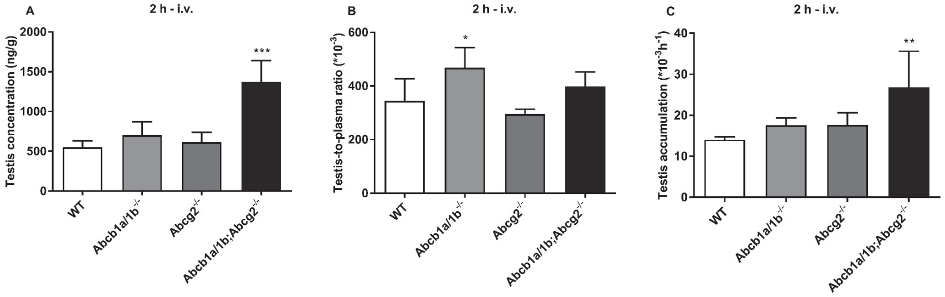

Supplemental Figure 8. Testis concentration (A), testis-to-plasma ratio (B) and testis accumulation (C) of encorafenib in male WT, *Abcb1a/1b*$^{-/-}$, *Abcg2*$^{-/-}$ and *Abcb1a/1b;Abcg2*$^{-/-}$ mice 2 h after intravenous injection of 10 mg/kg encorafenib (n = 4-5). *, $P < 0.05$; **, $P < 0.01$; ***, $P < 0.001$ compared to WT mice.

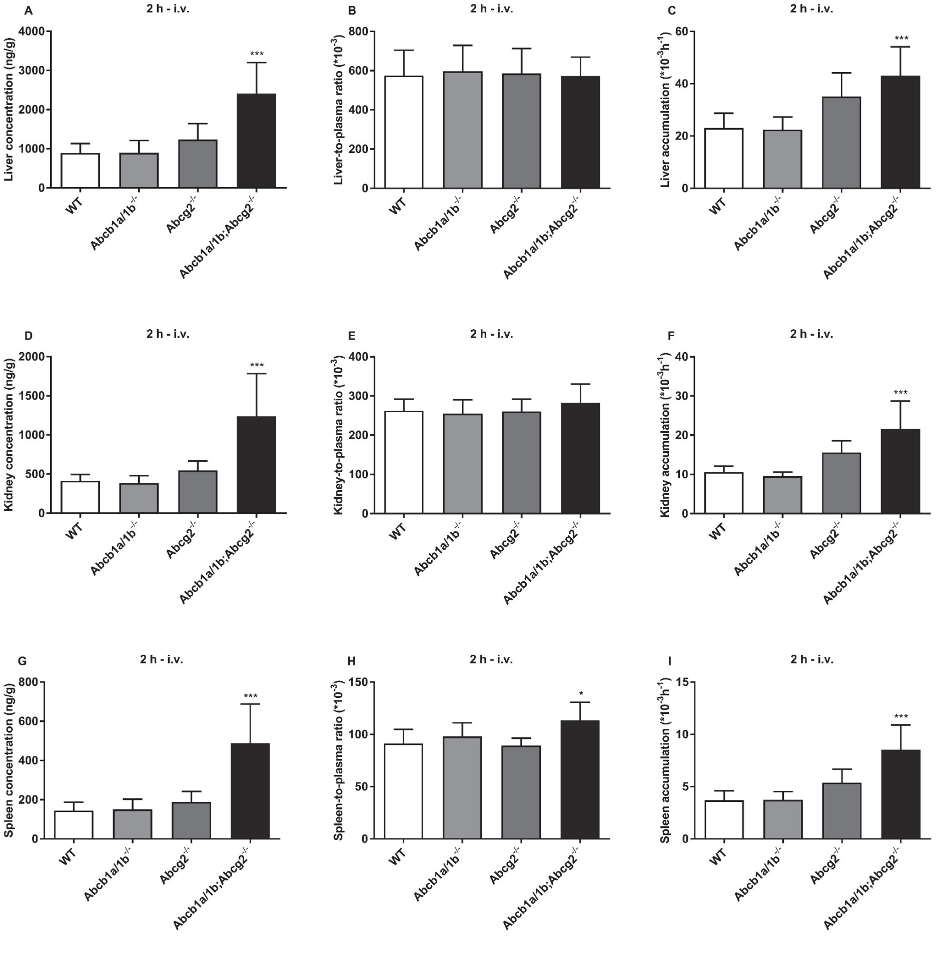

Supplemental Figure 9. Organ concentration (A, D, G), organ-to-plasma ratio (B, E, H) and organ accumulation (C, F, I) of encorafenib in male WT, *Abcb1a/1b*$^{-/-}$, *Abcg2*$^{-/-}$ and *Abcb1a/1b;Abcg2*$^{-/-}$ mice 2 h after intravenous injection of 10 mg/kg encorafenib. *, $P < 0.05$; **, $P < 0.01$; ***, $P < 0.001$ compared to WT mice.

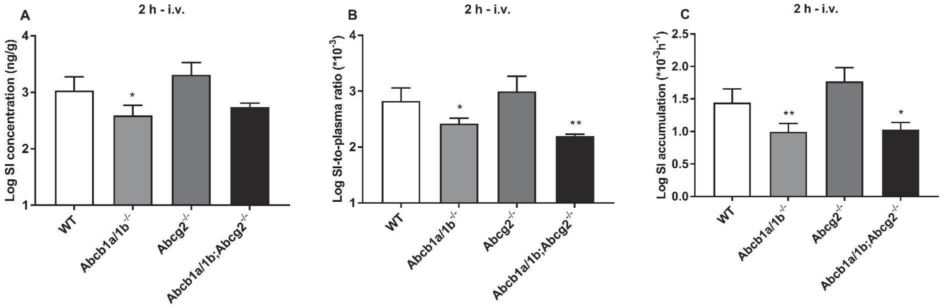

Supplemental Figure 10. Log-transformed small intestinal tissue (SI) concentration (A), log-transformed SI-to-plasma ratio (B) and log-transformed SI accumulation (C) of encorafenib in male WT, *Abcb1a/1b*$^{-/-}$, *Abcg2*$^{-/-}$ and *Abcb1a/1b;Abcg2*$^{-/-}$ mice 2 h after intravenous injection of 10 mg/kg encorafenib (n = 4-5). *, $P < 0.05$; **, $P < 0.01$; ***, $P < 0.001$ compared to WT mice.

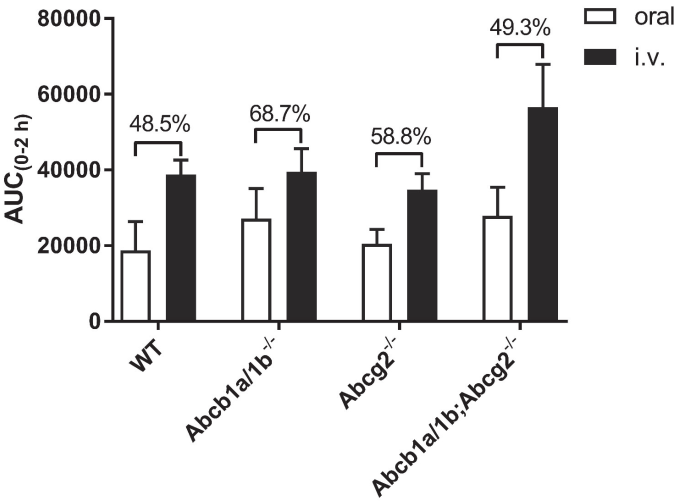

Supplemental Figure 11. Oral bioavailability of encorafenib. Percentage values indicate AUC$_{oral}$/AUC$_{i.v.}$ for each strain.

Supplemental Table 1. Plasma pharmacokinetic parameters and brain concentration 8 h after oral administration of 10 mg/kg encorafenib to female WT, *Abcb1a/1b;Abcg2*$^{-/-}$ and *Cyp3a*$^{-/-}$ mice.

Parameter	Genotype		
	WT	*Abcb1a/1b;Abcg2*$^{-/-}$	*Cyp3a*$^{-/-}$
Plasma $AUC_{0\text{-}8}$ (h*µg/ml)	15.4 ± 4.0	19.5 ± 6.9	26.8 ± 5.8 **
Fold change $AUC_{(0\text{-}8)}$	1.0	1.3	1.7
C_{max} (µg/ml)	8.7 ± 3.9	14.7 ± 7.3	25.0 ± 4.1 ***
T_{max} (min)	15	15	15
C_{brain} (ng/g)	8.4 ± 6.2	19.2 ± 23.6	12.7 ± 3.8
Fold change C_{brain}	1.0	2.3	1.5
Brain-to-plasma ratio ($*10^{-3}$)	9.8 ± 5.5	20.8 ± 17.2	18.0 ± 12.1
Fold change ratio	1.0	2.1	1.8
P_{brain} ($*10^{-3}h^{-1}$)	0.6 ± 0.5	1.2 ± 1.4	0.5 ± 0.1
Fold change P_{brain}	1.0	2.0	0.8

Data are given as mean ± S.D. (n = 4-10). C_{max}, maximum concentration in plasma; T_{max} , time point (h) of maximum plasma concentration; C_{brain}, brain concentration; P_{brain}, brain accumulation. *, $P < 0.05$; **, $P < 0.01$; ***, $P < 0.001$ compared to WT mice.

Supplemental Table 2. Small intestinal tissue concentration and small intestinal contents (SIC) percentage of dose 2 h after intravenous injection of 10 mg/kg encorafenib to male WT, *Abcb1a/1b*$^{-/-}$, *Abcg2*$^{-/-}$ and *Abcb1a/1b;Abcg2*$^{-/-}$ mice.

Parameter	Genotype			
	WT	*Abcb1a/1b*$^{-/-}$	*Abcg2*$^{-/-}$	*Abcb1a/1b;Abcg2*$^{-/-}$
C_{SI} (ng/g)	1221.7 ± 733.4	415.1 ± 152.3 *	2247.2 ± 1035.2	557.4 ± 88.7
Fold change C_{SI}	1.0	0.3	1.8	0.5
SI-to-plasma ratio ($*10^{-3}$)	735.7 ± 324.2	268.5 ± 52.1 *	1149.3 ± 651.5	156.9 ± 13.5 **
Fold change ratio	1.0	0.4	1.6	0.2
P_{SI} ($*10^{-3}h^{-1}$)	30.5 ± 15.3	10.3 ± 2.6 **	64.6 ± 29.0	10.9 ± 2.6 *
Fold change P_{SI}	1.0	0.3	2.1	0.4
SIC (percentage of dose)	1.17 ± 1.41	0.04 ± 0.02 ***	0.91 ± 0.24	0.02 ± 0.00 ***
Fold change SIC	1.00	0.04	0.78	0.02
SIC-to-plasma ratio ($*10^{-6}$)	638.6 ± 651.6	29.6 ± 11.6 ***	455.6 ± 149.5	4.9 ± 0.7 ***
Fold change ratio	1.00	0.05	0.71	0.08
P_{SIC} ($*10^{-6}h^{-1}$)	27.9 ± 31.4	1.1 ± 0.4 ***	26.7 ± 9.2	0.4 ± 0.1 ***
Fold change P_{SIC}	1.00	0.04	0.96	0.01

Data are given as mean ± S.D. (n = 4-5). *, $P < 0.05$; **, $P < 0.01$; ***, $P < 0.001$ compared to WT mice.

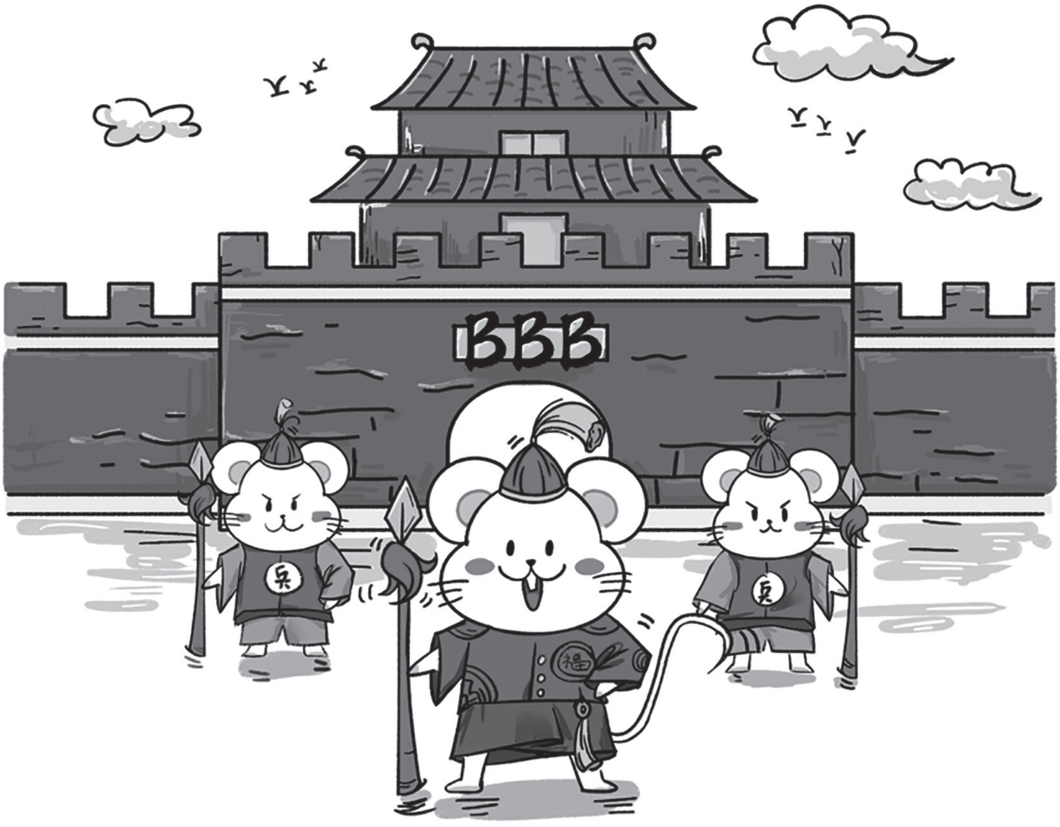
BBB
兵
福
兵

Chapter 3

P-glycoprotein (MDR1/ABCB1) and Breast Cancer Resistance Protein (BCRP/ABCG2) limit brain accumulation of the FLT3 inhibitor quizartinib in mice

Jing Wang
Changpei Gan
Irene A. Retmana
Rolf W. Sparidans
Wenlong Li
Maria C. Lebre
Jos H. Beijnen
Alfred H. Schinkel

International Journal of Pharmaceutics, 2019, 556: 172-180.

Abstract

Quizartinib, a second-generation FLT3 inhibitor, is in clinical development for the treatment of acute myeloid leukemia. We studied its pharmacokinetic interactions with the multidrug efflux transporters ABCB1 and ABCG2 and the multidrug metabolizing enzyme CYP3A, using *in vitro* transport assays and knockout and transgenic mouse models. Quizartinib was transported by human ABCB1 *in vitro*, and by mouse (m)Abcb1 and mAbcg2 *in vivo*. Upon oral administration, the brain accumulation of quizartinib was 6-fold restricted by mAbcb1 and 2-fold by mAbcg2 (together: 12-fold). Unexpectedly, the absence of mAbcb1 resulted in a ~2-fold lower plasma exposure in *Abcb1a/1b*$^{-/-}$ and *Abcb1a/1b;Abcg2*$^{-/-}$ mice, suggesting that loss of mAbcb1 causes compensatory alterations in alternative quizartinib elimination or uptake systems. mAbcb1 and mAbcg2 themselves did not appear to restrict quizartinib oral availability. Oral and intravenous pharmacokinetics of quizartinib were not substantially altered between wild-type, Cyp3a knockout and CYP3A4-humanized mice. All three strains showed relatively high (33-51%) oral bioavailability. If this also applies in humans, this would suggest a limited risk of CYP3A-related inter-individual variation in exposure for this drug. Our results provide a possible rationale for using pharmacological ABCB1/ABCG2 inhibitors together with quizartinib when treating malignant lesions situated in part or in whole behind the blood-brain barrier.

Keywords: ABCB1, ABCG2, CYP3A enzymes, quizartinib, brain penetration, FLT3

Graphical abstract:

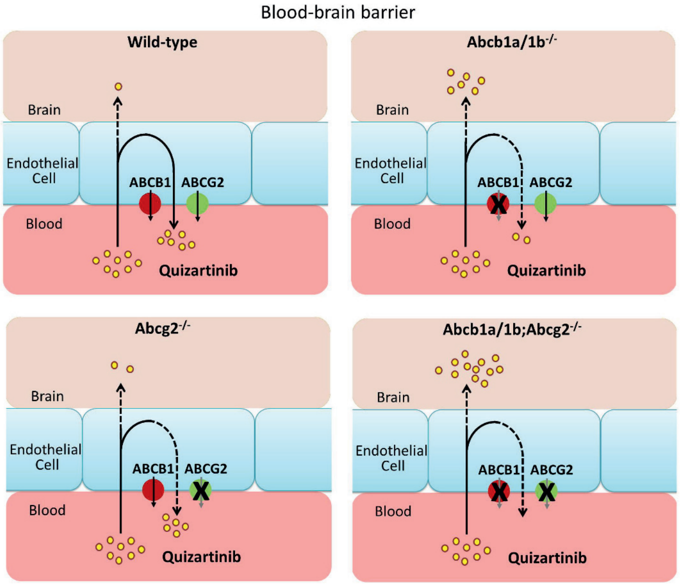
Blood-brain barrier
Wild-type
Brain
Endothelial Cell
ABCB1
ABCG2
Blood
Quizartinib
Abcb1a/1b-/-
Brain
Endothelial Cell
ABCB1
ABCG2
Blood
Quizartinib
Abcg2-/-
Brain
Endothelial Cell
ABCB1
ABCG2
Blood
Quizartinib
Abcb1a/1b;Abcg2-/-
Brain
Endothelial Cell
ABCB1
ABCG2
Blood
Quizartinib

1. Introduction

Acute myeloid leukemia (AML) accounts for 34% of all leukemia cases [1]. In 2017, 21,380 new cases were diagnosed, and more than 10,000 patients died from AML in the United States alone [1]. Different therapies have been used in treating AML, but despite initial remissions, relapses are frequent, with an overall cure rate of only 30-40% [2].

FMS-like tyrosine kinase 3 (FLT3) is a class III receptor tyrosine kinase (RTK) highly expressed in human hematopoietic stem and progenitor cells [3]. Activating mutations in FLT3 have been identified in up to 30% of AML patients [4, 5]. The commonest gain-of-function mutation in FLT3 is internal tandem duplications (ITDs), present in approximately 30% of cytogenetically normal AML [3, 6]. FLT3-ITD mutations are associated with increased relapse rates and reduced overall survival when treated with standard therapy [7-9], or after allogeneic haematopoietic stem cell transplantation [10]. These mutations are also negative prognostic factors for the survival of refractory or relapsed AML patients because of their poor response to rescue therapy [11-14].

Tyrosine kinase inhibitors (TKIs) are promising agents in the treatment of FLT3-ITD mutated AML, especially in combination with chemotherapy [15, 16]. The first-generation FLT3 inhibitors, sunitinib [17] and sorafenib, have been used in the treatment of AML, but treatment with sorafenib did not result in significant improvement in the median event-free survival or overall survival. The risk for bleeding events, fever, and hand-foot syndrome was significantly higher in the sorafenib arm of the study [18, 19]. Interestingly, sorafenib combined with conventional chemotherapy achieved complete remission in a study with FLT3-ITD–positive AML [20]. However, conventional cancer chemotherapy may cause a range of side effects which can adversely affect patients' health and quality of life.

Quizartinib (AC220) is a second-generation FLT3 inhibitor, with better pharmaceutical and pharmacokinetic properties, and much greater target specificity than sunitinib and sorafenib. *In vitro*, quizartinib is a potent inhibitor of both wild-type FLT3 and mutant FLT3-ITD. The inhibition of mutant-FLT3 isoforms results in inhibition of cellular proliferation and induction of apoptosis [21-23]. In phase 1 trials, quizartinib showed efficacy in patients with relapsed or refractory AML with wild-type FLT3 as well as FLT3-ITD [24], and it appears to be a safe single-dose agent with no serious adverse events [25]. Quizartinib is currently evaluated in clinical (phase 2/3) trials in combination with omacetaxine mepesuccinate or chemotherapy in newly diagnosed or relapsed/refractory AML carrying FLT3-ITD mutations (www.clinicaltrials.gov: NCT03135054, NCT02668653). Recent preclinical studies show that quizartinib may also be used to transiently induce quiescence in multipotent hematopoietic progenitor cells, thus circumventing myelosuppression by coadministered cytotoxic chemotherapeutics like 5-FU and gemcitabine [26]. If this turns out to also apply in humans, this could present a major advance in limiting myelosuppression, which is often dose-limiting in cytotoxic cancer chemotherapy.

ABCB1 (P-glycoprotein/MDR1) and ABCG2 (Breast Cancer Resistance Protein/BCRP) are multispecific drug efflux transporters localized at apical membranes of liver, kidney and intestine, where they pump their substrates into bile, urine, and feces, respectively. They also occur at pharmacological sanctuary site barriers such as the blood-brain barrier (BBB) and blood-testis barrier, where they pump their substrates back into blood. As a consequence, only small amounts of drug can accumulate in, for instance, the brain, which can compromise treatment of (micro-)metastases that are present behind a functionally intact BBB [27-29]. The FLT3 inhibitors sorafenib and sunitinib are good transport substrates of human (h) ABCB1 and ABCG2 and mouse (m) Abcg2, and their brain accumulation is effectively restricted by both mAbcb1 and mAbcg2 activity *in vivo* [30-33]. Current data suggest that quizartinib acts as an inhibitor of ABCB1 and ABCG2 *in vitro* [34] and of ABCG2 also *in vivo* [35], but there are no indications that it can be transported by ABCB1 or ABCG2. In fact, K562 cell lines overexpressing ABCB1 or ABCG2 even showed increased ("collateral") sensitivity to this drug, arguing against efficient export of quizartinib by ABCB1 and ABCG2 in this cell line [34].

Cytochrome P450-3A (CYP3A) is an abundant multispecific drug-metabolizing enzyme highly expressed in human liver and small intestine, and it plays a significant role in the metabolism of approximately half of the drugs in current clinical use [36, 37]. As CYP3A can display a high degree of inter- and intra-individual activity, it is a major player in variable drug exposure [38, 39]. Quizartinib is quite extensively metabolized in humans, and it may be an *in vitro* CYP3A substrate [24, 25].

Plasma pharmacokinetics as well as tissue and tumor distribution can have a major impact on the therapeutic efficacy of a drug. In this study we therefore aimed to investigate whether quizartinib is transported by ABCB1 and ABCG2 *in vitro*, and to establish the *in vivo* effects of these transporters and of CYP3A on oral availability and tissue distribution of quizartinib in wild-type and knockout mouse strains.

2. Material and methods

2.1. Chemicals

Quizartinib (98.5%, M_w = 560.7 g/mol) and zosuquidar were obtained from Sequoia Research Products (Pangbourne, UK). Ko143 was from Tocris Bioscience (Bristol, UK). Bovine Serum Albumin (BSA) Fraction V was obtained from Roche Diagnostics (Mannheim, Germany). Isoflurane was purchased from Pharmachemie (Haarlem, The Netherlands), heparin (5000 IU ml^{-1}) was from Leo Pharma (Breda, The Netherlands). Chemicals used in the quizartinib assay were described before [40]. All other chemicals and reagents were obtained from Sigma-Aldrich (Steinheim, Germany).

2.2. Transport assays

Polarized Madin-Darby Canine Kidney (MDCK-II) cell lines transduced with human (h)ABCB1, hABCG2 and mouse (m)Abcg2 cDNA were used (passage 10-20 after clonal selection) and cultured as described previously [41]. We never generated MDCKII cells overexpressing mAbcb1a or mAbcb1b, given the near-complete overlap in substrate specificity with hABCB1. Transepithelial transport assays were performed in triplicate using 12-well microporous polycarbonate membrane filters (3.0-μm pore size, Transwell 3402, Corning., Lowell, MA) as previously described [41]. In short, cells were seeded on the same day and at the same density (5×10^5 cells per well), and allowed to grow an intact monolayer in 3 days, which was monitored with transepithelial electrical resistance (TEER) measurements. 5 μM each of quizartinib, zosuquidar (ABCB1 inhibitor) and/or Ko143 (ABCG2/Abcg2 inhibitor) were used during the transport experiments. On the third day, if applicable, cells were pre-incubated with one or more of the inhibitors for 1 h in both compartments. The transport phase was initiated (t = 0) by replacing the medium in both compartments with fresh DMEM including 10% FBS and quizartinib at 5 μM, as well as the appropriate inhibitor(s). Cells were kept at 37°C in 5% (v/v) CO_2 during the experiment, and at 1, 2, 4 and 8 hours, 50 μl samples were taken from the acceptor compartment, and stored at -30°C until LC-MS/MS analysis. The amount of transported drug was calculated after correction for volume loss due to sampling at each time point. Active transport was expressed using the transport ratio (r), which is defined as the amount of apically directed drug transport divided by basolaterally directed drug translocation at a defined time point.

2.3. Animals

Mice were bred in the Netherlands Cancer Institute and housed and handled according to institutional guidelines complying with Dutch and EU legislation. All experiments were reviewed and approved by the Institutional Animal Care and Use Committee (IACUC). Animals used were female WT, *Abcb1a/1b*$^{-/-}$ [42], *Abcg2*$^{-/-}$ [43], *Abcb1a/1b;Abcg2*$^{-/-}$ [44] and *Cyp3a*$^{-/-}$ [45] mice of a >99% FVB genetic background. Homozygous CYP3A4 humanized transgenic mice (Cyp3aXAV) were generated by cross-breeding of transgenic mice with stable human CYP3A4 expression in liver or intestine, respectively, in a *Cyp3a*$^{-/-}$ background [45]. All the mice used were between 9 and 14 weeks of age, and generally between 23 and 35 gram of body weight. Animals were kept in a temperature-controlled environment with a 12 h light/12 h dark cycle and received a standard diet (Transbreed, SDS Diets, Technilab-BMI) and acidified water *ad libitum*.

2.4. Drug solutions

Quizartinib stock solution was in DMSO at a concentration of 33.3 mg/ml stored at -30˚C, and subsequently diluted with 50 mM sodium acetate buffer (pH 4.4) to yield a working concentration of 1 mg/ml. The final DMSO concentration in the formulation was 3%. All working solutions were prepared freshly on the day of the experiment.

2.5. Plasma and tissue pharmacokinetics of quizartinib

For the oral experiment, quizartinib (10 mg/kg) was administered to the mice by oral gavage using a blunt-ended needle. To minimize variation in absorption, mice were fasted for about 2 h before quizartinib was administered (n = 4-6). For the intravenous experiment, quizartinib (5 mg/kg) was injected into the tail vein (n = 4-6). For the 24 or 8 hour experiments, 50 µl blood samples were collected from the tail vein at 0.5, 1, 2, 4 and 8 h or 0.5, 1, 2 and 4 h, respectively, using heparin-coated capillaries (Sarstedt, Germany). At 24 or 8 h, mice were anesthetized with isoflurane and blood was collected by cardiac puncture. Immediately thereafter, mice were sacrificed by cervical dislocation, and the brain and a set of other tissues were removed, weighed and rapidly frozen at −30˚C. Tissues were homogenized on ice in an appropriate volume of 4% (w/v) BSA in water, and stored further at −30°C until analysis. Blood samples were centrifuged at 9,000 *g* for 6 min at 4°C immediately after collection, and the plasma fractions were collected and stored at −30°C until analysis.

2.6. LC-MS/MS analysis

Quizartinib concentrations in cell culture medium, plasma and tissue homogenates were analyzed with a previously reported liquid-chromatography tandem mass spectrometric (LC-MS/MS) assay, using a deuterated internal standard [40].

2.7. Statistics and pharmacokinetic calculations

Pharmacokinetic parameters were calculated by the software GraphPad Prism7 (GraphPad Software Inc., La Jolla, CA, USA). The area under the plasma concentration-time curve (AUC) was calculated using the trapezoidal rule with the Microsoft Excel plug in PKsolver [46], without extrapolating to infinity. Ordinary one-way analysis of variance (ANOVA) was used to determine significance of differences between groups, after which post-hoc tests with Tukey correction were performed for comparison between individual groups. The two-sided unpaired Student's t test was used when treatments or differences between two groups were compared. The peak plasma concentration (C_{max}) and the time to reach C_{max} (t_{max}) were estimated from the original data. Relative organ accumulation (P_{organ}) was calculated by dividing organ concentrations (C_{organ}) at either t = 24 h or t = 8 h by the $AUC_{0\text{-}24h}$ or $AUC_{0\text{-}8h}$, respectively. Differences were considered statistically significant when $P < 0.05$. Data are presented as mean ± SD with each experimental group containing 4-6 mice.

3. Results

3.1. Quizartinib is moderately transported by hABCB1 in vitro

We analyzed quizartinib (5 µM) transport across polarized Madin-Darby Canine Kidney (MDCK-II) cell lines stably transduced with human (h)ABCB1, hABCG2, or mouse (m)Abcg2 cDNA. The MDCK-II parental cells did not show significant apically directed transport (Figure 1A, efflux ratio r = 0.8), and addition of the ABCB1 inhibitor zosuquidar did not change this result (Figure 1B, r = 0.7). In hABCB1-overexpressing MDCKII cells, we observed clear apically directed transport of quizartinib (Figure 1C, r = 2.6), which was completely inhibited by co-incubation with zosuquidar (Figure 1D, r = 0.9). To suppress any possible transport contribution of quizartinib by the endogenous canine ABCB1, subsequent experiments were all done in the presence of zosuquidar (5 µM). In hABCG2-overexpressing MDCK-II cells, no clear net transport of quizartinib was detected, and addition of Ko143 did not alter this profile (r = 0.9 and 0.8, respectively, Figure 1E and F). In mAbcg2-overexpressing MDCK-II cells, there was a slight apically directed transport of quizartinib r = 1.5 (Figure 1G), and this could be reduced with the ABCG2 inhibitor Ko143 to an r of 1.2 (Figure 1H). These data demonstrate that quizartinib at 5 µM is moderately transported by hABCB1, but not noticeably by hABCG2, and perhaps by mAbcg2 *in vitro*, although the latter did not reach statistical significance.

3.2. Roles of Abcb1 and Abcg2 in quizartinib oral availability and tissue distribution

In view of the *in vitro* transport data, we also wanted to assess the *in vivo* impact of Abcb1 and Abcg2 on quizartinib oral availability and tissue distribution. Since quizartinib is given orally to patients at a dose of ~200 mg, we administered this drug to mice by oral gavage into the stomach at a physiologically roughly equivalent dose of 10 mg/kg.

We first performed a 24-hour pilot study in female WT and *Abcb1a/1b;Abcg2*$^{-/-}$ mice. After oral administration, the plasma concentrations were high, with a C_{max} of 1.6-2 µg/ml in both mouse strains, and a t_{max} around 8 h. At t = 24 h, the plasma concentrations in both strains were similar. The combined absence of Abcb1a/1b and Abcg2 resulted in 0.8-fold lower plasma $AUC_{0\text{-}24}$, although this was not statistically significant (Figure 2A; Supplemental Table 1). We next measured the brain, liver, kidney and spleen concentrations of quizartinib 24 h after oral administration. Although at t = 24 h the plasma concentrations in both strains were similar, the brain concentration in *Abcb1a/1b;Abcg2*$^{-/-}$ mice was markedly (17.8-fold) higher than that in WT mice (Figure 3A; Supplemental Table 1). The same applied for the brain-to-plasma ratio (12-fold) and the relative brain accumulation (24-fold) (Figure 3B and C; Supplemental Table 1). In contrast to the brain, we observed no significant differences between the strains in liver concentration, liver-to-plasma ratio (400-500%) and liver accumulation (Figure 3D-F). Qualitatively similar data were obtained for kidney and spleen concentrations, tissue-to-plasma ratios (150-250% for kidney and 140% for spleen), and tissue accumulations of quizartinib between these strains (Supplemental Figure 1A-F). The tissue-to-plasma distribution ratios for these organs in WT mice (140-500%) were all far higher than those observed for the WT brain (~10%). These data suggest that quizartinib is kept mostly out of the brain by mAbcb1a/1b and/or mAbcg2, but that these proteins have no substantial effect on relative quizartinib distribution to liver, kidney, and spleen after oral administration.

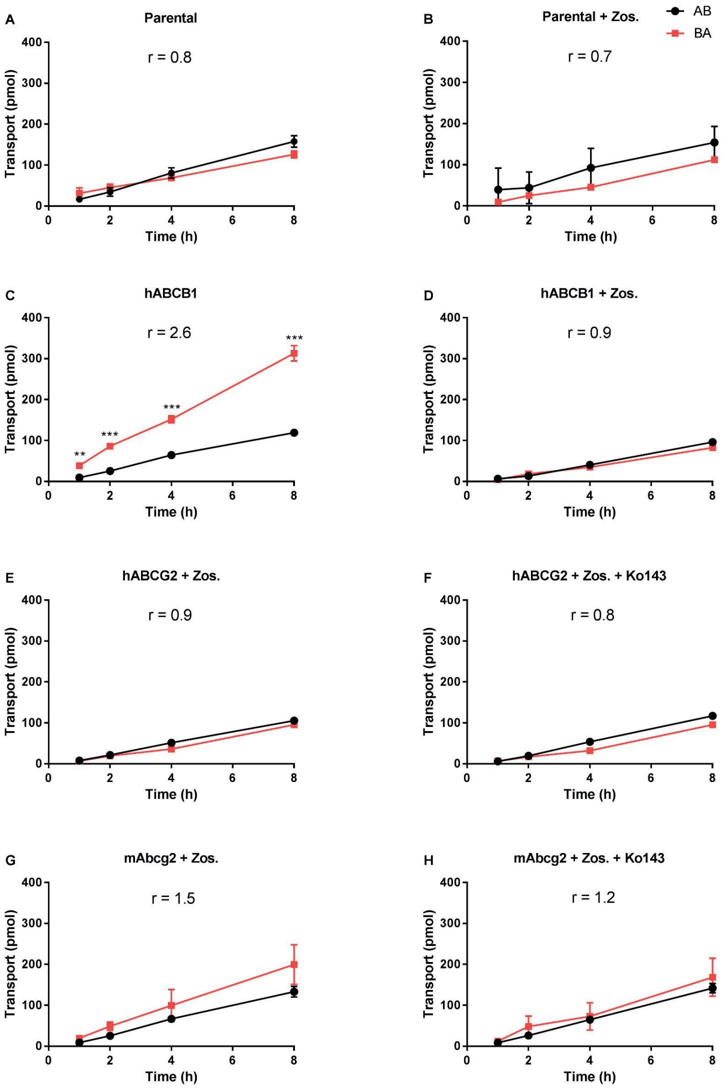

Figure 1. In vitro transport of quizartinib. Transepithelial transport of quizartinib (5 µM) was assessed in MDCK-II cells either non-transduced (A, B) or transduced with hABCB1 (C, D), hABCG2 (E, F) or mAbcg2 (G, H) cDNA. At t = 0 h, quizartinib was applied to the donor compartment and the concentrations in the acceptor compartment at t = 1, 2, 4 and 8 h were measured and plotted as total amount of transport (pmol) in the graphs (n = 3). B, D–H: Zos. (zosuquidar, 5 µM) and/or Ko143 (5 µM) were applied as indicated to inhibit ABCB1 and hABCG2 or mAbcg2, respectively. r, relative transport ratio. BA (■), translocation from the basolateral to the apical compartment; AB (●), translocation from the apical to the basolateral compartment. Points, mean; bars, SD. *, $P < 0.05$; **, $P < 0.01$; ***, $P < 0.001$ compared to AB.

To better assess the impact on plasma concentration and tissue distribution of quizartinib, as well as the possible single and overlapping pharmacokinetic roles of mAbcb1 and mAbcg2 at the BBB, we performed another oral quizartinib (10 mg/kg) experiment including WT, *Abcb1a/1b;Abcg2$^{-/-}$*, as well as single Abcg2 and Abcb1a/1b knockout mice. We terminated at t = 8 h, i.e. not far from the quizartinib C_{max} and t_{max} in each strain (Figure 2A and B). As shown in Figure 2B, the plasma AUC_{0-8} in the single Abcg2 knockout mice was lower than in WT mice, but this was not statistically significant (0.8-fold, $P > 0.05$). In contrast, the *Abcb1a/1b$^{-/-}$* and *Abcb1a/1b;Abcg2$^{-/-}$* mice both showed a significantly lower AUC_{0-8} than the WT mice (0.56-fold, $P < 0.01$; 0.47-fold, $P < 0.01$, respectively; Table 1). Of note, also in the preceding 24 h experiment the AUC_{0-8} in *Abcb1a/1b;Abcg2$^{-/-}$* mice had been significantly reduced compared to WT mice (0.65-fold, $P < 0.05$, Supplemental Table 1), indicating qualitative consistency between these experiments.

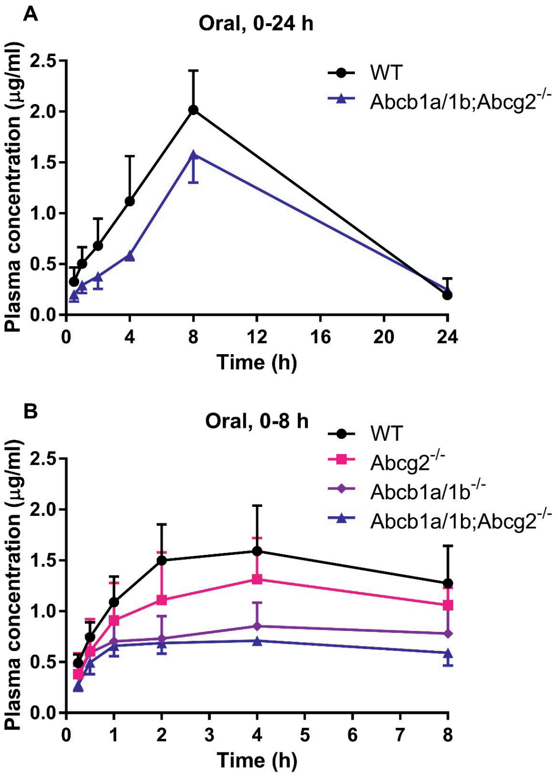

Figure 2. Plasma concentration-time curves of quizartinib in female WT and *Abcb1a/1b;Abcg2$^{-/-}$* mice over 24 h (A) or in WT, *Abcg2$^{-/-}$*, *Abcb1a/1b$^{-/-}$* and *Abcb1a/1b;Abcg2$^{-/-}$* mice over 8 h (B) after oral administration of 10 mg/kg quizartinib. Data are given as mean ± S.D. (n = 4-6). *, $P < 0.05$; **, $P < 0.01$; ***, $P < 0.001$ compared to WT mice.

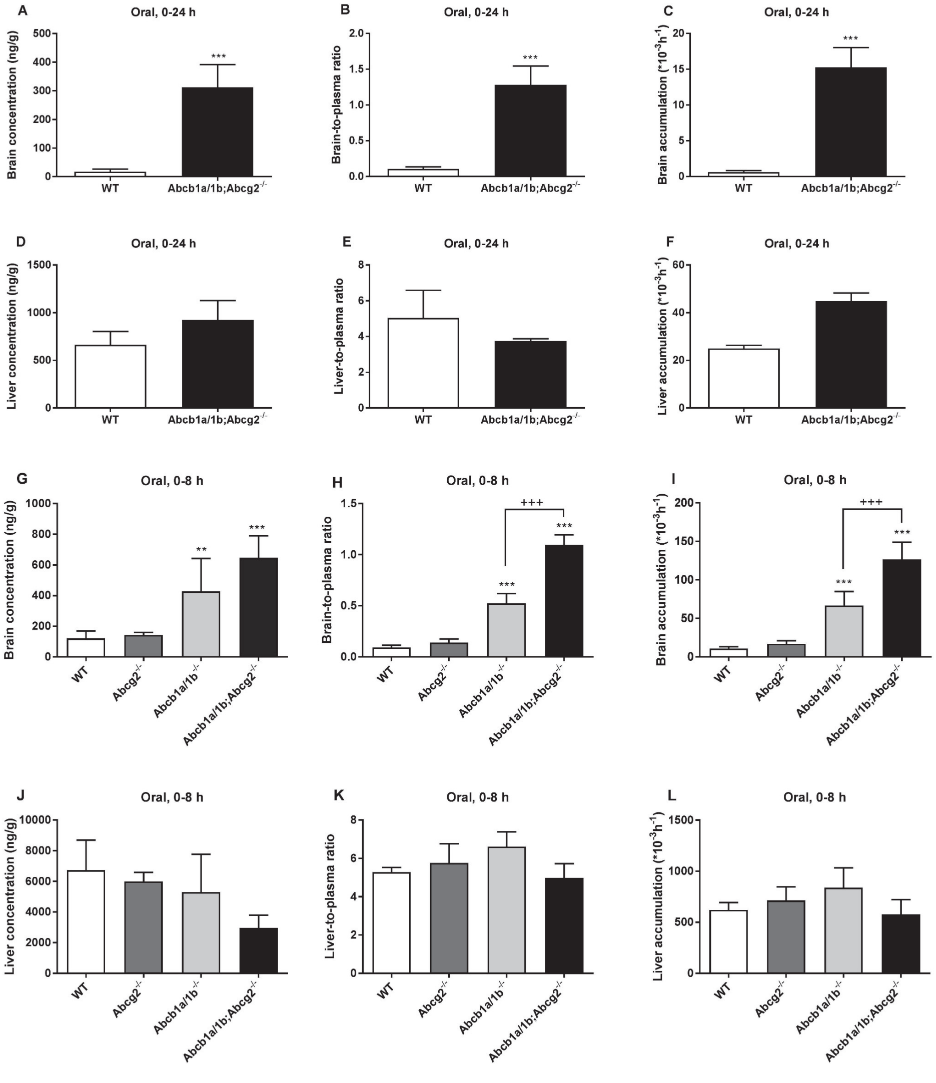

Figure 3. A-F: brain and liver concentration (A, D), tissue-to-plasma ratio (B, E) and tissue accumulation (C, F) of quizartinib in female WT and *Abcb1a/1b;Abcg2*$^{-/-}$ mice at 24 h after oral administration of quizartinib at 10 mg/kg (n = 4-6). G-L: brain and liver concentration (G, J), tissue-to-plasma ratio (H, K) and tissue accumulation (I, L) of quizartinib in female WT, *Abcg2*$^{-/-}$, *Abcb1a/1b*$^{-/-}$ and *Abcb1a/1b;Abcg2*$^{-/-}$ mice 8 h after oral administration of quizartinib at 10 mg/kg (n = 4-6). *, $P < 0.05$; **, $P < 0.01$; ***, $P < 0.001$ compared to WT mice.

Table 1. Plasma pharmacokinetic parameters and brain concentration 8 h after oral administration of 10 mg/kg quizartinib to female WT, *Abcg2*$^{-/-}$, *Abcb1a/1b*$^{-/-}$, *Abcb1a/1b;Abcg2*$^{-/-}$, *Cyp3a*$^{-/-}$ and Cyp3aXAV mice.

Parameter	Genotype					
	WT	*Abcg2*$^{-/-}$	*Abcb1a/1b*$^{-/-}$	*Abcb1a/1b;Abcg2*$^{-/-}$	*Cyp3a*$^{-/-}$	Cyp3aXAV
Plasma AUC$_{0-8}$ (h*µg/ml)	10.8 ± 2.5	8.7 ± 2.3	6.1 ± 1.7 **	5.12 ± 0.4 **	12.2 ± 1.8	13.9 ± 2.4
Fold change AUC$_{0-8}$	1	0.81	0.56	0.47	1.13	1.29
C_{max} (µg/ml)	1.7 ± 0.4	1.4 ± 0.4	0.9 ± 0.3	0.8 ± 0.1	1.9 ± 0.2	2.5 ± 0.3
t_{max} (h)	2-4	2-8	2-8	2-8	2-8	4-8
C_{brain} (ng/g)	121 ± 49	143 ± 16	428 ± 214 **	647 ± 142 ***	167 ± 24	244 ± 33
Fold change C_{brain}	1	1.2	3.5	5.4	1.4	2.0
Brain-to-plasma ratio	0.09 ± 0.02	0.14 ± 0.04	0.52 ± 0.10 **	1.10 ± 0.10 ***	0.10 ± 0.01	0.10± 0.00
Fold change ratio	1	1.5	5.6	11.8	1.0	1.1
P_{brain} (*$10^{-3}h^{-1}$)	10.8 ± 2.3	17.1 ± 3.8	66.8 ± 18.1 **	126.7 ± 22.4 ***	13.8 ± 1.3	17.8 ± 2.9
Fold change P_{brain}	1	1.6	6.2	11.7	1.3	1.7

Data are given as mean ± S.D. (n = 4-6). C_{max}, maximum concentration in plasma; t_{max} , time point (h) of maximum plasma concentration (range for individual mice); C_{brain}, brain concentration; P_{brain}, brain accumulation. *, $P < 0.05$; **, $P < 0.01$; ***, $P < 0.001$ compared to WT mice.

Table 2. Plasma pharmacokinetic parameters over 24 h after oral (10 mg/kg) or intravenous (5 mg/kg) administration of quizartinib to female WT, *Cyp3a*$^{-/-}$ and Cyp3aXAV mice.

Parameter	Dosing	Genotype		
		WT	*Cyp3a*$^{-/-}$	Cyp3aXAV
Plasma AUC$_{0-24}$ (h*µg/ml)	Oral,	43.0 ± 4.1	38.1 ± 8.5 $^{+++}$	67.1 ± 5.5 ***
Fold change AUC$_{0-24}$	10 mg/kg	1	0.9	1.6
C_{max} (µg/ml)		3.1 ± 0.3	2.1 ± 0.7	4.2 ± 0.4
t_{max} (h)		2-8	8	4-8
Plasma AUC$_{0-24}$ (h*µg/ml)	i.v.,	32.8 ± 2.2	40.1 ± 3.5 $^{++}$	45.2 ± 2.5 ***
Fold change AUC$_{0-24}$	5 mg/kg	1	1.2	1.4

Data are given as mean ± S.D. (n = 4-6). C_{max}, maximum concentration in plasma; t_{max} , time point (h) of maximum plasma concentration (range for individual mice). *, $P < 0.05$; **, $P < 0.01$; ***, $P < 0.001$ compared to WT mice. $^{+}$, $P < 0.05$; $^{++}$, $P < 0.01$; $^{+++}$, $P < 0.001$ compared to Cyp3aXAV mice.

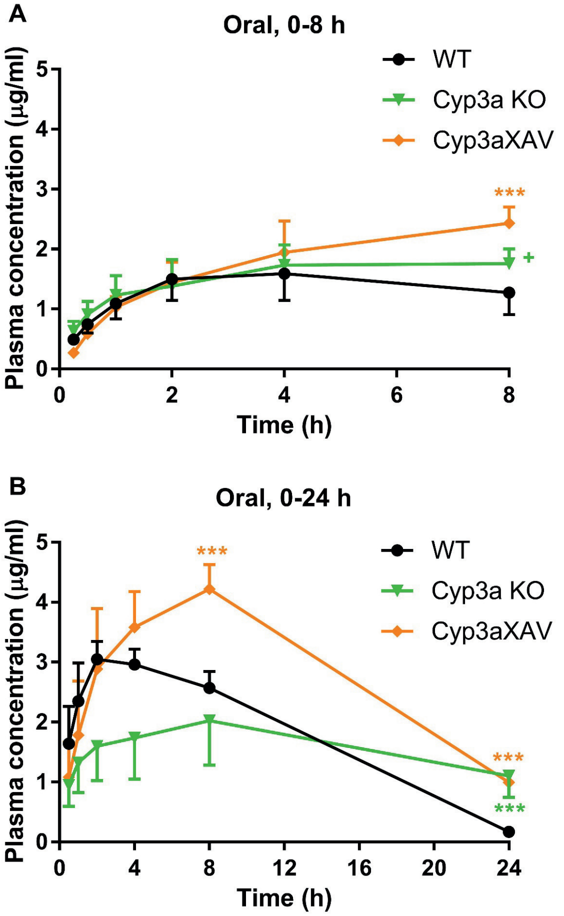

Figure 4. Plasma concentration-time curves of quizartinib in female WT, Cyp3a KO and Cyp3aXAV mice over 8 h (A) or 24 h (B) after oral administration of 10 mg/kg quizartinib. Data are given as mean ± S.D. (n = 4-6). *, $P < 0.05$; **, $P < 0.01$; ***, $P < 0.001$ compared to WT mice. +, $P < 0.05$ compared to Cyp3aXAV mice.

We also measured the brain concentrations of quizartinib at 8 h. The single *Abcg2*$^{-/-}$ mice did not display statistically significant changes in brain concentrations, brain-to-plasma ratios and brain accumulations compared to WT mice. However, in spite of the significantly lower plasma concentrations in *Abcb1a/1b*$^{-/-}$ and *Abcb1a/1b;Abcg2*$^{-/-}$ mice at 8 h, the quizartinib brain concentrations were greatly increased in these two mouse strains compared to WT mice, and accordingly also the brain-to-plasma ratios (5.6- and 11.8-

fold, respectively) and brain accumulations (Figure 3G-I; Table 1). The observation that the brain-to-plasma ratio was substantially higher in the *Abcb1a/1b;Abcg2*$^{-/-}$ mice than in the *Abcb1a/1b*$^{-/-}$ mice (Figure 3H) suggests that mAbcg2 also contributes to reducing the brain accumulation of quizartinib. Collectively, these data indicate that the brain penetration of quizartinib was limited by both mAbcb1 and mAbcg2, albeit with a substantially bigger role for mAbcb1. We further analyzed the liver (Figure 3J-L) as well as the kidney and spleen concentrations (Supplemental Figure 1G-L) of quizartinib at 8 h after oral administration. Like in the 24 h experiment, we found no substantial effect of mAbcb1 and mAbcg2 on relative quizartinib distribution to these organs after oral administration.

3.3. Limited in vivo role of Cyp3a in quizartinib pharmacokinetics

To investigate the possible impact of mCyp3a and hCYP3A4 on quizartinib pharmacokinetics in mice, we first performed an 8 h oral study in WT, Cyp3a knockout and Cyp3aXAV mice (Cyp3aXAV mice are humanized transgenic mice with stable human CYP3A4 expression in liver and intestine, in a Cyp3a knockout background). We found no meaningful differences in the plasma exposure of quizartinib over 8 h (AUC_{0-8}) in these three strains. The C_{max} in *Cyp3a*$^{-/-}$ and Cyp3aXAV mice occurred in both around 8 h. At this time point, Cyp3aXAV mice showed, somewhat unexpectedly, significantly higher plasma concentrations than WT and *Cyp3a*$^{-/-}$ mice, $P < 0.001$, $P < 0.05$, respectively (Figure 4A).

To further investigate the quizartinib pharmacokinetics, we also performed a 24 h oral and intravenous study in female WT, *Cyp3a*$^{-/-}$ and Cyp3aXAV mice, at a dose of 10 mg/kg (oral), and 5 mg/kg (intravenous, with reduced dose to accommodate quizartinib solubility limits). The oral plasma AUC_{0-24} was not significantly changed between *Cyp3a*$^{-/-}$ and WT mice, but Cyp3aXAV mice did show a significantly higher AUC_{0-24} than WT and *Cyp3a*$^{-/-}$ mice (1.6-fold; Figure 4B; Table 2). Upon intravenous administration of quizartinib, the plasma exposure of quizartinib over 24 h (AUC_{0-24}) was slightly but significantly increased in *Cyp3a*$^{-/-}$ and Cyp3aXAV mice compared to WT mice (Supplemental Figure 2A and B; Table 2). Collectively, the changes in plasma exposure observed between the strains were modest, albeit now and then significant. However, the direction of the changes was rather unexpected: assuming that mouse Cyp3a and human CYP3A4 would each substantially contribute to the metabolism of quizartinib, one would expect an increase in plasma AUC in *Cyp3a*$^{-/-}$ mice, and a subsequent decrease in Cyp3aXAV mice. Clearly that was not observed here. However, the modest shifts observed, and their unexpected direction suggest that Cyp3a itself is not a major determinant of quizartinib pharmacokinetics in mice.

When we measured the brain, liver, kidney, and spleen concentrations of quizartinib at 8 and 24 h after oral administration, we found no meaningful differences in tissue-to-plasma ratios after 8 h (Supplemental Figure 3) or 24 h (Supplemental Figure 4). These data suggest that mCyp3a and hCYP3A4 do not to have a substantial impact on quizartinib distribution to brain, liver, kidney, or spleen after oral administration. Liver and kidney appeared to equilibrate fairly efficiently with plasma levels of quizartinib also after intravenous administration, with very similar tissue-to-plasma ratios between the different strains after 24 h (Supplemental Figure 5). Tissue-to-plasma distribution ratios were also similar to those seen after oral quizartinib administration, with ~600% and ~250% for liver and kidney, respectively.

Because quizartinib was orally and intravenously administered to mice at different dosages (10 or 5 mg/kg), we used the normalized oral and i.v. AUC_{0-24} to estimate the oral bioavailability of quizartinib in the different CYP3A-modified mouse strains (Figure 5). The data suggest that the oral bioavailability of quizartinib was relatively high (33-51%) over 24 h in all three tested strains. Although the changes between the strains were very modest, the observed trends in the shifts were again in contrast with the assumption that mouse Cyp3a and human CYP3A4 limit the oral bioavailability of quizartinib, with ablation of mouse Cyp3a resulting in a small decrease in apparent bioavailability, and subsequent overexpression of human CYP3A4 resulting in a modest increase in apparent bioavailability. Perhaps (modest) secondary changes in expression of putative other detoxifying systems affecting quizartinib resulting from the engineered genetic modifications may have caused these minor shifts.

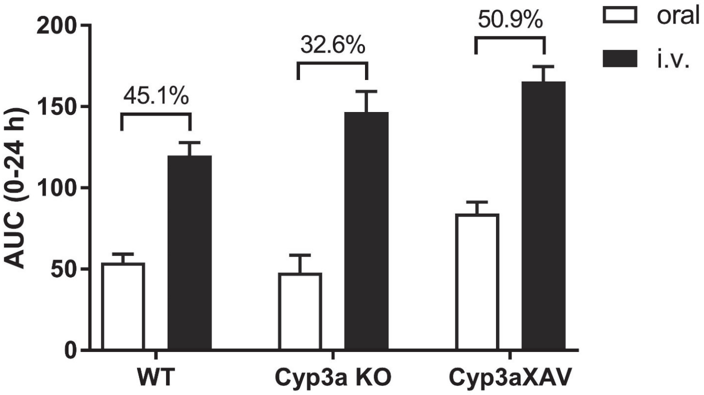

Figure 5. Oral and intravenous plasma AUC and oral bioavailability of quizartinib in female WT, Cyp3a KO and Cyp3aXAV mice over 24 h (n = 4-6). Percentage values indicate $AUC_{oral}/AUC_{i.v.}$ for each strain. The dose-normalized oral and i.v. plasma AUC_{0-24} was used.

4. Discussion

We found that quizartinib is moderately transported by hABCB1 and possibly slightly by mAbcg2, but not noticeably by hABCG2 *in vitro*. Consistent with a moderately transported Abcb1 substrate and a slightly transported Abcg2 substrate, the brain penetration of quizartinib in mice was clearly limited by the combined function of mAbcb1 and mAbcg2 (11.8-fold), and by single mAbcb1 activity as well (5.6-fold). Thus, both mAbcb1 and mAbcg2 can restrict brain accumulation of quizartinib in mice. mAbcb1 could fully compensate for the loss of mAbcg2 at the BBB, as *Abcg2*$^{-/-}$ and WT mice had similar quizartinib brain penetration levels. In contrast, mAbcg2 can only very partly take over the function of mAbcb1 at the BBB when mAbcb1 is absent. These data confirm that quizartinib is not only transported by mAbcb1 *in vivo*, but also by mAbcg2.

Somewhat unexpectedly, upon oral administration to mice, the absence of mAbcb1 resulted in a significantly, about 2-fold lower plasma AUC$_{0-8}$ in *Abcb1a/1b*$^{-/-}$ and *Abcb1a/1b;Abcg2*$^{-/-}$, but not *Abcg2*$^{-/-}$ mice. This suggests that loss of mouse Abcb1 (but not Abcg2) may perhaps secondarily cause compensatory upregulation of an alternative quizartinib elimination system or decrease of a quizartinib uptake system, resulting in decreased overall quizartinib exposure. It thus appears unlikely that Abcb1 and Abcg2 themselves in the intestine and/or liver can markedly reduce overall systemic uptake of quizartinib after oral administration, as this should have resulted in increased plasma levels upon ablation of these proteins. The nature of putative compensatorily altered detoxification system(s) responsible for the decreased systemic exposure to quizartinib in the Abcb1-deficient strains will be an interesting question for follow-up studies.

Our demonstration that quizartinib is clearly transported by hABCB1 *in vitro* and by mAbcb1 and mAbcg2 in the BBB of mice contrasts with a previous report suggesting that hABCB1 and hABCG2 overexpression caused no resistance, but instead substantial collateral sensitivity (8- and 5-fold, respectively) to quizartinib in the K562 myelogenous leukemia cell line [34]. It also contrasts with a report that hABCG2 does not confer significant resistance to quizartinib when overexpressed in H460 or HEK293 cell lines [35]. It may be that hABCG2 is only a poor transporter of quizartinib compared to the already modest transporter mAbcg2, and perhaps secondary changes in the hABCB1- and hABCG2-overexpressing K562 cells contributed to their increased sensitivity to quizartinib. Nonetheless, there can be little doubt that *in vivo* quizartinib is significantly transported by mAbcb1 and mAbcg2. The demonstration that quizartinib can directly interact with hABCB1 and hABCG2 through a number of assays including inhibition of transport of other drugs, and inhibition of photolabeling by a specific radioactive ligand of the transport proteins [34, 35] is in line with this, and suggests that these interactions occurred through competitive inhibition by transported quizartinib.

Looking at the collective data, one has to consider the possibility that ABCB1 and perhaps ABCG2 expression in AML cells may directly contribute to some level of resistance to quizartinib therapy, in which case it could be worthwhile to try and inhibit these transporters. Although Marzac et al. found that 22 out of 26 (85 %) patients with AML and FLT3-ITD did not express a functional ABCB1 [47], such patients do not appear to have significantly reduced ABCG2 mRNA [48, 49]. It will therefore be of interest to assess what fraction of FLT3-ITD AML patients might benefit from such an approach. Moreover, while CNS involvement is uncommon in AML among adults, in infants it is more frequent, and in such cases one could consider improving the CNS distribution of quizartinib using effective ABCB1 and ABCG2 inhibitors like elacridar, as previously demonstrated in mice for sunitinib [31]. In this respect it is worth noting that deficiency of mAbcb1 and mAbcg2 in mice resulted in quizartinib brain-to-plasma ratios of 1.1 (i.e., 110%), indicating a relatively good penetration of this drug into the brain once the BBB ABC efflux transporters were inactive.

There is very little publicly available information on the possible interaction of quizartinib with CYP3A, either *in vitro* or *in vivo*. In our 8 and 24 h oral experiments in Cyp3a knockout and Cyp3aXAV mice, we found there is some, most likely indirect, impact of mCyp3a and hCYP3A on the plasma levels and elimination of quizartinib in mice, with otherwise no significant effects on relative tissue distribution of the drug (Supplemental Figure 3 and 4). The plasma AUC in Cyp3a knockout mice was not significantly altered compared to WT mice in either the 8 h or 24 h oral experiment (Figure 4; Table 1 and 2) or in the 24 h i.v. experiment (Supplemental Figure 2; Table 2). However, in all tested conditions (oral 8 and 24 h, i.v. 8 h) the terminal elimination of quizartinib appeared to be significantly slower in the Cyp3a knockout mice (Figure 4 and Supplemental Figure 2), perhaps suggesting a limited role of mouse Cyp3a in the late elimination of quizartinib. Counterintuitively, the plasma AUC was increased in Cyp3aXAV mice compared to WT mice in the 8 h oral experiment (not significant, Table 1), 24 h oral experiment ($P < 0.001$, Table 2), and i.v. 24 h experiment ($P < 0.001$, Table 2). They were also increased relative to the $Cyp3a^{-/-}$ mice. This suggests that human CYP3A4 does not have a strong direct impact in reducing systemic availability of quizartinib, because then a decrease in plasma AUC would have been expected.

Collectively, these results suggest that loss of Cyp3a or overexpression of human CYP3A4 did not directly result in the predicted increase or decrease, respectively, of quizartinib availability in the case that CYP3A would be a dominant player in metabolizing quizartinib in mice. Rather, the data suggest that there is a secondary, perhaps compensatory, modulation of one or more other, as yet unidentified, quizartinib uptake or detoxification systems when CYP3A is removed or reintroduced, which is/are responsible for the modest pharmacokinetic changes that we observed between the strains. The most likely interpretation therefore is that CYP3A itself is not an important determinant of quizartinib pharmacokinetics in mice, but its absence or presence does affect activity of one or more other quizartinib detoxification systems. However, it is worth noting that we cannot exclude that, for instance, mouse Cyp2c enzymes, which are upregulated in $Cyp3a^{-/-}$ mice [50] may also metabolize quizartinib, thus potentially masking a more pronounced impact of CYP3A on quizartinib pharmacokinetics than suggested by our *in vivo* experiments.

In accordance with a limited direct impact of mCyp3a and human CYP3A4 on quizartinib metabolism in mice, we did not observe marked changes in absolute oral bioavailability between wild-type (45.1%), *Cyp3a*$^{-/-}$ (32.6%), and Cyp3aXAV (50.9%) mice (Figure 5). Interestingly, although the uptake rate of quizartinib after oral administration (for mice) is not very fast (t_{max} between 2 and 8 h), the oral availability is still quite good.

5. Conclusion

To the best of our knowledge, our study is the first to show that quizartinib can be transported by hABCB1, mAbcb1 and mAbcg2, and that the brain penetration of quizartinib, but not its oral availability, can be markedly limited by both mAbcb1 and mAbcg2. This could mean that it may be worthwhile to inhibit ABCB1 and ABCG2 with a pharmacological inhibitor when treating malignant lesions present in part or in whole behind the blood-brain barrier with quizartinib. Our *in vivo* experiments do not point to a prominent role of CYP3A in limiting the oral availability or tissue distribution of quizartinib, at least in mice, but we cannot exclude that there are significant changes in other quizartinib-detoxifying systems. Finally, the oral bioavailability of quizartinib in mice is quite high, in spite of a modest rate of net absorption. If this also applies in humans this could mean that there is a reduced risk of high CYP3A-related variation in exposure of this drug.

6. References

1. Siegel, R.L., K.D. Miller, and A. Jemal, Cancer statistics, 2017. CA: a cancer journal for clinicians, 2017. 67(1): p. 7-30.
2. Rowe, J.M. and M.S. Tallman, How I treat acute myeloid leukemia. Blood, 2010. 116(17): p. 3147-3156.
3. Meshinchi, S. and F.R. Appelbaum, Structural and functional alterations of FLT3 in acute myeloid leukemia. Clinical Cancer Research, 2009. 15(13): p. 4263-4269.
4. Gilliland, D.G. and J.D. Griffin, The roles of FLT3 in hematopoiesis and leukemia. Blood, 2002. 100(5): p. 1532-1542.
5. Levis, M. and D. Small, FLT3 tyrosine kinase inhibitors. International journal of hematology, 2005. 82(2): p. 100-107.
6. Döhner, H., D.J. Weisdorf, and C.D. Bloomfield, Acute myeloid leukemia. New England Journal of Medicine, 2015. 373(12): p. 1136-1152.
7. Thiede, C., et al., Analysis of FLT3-activating mutations in 979 patients with acute myelogenous leukemia: association with FAB subtypes and identification of subgroups with poor prognosis. Blood, 2002. 99(12): p. 4326-4335.
8. Schnittger, S., et al., Analysis of FLT3 length mutations in 1003 patients with acute myeloid leukemia: correlation to cytogenetics, FAB subtype, and prognosis in the AMLCG study and usefulness as a marker for the detection of minimal residual disease. Blood, 2002. 100(1): p. 59-66.
9. Kottaridis, P.D., et al., The presence of a FLT3 internal tandem duplication in patients with acute myeloid leukemia (AML) adds important prognostic information to cytogenetic risk group and response to the first cycle of chemotherapy: analysis of 854 patients from the United Kingdom Medical Research Council AML 10 and 12 trials. Blood, 2001. 98(6): p. 1752-1759.
10. Fleischmann, M., et al., Outcome of FLT3-ITD-positive acute myeloid leukemia: impact of allogeneic stem cell transplantation and tyrosine kinase inhibitor treatment. Journal of cancer research and clinical oncology, 2017. 143(2): p. 337-345.
11. Wattad, M., et al., Impact of salvage regimens on response and overall survival in acute myeloid leukemia with induction failure. Leukemia, 2017. 31(6): p. 1306-1313.
12. Schlenk, R., et al., Impact of pretreatment characteristics and salvage strategy on outcome in patients with relapsed acute myeloid leukemia. Leukemia, 2017.
13. Chevallier, P., et al., A new Leukemia Prognostic Scoring System for refractory/relapsed adult acute myelogeneous leukaemia patients: a GOELAMS study. Leukemia, 2011. 25(6): p. 939-944.
14. Wagner, K., et al., FLT3-internal tandem duplication and age are the major prognostic factors in patients with relapsed acute myeloid leukemia with normal karyotype. Haematologica, 2011. 96(5): p. 681-686.
15. Kindler, T., D.B. Lipka, and T. Fischer, FLT3 as a therapeutic target in AML: still challenging after all these years. Blood, 2010. 116(24): p. 5089-5102.
16. Benderra, Z., et al., MRP3, BCRP, and P-glycoprotein activities are prognostic factors in adult acute myeloid leukemia. Clinical cancer research, 2005. 11(21): p. 7764-7772.
17. Fiedler, W., et al., A phase I/II study of sunitinib and intensive chemotherapy in patients over 60 years of age with acute myeloid leukaemia and activating FLT3 mutations. British journal of haematology, 2015. 169(5): p. 694-700.
18. Serve, H., et al., Sorafenib in combination with intensive chemotherapy in elderly patients with acute myeloid leukemia: results from a randomized, placebo-controlled trial. Journal of Clinical Oncology, 2013. 31(25): p. 3110-3118.
19. Röllig, C., et al., Sorafenib versus placebo in addition to standard therapy in younger patients with newly diagnosed acute myeloid leukemia: results from 267 patients treated in the randomized placebo-controlled SAL-Soraml trial. 2014, Am Soc Hematology.
20. Baker, S.D., et al., Emergence of polyclonal FLT3 tyrosine kinase domain mutations during sequential therapy with sorafenib and sunitinib in FLT3-ITD–positive acute myeloid leukemia. Clinical Cancer Research, 2013. 19(20): p. 5758-5768.
21. Zarrinkar, P.P., et al., AC220 is a uniquely potent and selective inhibitor of FLT3 for the treatment of acute myeloid leukemia (AML). Blood, 2009. 114(14): p. 2984-2992.

22. Chao, Q., et al., Identification of N-(5-tert-butyl-isoxazol-3-yl)-N′-{4-[7-(2-morpholin-4-yl-ethoxy) imidazo [2, 1-b][1, 3] benzothiazol-2-yl] phenyl}C urea dihydrochloride (AC220), a uniquely potent, selective, and efficacious FMS-like tyrosine kinase-3 (FLT3) inhibitor. Journal of medicinal chemistry, 2009. 52(23): p. 7808-7816.
23. Kampa-Schittenhelm, K.M., et al., Quizartinib (AC220) is a potent second generation class III tyrosine kinase inhibitor that displays a distinct inhibition profile against mutant-FLT3,-PDGFRA and-KIT isoforms. Molecular cancer, 2013. 12(1): p. 19.
24. Cortes, J.E., et al., Phase I study of quizartinib administered daily to patients with relapsed or refractory acute myeloid leukemia irrespective of FMS-like tyrosine kinase 3–internal tandem duplication status. Journal of clinical oncology, 2013. 31(29): p. 3681-3687.
25. Sanga, M., et al., An open-label, single-dose, phase 1 study of the absorption, metabolism and excretion of quizartinib, a highly selective and potent FLT3 tyrosine kinase inhibitor, in healthy male subjects, for the treatment of acute myeloid leukemia. Xenobiotica, 2017. 47(10): p. 856-869.
26. Taylor, S.J., et al., Preventing chemotherapy-induced myelosuppression by repurposing the FLT3 inhibitor quizartinib. Science translational medicine, 2017. 9(402): p. eaam8060.
27. Borst, P. and R.O. Elferink, Mammalian ABC transporters in health and disease. Annual review of biochemistry, 2002. 71(1): p. 537-592.
28. Schinkel, A.H. and J.W. Jonker, Mammalian drug efflux transporters of the ATP binding cassette (ABC) family: an overview. Advanced drug delivery reviews, 2003. 55(1): p. 3-29.
29. Vlaming, M.L., J.S. Lagas, and A.H. Schinkel, Physiological and pharmacological roles of ABCG2 (BCRP): recent findings in Abcg2 knockout mice. Advanced drug delivery reviews, 2009. 61(1): p. 14-25.
30. Tang, S.C., et al., Impact of P-glycoprotein (ABCB1) and breast cancer resistance protein (ABCG2) gene dosage on plasma pharmacokinetics and brain accumulation of dasatinib, sorafenib, and sunitinib. Journal of Pharmacology and Experimental Therapeutics, 2013. 346(3): p. 486-494.
31. Tang, S.C., et al., Brain accumulation of sunitinib is restricted by P-glycoprotein (ABCB1) and breast cancer resistance protein (ABCG2) and can be enhanced by oral elacridar and sunitinib coadministration. International journal of cancer, 2012. 130(1): p. 223-233.
32. Lagas, J.S., et al., Breast cancer resistance protein and P-glycoprotein limit sorafenib brain accumulation. Molecular cancer therapeutics, 2010. 9(2): p. 319-326.
33. Tang, S.C., et al., P-glycoprotein (ABCB1) and breast cancer resistance protein (ABCG2) restrict brain accumulation of the active sunitinib metabolite N-desethyl sunitinib. Journal of Pharmacology and Experimental Therapeutics, 2012. 341(1): p. 164-173.
34. Bhullar, J., et al., The FLT3 inhibitor quizartinib inhibits ABCG2 at pharmacologically relevant concentrations, with implications for both chemosensitization and adverse drug interactions. PloS one, 2013. 8(8): p. e71266.
35. Li, J., et al., Quizartinib (AC220) reverses ABCG2-mediated multidrug resistance: In vitro and in vivo studies. Oncotarget, 2017. 8(55): p. 93785-93799.
36. Guengerich, F.P., Human cytochrome P450 enzymes, in Cytochrome P450. 1995, Springer. p. 473-535.
37. Zanger, U.M. and M. Schwab, Cytochrome P450 enzymes in drug metabolism: regulation of gene expression, enzyme activities, and impact of genetic variation. Pharmacology & therapeutics, 2013. 138(1): p. 103-141.
38. van Waterschoot, R.A., et al., Intestinal cytochrome P450 3A plays an important role in the regulation of detoxifying systems in the liver. The FASEB Journal, 2009. 23(1): p. 224-231.
39. van Hoppe, S., et al., Breast cancer resistance protein (BCRP/ABCG2) and P-glycoprotein (P-gp/ABCB1) transport afatinib and restrict its oral availability and brain accumulation. Pharmacological research, 2017. 120: p. 43-50.
40. Retmana, I.A., et al., Liquid chromatography-tandem mass spectrometric assay for the quantitative determination of the tyrosine kinase inhibitor quizartinib in mouse plasma using salting-out liquid-liquid extraction. Journal of Chromatography B, 2017. 1061: p. 300-305.
41. Durmus, S., et al., Oral availability and brain penetration of the B-RAFV600E inhibitor vemurafenib can be enhanced by the P-GLYCOprotein (ABCB1) and breast cancer resistance protein (ABCG2) inhibitor elacridar. Molecular pharmaceutics, 2012. 9(11): p. 3236-3245.

42. Schinkel, A.H., et al., Normal viability and altered pharmacokinetics in mice lacking mdr1-type (drug-transporting) P-glycoproteins. Proceedings of the National Academy of Sciences, 1997. 94(8): p. 4028-4033.
43. Jonker, J.W., et al., The breast cancer resistance protein protects against a major chlorophyll-derived dietary phototoxin and protoporphyria. Proceedings of the National Academy of Sciences, 2002. 99(24): p. 15649-15654.
44. Jonker, J.W., et al., Contribution of the ABC transporters Bcrp1 and Mdr1a/1b to the side population phenotype in mammary gland and bone marrow of mice. Stem cells, 2005. 23(8): p. 1059-1065.
45. van Herwaarden, A.E., et al., Knockout of cytochrome P450 3A yields new mouse models for understanding xenobiotic metabolism. The Journal of clinical investigation, 2007. 117(11): p. 3583-3592.
46. Zhang, Y., et al., PKSolver: An add-in program for pharmacokinetic and pharmacodynamic data analysis in Microsoft Excel. Computer methods and programs in biomedicine, 2010. 99(3): p. 306-314.
47. Marzac, C., et al., Flt3 internal tandem duplication and P-glycoprotein functionality in 171 patients with acute myeloid leukemia. Clinical Cancer Research, 2006. 12(23): p. 7018-7024.
48. Schaich, M., et al., MDR1 and MRP1 gene expression are independent predictors for treatment outcome in adult acute myeloid leukaemia. British journal of haematology, 2005. 128(3): p. 324-332.
49. Nasilowska-Adamska, B., et al., FLT3-ITD and MLL-PTD influence the expression of MDR-1, MRP-1, and BCRP mRNA but not LRP mRNA assessed with RQ-PCR method in adult acute myeloid leukemia. Annals of hematology, 2014. 93(4): p. 577-593.
50. van Waterschoot, R.A., et al., Midazolam metabolism in cytochrome P450 3A knockout mice can be attributed to up-regulated CYP2C enzymes. Molecular pharmacology, 2008. 73(3): p. 1029-1036.

7. Supplemental materials

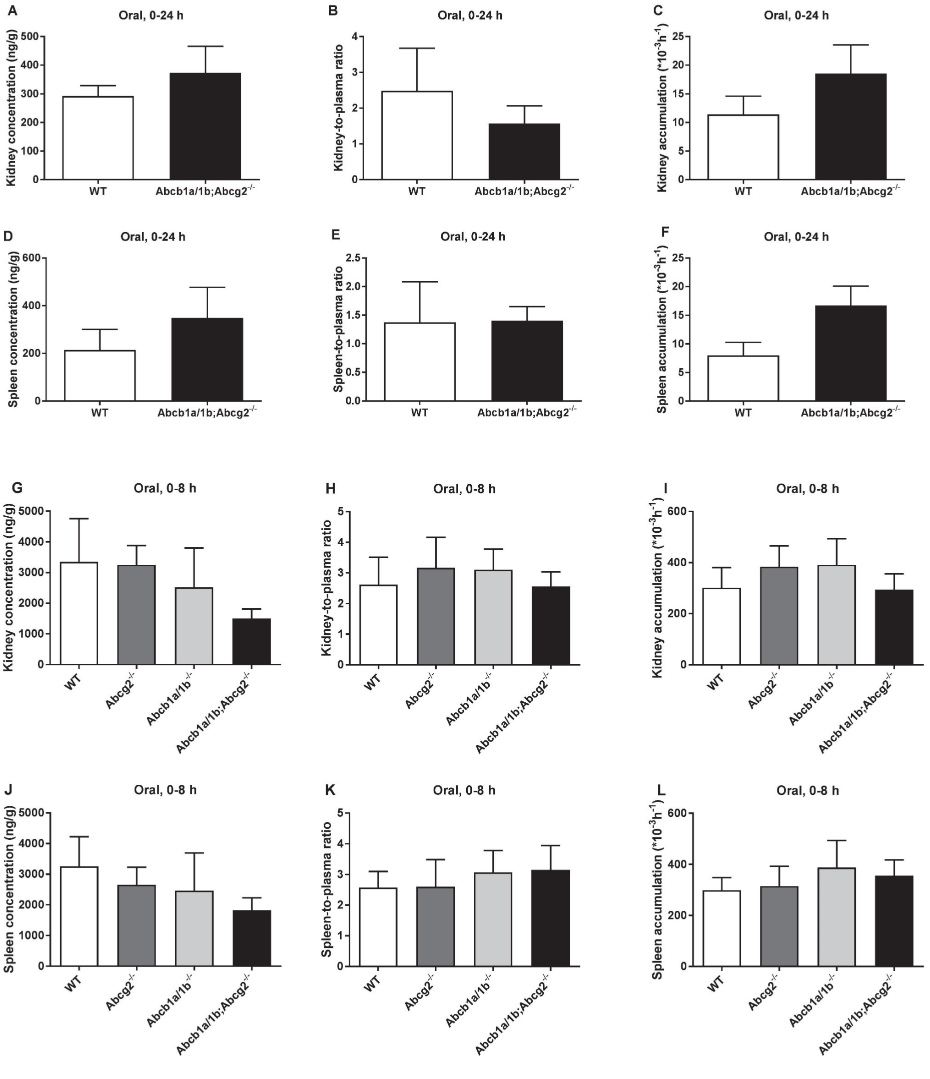

Supplemental Figure 1. A-F: kidney and spleen concentration (A, D), tissue-to-plasma ratio (B, E) and tissue accumulation (C, F) of quizartinib in female WT and *Abcb1a/1b;Abcg2*$^{-/-}$ mice at 24 h after oral administration of quizartinib at 10 mg/kg (n = 4-6). G-L: kidney and spleen concentration (G, J), tissue-to-plasma ratio (H, K) and tissue accumulation (I, L) of quizartinib in female WT, *Abcg2*$^{-/-}$, *Abcb1a/1b*$^{-/-}$ and *Abcb1a/1b;Abcg2*$^{-/-}$ mice 8 h after oral administration of quizartinib at 10 mg/kg (n = 4-6). $P > 0.05$.

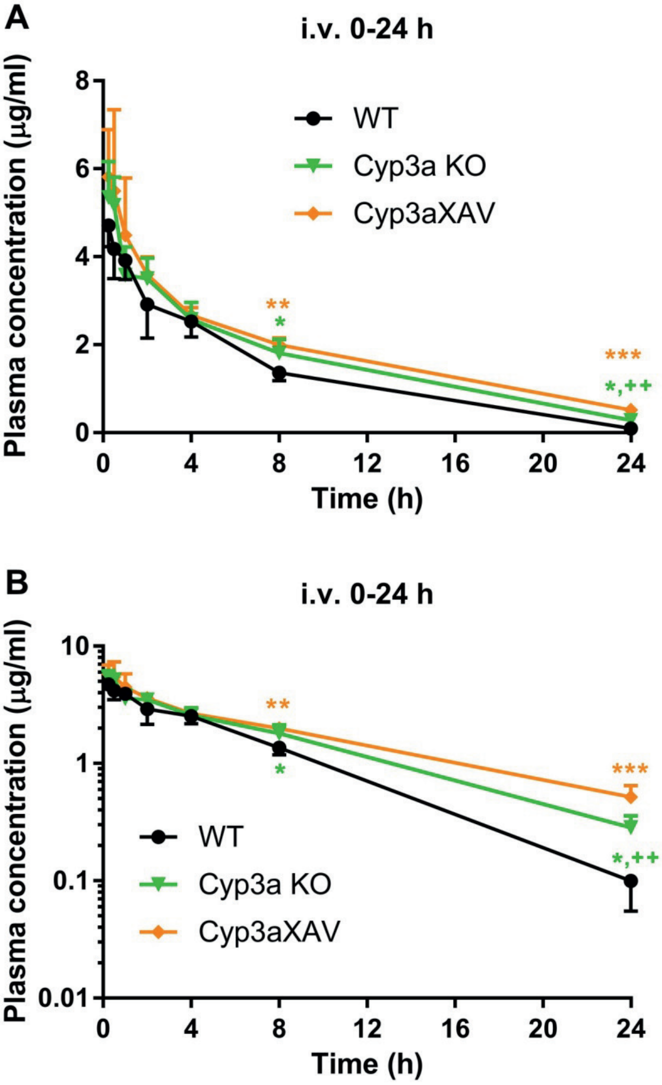

Supplemental Figure 2. Plasma concentration-time curves (A) and semi-log plots of plasma concentration-time curves (B) of quizartinib in female WT, Cyp3a KO and Cyp3aXAV mice over 24 h after intravenous injection of 5 mg/kg quizartinib. Data are given as mean ± S.D. (n = 4-6). *, $P < 0.05$; **, $P < 0.01$; ***, $P < 0.001$ compared to WT mice. $^{+}$, $P < 0.05$; $^{++}$, $P < 0.01$; $^{+++}$, $P < 0.001$ compared to Cyp3aXAV mice.

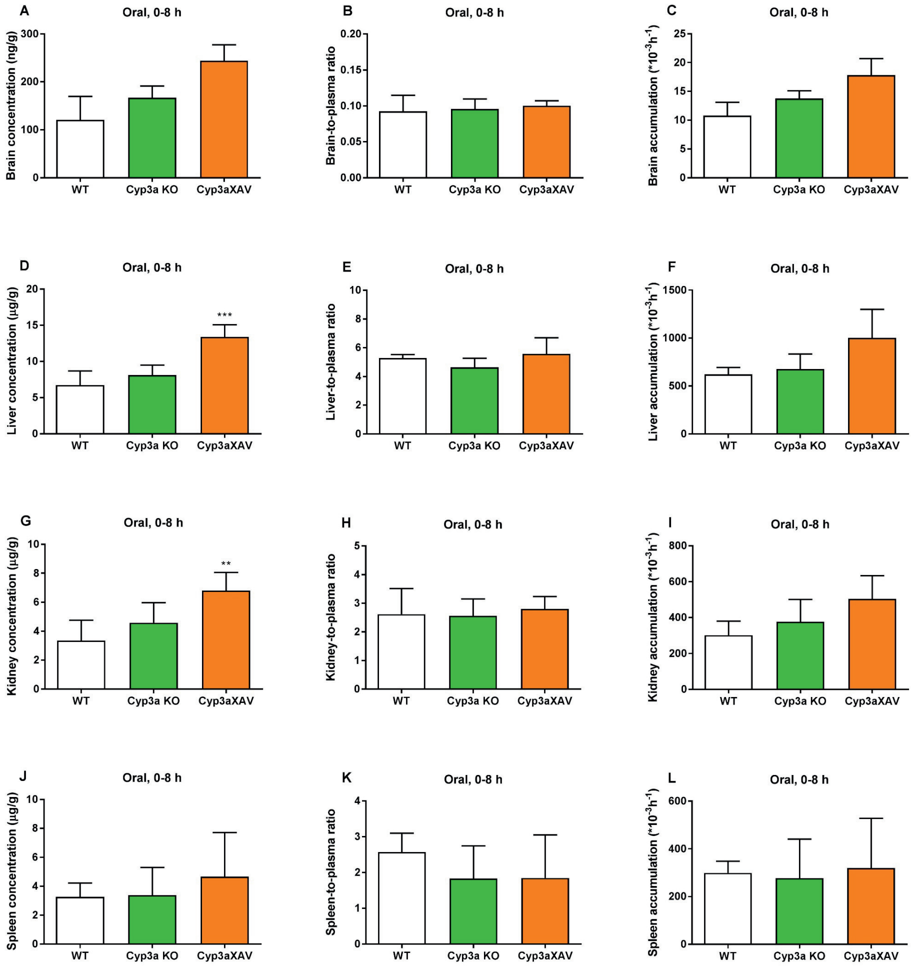

Supplemental Figure 3. Tissue concentration (A, D, G, J), tissue-to-plasma ratio (B, E, H, K) and tissue accumulation (C, F, I, L) of quizartinib in female WT, Cyp3a KO and Cyp3aXAV mice 8 h after oral administration of 10 mg/kg quizartinib (n = 4-6). *, $P < 0.05$; **, $P < 0.01$; ***, $P < 0.001$ compared to WT mice.

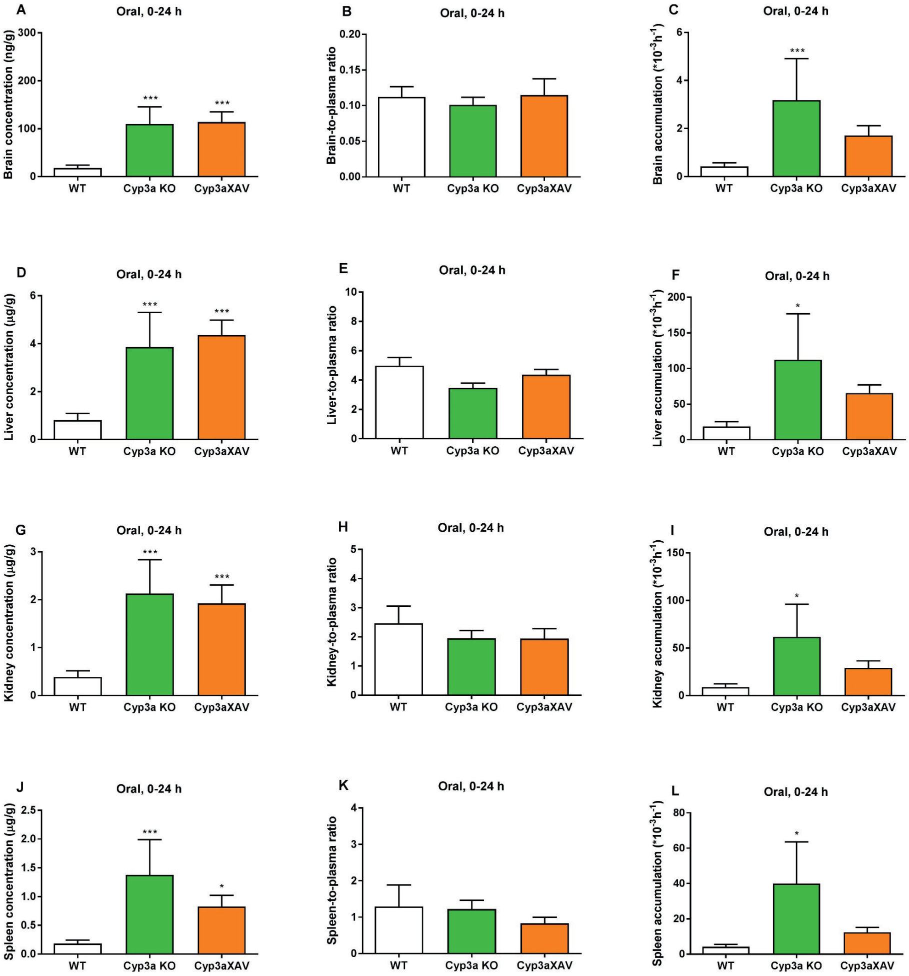

Supplemental Figure 4. Tissue concentration (A, D, G, J), tissue-to-plasma ratio (B, E, H, K) and tissue accumulation (C, F, I, L) of quizartinib in female WT, Cyp3a KO and Cyp3aXAV mice 24 h after oral administration of 10 mg/kg quizartinib (n = 4-6). *, $P < 0.05$; **, $P < 0.01$; ***, $P < 0.001$ compared to WT mice.

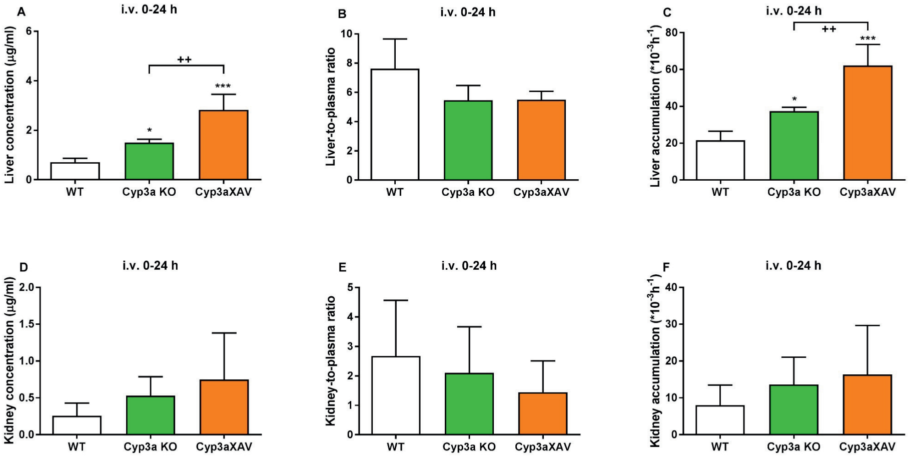

Supplemental Figure 5. Kidney and spleen concentration (A, D), tissue-to-plasma ratio (B, E) and tissue accumulation (C, F) of quizartinib in female WT and *Abcb1a/1b;Abcg2*$^{-/-}$ mice at 24 h after intravenously administered of quizartinib at 5 mg/kg (n = 4-6). *, $P < 0.05$; **, $P < 0.01$; ***, $P < 0.001$ compared to WT mice. $^{+}$, $P < 0.05$; $^{++}$, $P < 0.01$; $^{+++}$, $P < 0.001$ compared to Cyp3aXAV mice.

Supplemental Table 1. Plasma pharmacokinetic parameters and brain concentration 24 h after oral administration of 10 mg/kg quizartinib to female WT and *Abcb1a/1b;Abcg2*$^{-/-}$ mice.

Parameter	Genotype	
	WT	*Abcb1a/1b;Abcg2*$^{-/-}$
Plasma $AUC_{0\text{-}24}$ (h*μg/ml)	26.6 ± 6.0	20.4 ± 3.4
Fold change $AUC_{0\text{-}24}$	1	0.77
Plasma $AUC_{0\text{-}8}$ (h*μg/ml)	8.9 ± 2.3	5.8 ± 0.8 *
Fold change $AUC_{0\text{-}8}$	1	0.65
C_{max} (μg/ml)	2.0 ± 0.4	1.6 ± 0.3
t_{max} (h)	2-8	8
C_{brain} (ng/g)	17.6 ± 9.5	312.7 ± 78.9 ***
Fold change C_{brain}	1	17.8
Brain-to-plasma ratio	0.11 ± 0.01	1.28 ± 0.26 ***
Fold change ratio	1	12.0
P_{brain} ($*10^{-3}h^{-1}$)	0.6 ± 0.2	15.3 ± 2.8 ***
Fold change P_{brain}	1	24.1

Data are given as mean ± S.D. (n = 4-6). C_{max}, maximum concentration in plasma (range for individual mice); t_{max}, time point (h) of maximum plasma concentration; C_{brain}, brain concentration; P_{brain}, brain accumulation. *, $P < 0.05$; **, $P < 0.01$; ***, $P < 0.001$ compared to WT mice.

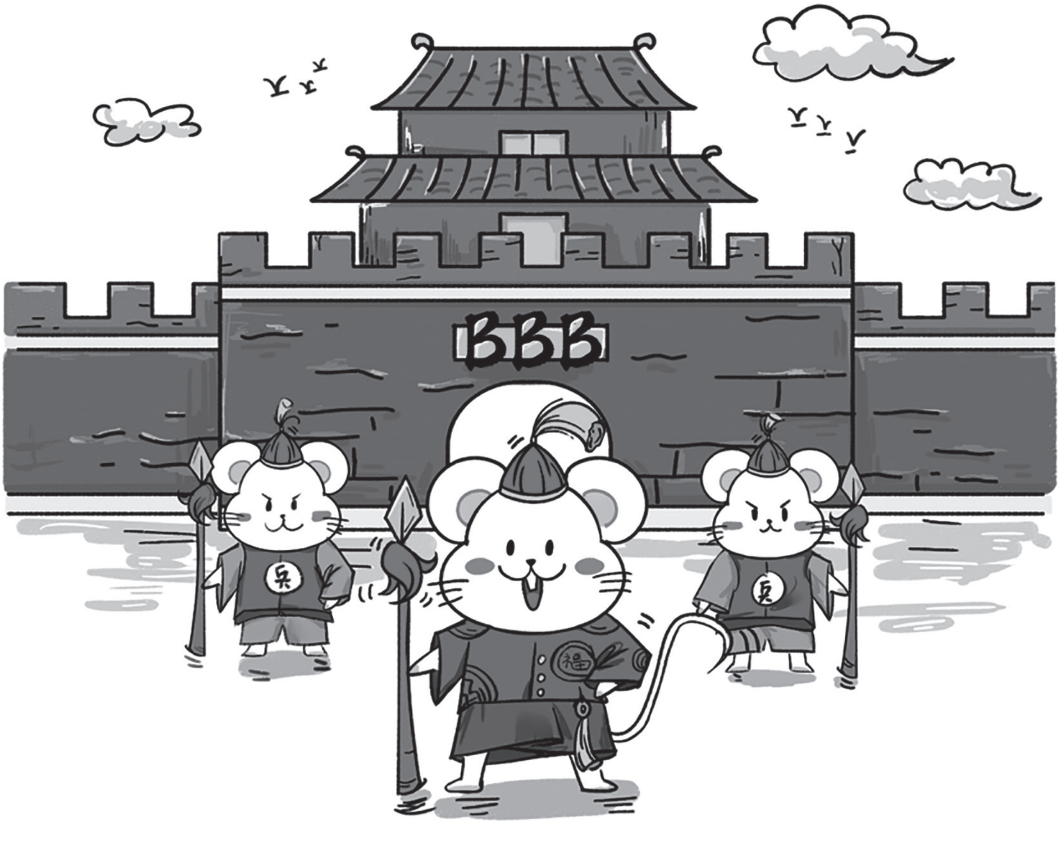
BBB
兵
福
兵

Chapter 4

Brain accumulation of tivozanib is restricted by ABCB1 (P-glycoprotein) and ABCG2 (breast cancer resistance protein) in mice

Jing Wang
Maaike A. C. Bruin
Changpei Gan
Maria C. Lebre
Hilde Rosing
Jos H. Beijnen
Alfred H. Schinkel

International Journal of Pharmaceutics, 2020, 581: 119277.

Abstract

Tivozanib is a potent and selective inhibitor of VEGFR1-3, recently approved by the EMA for first-line treatment of renal cell carcinoma. We used wild-type, knockout, and transgenic mouse strains to study the effects of the drug transporters ABCB1, ABCG2, and OATP1A/1B, and of the CYP3A enzymes on the oral availability and tissue distribution of tiavozanib. Tivozanib was transported by human ABCB1 and mouse Abcg2 in polarized MDCK-II cells. Upon oral administration, tivozanib showed rapid absorption and the plasma concentration-time curves showed secondary peaks in all mouse strains, suggesting enterohepatic recirculation. The brain-to-plasma ratios were significantly increased in *Abcb1a/1b*$^{-/-}$ (2.2-fold) and *Abcb1a/1b;Abcg2*$^{-/-}$ (2.6-fold) mice compared to wild-type mice, indicating a modest protective role of these transporters in the blood-brain barrier. *Slco1a/1b*$^{-/-}$ mice showed a 1.2-fold lower liver-to-plasma ratio than wild-type mice, suggesting a minor role of mOatp1a/1b in tivozanib liver distribution. Oral plasma pharmacokinetics of tivozanib was not significantly altered in these mouse strains, nor in Cyp3a knockout and CYP3A4-humanized mice. The modest effect of ABC transporters on tivozanib brain accumulation, if also true in humans, might mean that this drug is not strongly limited in its therapeutic efficacy against malignant lesions situated partly or completely behind the blood-brain barrier.

Keywords: Tivozanib, ABCB1, ABCG2, Oatp1a/1b, CYP3A enzymes, brain penetration

Graphical abstract:

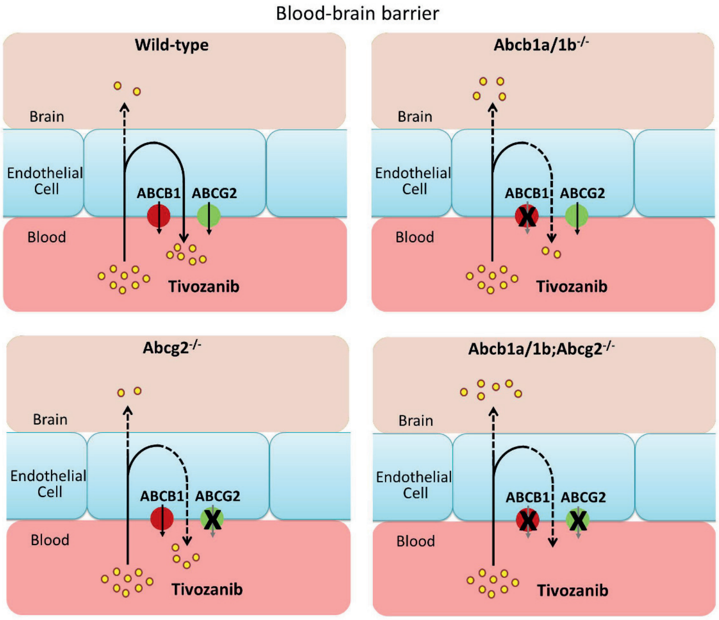
Blood-brain barrier
Wild-type
Brain
Endothelial Cell
ABCB1
ABCG2
Blood
Tivozanib
Abcb1a/1b-/-
Brain
Endothelial Cell
ABCB1
ABCG2
Blood
Tivozanib
Abcg2-/-
Brain
Endothelial Cell
ABCB1
ABCG2
Blood
Tivozanib
Abcb1a/1b;Abcg2-/-
Brain
Endothelial Cell
ABCB1
ABCG2
Blood
Tivozanib

1. Introduction

Renal cell carcinoma (RCC) is the most common type of kidney cancer, originating in the lining of the renal proximal convoluted tubule. It accounts for 90-95% of neoplasms arising from the kidney and for 2% to 3% of all adult malignancies [1]. In RCC, overexpression of vascular endothelial growth factor (VEGF) and platelet-derived growth factor promotes neoangiogenesis, which contributes to the development and progression of RCC. About 25-30% of patients have metastatic disease at diagnosis, the most common sites being lung (45%), bone (30%), lymph nodes (22%), liver (20%), adrenal (9%) and brain (9%) [2, 3].

Tivozanib (Fotivda, AV-951) is an oral, once-daily administered, VEGF receptor tyrosine kinase inhibitor (TKI). It has a long half-life and is a potent and selective inhibitor of all three VEGF receptors (VEGFR1-3), inhibiting angiogenesis and reducing the vascular permeability in tumor tissues. Tivozanib has been investigated in several tumor types, including renal cell, hepatocellular, colorectal and breast cancers. In August 2017, tivozanib was approved by the European Medicines Agency (EMA) for the first-line treatment of adult patients with advanced RCC and for adult patients who are VEGFR and mTOR pathway inhibitor-naive following disease progression after one prior treatment with cytokine therapy for advanced RCC [4]. One Phase III study showed that tivozanib was generally well tolerated, and significantly improved progression-free survival (PFS) compared with sorafenib (VEGFR inhibitor) in patients with metastatic RCC [5].

Transmembrane transporters can be major determinants of the pharmacokinetic, safety and efficacy profiles of drugs. Two major superfamilies - ATP-binding cassette (ABC) and solute carrier (SLC) transporters - have been annotated in the human genome. Many of these transporters have been cloned, characterized and localized to tissues and cellular membrane domains in the human body [6]. Multispecific efflux transporters of the ABC superfamily, like P-glycoprotein (P-gp; ABCB1) and breast cancer resistance protein (BCRP; ABCG2) are localized in the canalicular membranes of hepatocytes and in the apical membrane of epithelial cells of the intestinal tract and kidney; their distribution at these membrane locations allows these transporters to pump their substrates into bile, feces, and urine, respectively. They can thus potentially limit intestinal absorption of their substrates or mediate their direct intestinal, hepatobiliary, or renal excretion. ABCB1 and ABCG2 are also present at pharmacological sanctuary site barriers such as the blood-brain barrier (BBB), where they can pump their substrates back into the blood [7-9]. As a consequence, limited exposure of the brain to anticancer drugs due to these transporters may reduce their therapeutic efficacy, especially against brain metastases [10, 11]. One study showed that the ABCG2 mRNA expression was about 1.7-fold higher in clear cell RCC (ccRCC) tissue compared to non-tumor tissue, however, the ABCB1 mRNA expression was decreased in ccRCC compared to non-tumor tissue, and higher ABCB1 expression was associated with prolonged patient survival [12]. The underlying mechanism for this association is unknown.

Organic anion transporting polypeptides (human: OATP, gene *SLCO*; rodents: Oatp, gene *Slco*) are primarily uptake transporters, which can have profound roles in drug disposition and in drug-drug and drug-food interactions. For instance, the OATP1A and 1B subfamilies are expressed mainly in pharmacokinetically relevant tissues like liver, kidney and small intestine in both human and mice. They are believed to be important in the absorption, distribution and elimination of many drugs including anticancer drugs, antibiotics, statins and cardiac glycosides [13-15].

The cytochrome P450 system (CYP) is of particular relevance for drug-metabolizing enzymes. CYP3A is the most abundant subfamily highly expressed in human liver and small intestine, and it plays a significant role in the oxidative metabolism of approximately half of the drugs in current clinical use [16, 17]. As CYP3A can display a high degree of inter- and intra-individual activity, it is a major player in variable drug exposure [18, 19].

In this study we aimed to investigate whether tivozanib is transported by ABCB1 and ABCG2 *in vitro*, and to establish the individual and combined effects of the ABCB1, ABCG2, and OATP1A/1B drug transporters on the oral availability and tissue distribution of tivozanib using wild-type and transporter knockout mouse strains. We also studied to what extent mouse and human CYP3A can impact on the oral availability of tivozanib using Cyp3a knockout mice and transgenic mice.

2. Material and methods

2.1. Chemicals

Tivozanib free base (>99%, M_w = 454.9 g/mol) was obtained from Carbosynth (Compton, Berkshire, UK). Zosuquidar was obtained from Sequoia Research Products (Pangbourne, UK), and Ko143 was from Tocris Bioscience (Bristol, UK). Bovine Serum Albumin (BSA) Fraction V was obtained from Roche Diagnostics (Mannheim, Germany). Heparin (5000 IU ml^{-1}) was from Leo Pharma (Breda, The Netherlands), isoflurane was purchased from Pharmachemie (Haarlem, The Netherlands). Bovine Serum Albumin (BSA) Fraction V from Roche (Mannheim, Germany). All other chemicals and reagents were obtained from Sigma-Aldrich (Steinheim, Germany). All chemicals used in the tivozanib assay were described before [20].

2.2. Transport assays

Polarized Madin-Darby Canine Kidney (MDCK-II) cell lines transduced with either human (h)ABCB1, hABCG2 or mouse (m)Abcg2 cDNA were used (passage 10-20 after clonal selection) and cultured as described previously [21]. Transepithelial transport assays were performed on microporous polycarbonate membrane filters (3.0 mm pore size, 12 mm diameter, Transwell 3402, Corning Incorporated, Kennebunk, ME). In short, cells were allowed to grow an intact monolayer in 3 days, which was monitored with transepithelial electrical resistance (TEER) measurements, both before and after the transport phase. On the third day, if applicable, cells were pre-incubated with one or more of the inhibitors for 1 h, where 5 µM zosuquidar (ABCB1 inhibitor) and/or 5 µM Ko143 (ABCG2/Abcg2 inhibitor) were added to both apical and basolateral compartments. The transport phase was initiated (t = 0) by replacing the medium in both compartments with fresh Dulbecco's Modified Eagle's medium (DMEM medium) including 10% fetal bovine serum (FBS) and 2 µM tivozanib, as well as the appropriate inhibitor(s). Cells were kept at 37°C in 5% (v/v) CO_2 during the experiment, and at 1, 2, 4 and 8 hours, 50 µl samples were taken from the acceptor compartment, and stored at -30°C until LC-MS/MS analysis. The amount of transported drug was calculated after correction for volume loss due to sampling at each time point. Active transport was expressed using the transport ratio (*r)*, which is defined as the amount of apically directed drug transport divided by basolaterally directed drug translocation at a defined time point.

2.3. Animals

Mice (*Mus musculus*) were bred in the Netherlands Cancer Institute and housed and handled according to institutional guidelines complying with Dutch and EU legislation. Animals used were female WT, *Abcb1a/1b*$^{-/-}$ [22], *Abcg2*$^{-/-}$ [23], *Abcb1a/1b;Abcg2*$^{-/-}$ [24], *Cyp3a*$^{-/-}$ [25] and Slco*1a/1b*$^{-/-}$ [15] mice of a >99% FVB/N strain background. Homozygous CYP3A4 humanized transgenic mice (Cyp3aXAV) were generated by cross-breeding of transgenic mice with stable human CYP3A4 expression in liver or intestine, respectively, in a *Cyp3a*$^{-/-}$ background [25]. All the mice used were between 9 and 14 weeks of age, and generally between 23 and 35 gram of body weight. Animals were kept in a temperature-controlled environment with a 12 h light/12 h dark cycle and received a standard diet (Transbreed, SDS Diets, Technilab-BMI) and acidified water *ad libitum*. Depending on the type of experiment, between 4 and 6 mice were tested in each experimental group. All experiments were reviewed and approved by the Institutional Animal Care and Use Committee (IACUC).

2.4. Drug solutions

Tivozanib stock solution in dimethyl sulfoxide (DMSO) at a concentration of 5 mg/ml was stored at -30˚C, and additionally 2:3 (v/v) diluted with a mixture of polysorbate 80/ethanol (1:1, v/v). It was then further diluted with 5% (w/v) glucose in water to yield a working concentration of 0.1 mg/ml. The final tivozanib solution in water contains 2% DMSO, 1.5% (v/v) polysorbate 80, 1.5% (v/v) ethanol, and 4.75% (w/v) glucose. All working solutions were freshly prepared on the day of the experiment.

2.5. Plasma and tissue pharmacokinetics of tivozanib

To minimize variation in absorption, mice were fasted for about 3 h before tivozanib was administered by gavage into the stomach (n = 5-7), using a blunt-ended needle. For the 24 or 8 hour experiments, 50 µl blood samples were collected from the tail vein at 5 min, 30 min, 1, 2, 4 and 8 h or 5 min, 30 min, 1, 2 and 4 h, respectively, using heparin-coated capillaries (Sarstedt, Germany). At 24 or 8 h, mice were anesthetized with isoflurane and blood was collected by cardiac puncture. The mice were then sacrificed by cervical dislocation, and the brain and a set of other tissues were rapidly removed, weighed and rapidly frozen at −30˚C. Organs were homogenized on ice in appropriate volumes of 4% (w/v) BSA in water using a FastPrep®-24 device (MP Biomedicals, SA, California, USA), and then stored at −30°C until analysis. Blood samples were centrifuged at 9,000 *g* for 6 min at 4°C immediately after collection, and plasma was collected and stored at −30°C until analysis.

2.6. LC-MS/MS analysis

Tivozanib concentrations in cell culture medium, plasma and tissue homogenates were analyzed with a previously reported liquid-chromatography tandem mass spectrometric (LC-MS/MS) assay, using a deuterated internal standard [20].

2.7. Pharmacokinetic and statistics calculations

Pharmacokinetic parameters were calculated by the software GraphPad Prism7 (GraphPad Software Inc., La Jolla, CA, USA). Ordinary one-way analysis of variance (ANOVA) was used to determine significance of differences between groups, after which post-hoc tests with Tukey correction were performed for comparison between individual groups. The two-sided unpaired Student's t test was used when treatments or differences between two groups were compared. The area under the plasma concentration-time curve (AUC) was calculated using the trapezoidal rule with the Microsoft Excel plug in PKsolver [26], without extrapolating to infinity. The peak plasma concentration (C_{max}) and the time to reach C_{max} (t_{max}) were estimated from the original data. Differences were considered statistically significant when $P < 0.05$. Data are presented as mean ± SD with each experimental group containing 5-7 mice.

3. Results

3.1. Tivozanib is moderately transported by hABCB1 and mAbcg2 in vitro

We analyzed tivozanib (2 μM) transport across polarized monolayers of Madin-Darby Canine Kidney (MDCK-II) cell lines stably transduced with hABCB1, hABCG2 or mAbcg2 cDNAs. The parental MDCK-II cell line did not show apically directed transport (Figure 1A, r = 0.8) and addition of the potent ABCB1 inhibitor zosuquidar did not change this result (Figure 1B, r = 0.9). This indicates that endogenously present canine ABCB1 did not noticeably transport tivozanib in the parental cells. In the hABCB1 overexpressing cells, we observed modest apically directed transport of tivozanib (Figure 1C, r = 1.8), which was effectively inhibited by addition of zosuquidar (Figure 1D, r = 1.1). To evaluate the interaction between ABCG2 and tivozanib, zosuquidar was added to inhibit any endogenous canine ABCB1 in experiments with MDCK-II cells overexpressing hABCG2 and mAbcg2. In the hABCG2 subclone we did not detect active transport of tivozanib and addition of Ko143 did not alter this profile (respective r = 1.0 and 0.8, Figure 1E and F). However, mAbcg2 modestly transported tivozanib in the apical direction (Figure 1G, r = 1.8), and this transport was completely abrogated by treatment with the ABCG2 inhibitor Ko143 (Figure 1H, r = 1.0). Overall, tivozanib appears to be modestly transported by hABCB1 and mAbcg2 *in vitro*.

3.2. Brain accumulation of tivozanib was limited by mAbcb1 and mAbcg2 activity after oral administration

Tivozanib is orally administered to patients at a dose of 1.5 mg/d. To allow sensitive detection in tissues, mice received tivozanib by oral gavage into the stomach at a relatively higher dose of 1 mg/kg, yielding maximal plasma levels that were about 5-fold higher than steady state levels in chronically treated patients. We first performed a pilot study using female wild-type (WT) and combination mAbcb1a/1b and mAbcg2 knockout mice, analyzing tivozanib oral availability and tissue disposition over 24 h. As shown in Figure 2A and Table 1, oral absorption of tivozanib was rapid, with the highest concentrations observed 30 minutes after dosing. The plasma concentration-time curves showed secondary plasma peaks in individual mice, resulting in plateau-like exposure levels between 0.5 and 8 h. The plasma $AUC_{0\text{-}24h}$ revealed no significant differences in tivozanib oral availability between WT and *Abcb1a/1b;Abcg2*$^{-/-}$ mice. Moreover, the semi-log plot of the plasma concentrations showed similar elimination rates of tivozanib between 8-24 h in these two mouse strains (Supplemental Figure 1A).

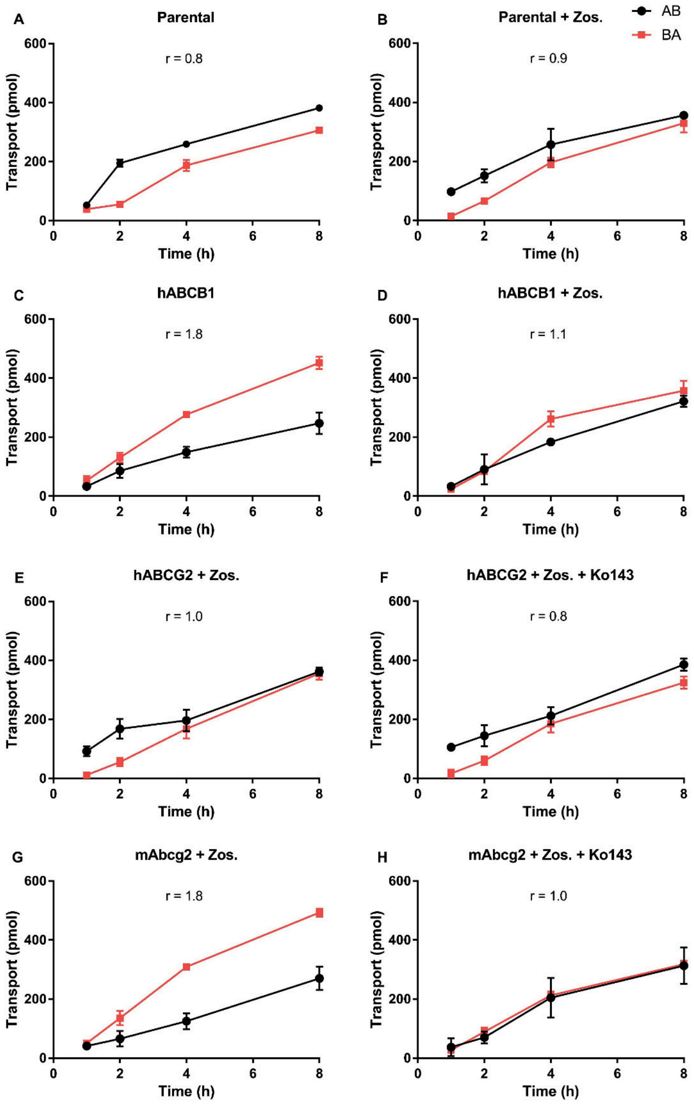

Figure 1. Transepithelial transport of tivozanib (2 μM) assessed in MDCK-II cells either non-transduced (A, B), or transduced with hABCB1 (C, D), hABCG2 (E, F) or mAbcg2 (G, H) cDNA. At t = 0 h, tivozanib was applied in the donor compartment and the concentrations in the acceptor compartment at t = 1, 2, 4 and 8 h were measured and plotted as tivozanib transport (pmol) in the graph (n = 3). B, D–H: Zos. (zosuquidar, 5 μM) was applied to inhibit endogenous and/or human canine ABCB1. F and H: the ABCG2 inhibitor Ko143 (5 μM) was applied to inhibit ABCG2/Abcg2–mediated transport. r, relative transport ratio at 8 h. BA (■), translocation from the basolateral to the apical compartment; AB (●), translocation from the apical to the basolateral compartment. Points, mean; bars, S.D.

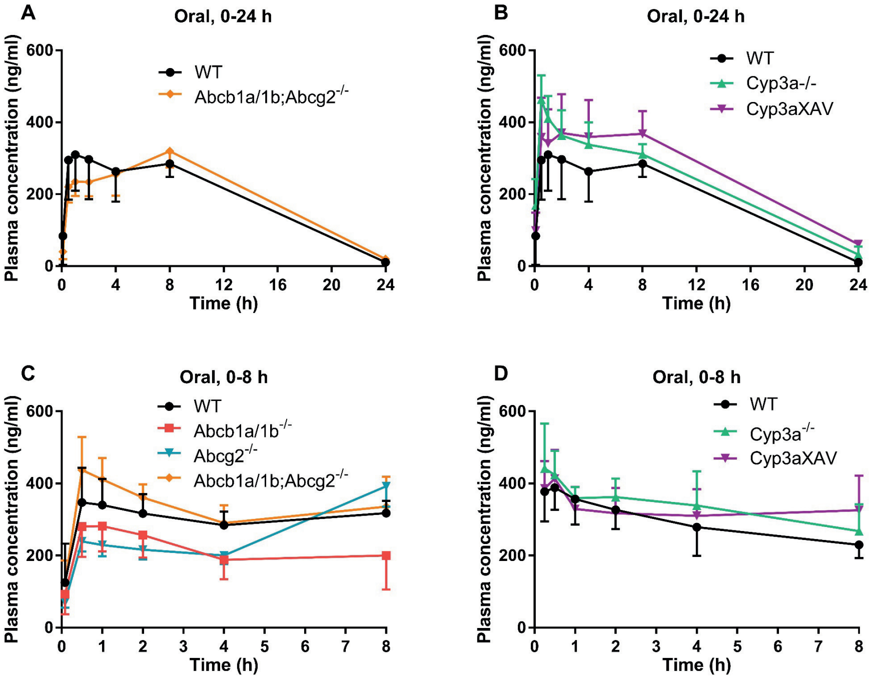

Figure 2. Plasma concentration-time curves of tivozanib in female mice after oral administration of 1 mg/kg tivozanib. Data are given as mean ± S.D. (n = 5-7). A: 0-24 h experiment in WT and *Abcb1a/1b;Abcg2*$^{-/-}$ mice. B: 0-24 h experiment in WT, *Cyp3a*$^{-/-}$, and Cyp3aXAV mice. C: 0-8 h experiment in WT, *Abcb1a/1b*$^{-/-}$, *Abcg2*$^{-/-}$ and *Abcb1a/1b;Abcg2*$^{-/-}$ mice. D: 0-8 h experiment in WT, *Cyp3a*$^{-/-}$, and Cyp3aXAV mice.

Table 1. Plasma pharmacokinetic parameters and tissue concentrations over 24 h after oral administration of 1 mg/kg tivozanib to female WT, *Abcb1a/1b;Abcg2*$^{-/-}$, *Cyp3a*$^{-/-}$ and Cyp3aXAV mice.

Parameter	Genotype			
	WT	*Abcb1a/1b;Abcg2*$^{-/-}$	*Cyp3a*$^{-/-}$	Cyp3aXAV
Plasma AUC$_{0\text{-}24h}$ (h*ng/ml)	4557 ± 683	4756 ± 674	5481 ± 179	6227 ± 936
Fold change AUC$_{0\text{-}24h}$	1.0	1.04	1.20	1.37
C$_{max}$ (ng/ml)	341 ± 76	322 ± 46	463 ± 67	417 ± 58
t$_{max}$ (h)	0.5-8	4-8	0.5	0.5-8
C$_{brain}$ (ng/g)	1.76 ± 0.88	7.13 ± 3.82 *	4.38 ± 3.19	8.32 ± 1.05 ***
Fold change C$_{brain}$	1.0	4.1	2.5	4.7
Brain-to-plasma ratio	0.17 ± 0.02	0.36 ± 0.04 ***	0.14 ± 0.01	0.14 ± 0.01
Fold change ratio	1.0	2.1	0.8	0.8

Data are given as mean ± S.D. (n = 5-7). C$_{brain}$, brain concentration. *, $P < 0.05$; **, $P < 0.01$; ***, $P < 0.001$ compared to WT mice.

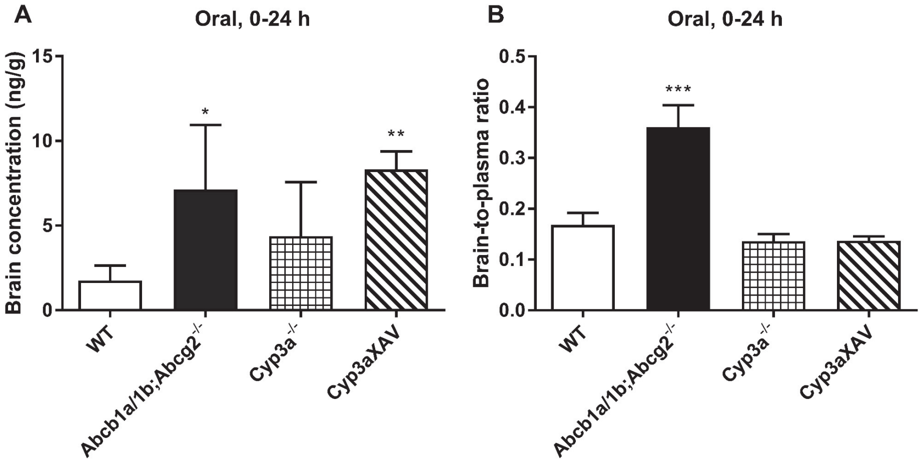

Figure 3. Brain concentration (A) and brain-to-plasma ratio (B) of tivozanib in female WT, *Abcb1a/1b*;*Abcg2*$^{-/-}$, *Cyp3a*$^{-/-}$ and Cyp3aXAV mice 24 h after oral administration of 1 mg/kg tivozanib. Data are given as mean ± S.D. (n = 5-7). *, *P* < 0.05; **, *P* < 0.01; ***, *P* < 0.001 compared to WT mice.

We also measured the impact of the ABC transporters on the brain concentration of tivozanib at 24 h. Although plasma AUC over 24 hours showed no significant differences between WT and *Abcb1a/1b;Abcg2*$^{-/-}$ mice, the brain concentration was 4.1-fold increased in the *Abcb1a/1b;Abcg2*$^{-/-}$ mice compared to WT mice, and 2.1-fold increased when considering the brain-to-plasma ratio (Figure 3A, B; Table 1). Next, we analyzed liver, kidney, spleen, and small intestinal tissue (SI) concentrations of tivozanib at 24 h. We found no meaningful differences in tissue concentrations or tissue-to-plasma ratios between WT and *Abcb1a/1b;Abcg2*$^{-/-}$ mice (Supplemental Figures 2 and 3A, B). Tissue to plasma distribution ratios were about 200%, 150%, 60% and 150% for liver, kidney, spleen, and SI, respectively, which was far higher than observed for the brain (17%) in WT mice. When the percentage of dose of tivozanib retrieved from the small intestinal contents (SIC%) was measured, it was low in both strains, about 0.03% at this time point (Supplemental Figure 3C).

3.3. CYP3A has little impact on tivozanib plasma pharmacokinetics and tissue disposition 24 h after oral administration

To investigate the impact of CYP3A-mediated metabolism on tivozanib kinetics, we performed a 24 h pilot study using *Cyp3a*$^{-/-}$, and mice with specific transgenic overexpression of human CYP3A4 in liver and intestine in a *Cyp3a*$^{-/-}$ background (Cyp3aXAV mice). After oral administration, tivozanib was rapidly absorbed in all strains, with a t_{max} at or before 30 min, and the plasma curve again showed secondary peaks in all strains (Figure 2B). Plasma exposure of tivozanib over 24 h (AUC_{0-24}) was not significantly different between the strains, but the semi-log plot of the plasma concentrations suggested a slower elimination rate between 8 to 24 h in *Cyp3a*$^{-/-}$ and Cyp3aXAV mice compared to WT mice (Supplemental Figure 1B).

After oral administration, *Cyp3a*$^{-/-}$ and Cyp3aXAV mice showed 2.5-fold and 4.7-fold higher brain concentration than WT mice at 24 h. However, these differences likely reflect the differences in plasma tivozanib concentration at this time point, as suggested by the absence of differences in brain-to-plasma ratios between the strains (Figure 3A, B; Table 1). The same applied for tivozanib distribution to the liver, kidney, spleen, SI and SIC% of these mouse strains when considering the tissue-to-plasma ratios, expect for a borderline difference observed for spleen in Cyp3aXAV mice (Supplemental Figures 2 and 3). The total amount of tivozanib retrieved from small intestinal content was again low in all strains (Supplemental Figure 3C).

3.4. Brain accumulation of tivozanib was limited by mAbcb1 and mAbcg2 activity after oral administration at 8 h

Upon oral administration over 24 h of tivozanib, we observed secondary plasma peaks at ~8 h in WT and *Abcb1a/1b;Abcg2*$^{-/-}$ mice. Therefore we performed an 8 h pilot study with oral tivozanib at 1 mg/kg in female WT and *Abcb1a/1b;Abcg2*$^{-/-}$ mice to assess tissue distribution when the plasma concentration was still high. We collected the first plasma samples at 15 min in this study.

As shown in Supplemental Figure 4A, tivozanib showed an average plasma t_{max} at the first time point, 15 min, and the plasma AUC_{0-8h} showed no significant differences. However, at 8 h we observed significant increases in brain concentration (3.3-fold) and brain-to-plasma ratio (2.5-fold) in *Abcb1a/1b;Abcg2*$^{-/-}$ mice in comparison to WT mice (Supplemental Figure 5A, B; Supplemental Table 1). In contrast to the brain-to-plasma ratio, we found 1.4-fold decreased liver-to-plasma ratio in *Abcb1a/1b;Abcg2*$^{-/-}$ mice compared to WT mice (*P* < 0.001. Supplemental Figure 5D; Supplemental Table 1). We next measured kidney, spleen, lung, SI and SIC% concentrations of tivozanib at 8 h after oral administration (Supplemental Figures 5 and 6; Supplemental Table 1). The tissue-to-plasma ratios showed no statistically significant differences between WT and *Abcb1a/1b;Abcg2*$^{-/-}$ mice.

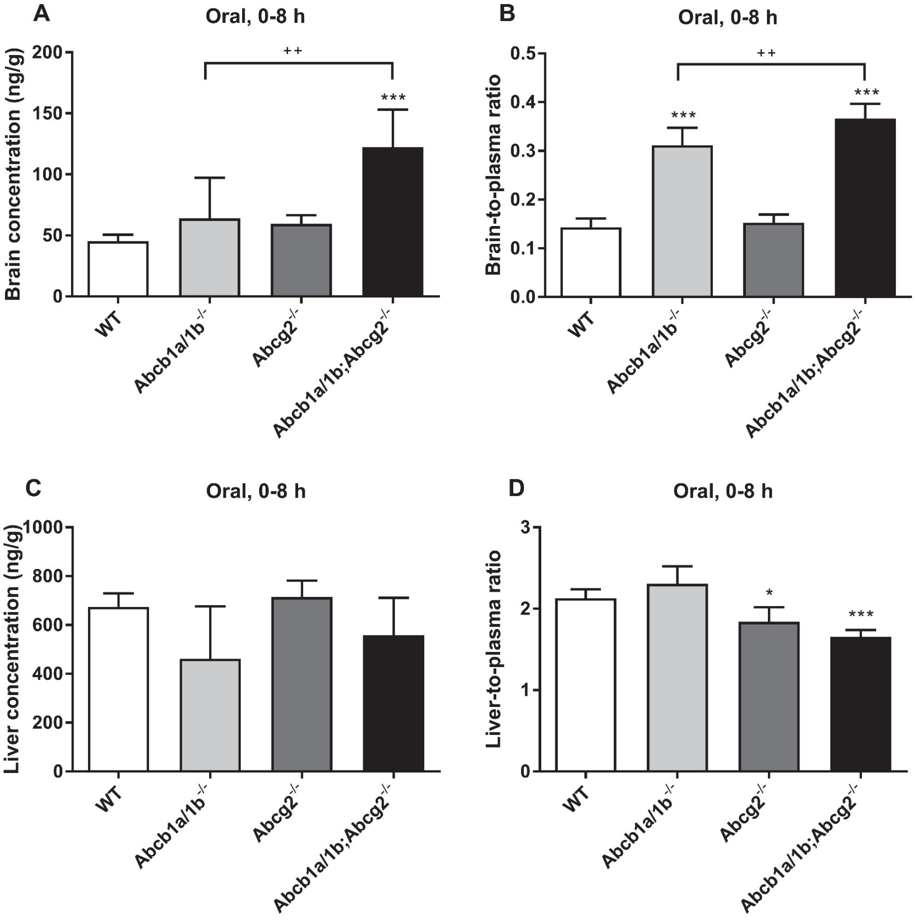

Figure 4. Brain and liver concentrations (A, C) and brain- and liver-to-plasma ratios (B, D) of tivozanib in female WT, *Abcb1a/1b*$^{-/-}$, *Abcg2*$^{-/-}$, and *Abcb1a/1b;Abcg2*$^{-/-}$ mice 8 h after oral administration of 1 mg/kg tivozanib. Data are given as mean ± S.D. (n = 5-7). *, $P < 0.05$; **, $P < 0.01$; ***, $P < 0.001$ compared to WT mice. $^{++}$, $P < 0.01$ comparing *Abcb1a/1b*$^{-/-}$ and *Abcb1a/1b;Abcg2*$^{-/-}$ mice.

3.5. CYP3A has little impact on tivozanib plasma pharmacokinetics and tissue disposition 8 h after oral administration

A similar pilot experiment over 8 h was done in WT, *Cyp3a$^{-/-}$* and Cyp3aXAV mice. After oral administration, the highest plasma levels occurred at 15 min, and the plasma AUC$_{0\text{-}8h}$ showed no significant differences between these three mouse strains (Figure 2D). The tivozanib tissue distribution in the major organs tested (brain, liver, kidney, spleen, lung, SI and SIC%) showed no meaningful differences (Supplemental Figures 5 and 6), in line with the 24 h experiment. This suggests that Cyp3a does not have a marked impact on the tissue concentrations of tivozanib after oral administration.

3.6. Brain accumulation of tivozanib was limited by both mAbcb1 and mAbcg2 after oral administration over 8 h

Upon oral administration of tivozanib over 24 h and 8 h, the brain penetration of tivozanib was enhanced by combined deficiency of mAbcb1a/1b and mAbcg2. We therefore performed an 8 h main experiment in WT and *Abcb1a/1b;Abcg2$^{-/-}$* mice, as well as in separate Abcb1a/1b and Abcg2 knockout strains to look at possible single and overlapping pharmacokinetic roles of these transporters. Since in the previous 8 h pilot experiment we observed t$_{max}$ at the first time point (15 min) after dosing, in this main experiment the first plasma sample was collected at 5 min after dosing.

As before, no significant differences were observed in the oral plasma AUC$_{0\text{-}8}$ in all the mouse strains, even though there was a tendency for the AUC$_{0\text{-}8}$ to be lower in the single Abcb1a/1b knockout mice (Figure 2C; Table 2). Plasma concentration-time curves showed secondary peaks in all strains (Figure 2C). We also measured brain, liver, kidney and spleen concentrations of tivozanib at 8 h. The single *Abcg2$^{-/-}$* mice did not display statistically significant changes in brain concentrations or brain-to-plasma ratios compared to WT mice. However, in spite of the different plasma concentrations at 8 h, the tivozanib brain concentrations were increased about 2.7-fold in *Abcb1a/1b;Abcg2$^{-/-}$* mice compared to WT mice (Figure 4A), and the brain-to-plasma ratios were significantly increased in both *Abcb1a/1b$^{-/-}$* (2.2-fold) and *Abcb1a/1b;Abcg2$^{-/-}$* (2.6-fold) mice compared to WT mice (Figure 4B; Table 2). The observation that the brain-to-plasma ratio was significantly higher in the *Abcb1a/1b;Abcg2$^{-/-}$* mice than in the *Abcb1a/1b$^{-/-}$* mice ($P < 0.01$) suggests that mAbcg2 also contributed to reducing the brain accumulation of tivozanib (Figure 4B). Collectively, these data indicate that the brain penetration of tivozanib was limited by both mAbcb1 and mAbcg2, albeit with a substantially bigger role for mAbcb1.

In contrast to the brain, loss of both Abcb1 and Abcg2 transporters resulted in a 1.3-fold lower liver-to-plasma ratio in *Abcb1a/1b;Abcg2$^{-/-}$* compared to WT mice (Figure 4B; Table 2). This result was in line with our previous 8 h pilot experiment, which showed a 1.4-fold lower liver-to-plasma ratio (Supplemental Figure 5D; Supplemental Table 1). We further analyzed the kidney and spleen concentrations (Supplemental

Figure 7) of tivozanib. As in the previous 24 h and 8 h experiments, we found no substantial effect of mAbcb1 and mAbcg2 on relative tivozanib distribution to kidney and spleen after oral administration.

3.7. mOatp1a/1b transporters may have a minor role in the distribution of tivozanib to the liver

To investigate the roles of the Oatp1a/1b uptake transporters in tivozanib disposition, we also performed an 8 h oral experiment in WT and Oatp1a/1b knockout mice (*Slco1a1b*$^{-/-}$). In this 8 h experiment, no significant differences were observed in the plasma AUC over 8 h between WT and *Slco1a1b*$^{-/-}$ mice, and the plasma concentrations remained at relatively high levels until 8 h (Supplemental Figure 4B).

For the *Slco1a/1b*$^{-/-}$ mice, we observed a significant decrease (1.2-fold) in liver-to-plasma ratio compared to WT mice (Supplemental Figure 8D; Supplemental Table 2).However, this difference was small, indicating that there could be at best a small contribution of Oatp1a/1b to the uptake of tivozanib into liver. In contrast to the liver-to-plasma ratio, there were no significant differences in brain-, kidney- and spleen-to-plasma ratios of tivozanib, suggesting that there is no meaningful impact of mouse Oatp1a/1b transporters on tivozanib exposure to brain, kidney, and spleen (Supplemental Figure 8; Supplemental Table 2).

Table 2. Plasma pharmacokinetic parameters and tissue concentrations over 8 h after oral administration of 1 mg/kg tivozanib to female WT, *Abcb1a/1b*$^{-/-}$, *Abcg2*$^{-/-}$, and *Abcb1a/1b;Abcg2*$^{-/-}$ mice.

Parameter	Genotype			
	WT	*Abcb1a/1b*$^{-/-}$	*Abcg2*$^{-/-}$	*Abcb1a/1b;Abcg2*$^{-/-}$
Plasma $AUC_{0\text{-}8h}$ (h*ng/ml)	2408 ± 229	1713 ± 511	2008 ± 228	2623 ± 322
Fold change $AUC_{0\text{-}8h}$	1.0	0.71	0.83	1.09
C_{max} (ng/ml)	376 ± 82	293 ± 80	392 ± 56	450 ± 80
t_{max} (h)	0.5-8	0.5-8	8	0.5-8
C_{brain} (ng/g)	45.3 ± 5.4	63.8 ± 33.3 $^{++}$	59.4 ± 7.2	122 ± 31 ***
Fold change C_{brain}	1.0	1.41	1.31	2.70
Brain-to-plasma ratio	0.14 ± 0.02	0.31 ± 0.04 $^{++}$	0.15 ± 0.02	0.37 ± 0.03 ***
Fold change ratio	1.0	2.2	1.1	2.6
C_{liver} (ng/g)	675 ± 55	462 ± 215	715 ± 67	558 ± 153
Fold change C_{liver}	1.0	0.7	1.1	0.8
Liver-to-plasma ratio	2.13 ± 0.11	2.31 ± 0.22	1.84 ± 0.18	1.65 ± 0.09 ***
Fold change ratio	1.0	1.1	0.9	0.8

Data are given as mean ± S.D. (n = 5-7). C_{tissue}, tissue concentration. *, $P < 0.05$; **, $P < 0.01$; ***, $P < 0.001$ compared to WT mice. $^{++}$, $P < 0.01$ comparing *Abcb1a/1b*$^{-/-}$ to *Abcb1a/1b;Abcg2*$^{-/-}$ mice.

4. Discussion

In this study, we found that tivozanib is transported by hABCB1 and mAbcg2 *in vitro*, and that this transport can be inhibited with specific inhibitors. However, we did not observe a clear limiting effect of mAbcb1a/1b and/or mAbcg2 on the oral availability of tivozanib in mice. Tivozanib was absorbed quickly between 5 to 15 minutes, with a t_{max} at or before 15 min, and the plasma concentrations stayed at high levels between 15 min and 8 h. Secondary peaks were detected in many individual mouse plasma curves up to around 8 h, suggesting the presence of enterohepatic circulation. The brain penetration of tivozanib was limited by the combined function of mAbcb1 and mAbcg2 (2.6-fold), and by single mAbcb1 activity as well (2.2-fold) (Figures 3 and 4A, B). Thus, both mAbcb1 and, to a lesser extent, mAbcg2 can modestly restrict brain accumulation of tivozanib in mice. mAbcb1 could fully compensate for the loss of mAbcg2 at the BBB, whereas mAbcg2 could only very partly take over the function of mAbcb1 at the BBB. Qualitatively, this ABC transporter-drug interaction behavior at the BBB is similar to that seen for a number of other targeted anticancer drugs, including the VEGFR inhibitors sorafenib [27], sunitinib [28] and axitinib [29].

It is worth noting that the administered dose we used in mice (1 mg/kg) was substantially higher than the recommended therapeutic dose for tivozanib (1.5 mg/d) in patients, primarily to facilitate ready detection in tissues. We indeed found C_{max} and plateau plasma levels in our mice of around 300 ng/ml, about 4-5-fold higher than therapeutic C_{max} levels in chronically treated patients [30]. Nonetheless, the plasma exposure was still of the same order of magnitude as used in patients. At this relatively high single dose we did not observe any acute toxicity, suggesting that tivozanib was well tolerated in mice under these conditions. Compared to other VEGFR inhibitors, the recommended therapeutic dose for tivozanib (1.5 mg/d) is far lower than for sorafenib (400 mg/d) and sunitinib (50 mg/d). The brain-to-plasma ratio in WT mice for tivozanib (~14%) was higher than that of sorafenib (~3%), lower than that of sunitinib (30%), and similar to that for axitinib (~12%) [27, 29]. This suggests that tivozanib has a relatively good ability to accumulate into the mouse brain. As 9% of RCC patients have brain metastases, theoretically, one could therefore consider to try and further improve the brain concentration of tivozanib by co-administration of a strong ABCB1 and ABCG2 inhibitor, such as elacridar, as was previously demonstrated in mice for sunitinib [28]. This might help to enhance drug exposure for tumors that are positioned in part or in whole behind the BBB, and thus possibly improve therapeutic efficacy. However, the effect of Abcb1 and Abcg2 on brain penetration of tivozanib was relatively modest.. If this would also apply to the human brain, this might perhaps mean that the gain from such a co-administration approach would be relatively limited.

The plasma pharmacokinetic profile of tivozanib showed quick absorption, and plasma concentration-time curves from patients and mice both show secondary peaks, indicating that tivozanib may undergo enterohepatic recirculation. This would likely be a contributing factor in the observed late t_{max}. In our 24 h experiment, the average half-life ($t_{1/2}$) was 335 minutes (188-588 minutes), i.e. 3.1-9.8 hours (average 5.6 hours) in mice. This long half-life and high variability between mice is in line with the clinical experiment of

Eskens *et al.*, which revealed a $t_{1/2}$ of 4.7 days (112 hours), range 31 to 233 hours in patients [31]. Compared to other VEGFR inhibitors (sunitinib ($t_{1/2}$, 41-86 hours) [32], sorafenib ($t_{1/2}$, 20-36 hours) [33], and axitinib ($t_{1/2}$, 2-5 hours) [34]) in patients, tivozanib's extended half-life could enhance the exposure of tumors to tivozanib, which has positive clinical implications. The plateau-like pharmacokinetic profile of tivozanib may also allow for more consistent therapeutic levels without large fluctuations in concentration between daily doses and allows the current once-daily dosing schedule.

Somewhat unexpectedly, after oral administration, the *Abcg2*$^{-/-}$ and *Abcb1a/1b;Abcg2*$^{-/-}$ mice demonstrated modestly reduced liver-to-plasma ratios of tivozanib at 8 h (Figure 4D, Supplemental Figure 5D). This may perhaps reflect a partially reduced Abcg2-mediated biliary excretion from the hepatocytes into bile. As a result, the reduced intrahepatic biliary tivozanib concentration may have slightly reduced overall liver-to-plasma ratios of tivozanib in *Abcg2*$^{-/-}$ and *Abcb1a/1b;Abcg2*$^{-/-}$ mice (gall bladders were always removed from the liver before homogenization), assuming that the intrahepatic bile contributes importantly to overall hepatic tivozanib concentration. However, the direct functions of Abcg2 and Abcb1 in this putative process are limited, considering the small difference between the WT and *Abcb1a/1b;Abcg2*$^{-/-}$ mice (~0.8-fold).

Looking at the collective *in vitro* and *in vivo* data, it is possible that ABCB1 and ABCG2 expression in RCC cells might directly contribute to some level of resistance to tivozanib therapy. However, its absolute contribution, if any, is likely to be small. Reustle et al. found decreased ABCB1 mRNA expression, but increased ABCG2 mRNA expression in clear cell RCC tissue compared to non-tumor tissue [12], which might perhaps also affect tivozanib resistance.

Very little literature is available on the possible interaction of tivozanib with OATPs. Our experiments in *Slco1a/1b*$^{-/-}$ mice suggest there might perhaps be a modest uptake function of mOatp1a/1b transporters in tivozanib liver accumulation, but the differences in liver-to-plasma ratio between WT and *Slco1a/1b*$^{-/-}$ mice were small (1.2-fold), and plasma levels were not affected. Any broader *in vivo* pharmacokinetic impact is therefore likely to be small.

In the experiments in Cyp3a knockout and Cyp3aXAV mice over 24 h, we found no significant differences in the plasma AUCs and tissue-to-plasma ratios in WT, *Cyp3a*$^{-/-}$ and Cyp3aXAV mice (Figure 2B; Table 1). However, the semi-log plot of the plasma concentrations suggested a somewhat slower elimination between 8 to 24 h in both *Cyp3a*$^{-/-}$ and Cyp3aXAV mice compared to WT mice (Supplemental Figure 1B). The data suggest that mCyp3a or hCYP3A4 in themselves do not significantly affect tivozanib detoxification. According to the EMA report, CYP1A1 and CYP3A4 can metabolize tivozanib *in vitro* [1], but it may be that the *in vivo* impact of CYP3A is negligible. The modest reduction in late clearance in both CYP3A-modified strains suggests that the absence of mouse Cyp3a (but not the presence of human CYP3A4) alters some other tivozanib-eliminating process. We have earlier documented some compensatory changes in Cyp3a knockout mice, primarily upregulation of Cyp32c enzymes [35]. However, this could not explain decreased clearance of tivozanib, so some other unidentified detoxification system may have been (modestly) altered.

5. Conclusion

Our data indicate that both Abcb1a/1b and Abcg2 can restrict the net accumulation of tivozanib in the brain, but not its oral availability. If also true in humans, the observed modest effect of ABC transporters on brain accumulation of tivozanib suggests that this drug, in contrast to most other TKIs, will only be modestly limited in its therapeutic efficacy against malignant lesions situated in part or in whole behind the BBB. We further found that mOatp1a/1bs had at best a very modest uptake function for tivozanib into liver, without affecting overall plasma kinetics. Finally, both mCyp3a and human CYP3A4 appear to have little if any direct impact on the *in vivo* oral availability and tissue distribution of tivozanib. This suggests that CYP3A-mediated drug-drug interactions are probably of minor concern for tivozanib.

6. References

1. EMA, Committee for Medicinal Products for Human Use (CHMP), European Medicines Agency (EMA), Assessment Report: Fotivda (Tivozanib). 2017, https://www.ema.europa.eu/en/medicines/human/EPAR/fotivda.
2. Bianchi, M., et al., Distribution of metastatic sites in renal cell carcinoma: a population-based analysis. Annals of Oncology, 2011. 23(4): p. 973-980.
3. Gong, J., et al., Metastasis in renal cell carcinoma: Biology and implications for therapy. Asian journal of urology, 2016. 3(4): p. 286-292.
4. AVEO Oncology, AVEO Oncology announces FOTIVDA® (tivozanib) approved in the European Union for the Treatment of advanced renal cell carcinoma. 2017, http://www.aveooncology.com/.
5. Motzer, R.J., et al., Tivozanib versus sorafenib as initial targeted therapy for patients with metastatic renal cell carcinoma: results from a phase III trial. Journal of clinical oncology, 2013. 31(30): p. 3791.
6. Giacomini, K.M., et al., Membrane transporters in drug development. Nature reviews Drug discovery, 2010. 9(3): p. 215.
7. Borst, P. and R.O. Elferink, Mammalian ABC transporters in health and disease. Annual review of biochemistry, 2002. 71(1): p. 537-592.
8. Schinkel, A.H. and J.W. Jonker, Mammalian drug efflux transporters of the ATP binding cassette (ABC) family: an overview. Advanced drug delivery reviews, 2003. 55(1): p. 3-29.
9. Vlaming, M.L., J.S. Lagas, and A.H. Schinkel, Physiological and pharmacological roles of ABCG2 (BCRP): recent findings in Abcg2 knockout mice. Advanced drug delivery reviews, 2009. 61(1): p. 14-25.
10. Wang, J., et al., P-glycoprotein (MDR1/ABCB1) and breast cancer resistance protein (BCRP/ABCG2) affect brain accumulation and intestinal disposition of encorafenib in mice. Pharmacological research, 2018. 129: p. 414-423.
11. Wang, J., et al., P-glycoprotein (MDR1/ABCB1) and Breast Cancer Resistance Protein (BCRP/ABCG2) limit brain accumulation of the FLT3 inhibitor quizartinib in mice. International journal of pharmaceutics, 2019. 556: p. 172-180.
12. Reustle, A., et al., Characterization of the breast cancer resistance protein (BCRP/ABCG2) in clear cell renal cell carcinoma. International Journal of Cancer, 2018. 143(12): p. 3181-3193.
13. Cheng, X., et al., Tissue distribution and ontogeny of mouse organic anion transporting polypeptides (Oatps). Drug metabolism and Disposition, 2005. 33(7): p. 1062-1073.
14. Cheng, X. and C.D. Klaassen, Tissue distribution, ontogeny, and hormonal regulation of xenobiotic transporters in mouse kidneys. Drug Metabolism and Disposition, 2009. 37(11): p. 2178-2185.
15. van de Steeg, E., et al., Organic anion transporting polypeptide 1a/1b–knockout mice provide insights into hepatic handling of bilirubin, bile acids, and drugs. The Journal of clinical investigation, 2010. 120(8): p. 2942-2952.
16. Guengerich, F.P., Human cytochrome P450 enzymes, in Cytochrome P450. 1995, Springer. p. 473-535.
17. Zanger, U.M. and M. Schwab, Cytochrome P450 enzymes in drug metabolism: regulation of gene expression, enzyme activities, and impact of genetic variation. Pharmacology & therapeutics, 2013. 138(1): p. 103-141.
18. van Waterschoot, R.A., et al., Intestinal cytochrome P450 3A plays an important role in the regulation of detoxifying systems in the liver. The FASEB Journal, 2009. 23(1): p. 224-231.
19. van Hoppe, S., et al., Breast cancer resistance protein (BCRP/ABCG2) and P-glycoprotein (P-gp/ABCB1) transport afatinib and restrict its oral availability and brain accumulation. Pharmacological research, 2017. 120: p. 43-50.
20. Bruin, M.A.C., et al., Development and validation of an LC-MS/MS method with a broad linear dynamic range for the quantification of tivozanib in human and mouse plasma, mouse tissue homogenates, and culture medium. Journal of Chromatography B, 2019. 1125: p. 121723.
21. Durmus, S., et al., Oral availability and brain penetration of the B-RAFV600E inhibitor vemurafenib can be enhanced by the P-GLYCOprotein (ABCB1) and breast cancer resistance protein (ABCG2) inhibitor elacridar. Molecular pharmaceutics, 2012. 9(11): p. 3236-3245.

22. Schinkel, A.H., et al., Normal viability and altered pharmacokinetics in mice lacking mdr1-type (drug-transporting) P-glycoproteins. Proceedings of the National Academy of Sciences, 1997. 94(8): p. 4028-4033.
23. Jonker, J.W., et al., The breast cancer resistance protein protects against a major chlorophyll-derived dietary phototoxin and protoporphyria. Proceedings of the National Academy of Sciences, 2002. 99(24): p. 15649-15654.
24. Jonker, J.W., et al., Contribution of the ABC transporters Bcrp1 and Mdr1a/1b to the side population phenotype in mammary gland and bone marrow of mice. Stem cells, 2005. 23(8): p. 1059-1065.
25. van Herwaarden, A.E., et al., Knockout of cytochrome P450 3A yields new mouse models for understanding xenobiotic metabolism. The Journal of clinical investigation, 2007. 117(11): p. 3583-3592.
26. Zhang, Y., et al., PKSolver: An add-in program for pharmacokinetic and pharmacodynamic data analysis in Microsoft Excel. Computer methods and programs in biomedicine, 2010. 99(3): p. 306-314.
27. Tang, S.C., et al., Impact of P-glycoprotein (ABCB1) and breast cancer resistance protein (ABCG2) gene dosage on plasma pharmacokinetics and brain accumulation of dasatinib, sorafenib, and sunitinib. Journal of Pharmacology and Experimental Therapeutics, 2013. 346(3): p. 486-494.
28. Tang, S.C., et al., Brain accumulation of sunitinib is restricted by P-glycoprotein (ABCB1) and breast cancer resistance protein (ABCG2) and can be enhanced by oral elacridar and sunitinib coadministration. International journal of cancer, 2012. 130(1): p. 223-233.
29. Poller, B., et al., Differential impact of P-glycoprotein (ABCB1) and breast cancer resistance protein (ABCG2) on axitinib brain accumulation and oral plasma pharmacokinetics. Drug Metabolism and Disposition, 2011. 39(5): p. 729-735.
30. Jang, S. and M. Atkins, Treatment of BRAF-mutant melanoma: the role of vemurafenib and other therapies. Clinical Pharmacology & Therapeutics, 2014. 95(1): p. 24-31.
31. Eskens, F.A., et al., Biologic and clinical activity of tivozanib (AV-951, KRN-951), a selective inhibitor of VEGF receptor-1,-2, and-3 tyrosine kinases, in a 4-week-on, 2-week-off schedule in patients with advanced solid tumors. Clinical Cancer Research, 2011. 17(22): p. 7156-7163.
32. Faivre, S., et al., Safety, pharmacokinetic, and antitumor activity of SU11248, a novel oral multitarget tyrosine kinase inhibitor, in patients with cancer. Journal of clinical oncology, 2006. 24(1): p. 25-35.
33. Moore, M., et al., Phase I study to determine the safety and pharmacokinetics of the novel Raf kinase and VEGFR inhibitor BAY 43-9006, administered for 28 days on/7 days off in patients with advanced, refractory solid tumors. Annals of oncology, 2005. 16(10): p. 1688-1694.
34. Rugo, H.S., et al., Phase I trial of the oral antiangiogenesis agent AG-013736 in patients with advanced solid tumors: pharmacokinetic and clinical results. Journal of Clinical Oncology, 2005. 23(24): p. 5474-5483.
35. van Waterschoot, R.A., et al., Midazolam metabolism in cytochrome P450 3A knockout mice can be attributed to up-regulated CYP2C enzymes. Molecular pharmacology, 2008. 73(3): p. 1029-1036.

7. Supplemental materials

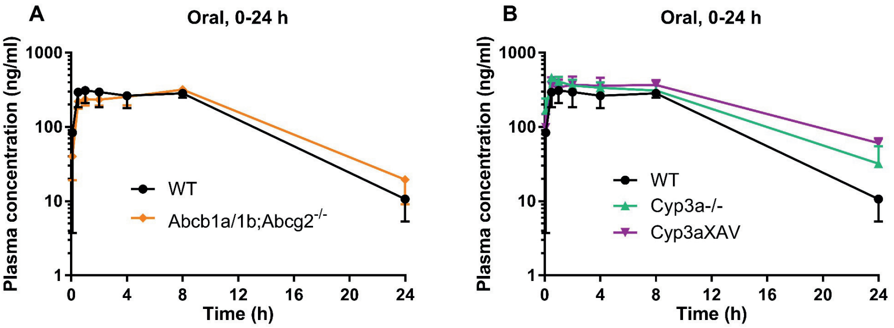

Supplemental Figure 1. Semi-log plots of plasma concentration-time curves of tivozanib in female mice after oral administration of 1 mg/kg tivozanib. Data are given as mean ± S.D. (n = 5-7). A: 0-24 h experiment in WT and *Abcb1a/1b;Abcg2*$^{-/-}$ mice. B: 0-24 h experiment in WT, *Cyp3a*$^{-/-}$, and Cyp3aXAV mice.

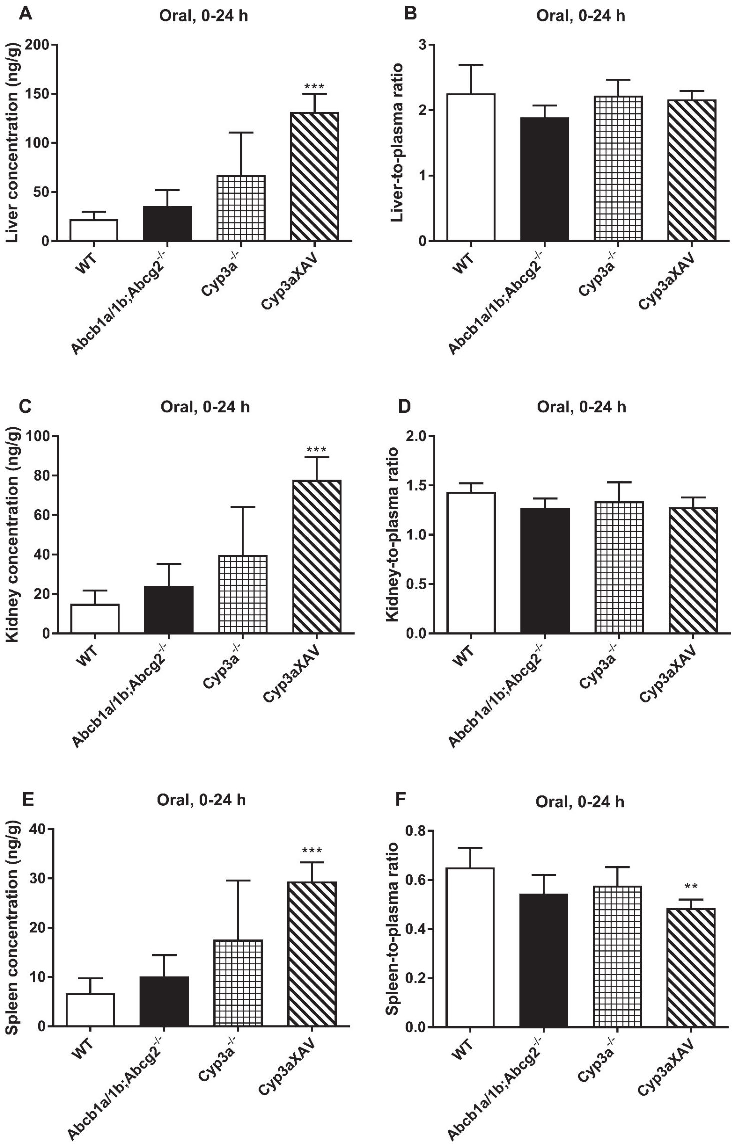

Supplemental Figure 2. Organ concentration (A, C, E) and organ-to-plasma ratio (B, D, F) of tivozanib in female WT, *Abcb1a/1b*;*Abcg2*$^{-/-}$, *Cyp3a*$^{-/-}$ and Cyp3aXAV mice 24 h after oral administration of 1 mg/kg tivozanib. Data are given as mean ± S.D. (n = 5-7). *, *P* < 0.05; **, *P* < 0.01; ***, *P* < 0.001 compared to WT mice.

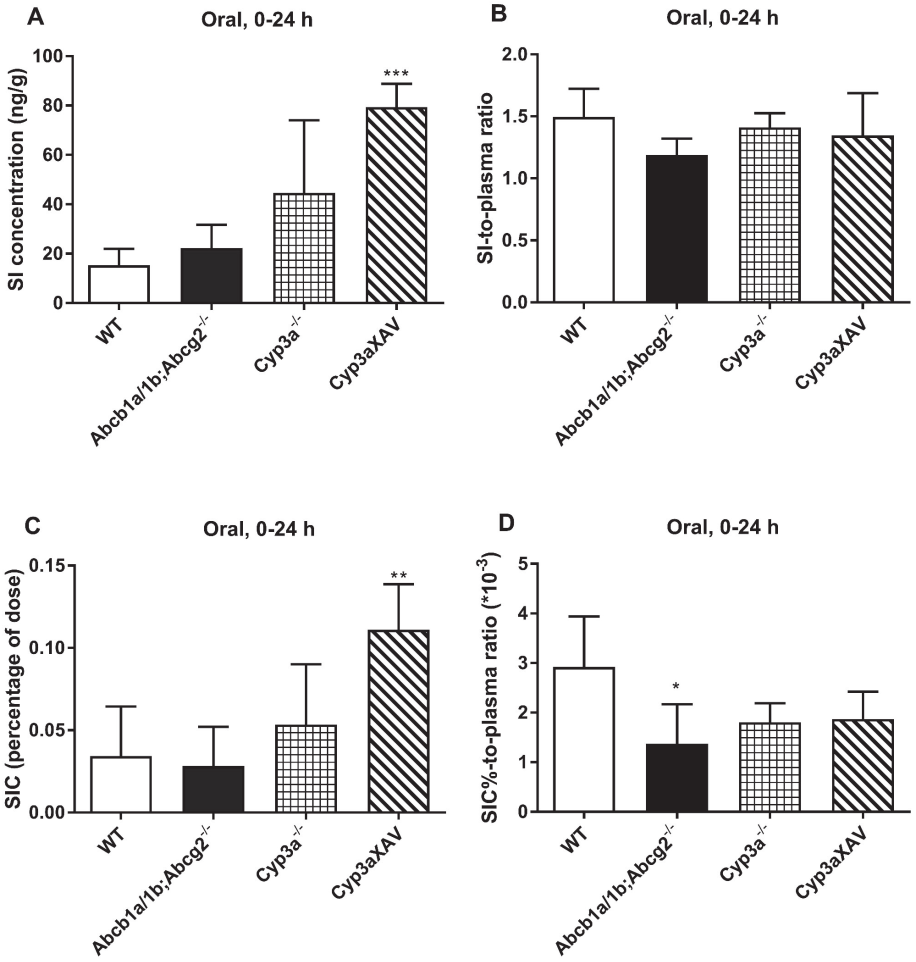

Supplemental Figure 3. Small intestinal tissue (SI) and small intestinal content percentage of dose (SIC%) (A, C), and SI-to-plasma and SIC%-to-plasma ratio (B, D) of tivozanib in female WT, *Abcb1a/1b*;*Abcg2*$^{-/-}$, *Cyp3a*$^{-/-}$ and Cyp3aXAV mice 24 h after oral administration of 1 mg/kg tivozanib. Data are given as mean ± S.D. (n = 5-7). C: Drug percentage of dose in SIC, which was expressed as total drug (ng) in SIC divided by total drug administered (ng). D, expressed as A divided by last time point plasma concentration. *, $P < 0.05$; **, $P < 0.01$; ***, $P < 0.001$ compared to WT mice.

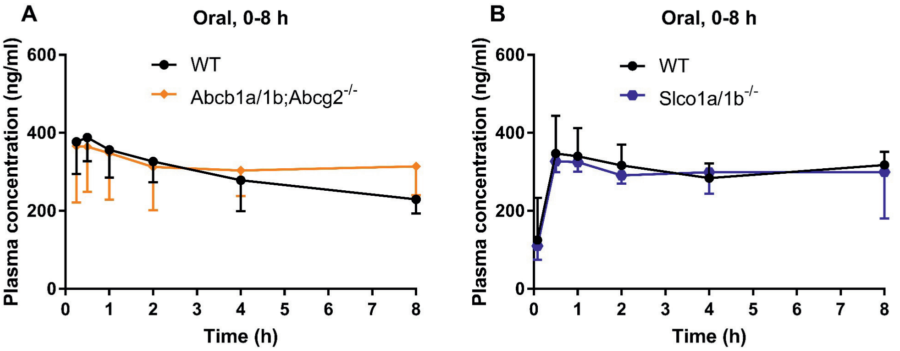

Supplemental Figure 4. Plasma concentration-time curves of tivozanib in female mice after oral administration of 1 mg/kg tivozanib. Data are given as mean ± S.D. (n = 5-7). A: 0-8 h experiment in WT and *Abcb1a/1b;Abcg2*$^{-/-}$ mice. B: 0-8 h experiment in WT and *Slco1a/1b*$^{-/-}$ mice.

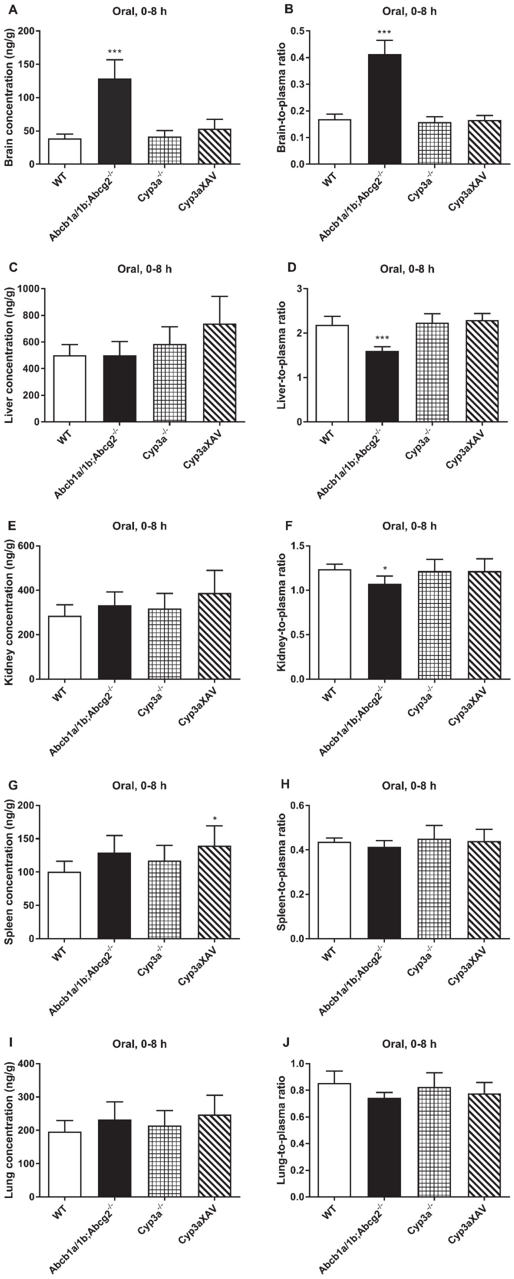

Supplemental Figure 5.
Organ concentration (A, C, E, G, I) and organ-to-plasma ratio (B, D, F, H, J) of tivozanib in female WT, *Abcb1a/1b*;*Abcg2*$^{-/-}$, *Cyp3a*$^{-/-}$ and Cyp3aXAV mice 8 h after oral administration of 1 mg/kg tivozanib. Data are given as mean ± S.D. (n = 5-7). *, *P* < 0.05; **, *P* < 0.01; ***, *P* < 0.001 compared to WT mice.

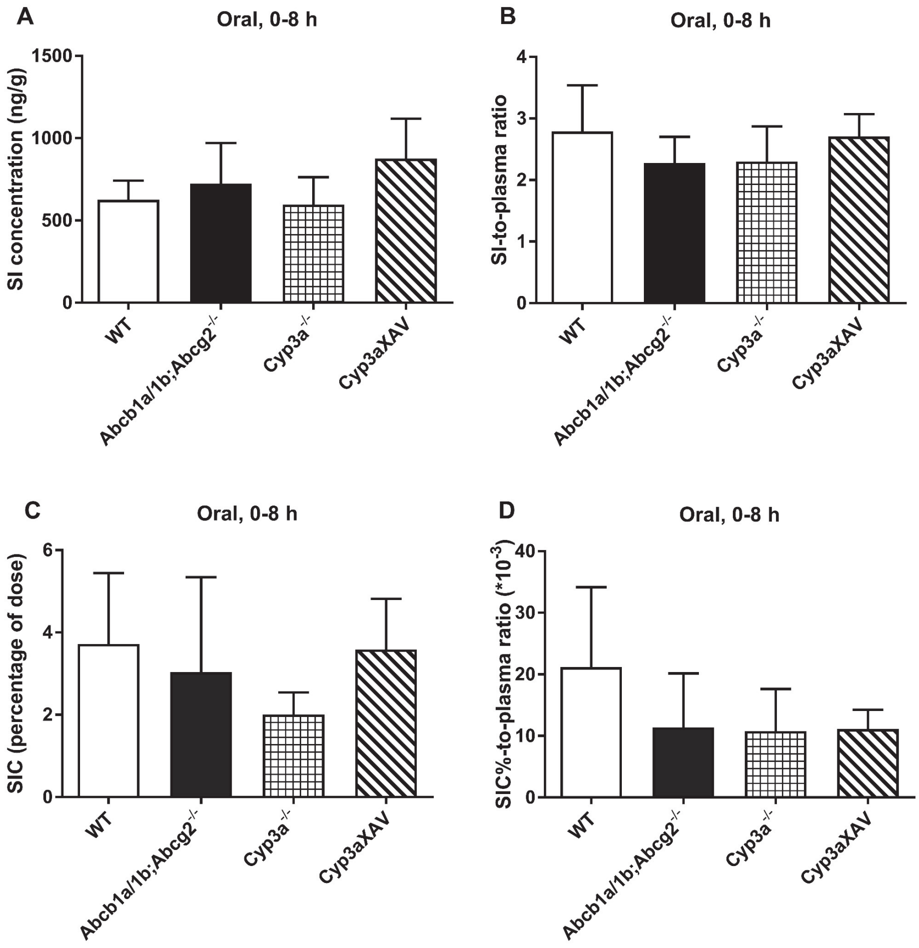

Supplemental Figure 6. Small intestinal tissue (SI) and small intestinal content percentage of dose (SIC%) (A, C) and SI-to-plasma and SIC%-to-plasma ratio (B, D) of tivozanib in female WT, *Abcb1a/1b*;*Abcg2*$^{-/-}$, *Cyp3a*$^{-/-}$ and Cyp3aXAV mice 8 h after oral administration of 1 mg/kg tivozanib. Data are given as mean ± S.D. (n = 5-7). C: Drug percentage of dose in SIC, which was expressed as total drug (ng) in SIC divided by total drug administered (ng). D, expressed as A divided by last time point plasma concentration. No statistically significant differences compared to WT mice were observed ($P > 0.05$).

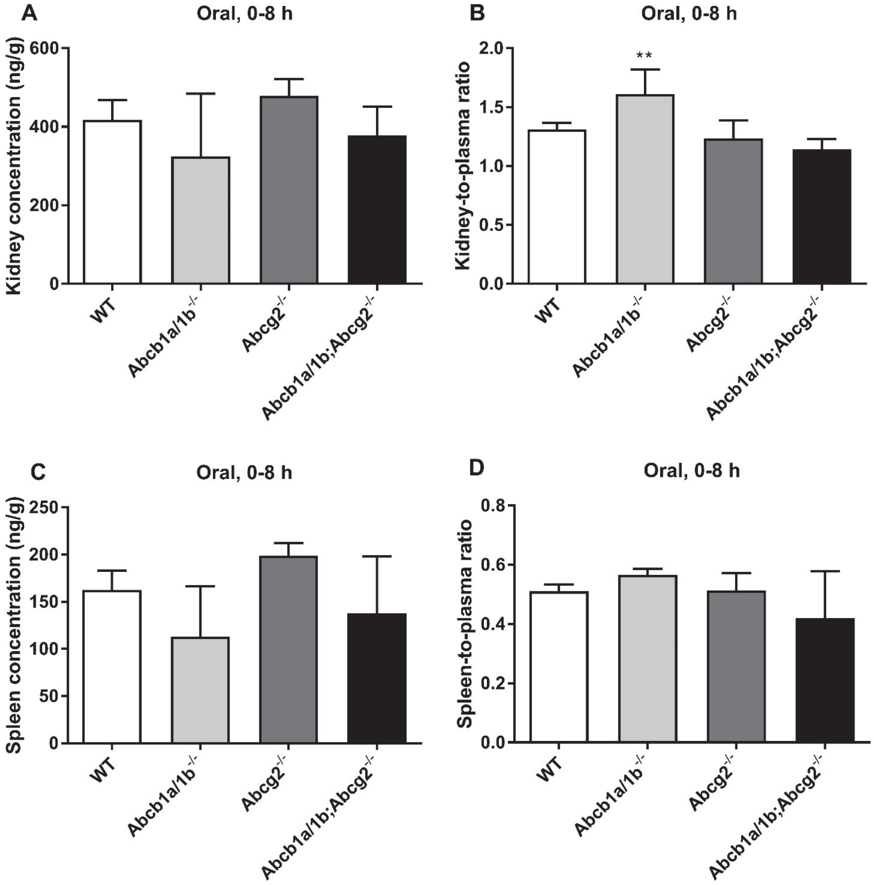

Supplemental Figure 7. Kidney and spleen concentration (A, C) and kidney- and spleen-to-plasma ratio (B, D) of tivozanib in female WT, *Abcb1a/1b*$^{-/-}$, *Abcg2*$^{-/-}$,and *Abcb1a/1b;Abcg2*$^{-/-}$ mice 8 h after oral administration of 1 mg/kg tivozanib. Data are given as mean ± S.D. (n = 5-7). *, $P < 0.05$; **, $P < 0.01$; ***, $P < 0.001$ compared to WT mice.

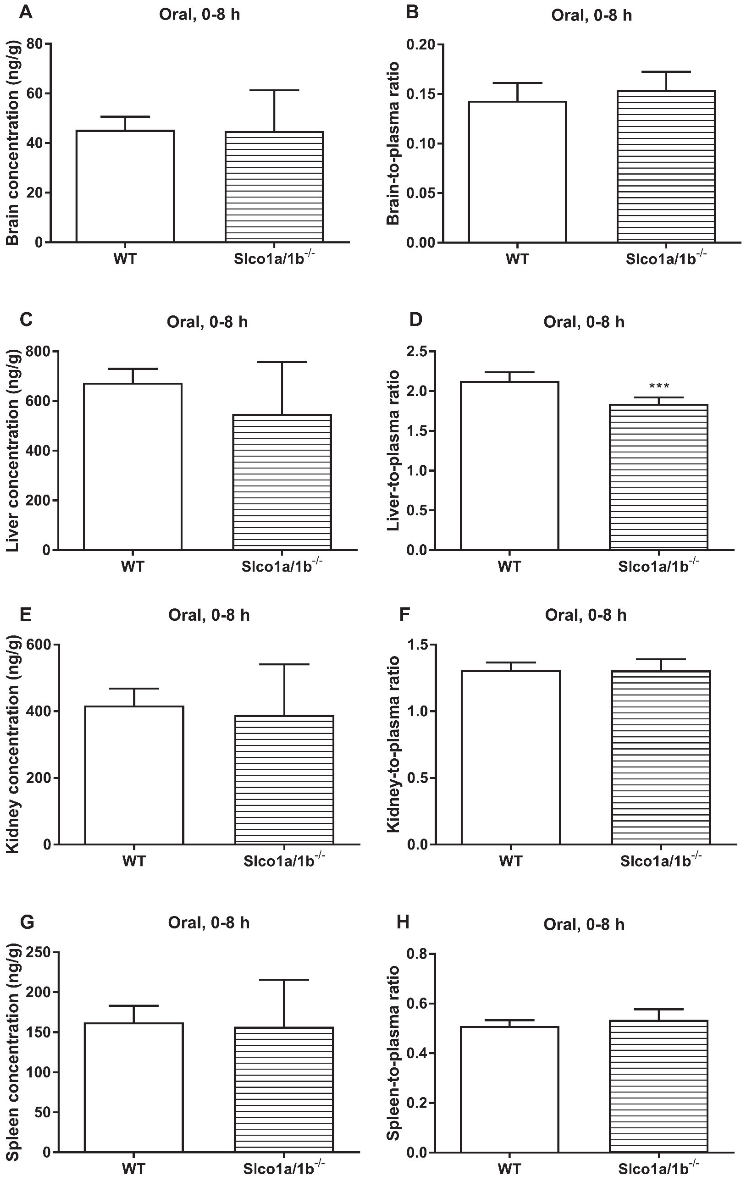

Supplemental Figure 8. Organ concentration (A, C, E, G) and organ-to-plasma ratio (B, D, F, H) of tivozanib in female WT, and *Slco1a/1b*$^{-/-}$ mice 8 h after oral administration of 1 mg/kg tivozanib. Data are given as mean ± S.D. (n = 5-7). *, *P* < 0.05; **, *P* < 0.01; ***, *P* < 0.001 compared to WT mice.

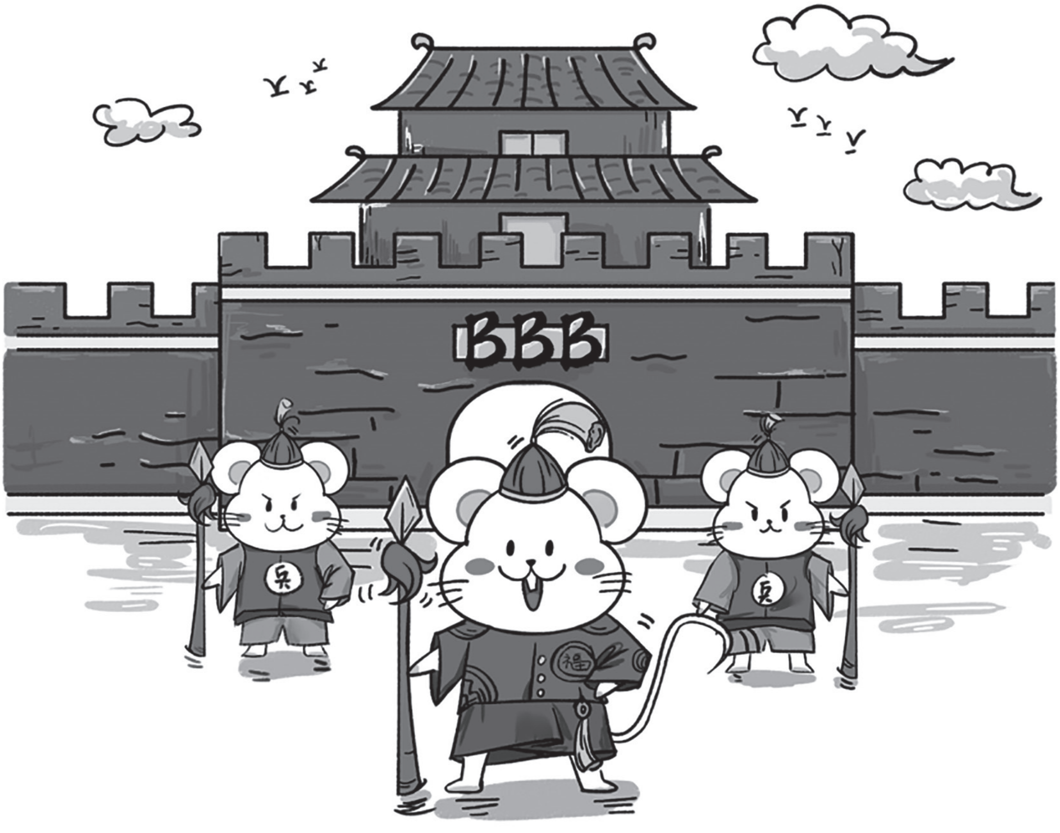
BBB
兵
福
兵

Chapter 5

P-glycoprotein (MDR1/ABCB1) restricts brain accumulation of the novel EGFR inhibitor EAI045 and oral elacridar coadministration enhances its brain accumulation and oral exposure

Jing Wang
M. Merve Susam
Changpei Gan
Rolf W. Sparidans
Maria C. Lebre
Jos H. Beijnen
Alfred H. Schinkel

To be submitted

Abstract

EAI045 is a fourth-generation allosteric epidermal growth factor receptor (EGFR) tyrosine kinase inhibitor (TKI) which targets T790M and C797S EGFR mutants in treatment of non-small cell lung cancer (NSCLC). The combination of EAI045 and cetuximab induces tumour regression in mouse models of EGFR-mutant lung cancer. Using genetically modified mouse models, we investigated the roles of the multidrug efflux and uptake transporters ABCB1 (P-gp), ABCG2 (BCRP), OATP1A/1B, and of the drug-metabolizing enzyme CYP3A in plasma pharmacokinetics and tissue distribution of EAI045 and its metabolites. *In vitro*, EAI045 was a good transport substrate of human ABCB1. *In vivo*, orally administered EAI045 (20 mg/kg) was very rapidly absorbed. EAI045 brain-to-plasma ratios were increased by 3.9-fold in *Abcb1a/1b*$^{-/-}$ and 4.8-fold in *Abcb1a/1b;Abcg2*$^{-/-}$ mice compared to wild-type mice, but not in single *Abcg2*$^{-/-}$ mice. EAI045 oral availability was not markedly affected. Coadministration of elacridar, an ABCB1/ABCG2 inhibitor, increased the plasma $AUC_{0\text{-}30min}$ and brain-to-plasma ratios of EAI045 by 4.0-fold and 5.4-fold, respectively, in wild-type mice. EAI045 glucuronide showed an increased plasma $AUC_{0\text{-}30min}$ and a markedly decreased accumulation and tissue-to-plasma ratio in the small intestinal content in the absence of Abcb1a/1b and Abcg2. A large fraction of oral EAI045 was converted to its metabolite PIA, but Abcb1a/1b, Abcg2 and Oatp1a/1b had little impact on its pharmacokinetics. Mouse Cyp3a knockout or transgenic human CYP3A4 overexpression did not significantly affect oral EAI045 pharmacokinetics. Our data indicate that EAI045 brain accumulation is substantially limited by ABCB1 in the blood-brain barrier, but this can be effectively reversed by elacridar coadministration.

Keywords: EAI045, ABCB1, ABCG2, Brain accumulation, Elacridar, Oatp1a/1b, CYP3A4

1. Introduction

Lung cancer is the leading cause of cancer death among women and men in many developed countries. For instance, for 2021, 235,760 new cases were expected and 131,880 persons are projected to die from the disease in the United States alone [1]. Non-small cell lung cancer (NSCLC) accounts for about 80% to 85% of all cases [2-5]. The past 20 years have seen tremendous progress in the understanding of the biology and management of NSCLC. The development of the third-generation epidermal growth factor receptor (EGFR) tyrosine kinase inhibitors (TKIs) represented a significant breakthrough in the treatment of patients with EGFR mutant and especially T790M mutant NSCLC. However, the C797S mutation in the tyrosine kinase domain of EGFR is a leading mechanism of resistance to the third-generation irreversible EGFR inhibitors targeting the T790M mutation [6-9]. To overcome this C797S mutation, Jia et al. screened a library of approximately 2.5 million compounds against the L858R/T790M EGFR mutant kinase peptide. Among these compounds, an EGFR allosteric inhibitor-1 (EAI001) was discovered. However, it only had modest potency against individual L858R and T790M mutants. With further modification and characterization, EGFR allosteric inhibitor -45 (EAI045) was found to have the most selective inhibition of the EFGR mutant over wild-type EGFR [10]. Moreover, EAI045 shows marked synergy with cetuximab, an antibody therapeutic that blocks EGFR dimerization [11, 12]. The combination of EAI045 with cetuximab is effective against lung cancer driven by EGFR(L858R/T790M) and by EGFR(L858R/T790M/C797S) in mouse models; EAI045 or cetuximab alone had a very modest effect in the L858R/T790M mutant mice, but marked tumor regressions were observed in these mice in the combination treatment [10, 13].

Transmembrane transporters can be major determinants of the pharmacokinetic, safety and efficacy profiles of drugs. Two major superfamilies, the ATP-binding cassette (ABC) and solute carrier (SLC) transporters, are widely expressed (e.g. brain, liver, small intestine and kidney) and thought to have profound roles in drug disposition and in drug-drug and drug-food interactions [14, 15]. Two important ABC efflux transporters, P-glycoprotein (P-gp, ABCB1, MDR1) and breast cancer resistance protein (BCRP, ABCG2), are expressed in the apical membrane of organs with absorptive and eliminatory functions, like liver, intestine, and kidneys. They are also expressed in the endothelial cells constituting blood-tissue interfaces (such as the blood-brain, blood-testis, blood-ovarian, and blood-retinal barriers) [16-24]. This expression profile of these two transporters suggests that the central roles of ABCB1 and ABCG2 may be to prevent the entry of toxins or drugs into sensitive tissues and to facilitate their elimination through hepatobiliary, intestinal, and renal excretory pathways [22-24].

Organic anion transporting polypeptides (human: OATP, gene *SLCO*; rodents: Oatp, gene *Slco*) are primarily uptake transporters. They can transport a wide range of endogenous and exogenous compounds, including bile salts, steroid conjugates, thyroid hormones, anionic oligopeptides, and numerous drugs as well as other xenobiotics [25]. For instance, the OATP1A and 1B subfamilies are highly expressed in the liver, and are thought to play a key role in the hepatic uptake and plasma clearance of substrate drugs [26].

In the present study, we aimed to investigate the pharmacokinetic functions of ABCB1 and ABCG2 *in vitro* and *in vivo*, and the roles of OATP1A/1B *in vivo*, with respect to systemic exposure upon oral administration (in short: oral exposure) and tissue distribution of EAI045. We also studied the effect of co-administration of the ABCB1 and ABCG2 inhibitor elacridar. Finally, we determined to what extent EAI045 oral exposure and tissue accumulation is affected by multispecific drug-metabolizing enzymes of the cytochrome P4503A (CYP3A) family.

2. Materials and methods

2.1. Chemicals

EAI045 was obtained from Carbosynth (Berkshire, UK). Elacridar HCl and Zosuquidar were purchased from Sequoia Research Products (Pangbourne, UK). Ko143 was from Tocris Bioscience (Bristol, UK). Bovine Serum Albumin (BSA) Fraction V was obtained from Roche Diagnostics GmbH (Mannheim, Germany). Glucose water (5%, w/v) was supplied by B. Braun Medical Supplies (Melsungen, Germany). Isoflurane was from Pharmachemie (Haarlem, The Netherlands), heparin (5000 IU ml^{-1}) was purchased from Leo Pharma (Breda, The Netherlands). Other chemicals used in the EAI045 assays were described before [27, 28], and all other chemicals and reagents were obtained from Sigma-Aldrich (Steinheim, Germany).

2.2. Transport assays

Madin-Darby Canine Kidney (MDCK-II) cells (ECACC 00062107) stably transduced with human (h) ABCB1, hABCG2, or mouse (m) Abcg2 cDNA were generated in our institute between 1998-2005. Transepithelial transport assays were performed on microporous polycarbonate membrane filters (3.0 mm pore size, 12 mm diameter, Transwell 3402, Corning Incorporated, Kennebunk, ME). In short, cells were allowed to grow an intact monolayer in 3 days, which was monitored with transepithelial electrical resistance (TEER) measurements, both before and after the transport phase. On the day of experiment, when appropriate cells were pre-incubated (1 h) with 5 μM zosuquidar (ABCB1 inhibitor) and/or 5 μM Ko143 (ABCG2/Abcg2 inhibitor) in both compartments. The transport phase was then initiated (t = 0) by replacing the medium in apical or basolateral compartments with fresh Dulbecco's Modified Eagle's medium (DMEM medium) including 10% (v/v) fetal bovine serum (FBS) and 5 μM EAI045, as well as the appropriate inhibitor(s). Cells were kept at 37°C in 5% (v/v) CO_2 during the experiment. 50 μl samples were taken from the acceptor compartment at 1, 2, 4 and 8 hours, and stored at -30°C until LC-MS/MS analysis. Active transport was expressed using the transport ratio (r), which is defined as the amount of apically directed drug transport divided by basolaterally directed drug translocation at a defined time point. Proper functionality of these cell lines was monitored by continual testing with a variety of drug substrates.

2.3. Animals

Mice (*Mus musculus*) were bred in the Netherlands Cancer Institute and housed and handled according to institutional guidelines complying with Dutch and EU legislation. Animals used were WT, *Abcb1a/1b*$^{-/-}$ [29], *Abcg2*$^{-/-}$ [30], *Abcb1a/1b;Abcg2*$^{-/-}$ [31], *Cyp3a*$^{-/-}$ [32] and *Oatp1a/1b*$^{-/-}$ [33] mice of a >99% FVB/N strain background. Homozygous CYP3A4 humanized transgenic mice (Cyp3aXAV) were generated by cross-breeding of transgenic mice with stable human CYP3A4 expression in liver or intestine, respectively, in a *Cyp3a*$^{-/-}$ background [32]. Proper functionality of the knockout and transgenic strains was monitored by regular testing with a variety of drug substrates. All the mice used were between 10 and 15 weeks of age. Animals were kept in a temperature-controlled environment with a 12 h light/12 h dark cycle and received a standard diet (Transbreed, SDS Diets, Technilab-BMI, The Netherlands) and acidified water *ad libitum*. Depending on the type of experiment, 5 or 6 mice were tested in each experimental group. All experimental animal protocols including power calculations were designed under the nationally approved DEC/CCD project AVD301002016595 and evaluated and approved by the institutional animal care and use committee (IACUC) of the Netherlands Cancer Institute.

2.4. Working solutions

EAI045 was dissolved in dimethyl sulfoxide (DMSO) at a concentration of 4 mg/ml, and further diluted with a mixture of polysorbate 80/ethanol (1:1, v/v), and then 5% (w/v) glucose in water to yield a concentration of 2 mg/ml. Final concentrations for DMSO, polysorbate 80, ethanol and glucose in the dosing solution were 5%, 2.5%, 2.5% and 4.5% (v/v/v/w), respectively. Elacridar hydrochloride was dissolved in DMSO at a concentration of 53 mg/ml, then further diluted with a mixture of polysorbate 80, ethanol and water [20:13:67, (v/v/v)] to yield a concentration of 5 mg/ml elacridar, and orally administered at a dose of 50 mg/kg body weight. All dosing solutions were prepared freshly on the day of experiment.

2.5. Plasma and tissue pharmacokinetics of EAI045

To minimize variation in absorption, mice were fasted for about 3 h before EAI045 was administered by gavage into the stomach (n = 5-6), using a blunt-ended needle. EAI045 was administered orally at dose of 20 mg/kg. Elacridar was administered orally at a dose of 50 mg/kg, 3 h prior to oral EAI045 administration. For the 24 or 4 hour experiments, tail vein blood samplings were performed at 5 min, 30 min, 1, 2, 4, and 8 h or 5 min, 15 min, 30 min, 1 and 2 h time points after oral administration of EAI045, respectively, using microvettes containing heparin. For the 30 min experiments, blood samplings were performed at 5, 10, and 20 min from the tail vein. At the last time point (24 h, 4 h or 30 min), mice were anesthetized with isoflurane and blood was collected by cardiac puncture. Then mice were sacrificed by cervical dislocation and brain, liver, spleen, kidneys, lung, small intestine with content (SIWC) and testis were rapidly removed and weighed. Tissues were homogenized on ice in appropriate volumes of 2% (w/v) BSA. Blood samples were centrifuged at 9,000 *g* for 6 min at 4°C immediately after collection. All samples were stored at -30°C until analysis.

2.6. LC-MS/MS analysis

Concentrations of EAI045 (Supplemental Figure 1A) and its hydrolyzed metabolite, 5-fluoro-2-hydroxyphenyl)(1-oxo-1,3-dihydro-2H-isoindol-2-yl)acetic acid, abbreviated PIA for (phenyl-(iso)indol-acetic acid) (Supplemental Figure 1B), and EAI045 glucuronide response relative to EAI045. in cell culture medium, plasma and tissue homogenates were analyzed with a liquid-chromatography tandem mass spectrometric (LC-MS/MS) assay (method to be submitted).

2.7. Pharmacokinetic and statistical calculations

Pharmacokinetic parameters were calculated using the software GraphPad Prism7 (GraphPad Software Inc., La Jolla, CA, USA). The area under the plasma concentration-time curve (AUC) was calculated using the trapezoidal rule with the Microsoft Excel plug in PKsolver [34], without extrapolating to infinity. The peak plasma concentration (C_{max}) and the time to reach C_{max} (t_{max}) were estimated from the original data. Ordinary one-way analysis of variance (ANOVA) was used to determine significance of differences between groups, after which post-hoc tests with Tukey correction were performed for comparison between individual groups. The two-sided unpaired Student's t test was used when treatments or differences between two groups were compared. When variances were not homogeneously distributed, data were log-transformed before statistical tests were applied. Differences were considered statistically significant when $P < 0.05$. Data are presented as mean ± SD.

3. Results

3.1. *In vitro* transport of EAI045

Transepithelial drug transport of EAI045 (5 μM) was tested using polarized monolayers of Madin-Darby Canine Kidney (MDCK-II) parental cells and its subclones overexpressing hABCB1, hABCG2 or mAbcg2 cDNA. In the parental line, EAI045 was modestly transported to the apical side (efflux ratio r = 1.7, Figure 1A). This transport was completely inhibited by the ABCB1 inhibitor zosuquidar (r = 1.1, Figure 1B). This suggests that the EAI045 transport may be due to the low-level endogenous canine ABCB1 known to be expressed in the parental cell line [35]. In cells overexpressing hABCB1, there was clear apically directed transport of EAI045 (r = 5.5, Figure 1C), which was extensively inhibited by zosuquidar (r = 1.3, Figure 1D). To evaluate the interaction between hABCG2 and mAbcg2 and EAI045, zosuquidar (5 μM) was added to inhibit any endogenous canine ABCB1. In cells overexpressing hABCG2, the BA transport of EAI045 was slightly higher than the AB transport, resulting in an efflux ratio of 1.4 (Figure 1E). When the ABCG2 inhibitor

Ko143 was added, the efflux ratio was reduced to 1.1 (Figure 1F). In mAbcg2-overexpressing MDCK-II cells, there was a slight apically directed transport of EAI045 r = 1.8 (Figure 1G), and this could be reduced with Ko143 to an r of 1.4 (Figure 1H). EAI045 thus appears to be a good transport substrate of hABCB1, a moderate transport substrate of the endogenous canine ABCB1, whereas it is at best slightly transported by mouse Abcg2 or human ABCG2 *in vitro*.

3.2. Impact of ABCB1 and ABCG2 on EAI045 plasma pharmacokinetics and tissue distribution over 4 hours

Based on the *in vitro* transport results, we evaluated a possible effect of both transporters on EAI045 plasma pharmacokinetics (systemic exposure upon oral drug administration, or oral exposure in short) and tissue distribution in mice. A 4-h pilot experiment was performed in female wild-type (WT) and combination *Abcb1a/1b;Abcg2*$^{-/-}$ mice, using oral administration of 20 mg/kg EAI045. As shown in Supplemental Figure 2A-B, EAI045 was very rapidly absorbed in all strains, with an apparent t_{max} around 5 min. The plasma exposure of EAI045 over 4 h (AUC_{0-4h}) was not significantly different between WT and *Abcb1a/1b;Abcg2*$^{-/-}$ mice (Supplemental Figure 2C). However, inter-individual variation was high, as we often observe shortly after oral drug administration.

We next measured the brain, liver, kidney, spleen, lung, and small intestine with content (SIWC) concentrations of EAI045 4 h after oral administration. Although at t = 4 h the plasma concentrations in both strains were similar, the brain concentrations and brain-to-plasma ratios in *Abcb1a/1b;Abcg2*$^{-/-}$ mice were dramatically higher than those in WT mice (25-fold and 12-fold, respectively, Supplemental Figure 3A-B). We also observed a modest but significantly higher liver concentration (2.8-fold) and liver-to-plasma ratio (1.6-fold) (Supplemental Figure 3C-D) in *Abcb1a/1b;Abcg2*$^{-/-}$ mice compared to WT mice. In contrast, the small intestine with content (SIWC) percentage of dose (SIWC%) and SIWC%-to-plasma ratio was reduced in *Abcb1a/1b;Abcg2*$^{-/-}$ mice (Supplemental Figure 3K-L). No significant differences were detected between the strains in kidney-, spleen- and lung-to-plasma ratios (Supplemental Figure 3E-J). Collectively, these results indicate that Abcb1a/1b and/or Abcg2 can efficiently limit the brain penetration of EAI045, and possibly they are involved in its hepatic and intestinal disposition.

EAI045 is hydrolyzed to a major metabolite, which would be negatively charged under physiological conditions (PIA, Supplemental Figure 1B). We therefore studied the plasma and tissue concentration of PIA over 4 h after oral EAI045 administration at 20 mg/kg. There were no significant differences in plasma concentration (Supplemental Figure 2D-F), tissue concentrations, and tissue-to-plasma ratios (data not shown) of PIA between the mouse strains. This suggests that Abcb1a/1b and/or Abcg2 play little or no role in limiting PIA availability and tissue distribution.

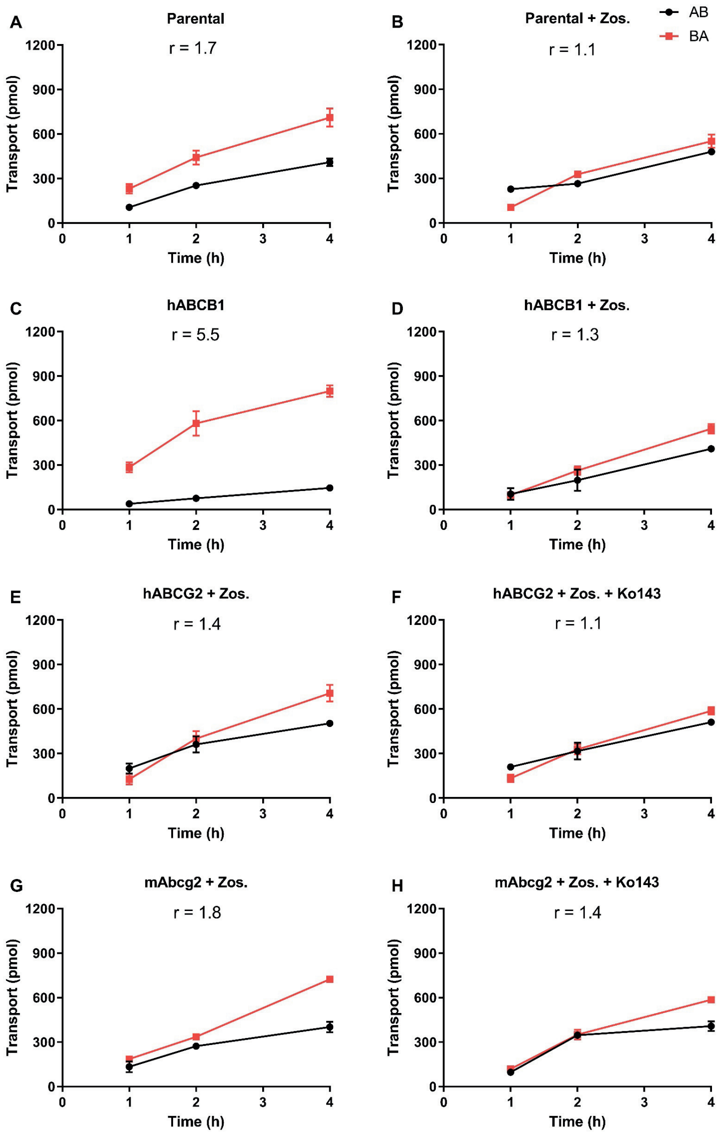

Figure 1. *In vitro* transepithelial transport of EAI045 (5 µM) using MCDK-II parental cells (A, B) or transduced with human ABCB1 (C, D), human ABCG2 (E, F), or murine Abcg2 (G, H) cDNA. At t = 0 EAI045 was added in the donor compartment (either apical or basolateral). At 1, 2 and 4 h EAI045 was quantified in the acceptor compartment and the cumulative total transported amount per well was plotted (n = 3). Zosuquidar (5 µM) was added to inhibit the human and/or the endogenous ABCB1, while Ko143 (5 µM) was added to inhibit the human or murine ABCG2. r, relative transport ratio. BA (■), translocation from the basolateral to the apical compartment; AB (●), translocation from the apical to the basolateral compartment. Points, mean; bars, SD.

3.3. Impact of ABCB1 and ABCG2 on EAI045 plasma pharmacokinetics and tissue distribution over 30 minutes

We next studied in more detail the single and combined effects of Abcb1 and Abcg2 deficiencies on EAI045 plasma pharmacokinetics and organ accumulation using male WT, *Abcg2*$^{-/-}$, *Abcb1a/1b*$^{-/-}$, and *Abcb1a/1b;Abcg2*$^{-/-}$ mice. As we wanted to assess tissue concentrations while plasma concentrations were still relatively high, we terminated this experiment at 30 min. As shown in Figure 2A-B, there were only limited differences in plasma EAI045 levels over 30 min ($AUC_{0\text{-}30min}$) due to the absence of Abcb1a/1b or Abcg2. Loss of both Abcb1a/1b and Abcg2 resulted in a 1.7-fold increase in plasma $AUC_{0\text{-}30min}$, which was not significant compared to WT mice, but also in a significant 2.1-fold increase relative to single *Abcb1a/1b*$^{-/-}$ mice (Figure 2A-B; Table 1). These results suggest that each of these transporters may have a minor limiting impact on the oral exposure of EAI045 in mice. As we had observed in the 4-h experiment, there was also high inter-individual variation for this 30-min experiment, especially during the first 10 min after administration in all mouse strains. This may be due to variable rates of stomach emptying for this drug.

At 30 min, *Abcb1a/1b*$^{-/-}$ and *Abcb1a/1b;Abcg2*$^{-/-}$ mice showed increased brain concentrations compared to WT mice, by 3.5-fold and 7.2-fold, respectively (Figure 3A; Table 1). After correcting for the plasma concentrations, *Abcb1a/1b*$^{-/-}$ and *Abcb1a/1b;Abcg2*$^{-/-}$ mice showed significant increases in brain-to-plasma ratios, by 3.9-fold and 4.8-fold, respectively. However, no significant difference was seen between *Abcg2*$^{-/-}$ mice and WT mice (Figure 3B; Table 1). Moreover, for *Abcb1a/1b;Abcg2*$^{-/-}$ mice, the brain-to-plasma ratio was 4.8-fold increased ($P < 0.001$) compared to that in WT mice, and 5.2-fold increased ($P < 0.001$) compared to *Abcg2*$^{-/-}$ mice, but with no significant difference compared to *Abcb1a/1b*$^{-/-}$ mice (Figure 3B; Table 1). This indicates that primarily Abcb1a/1b can markedly restrict the brain penetration of EAI045. The testis distribution of EAI045 behaved qualitatively similar to that in the brain. The testis-to-plasma ratios in *Abcb1a/1b*$^{-/-}$ and *Abcb1a/1b;Abcg2*$^{-/-}$ mice were significantly increased by 3.1-fold and 2.2-fold compared to WT mice, and by 4.5-fold and 3.1-fold compared to *Abcg2*$^{-/-}$ mice, respectively (Figure 3D; Table 1).

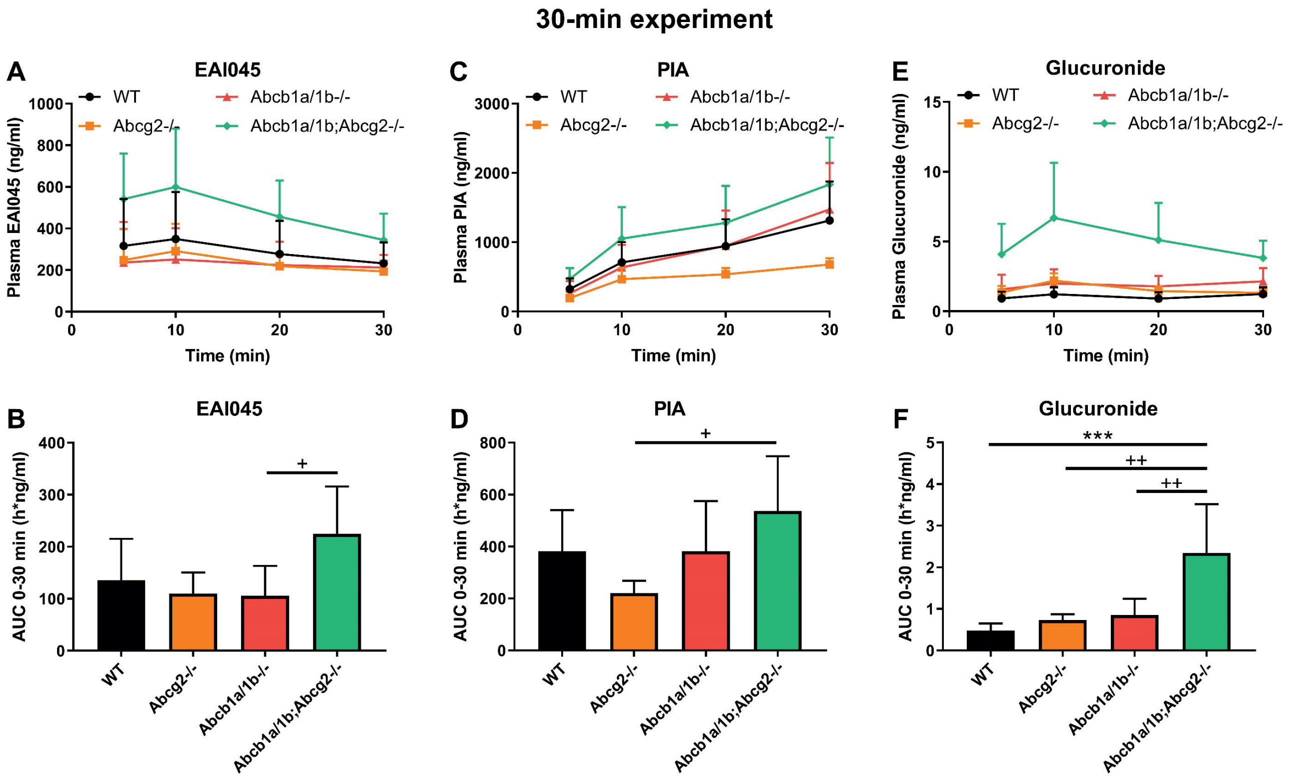

Figure 2. Plasma concentration-time curves and AUC$_{0\text{-}30min}$ of EAI045 (A, B), PIA (C, D), and EAI045 glucuronide (E, F) in male WT, *Abcb1a/1b*$^{-/-}$, *Abcg2*$^{-/-}$ and *Abcb1a/1b;Abcg2*$^{-/-}$ mice 30 minutes after oral administration of 20 mg/kg EAI045. Data are given as mean ± S.D. (n = 6-7). *, $P < 0.05$; **, $P < 0.01$; ***, $P < 0.001$ compared to WT mice. $^{+}$, $P < 0.05$; $^{++}$, $P < 0.01$; $^{+++}$, $P < 0.001$ compared to *Abcb1a/1b;Abcg2*$^{-/-}$ mice.

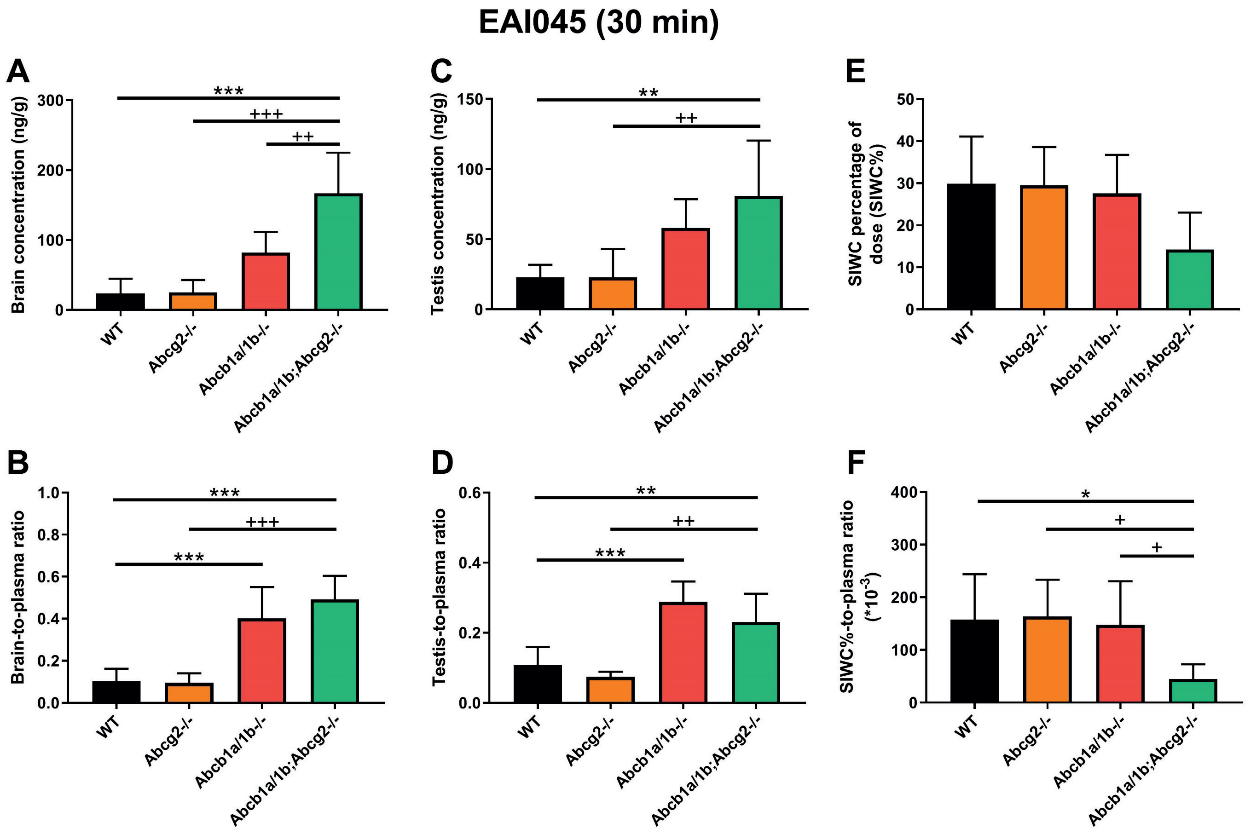

Figure 3. Organ concentration (A, C, E), and organ-to-plasma ratio (B, D, F) of EAI045 in male WT, *Abcb1a/1b*$^{-/-}$, *Abcg2*$^{-/-}$ and *Abcb1a/1b;Abcg2*$^{-/-}$ mice 30 minutes after oral administration of 20 mg/kg EAI045. Data are given as mean ± S.D. (n = 6-7). *, $P < 0.05$; **, $P < 0.01$; ***, $P < 0.001$ compared to WT mice. $^{+}$, $P < 0.05$; $^{++}$, $P < 0.01$; $^{+++}$, $P < 0.001$ compared to *Abcb1a/1b;Abcg2*$^{-/-}$ mice.

In contrast to brain and testis, the recovery of EAI045 (percentage of dose) in the SIWC was substantially reduced in the *Abcb1a/1b;Abcg2*$^{-/-}$ mice compared with the other mouse strains, especially when corrected for plasma exposure, but the single knockout strains were not reduced compared to WT mice (Figure 3E and F, Table 1). This observation suggests that both Abcb1a/1b and Abcg2 may affect enterohepatic circulation of EAI045 by mediating intestinal excretion, and thus limiting net absorption across the intestinal wall. In this way the absence of Abcb1a/1b and Abcg2 could reduce the amount of drug recovered from the intestinal content. At this early time point after EAI045 oral administration (30 min), a large amount of EAI045 was recovered from the intestinal lumen in WT mice (29.9%), and about half that amount in *Abcb1a/1b;Abcg2*$^{-/-}$ mice (14.2%) (Figure 3E, Table 1). However, at 4 h, there was only 1.7% left in WT intestinal lumen (Supplemental Figure 3K), suggesting that longer term EAI045 was not retained extensively in the intestinal lumen.

The other tested tissues including liver, kidney, spleen and lung demonstrated no meaningful differences in tissue concentrations or tissue-to-plasma ratios between the mouse strains, except for one, likely spurious, outlier for the liver-to-plasma ratio in *Abcb1a/1b*$^{-/-}$ but not *Abcb1a/1b;Abcg2*$^{-/-}$ mice. Typical tissue-to-plasma ratios were about 5.7, 2.8, 1.1, and 2.6 for liver, kidney, spleen and lung, respectively (Supplemental Figure 4), so far higher than those observed for (WT) brain (0.10) and testis (0.11).

3.4. Impact of ABCB1 and ABCG2 on plasma pharmacokinetics and tissue distribution of EAI045 metabolites

After oral administration of EAI045, we also measured the PIA concentration in plasma and different tissues. Within 10 min PIA was more abundant in plasma than the parent drug in all strains, suggesting a relatively rapid conversion to this metabolite (Figure 2A and C). However, there were no meaningful differences in oral $AUC_{0\text{-}30min}$ between the strains (Figure 2C-D). The PIA/EAI045 $AUC_{0\text{-}30min}$ ratios ranged between 270-480% and also did not show meaningful differences between the strains (Supplemental Figure 5A-B). This suggests that any differences between the strains mainly reflected the higher EAI045 levels in the *Abcb1a/1b;Abcg2*$^{-/-}$ mice. For tissues, we found only a significant decrease in SIWC% (1.8-fold, $P < 0.05$) and SIWC%-to-plasma ratios (2.7-fold, $P < 0.05$) in *Abcb1a/1b;Abcg2*$^{-/-}$ mice compared to WT mice, again in line with the results found for EAI045. The absolute amount of PIA retrieved from SIWC at this time point was much smaller than that of EAI045 (~0.3% vs ~30% of the EAI045 dose in WT mice), although the latter may well have represented yet unabsorbed EAI045 from the dosing. Furthermore, there were no significant differences in tissue-to-plasma ratios among these strains for brain, testis, liver, kidney, spleen, and lung (Supplemental Figure 5C-P). Brain penetration was extremely low, with the brain-to-plasma ratio at only 0.014 in WT mice, consistent with the negatively charged nature of PIA. Also distribution of PIA to other tissues was generally much lower than that of the parent compound, with the possible exception of kidney.

Altogether, the data suggest a very limited impact of the ABC transporters on PIA disposition, with the possible exception of intestinal excretion.

Table 1. Plasma and tissue pharmacokinetic parameters of EAI045 in male WT, *Abcb1a/1b*$^{-/-}$, *Abcg2*$^{-/-}$ and *Abcb1a/1b;Abcg2*$^{-/-}$ mice over 30 minutes after oral administration of 20 mg/kg EAI045 without or with inhibitor elacridar (Ela, only for WT mice).

Parameter (EAI045)	Genotype				
	WT	*Abcg2*$^{-/-}$	*Abcb1a/1b*$^{-/-}$	*Abcb1a/1b;Abcg2*$^{-/-}$	WT+Ela
Plasma $AUC_{0\text{-}30min}$ (h*ng/ml)	136 ± 80	110 ± 41	106 ± 57^{+}	225 ± 91	549 ± 82$^{***,\ +++}$
Fold change AUC	1.0	0.81	0.78	1.7	4.0
t_{max} (min)	5-30	10-30	10-30	10-30	10-30
C_{max} (ng/ml)	354 ± 225	310 ± 114	201 ± 79	603 ± 277	1512 ± 260
C_{brain} (ng/g)	23.3 ± 21.3	25.2 ± 17.6^{+++}	82.0 ± 29.7^{++}	166.9 ± 58.4***	395.9 ± 123.1$^{***,\ +++}$
Fold change C_{brain}	1.0	1.1	3.5	7.2	17.0
$K_{p.brain}$	0.103 ± 0.059	0.094 ± 0.046^{+++}	0.401 ± 0.149***	0.492 ± 0.112***	0.560 ± 0.200***
Fold change $K_{p.brain}$	1.0	0.92	3.9	4.8	5.4
C_{testis} (ng/g)	22.8 ± 8.9	22.8 ± 20.2^{++}	70.9 ± 36.2	80.9 ± 39.4**	198.7 ± 58.9$^{***,\ +++}$
Fold change C_{testis}	1.0	1.0	3.1	3.5	8.7
$K_{p.testis}$	0.107 ± 0.052	0.074 ± 0.015^{++}	0.329 ± 0.114***	0.231 ± 0.080**	0.280 ± 0.096**
Fold change $K_{p.testis}$	1.0	0.69	3.1	2.2	2.6
SIWC%	29.9 ± 11.3	29.5 ± 9.1	27.6 ± 9.2	14.2 ± 8.8	4.00 ± 2.57***
Fold change SIWC%	1.0	0.99	0.92	0.48	0.13
$K_{p.SIWC\%}$	158 ± 86	164 ± 70^{+}	148 ± 82^{+}	44.4 ± 28.3*	5.13 ± 2.63***
Fold change $K_{p.SIWC\%}$	1.0	1.04	0.94	0.28	0.032

Data are given as mean ± S.D. (n = 6-7). $AUC_{0\text{-}30min}$, area under the plasma concentration-time curve; C_{max}, maximum concentration in plasma; t_{max}, time point (min) of maximum plasma concentration; C_{tissue}, tissue concentration; $K_{p.tissue}$, tissue-to-plasma ratio. SIWC, small intestine with contents; SIWC%, Drug percentage of dose in SIWC, expressed as total drug (ng) in SIWC divided by total drug administered (ng). *, $P < 0.05$; **, $P < 0.01$; ***, $P < 0.001$ compared to WT mice. $^{+}$, $P < 0.05$; $^{++}$, $P < 0.01$; $^{+++}$, $P < 0.001$ compared to *Abcb1a/1b;Abcg2*$^{-/-}$ mice.

EAI045 itself is also conjugated to form EAI045 glucuronide, although the exact location of the glucuronide is as yet unclear. We therefore studied the plasma concentration of EAI045 glucuronide over time after oral EAI045 administration at 20 mg/kg. For the EAI045 glucuronide, the plasma $AUC_{0\text{-}30min}$ was significantly increased in *Abcb1a/1b;Abcg2*$^{-/-}$ mice, by 4.9-fold ($P < 0.001$) compared to WT mice, and by 3.2-fold and 2.7-fold compared to *Abcg2*$^{-/-}$ and *Abcb1a/1b*$^{-/-}$ mice (Figure 2E-F). Due to absence of an internal standard, EAI045 glucuronide could only be semi-quantified relative to the EAI045 detector response, but this semiquantification does allow relative concentration comparisons to be made within one tissue or matrix. Due to the higher plasma exposure of the glucuronide in *Abcb1a/1b;Abcg2*$^{-/-}$ mice, kidney and liver also had significantly higher glucuronide concentrations in this strain. However, the tissue-to-plasma ratios revealed no meaningful differences among all the mouse strains (Supplemental Figure 6A-H). Interestingly, both SIWC%-to-plasma ratio and SIWC% accumulation were clearly reduced in *Abcb1a/1b;Abcg2*$^{-/-}$ mice compared to WT mice (4.4-fold and 5.5-fold), as well as to *Abcg2*$^{-/-}$ mice (2.6-fold and 2.5-fold) (Supplemental Figure 6I-M). The data suggest that Abcb1a/1b and Abcg2 are to some extent involved in the plasma clearance of EAI045 glucuronide, possibly through a relatively reduced hepatobiliary and/or direct intestinal excretion in *Abcb1a/1b;Abcg2*$^{-/-}$ mice. It should be noted, however, that the glucuronide response relative to EAI045 was low, 2.9% for kidney, 1.8% for liver, and 0.17% for SIWC (Supplemental Figure 6A, E, I), suggesting a very low amount of EAI045 glucuronide formed overall.

3.5. Co-administration of elacridar boosts brain and testis distribution of EAI045

As shown in Figure 3 and Table 1, there were substantial differences between WT and *Abcb1a/1b;Abcg2*$^{-/-}$ mice in brain-to-plasma ratios, as well as testis and intestinal disposition. In view of the potential therapeutic benefit of enhancing EAI045 brain accumulation, and possibly also plasma exposure, we wanted to investigate to what extent the dual ABCB1 and ABCG2 inhibitor elacridar could increase the oral exposure and brain accumulation of EAI045. We performed a 30-min pharmacokinetic experiment with an EAI045 dose of 20 mg/kg, and elacridar at 50 mg/kg. As elacridar plasma concentration peaks around 3-4 hours after oral administration, elacridar was administered orally 3 h prior to oral EAI045 administration to male WT mice. Plasma and tissue EAI045 levels were assessed 30 min later. In elacridar-treated WT (WT+Ela) mice, the EAI045 plasma $AUC_{0\text{-}30min}$ was markedly increased compared to WT without elacridar treatment (4-fold, $P < 0.001$). Unexpectedly, in the presence of elacridar, the plasma $AUC_{0\text{-}30min}$ of EAI045 was further increased significantly by 2.4-fold ($P < 0.001$) in WT+Ela mice compared to that in *Abcb1a/1b;Abcg2*$^{-/-}$ mice (Figure 4A-B; Table 1). These results indicate that EAI045 oral plasma exposure in WT mice could be markedly increased by elacridar, but that likely other systems in addition to ABC transporters were affected by the elacridar treatment that can normally restrict EAI045 plasma exposure.

With respect to tissue distribution, elacridar treatment dramatically increased the brain concentration of EAI045 in WT mice by 17-fold ($P < 0.001$), and brain-to-plasma ratios by 5.4-fold ($P < 0.001$). The brain-to-plasma ratio was thus similar to that observed in *Abcb1a/1b;Abcg2*$^{-/-}$ mice without elacridar (Figure 4C-D; Table 1). Pretreatment with elacridar also increased the EAI045 testis distribution in WT mice, in a pattern very similar to that seen for brain (Figure 4 E-F; Table 1). In contrast, the liver-, kidney-, spleen- and lung-to-plasma ratios of EAI045 were not noticeably affected by elacridar treatment in the WT mouse strain compared to WT and *Abcb1a/1b;Abcg2*$^{-/-}$ mice without elacridar treatment (Supplemental Figure 7A-H).

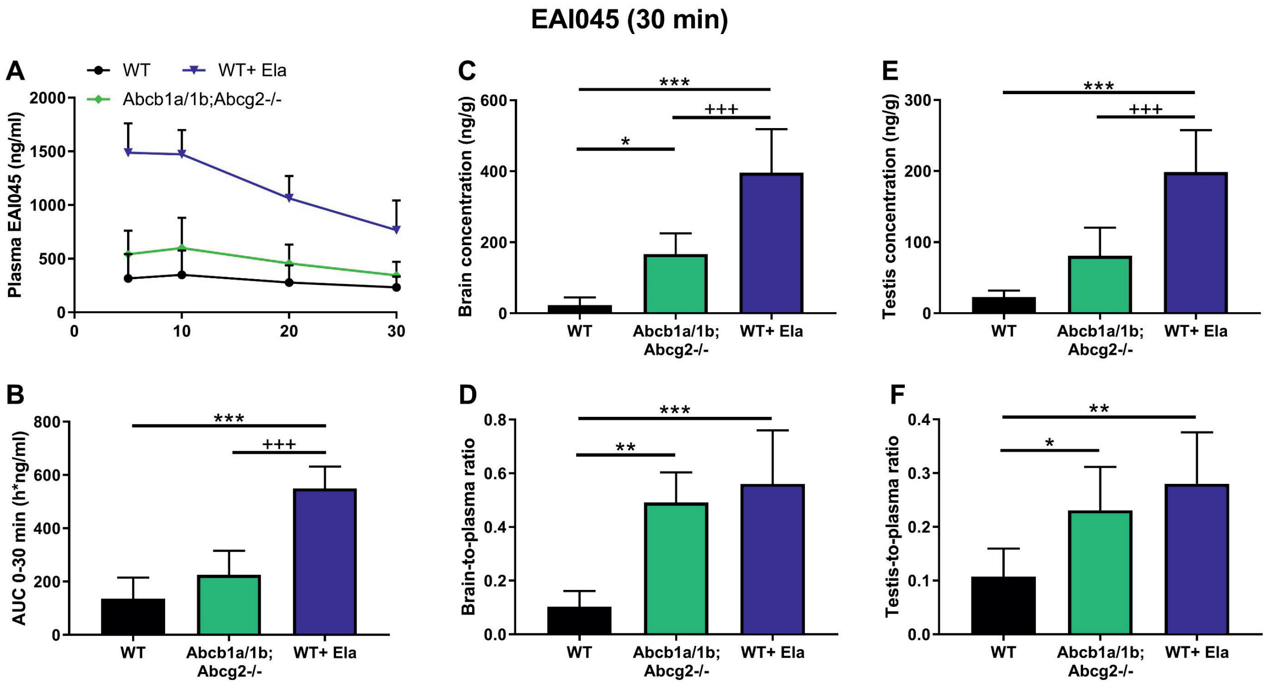

Figure 4. Plasma concentration-time curves (A), plasma $AUC_{0\text{-}30min}$ (B), brain and testis concentration (C, E), and brain- and testis-to-plasma ratio of EAI045 (D, F) in male WT and *Abcb1a/1b;Abcg2*$^{-/-}$ mice over 30 minutes after oral administration of 20 mg/kg EAI045 with or without co-administration of elacridar (Ela). Data are given as mean ± S.D. (n = 6-7). *, $P < 0.05$; **, $P < 0.01$; ***, $P < 0.001$ compared to WT mice. $^{+}$, $P < 0.05$; $^{++}$, $P < 0.01$; $^{+++}$, $P < 0.001$ compared to *Abcb1a/1b;Abcg2*$^{-/-}$ mice.

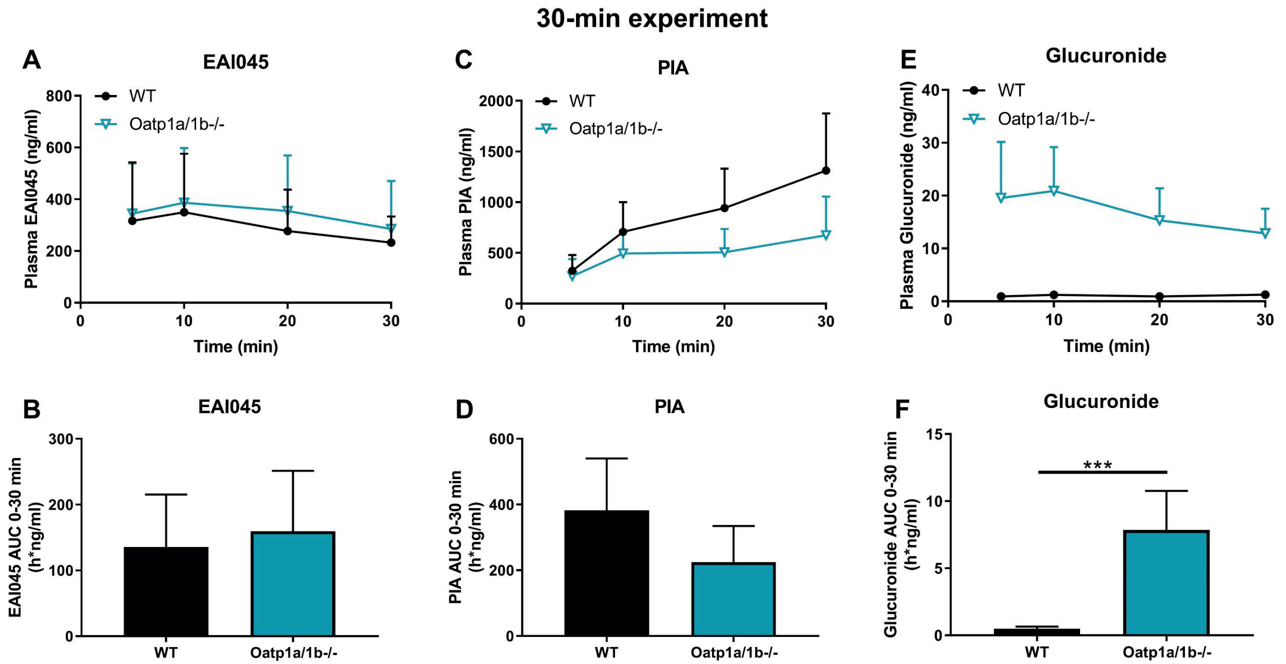

Figure 5. Plasma concentration-time curves and AUC$_{0\text{-}30\text{min}}$ of EAI045 (A, B), PIA (C, D), and EAI045 glucuronide (E, F) in male WT and *Oatp1a/1b*$^{-/-}$ mice 30 minutes after oral administration of 20 mg/kg EAI045. Data are given as mean ± S.D. (n = 6-7). *, $P < 0.05$; **, $P < 0.01$; ***, $P < 0.001$ compared to WT mice.

Interestingly, in the presence of elacridar, the percentage of dose present in the SIWC and the relative SIWC%-to-plasma ratio in WT+Ela mice were significantly decreased by 7.5-fold and 30.8-fold, respectively, compared to WT mice without elacridar treatment. Moreover, these differences were also found between WT+Ela and *Abcb1a/1b;Abcg2*$^{-/-}$ mice, i.e., WT+Ela showed 3.5-fold and 8.6-fold decreases for SIWC% and SIWC%-to-plasma ratio, respectively, compared to *Abcb1a/1b;Abcg2*$^{-/-}$ mice (Supplemental Figure 7I-J). In conjunction with the disproportionately increased plasma levels of EAI045 in WT+Ela mice, this suggests that elacridar treatment can markedly improve the net intestinal uptake of EAI045. It therefore appears that elacridar can not only inhibit Abcb1a/1b and Abcg2 in intestine and liver, but also some other system(s), perhaps another efflux transporter, that can restrict the net intestinal uptake of EAI045.

Collectively, these data indicate that oral elacridar pretreatment can extensively and specifically inhibit the activity of mouse Abcb1 and Abcg2 in the BBB and BTB, leading to markedly increased EAI045 distribution to the brain and testis after oral administration. Furthermore, elacridar might also inhibit some EAI045 elimination system(s) other than Abcb1 and Abcg2, causing increased net drug absorption from the gut, leading to additionally increased plasma exposure and decreased small intestinal content retention of EAI045.

3.6. Impact of OATP1A/1B on plasma pharmacokinetics and tissue disposition of EAI045 and its metabolites

OATP-mediated liver uptake can also affect the (oral) plasma exposure and elimination of a number of substrate drugs. Very little is known about possible interactions of EAI045 with OATP/SLCO uptake transporters. We therefore performed an experiment administering oral EAI045 (20 mg/kg) to male WT and *Oatp1a/1b*$^{-/-}$ mice and analyzed the plasma concentrations over 30 min as well as the liver-to-plasma ratios at 30 min. Systemic exposure of EAI045 was not changed in *Oatp1a/1b*$^{-/-}$ mice compared to the WT mice (Figure 5A-B). We further observed no significant differences between WT and *Oatp1a/1b*$^{-/-}$ mice in tissue concentration or tissue-to-plasma ratios of EAI045 for brain, testis, spleen, lung, liver and SIWC (Supplemental Figure 8A-H, K-N). This suggests that there is no meaningful impact of the mouse Oatp1a/1b transporters on EAI045 oral exposure and distribution to these tissues. We did observe modestly but significantly higher kidney concentration and kidney-to-plasma ratio in *Oatp1a/1b*$^{-/-}$ mice compared to WT mice, but given the high experimental variation an the large number of tissues assessed, it is uncertain whether these differences are meaningful (Supplemental Figure 8I-J).

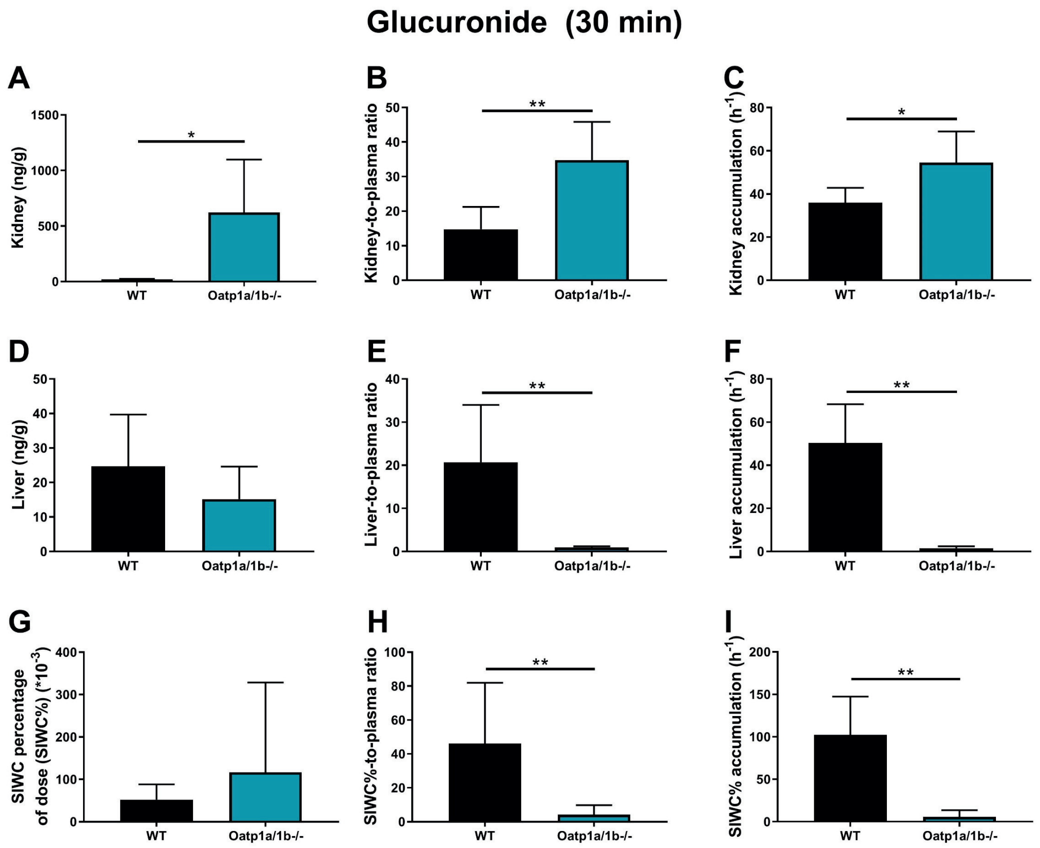

Figure 6. EAI045 glucuronide response relative to EAI045 concentration in each tissue and matrix (A, D, G), response-to-plasma ratio (B, E, H) and response accumulation (C, F, I) in male WT and *Oatp1a/1b*$^{-/-}$ mice 30 minutes after oral administration of 20 mg/kg EAI045. Data are given as mean ± S.D. (n = 6-7). *, $P < 0.05$; **, $P < 0.01$; ***, $P < 0.001$ compared to WT mice.

The potential effect of Oatp1a/1b on the pharmacokinetics of the, negatively charged, metabolite PIA was investigated also. Whereas the plasma concentrations of PIA were somewhat lower in *Oatp1a/1b*$^{-/-}$ than in WT mice, this difference was not statistically significant (Figure 5C-D). Loss of Oatp1a/1b further resulted in a 4.2-fold increase in kidney-to-plasma ratio, and a 3.3-fold increase in brain-to-plasma ratio (Supplemental Figure 9), suggesting that one or more of the Oatp1a/1b transporters might be involved in net efflux of PIA from these tissues. Perhaps more conventionally, we observed a 1.5-fold decrease in liver-to-plasma ratio of this metabolite, which might be consistent with reduced hepatic uptake of PIA due to Oatp1a/1b deficiency. No significant differences were found for testis, spleen, lung, and SIWC (Supplemental Figure 9).

For EAI045 glucuronide, the C_{max} and $AUC_{0\text{-}30min}$ in plasma were 15-fold and 16-fold increased in *Oatp1a/1b*$^{-/-}$ compared to WT mice (Figure 5E-F; Table 2). In *Oatp1a/1b*$^{-/-}$ mice the extrapolated plasma $AUC_{0\text{-}30min}$ of the glucuronide was 7.86 h*ng/ml, so still very low compared to the EAI045 $AUC_{0\text{-}30min}$ (136 h*ng/ml) in WT mice). Perhaps not surprisingly, loss of mOatp1a/1b resulted in a 22.6-fold decreased liver-to-plasma ratio and a 32.6-fold decreased liver accumulation (Figure 6D-F; Table 2) in *Oatp1a/1b*$^{-/-}$ mice compared to WT mice. This indicates that EAI045 glucuronide was efficiently taken up by mouse mOatp1a/1b into the liver. We also observed a significant decrease in SIWC%-to-plasma ratio (11.3-fold) and SIWC% accumulation (17.6-fold) in *Oatp1a/1b*$^{-/-}$ mice compared to WT mice (Figure 6G-I; Table 2). This probably reflects the dramatically reduced liver accumulation of the glucuronide, and likely subsequent biliary excretion into the intestinal lumen. In contrast, the kidney concentration was about 35-fold higher in *Oatp1a/1b*$^{-/-}$ mice, and after correction for the plasma concentration and $AUC_{0\text{-}30min}$, the increases were still about 2.4-fold and 1.5-fold compared to WT mice (Figure 6A-C; Table 2). Possibly Oatp1a/1b plays a minor role in release of the glucuronide from kidney.

3.7. Limited *in vivo* role of CYP3A in EAI045 pharmacokinetics

To assess the interaction between EAI045 and CYP3A *in vivo*, we performed a 24 h pharmacokinetic pilot experiment with oral EAI045 at 20 mg/kg in female WT, Cyp3a knockout (*Cyp3a*$^{-/-}$), and transgenic Cyp3aXAV mice (humanized model that expresses the human CYP3A4 in liver and small intestine in a *Cyp3a*$^{-/-}$ background). The plasma exposure and tissue distribution of EAI045 and PIA were assessed. The t_{max} in all strains was around 5-30 min. The plasma exposure of EAI045 over 30 min ($AUC_{0\text{-}30min}$), somewhat unexpectedly, was slightly but significantly lower in *Cyp3a*$^{-/-}$ mice than WT mice (1.6-fold). In contrast, relative to *Cyp3a*$^{-/-}$ or WT mice, the $AUC_{0\text{-}30min}$ and C_{max} were not changed in Cyp3aXAV mice (Supplemental Figure 10A-C). Similar results were obtained for PIA (Supplemental Figure 10D-F). While not plotted separately, the PIA/EAI045 AUC ratios were also hardly changed between the three mouse strains. Overall, the modest shifts observed, and their unexpected direction, suggest that mouse Cyp3a and human CYP3A4 itself are not major determinants of EAI045 or PIA pharmacokinetics in mice.

Table 2. Plasma and tissue pharmacokinetic parameters of EAI045 glucuronide in male WT and *Oatp1a/1b*$^{-/-}$ mice over 30 minutes after oral administration of 20 mg/kg EAI045.

Parameter (glucuronide)	Genotype	
	WT	*Oatp1a/1b*$^{-/-}$
Plasma AUC$_{0\text{-}30min}$ (h*ng/ml)	0.483 ± 0.168	7.86 ± 2.91***
Fold change AUC	1.0	16
t$_{max}$ (min)	5-30	5-30
C$_{max}$ (ng/ml)	1.53 ± 0.55	22.2 ± 8.9
Kidney	17.6 ± 7.3	622 ± 475*
Fold change kidney	1.0	35
K$_{p.Kidney}$	14.8 ± 6.5	34.8 ± 11.1**
Fold change K$_{p.Kidney}$	1.0	2.4
P$_{Kidney}$ (*10^{-6}h^{-1})	36.0 ± 6.8	54.6 ± 14.3*
Fold change P$_{Kidney}$	1.0	1.5
Liver	24.7 ± 15.0	15.2 ± 9.4
Fold change liver	1.0	0.62
K$_{p.Liver}$	20.7 ± 13.3	0.915 ± 0.315**
Fold change K$_{p.Liver}$	1.0	0.044
P$_{Liver}$ (*10^{-6}h^{-1})	50.3 ± 18.0	1.54 ± 0.87**
Fold change P$_{Liver}$	1.0	0.031
SIWC%	52.3 ± 36.1	117 ± 211
Fold change SIWC%	1.0	2.2
K$_{p.SIWC\%}$	46.2 ± 35.7	4.08 ± 5.72**
Fold change K$_{p.SIWC\%}$	1.0	0.088
P$_{SIWC\%}$ (*10^{-6}h^{-1})	102 ± 45	5.80 ± 7.84**
Fold change P$_{SIWC\%}$	1.0	0.057

Data are given as mean ± S.D. (n = 6-7). AUC$_{0\text{-}30min}$, area under the plasma concentration-time curve; C$_{max}$, maximum concentration in plasma; t$_{max}$, time point (min) of maximum plasma concentration; C$_{tissue}$, tissue concentration; K$_{p.tissue}$, tissue-to-plasma ratio. SIWC, small intestine tissue with contents; SIWC%, C: Drug percentage of dose in SIWC, which was expressed as total drug (ng) in SIWC divided by total drug administered (ng). *, $P < 0.05$; **, $P < 0.01$; ***, $P < 0.001$ compared to WT mice.

4. Discussion

In this study we show that EAI045 is transported well *in vitro* by human ABCB1, moderately by canine ABCB1 and at best slightly by mouse Abcg2 and human ABCG2. *In vivo* mAbcb1a/1b had a significant impact on EAI045 pharmacokinetics and tissue distribution, with perhaps a slight contribution of mAbcg2. Although the absence of Abcb1a/1b and Abcg2 did not substantially increase the oral exposure of EAI045, the relative brain penetration of EAI045 was clearly increased when both Abcb1 and Abcg2 were ablated (by 4.8-fold), and also by the absence of single Abcb1a/1b (3.9-fold). Similarly, the relative testis penetration of EAI045 was increased when both Abcb1a/1b and Abcg2 were absent (by 2.2-fold), and by the loss of single Abcb1a/1b (by 3.1-fold). These results demonstrate that Abcb1a/1b plays an important role in the BBB and BTB in limiting the brain and testis penetration of EAI045. We observed a significantly decreased SIWC%-to-plasma ratio of EAI045 in small intestine with content in the mice lacking both Abcb1a/1b and Abcg2 (3.6-fold), but not in mice lacking only one of these systems. These findings support a role for both Abcb1a/1b and Abcg2 in the intestinal disposition of EAI045. As liver accumulation was not substantially altered by Abcb1a/1b and Abcg2 deficiency in the 30-min experiment, this suggests that Abcb1a/1b and Abcg2 primarily exert their effect by mediating direct efflux of EAI045 across the intestinal wall (also reducing net intestinal uptake). In contrast, EAI045 distribution to kidney, spleen, and lung was not markedly affected by Abcb1a/1b and Abcg2 deficiency.

The brain penetration of EAI045 was considerably increased in the absence of both Abcb1 and Abcg2 or in the absence of Abcb1 alone, but not in the absence of Abcg2. Since single Abcb1a/1b-deficient mice showed an increase in EAI045 brain penetration almost equal to that in the combination knockout, Abcg2 makes at best a minor contribution in the BBB. Clearly Abcb1a/1b has a dominant role, and this also appears to apply to the BTB. These results are consistent with the *in vitro* transport data, showing that EAI045 is only a (very) weak substrate of mAbcg2 and hABCG2. Overall, it seems unlikely that hABCG2 will have a substantial impact on human EAI045 pharmacokinetics and tissue distribution, although it should be kept in mind that protein expression of ABCG2 relative to ABCB1 in the human BBB is higher than in the mouse BBB [36]. This might result in a somewhat more prominent role of hABCG2 in the human BBB compared to mAbcg2 in the mouse BBB.

As brain metastases can easily occur in NSCLC, it is important to know whether EAI045 can achieve high intrinsic BBB permeability and how it interacts with ABCB1 and ABCG2 in the BBB. So far, the penetration of EAI045 into the central nervous system (CNS) has not been fully characterized, and there is little human data on the brain penetration or accumulation of EAI045. In the present study we found that in WT mice, the brain-to-plasma ratio was 0.10 at 30 min and 0.15 at 4 h after oral administration of 20 mg/kg of EAI045. Therefore, compared to many other targeted anticancer drugs, EAI045 has an intermediate ability to cross the BBB even in WT mice, but its penetration to the brain is still strongly limited by Abcb1a/1b. The high efflux ratio in ABCB1-overexpressing cells *in vitro* correlates well with the *in vivo* role of Abcb1a/1b in the

BBB. This implies that also in the human situation ABCB1 activity may considerably limit EAI045 brain penetration.

Similar results of the single and combined effects of Abcg2 and Abcb1 have been observed for other EGFR-targeting anticancer agents, including afatinib [37], brigatinib [38], and osimertinib [39]. While these drugs and EAI045 are all substrates for ABCB1 and ABCG2 to varying extents, marked differences were seen in brain penetrance. Reported increases in brain penetration in *Abcb1a/1b;Abcg2*$^{-/-}$ compared to WT mice were as follows: brigatinib (38-fold), afatinib (28-fold), osimertinib (6.4-fold), and EAI045 (4.8-fold). Overall, the effect of Abcb1 and Abcg2 on brain penetration of EAI045 was relatively modest compared to that for other EGFR inhibitors.

We further found that the dual ABCB1 and ABCG2 inhibitor elacridar could virtually completely reverse the effect of Abcb1a/1b and Abcg2 on limiting brain and testis penetration of EAI045, as well as limiting its net intestinal absorption. This suggests that elacridar coadministration could be considered to enhance the brain (and tumor) penetration of EAI045 in patients suffering from suitable EGFR mutant brain metastases. However, the 2.4-fold further increase in plasma $AUC_{0\text{-}30min}$ of EAI045 seen in WT mice relative to *Abcb1a/1b;Abcg2*$^{-/-}$ mice upon elacridar coadministration shows an additional effect on its plasma kinetics independent of Abcb1a/1b and Abcg2 inhibition. This increase in oral exposure might present a toxicity risk of this combination treatment, although we did not observe any acute externally visible toxicity in the mice during the experiment. Nonetheless, coadministration of elacridar with EAI045 in patients should only be considered with extreme caution, and it would be preferable if the alternative EAI045 clearance system affected by elacridar that appears to be present in mice would be first identified. Intriguingly, no additional changes in tissue distribution of EAI045 due to the elacridar treatment were found in other tested tissues. On the one hand this can be considered positive, as it reduces the risks of unexpected toxicities of elacridar co-treatment. On the other hand, this also does not provide any clues to the identity of the candidate EAI045 clearance system affected by elacridar.

All in all, it might be possible to enhance the efficacy of EAI045 to treat (metastatic) brain tumors in the clinic by inhibiting hABCB1, since we have shown that EAI045 is also highly transported by hABCB1 *in vitro*. Furthermore, since cancer cells themselves also often express ABCB1, they can therefore be resistant to EAI045, and ABCB1 inhibitors (like elacridar) could be co-administered to improve the efficacy of EAI045 against such tumors. It may thus be possible to further improve the efficacy of EAI045 against brain metastases and possibly also primary brain tumors by co-administration with an efficacious ABCB1/ABCG2 inhibitor. However, given the possible complications of elacridar with respect to EAI045 pharmacokinetics we observed, it might be worth considering alternative ABCB1/ABCG2 inhibitors.

Very little literature is available on the possible interaction of EAI045 with OATPs. We found that Oatp1a/1b deficiency did not markedly alter oral EAI045 plasma pharmacokinetics and liver distribution. Although there might perhaps be a modest uptake function of mOatp1a/1b transporters in EAI045 kidney accumulation, the differences in kidney-to-plasma ratio between WT and *Oatp1a/1b*$^{-/-}$ mice were small (1.6-fold) (Supplemental Figure 8J). Moreover, the plasma and liver levels were not affected. Any broader *in vivo* pharmacokinetic impact of variable OATP activity in patients on EAI045 is therefore likely to be small.

Not much is known about possible toxicity or drug-drug interactions mediated by the main EAI045 metabolites. There was little impact of Abcb1a/1b, Abcg2 and Oatp1a/1b on the plasma exposure and tissue penetration of the EAI045 hydrolyzed metabolite PIA. It is worth noting that in WT mice, the PIA/EAI045 AUC ratio was about 400% (Supplemental Figure 5A-B), suggesting that a large amount of EAI045 was converted to PIA. However, the ratios did not differ significantly between strains, indicating that Abcb1a/1b, Abcg2 or Oatp1a/1b do not have a substantial role in, or effect on, the availability, metabolism, or elimination of PIA after oral EAI045 administration.

We observed an increased plasma $AUC_{0\text{-}30min}$ and a markedly decreased accumulation and tissue-to-plasma ratio of EAI045 glucuronide in the SIWC% in the absence of Abcb1a/1b and Abcg2. This suggests that Abcb1a/1b and Abcg2 are involved in the intestinal disposition of the glucuronide, possibly by mediating hepatobiliary excretion, or direct intestinal excretion, or both. Moreover, our data show that whereas the plasma $AUC_{0\text{-}30min}$ of EAI045 was similar in WT and *Oatp1a/1b*$^{-/-}$ mice, the EAI045 glucuronide $AUC_{0\text{-}30min}$ was 16.3-fold increased in *Oatp1a/1b*$^{-/-}$ mice (Figure 5E-F; Table 2). Accordingly, there was a dramatic decrease in liver concentration of EAI045 glucuronide, from 1.8% of the administered EAI045 dose in WT mice to less than 0.8% in the Oatp1a/1b knockout mice (Supplemental Figure 6E), with a 22.6-fold decreased liver-to-plasma ratio (Figure 6F-H) in *Oatp1a/1b*$^{-/-}$ mice compared to WT mice. This clearly demonstrates that Oatp1a/1b is substantially involved in the transport of EAI045 glucuronide from blood into the liver. Also SIWC levels of EAI045 glucuronide were strongly decreased in the Oatp1a/1b knockout mice. This was most likely because of relatively reduced hepatobiliary excretion as a consequence of the reduced liver levels of the glucuronide.

Our 24-hour experiments on oral EAI045 in *Cyp3a*$^{-/-}$ and Cyp3aXAV mice suggest there may at best be a very limited effect of mouse Cyp3a or human CYP3A4 on EAI045 oral exposure (Supplemental Figure 10). Also the conversion of EAI045 to PIA is unlikely to be primarily mediated by CYP3A, given minimal changes in PIA/EAI045 ratios between the strains. However, the slightly decreased plasma $AUC_{0\text{-}30min}$ in *Cyp3a*$^{-/-}$ mice (1.6-fold) suggests that there might be other system(s) that can metabolize EAI045, perhaps Cyp2c enzymes, which are known to be compensatorily upregulated in *Cyp3a*$^{-/-}$ mice [40].

In summary, the most striking finding for this study is that Abcb1a/1b was responsible mostly for limiting the EAI045 brain and testis penetration, but not its oral exposure. Furthermore, elacridar co-administration could markedly enhance the oral availability and brain penetration of oral EAI045. Additionally, we demonstrated that Oatp1a/1b is substantially involved in the transport of EAI045 glucuronide from the blood into the liver. Finally, both mCyp3a and human CYP3A4 appear to have little, if any, direct impact on the *in vivo* oral exposure of EAI045, but we cannot exclude that there are significant changes in other EAI045-detoxifying systems. All together, these results may be considered positive for the therapeutic application of EAI045, since a low risk of affecting its oral plasma exposure by drug-drug interactions via these transporters or CYP3A4 is predicted.

5. References

1. Siegel, R.L., et al., Cancer statistics, 2021. CA: a cancer journal for clinicians, 2021. 71(1): p. 7-33.
2. Zarogoulidis, K., et al., Treatment of non-small cell lung cancer (NSCLC). Journal of thoracic disease, 2013. 5(Suppl 4): p. S389.
3. Navada, S., et al., Temporal trends in small cell lung cancer: analysis of the national Surveillance, Epidemiology, and End-Results (SEER) database. Journal of Clinical Oncology, 2006. 24(18_suppl): p. 7082-7082.
4. Sher, T., G.K. Dy, and A.A. Adjei. Small cell lung cancer. in Mayo Clinic Proceedings. 2008. Elsevier.
5. Molina, J.R., et al. Non-small cell lung cancer: epidemiology, risk factors, treatment, and survivorship. in Mayo clinic proceedings. 2008. Elsevier.
6. Thress, K.S., et al., Acquired EGFR C797S mutation mediates resistance to AZD9291 in non–small cell lung cancer harboring EGFR T790M. Nature medicine, 2015. 21(6): p. 560-562.
7. Niederst, M.J., et al., The allelic context of the C797S mutation acquired upon treatment with third-generation EGFR inhibitors impacts sensitivity to subsequent treatment strategies. Clinical Cancer Research, 2015. 21(17): p. 3924-3933.
8. Helena, A.Y., et al., Acquired resistance of EGFR-mutant lung cancer to a T790M-specific EGFR inhibitor: emergence of a third mutation (C797S) in the EGFR tyrosine kinase domain. JAMA oncology, 2015. 1(7): p. 982-984.
9. Wang, S., et al., EGFR C797S mutation mediates resistance to third-generation inhibitors in T790M-positive non-small cell lung cancer. Journal of hematology & oncology, 2016. 9(1): p. 1-5.
10. Jia, Y., et al., Overcoming EGFR (T790M) and EGFR (C797S) resistance with mutant-selective allosteric inhibitors. Nature, 2016. 534(7605): p. 129-132.
11. Goldstein, N.I., et al., Biological efficacy of a chimeric antibody to the epidermal growth factor receptor in a human tumor xenograft model. Clinical Cancer Research, 1995. 1(11): p. 1311-1318.
12. Li, S., et al., Structural basis for inhibition of the epidermal growth factor receptor by cetuximab. Cancer cell, 2005. 7(4): p. 301-311.
13. Cho, J., et al., Cetuximab response of lung cancer–derived EGF receptor mutants is associated with asymmetric dimerization. Cancer research, 2013. 73(22): p. 6770-6779.
14. Cheng, X., et al., Tissue distribution and ontogeny of mouse organic anion transporting polypeptides (Oatps). Drug metabolism and Disposition, 2005. 33(7): p. 1062-1073.
15. Cheng, X. and C.D. Klaassen, Tissue distribution, ontogeny, and hormonal regulation of xenobiotic transporters in mouse kidneys. Drug Metabolism and Disposition, 2009. 37(11): p. 2178-2185.
16. Endicott, J.A. and V. Ling, The biochemistry of P-glycoprotein-mediated multidrug resistance. Annual review of biochemistry, 1989. 58(1): p. 137-171.
17. Gottesman, M.M. and I. Pastan, Biochemistry of multidrug resistance mediated by the multidrug transporter. Annual review of biochemistry, 1993. 62(1): p. 385-427.
18. Gottesman, M.M., T. Fojo, and S.E. Bates, Multidrug resistance in cancer: role of ATP–dependent transporters. Nature Reviews Cancer, 2002. 2(1): p. 48-58.
19. Thiebaut, F., et al., Cellular localization of the multidrug-resistance gene product P-glycoprotein in normal human tissues. Proceedings of the National Academy of Sciences, 1987. 84(21): p. 7735-7738.
20. Sugawara, I., et al., Tissue distribution of P-glycoprotein encoded by a multidrug-resistant gene as revealed by a monoclonal antibody, MRK 16. Cancer research, 1988. 48(7): p. 1926-1929.
21. Cordon-Cardo, C., et al., Multidrug-resistance gene (P-glycoprotein) is expressed by endothelial cells at blood-brain barrier sites. Proceedings of the National Academy of Sciences, 1989. 86(2): p. 695-698.
22. Kennedy, B.G. and N.J. Mangini, P-glycoprotein expression in human retinal pigment epithelium. Mol Vis, 2002. 8: p. 422-430.
23. Constable, P.A., et al., P-Glycoprotein expression in human retinal pigment epithelium cell lines. Experimental eye research, 2006. 83(1): p. 24-30.

24. Schinkel, A.H. and J.W. Jonker, Mammalian drug efflux transporters of the ATP binding cassette (ABC) family: an overview. Advanced drug delivery reviews, 2003. 55(1): p. 3-29.
25. Hagenbuch, B. and P.J. Meier, Organic anion transporting polypeptides of the OATP/SLC21 family: phylogenetic classification as OATP/SLCO superfamily, new nomenclature and molecular/functional properties. Pflügers Archiv, 2004. 447(5): p. 653-665.
26. Iusuf, D., et al., Murine Oatp1a/1b uptake transporters control rosuvastatin systemic exposure without affecting its apparent liver exposure. Molecular pharmacology, 2013. 83(5): p. 919-929.
27. Wang, J., et al., P-glycoprotein (MDR1/ABCB1) and breast cancer resistance protein (BCRP/ABCG2) affect brain accumulation and intestinal disposition of encorafenib in mice. Pharmacological research, 2018. 129: p. 414-423.
28. Wang, J., et al., P-glycoprotein (MDR1/ABCB1) and Breast Cancer Resistance Protein (BCRP/ABCG2) limit brain accumulation of the FLT3 inhibitor quizartinib in mice. International journal of pharmaceutics, 2019. 556: p. 172-180.
29. Schinkel, A.H., et al., Normal viability and altered pharmacokinetics in mice lacking mdr1-type (drug-transporting) P-glycoproteins. Proceedings of the National Academy of Sciences, 1997. 94(8): p. 4028-4033.
30. Jonker, J.W., et al., The breast cancer resistance protein protects against a major chlorophyll-derived dietary phototoxin and protoporphyria. Proceedings of the National Academy of Sciences, 2002. 99(24): p. 15649-15654.
31. Jonker, J.W., et al., Contribution of the ABC transporters Bcrp1 and Mdr1a/1b to the side population phenotype in mammary gland and bone marrow of mice. Stem cells, 2005. 23(8): p. 1059-1065.
32. van Herwaarden, A.E., et al., Knockout of cytochrome P450 3A yields new mouse models for understanding xenobiotic metabolism. The Journal of clinical investigation, 2007. 117(11): p. 3583-3592.
33. van de Steeg, E., et al., Organic anion transporting polypeptide 1a/1b–knockout mice provide insights into hepatic handling of bilirubin, bile acids, and drugs. The Journal of clinical investigation, 2010. 120(8): p. 2942-2952.
34. Zhang, Y., et al., PKSolver: An add-in program for pharmacokinetic and pharmacodynamic data analysis in Microsoft Excel. Computer methods and programs in biomedicine, 2010. 99(3): p. 306-314.
35. Gartzke, D., et al., Genomic knockout of endogenous canine P-glycoprotein in wild-type, human P-glycoprotein and human BCRP transfected MDCKII cell lines by zinc finger nucleases. Pharmaceutical research, 2015. 32(6): p. 2060-2071.
36. Kamiie, J., et al., Quantitative atlas of membrane transporter proteins: development and application of a highly sensitive simultaneous LC/MS/MS method combined with novel in-silico peptide selection criteria. Pharmaceutical research, 2008. 25(6): p. 1469-1483.
37. van Hoppe, S., et al., Breast cancer resistance protein (BCRP/ABCG2) and P-glycoprotein (P-gp/ABCB1) transport afatinib and restrict its oral availability and brain accumulation. Pharmacological research, 2017. 120: p. 43-50.
38. Li, W., et al., P-glycoprotein and breast cancer resistance protein restrict brigatinib brain accumulation and toxicity, and, alongside CYP3A, limit its oral availability. Pharmacological research, 2018. 137: p. 47-55.
39. van Hoppe, S., et al., Brain accumulation of osimertinib and its active metabolite AZ5104 is restricted by ABCB1 (P-glycoprotein) and ABCG2 (breast cancer resistance protein). Pharmacological research, 2019. 146: p. 104297.
40. van Waterschoot, R.A., et al., Midazolam metabolism in cytochrome P450 3A knockout mice can be attributed to up-regulated CYP2C enzymes. Molecular pharmacology, 2008. 73(3): p. 1029-1036.

6. Supplemental materials

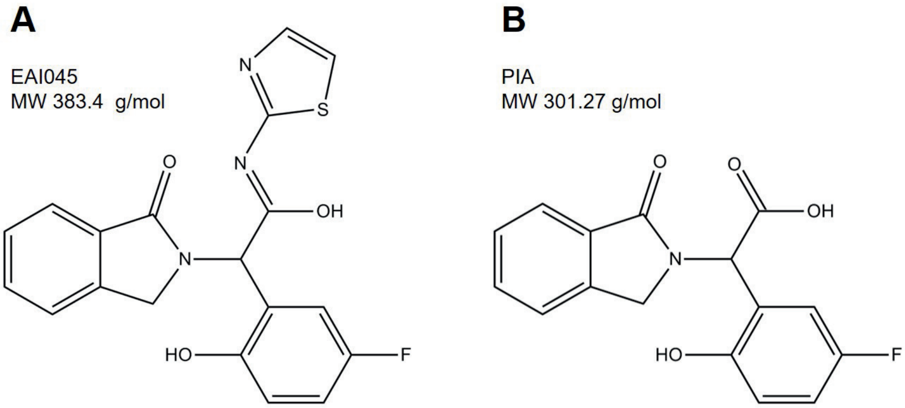

Supplemental Figure 1. Molecular structure of EAI045 (A) and its hydrolyzed metabolite, (5-fluoro-2-hydroxyphenyl)(1-oxo-1,3-dihydro-2H-isoindol-2-yl)acetic acid, abbreviated PIA for (phenyl-(iso)indol-acetic acid) (B). The exact structure of the EAI045 glucuronide is as yet unknown.

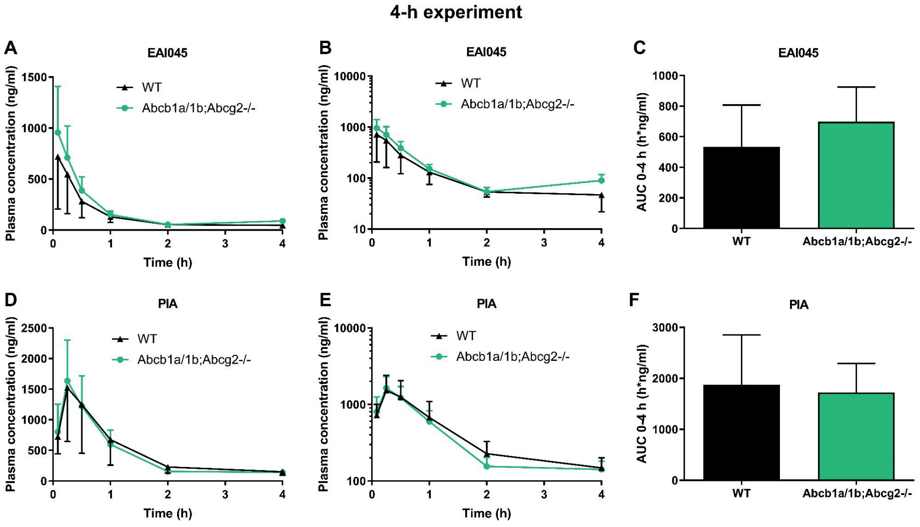

Supplemental Figure 2. Plasma concentration-time curves (A, D), Semi-log plots of plasma concentration-time curves (B, E), and AUC$_{0\text{-}30min}$ (C, F) of EAI045 and PIA in female WT and *Abcb1a/1b;Abcg2*$^{-/-}$ mice 4 h after oral administration of 20 mg/kg EAI045. Data are given as mean ± S.D. (n = 6-7).

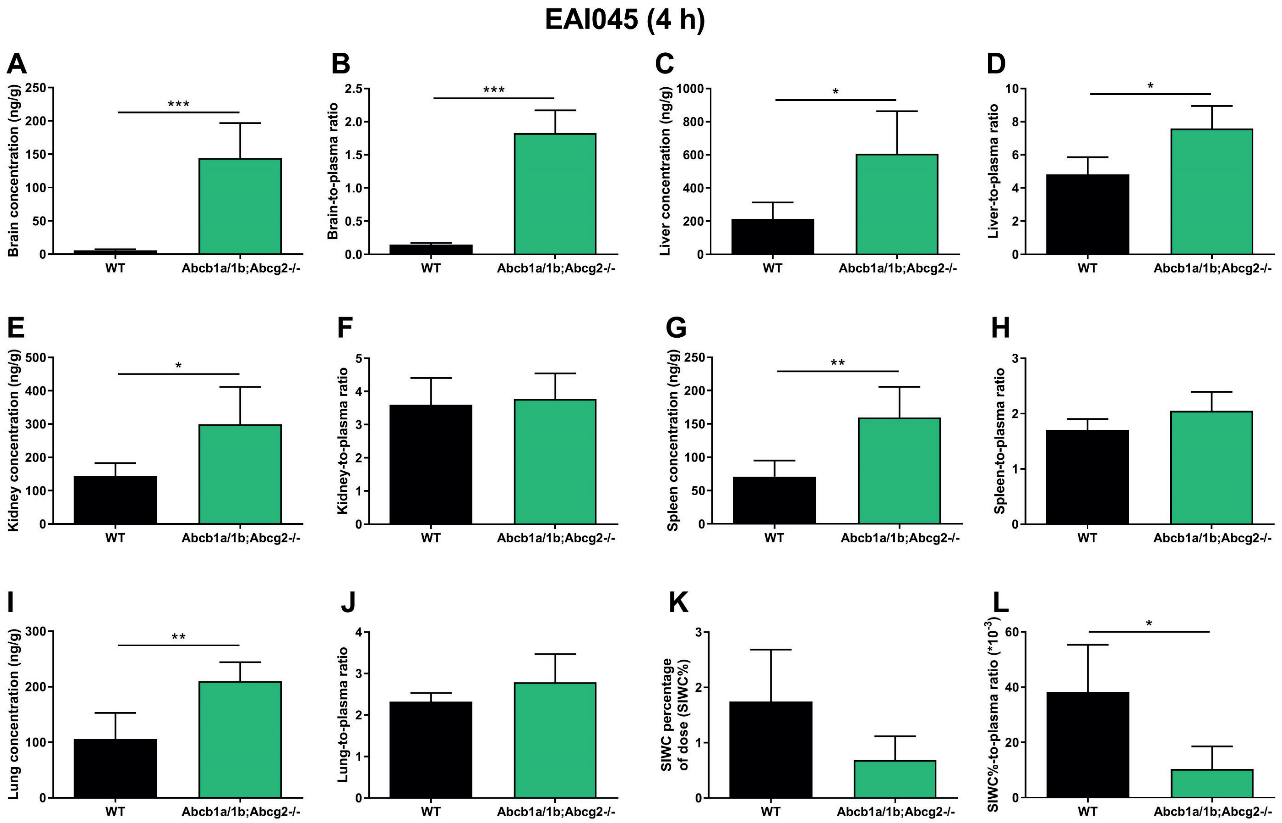

Supplemental Figure 3. Tissue concentration (A, C, E, G, I, K), and tissue-to-plasma ratio (B, D, F, H, J, L) of EAI045 in female WT and *Abcb1a/1b;Abcg2*$^{-/-}$ mice 4 h after oral administration of 20 mg/kg EAI045. Data are given as mean ± S.D. (n = 6-7). *, *P* < 0.05; **, *P* < 0.01; ***, *P* < 0.001 compared to WT mice.

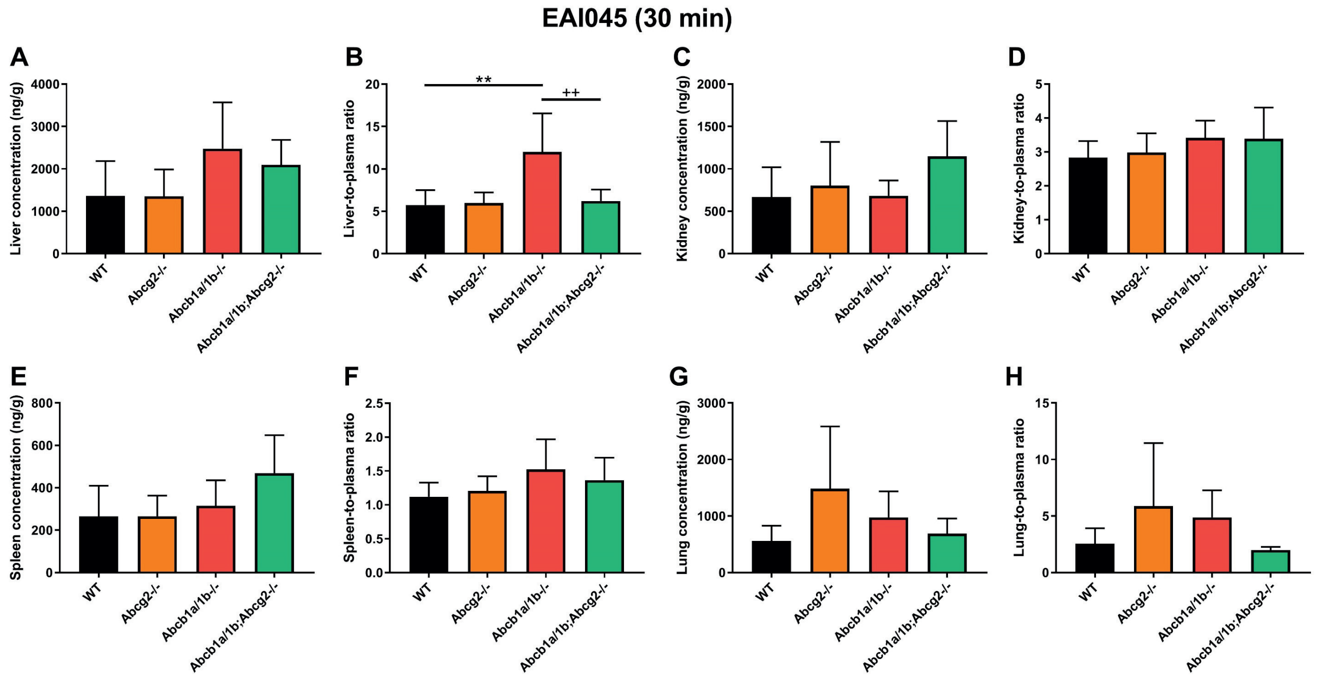

Supplemental Figure 4. Tissue concentration (A, C, E, G), and tissue-to-plasma ratio (B, D, F, H) of EAI045 in WT, *Abcb1a/1b*$^{-/-}$, *Abcg2*$^{-/-}$ and *Abcb1a/1b;Abcg2*$^{-/-}$ mice 30 minutes after oral administration of 20 mg/kg EAI045. Data are given as mean ± S.D. (n = 6-7). *, $P < 0.05$; **, $P < 0.01$; ***, $P < 0.001$ compared to WT mice. $^{+}$, $P < 0.05$; $^{++}$, $P < 0.01$; $^{+++}$, $P < 0.001$ compared to *Abcb1a/1b;Abcg2*$^{-/-}$ mice.

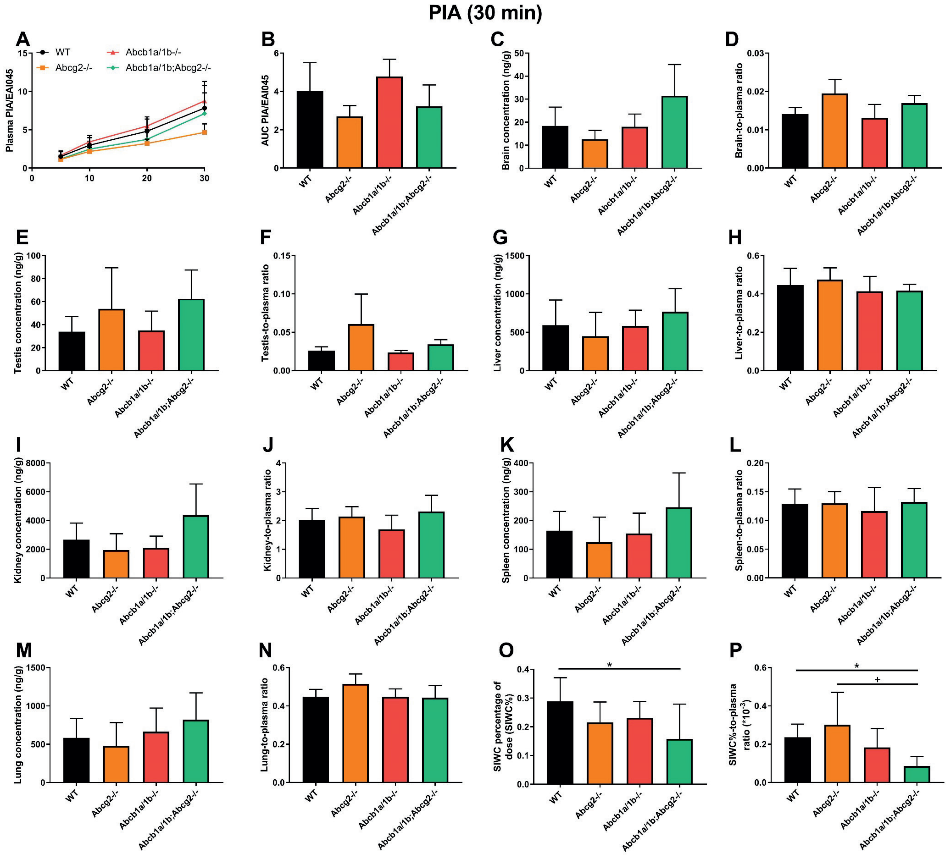

Supplemental Figure 5. PIA pharmacokinetic parameters in male WT, *Abcb1a/1b*$^{-/-}$, *Abcg2*$^{-/-}$, and *Abcb1a/1b;Abcg2*$^{-/-}$ mice 30 minutes after oral administration of 20 mg/kg EAI045. Data are given as mean ± S.D. (n = 6-7). *, $P < 0.05$; **, $P < 0.01$; ***, $P < 0.001$ compared to WT mice.

A: PIA/EAI045 concentration ratios for plasma.

B: PIA/EAI045 AUC$_{0\text{-}30\text{min}}$ ratios for plasma.

C, E, G, I, K, M, O: PIA tissue concentrations.

D, F, H, J, L, N, P: PIA tissue-to-plasma ratios.

O, P: data log transformed before applying statistical tests.

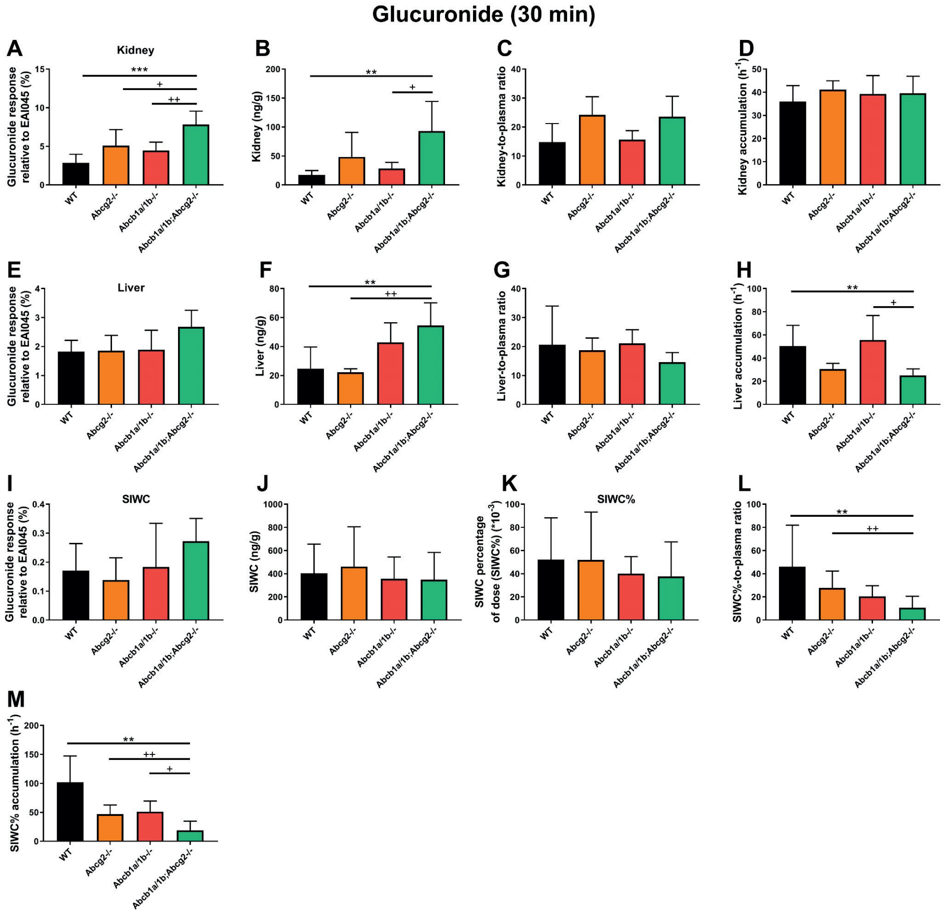

Supplemental Figure 6. EAI045 glucuronide response relative to EAI045 (%) (A, E, I), and accordingly extrapolated glucuronide concentrations (B, F, J, K), glucuronide-to-plasma ratios (C, G, L) and accumulations (D, H, M) in male WT, *Abcb1a/1b*$^{-/-}$, *Abcg2*$^{-/-}$ and *Abcb1a/1b;Abcg2*$^{-/-}$ mice 30 minutes after oral administration of 20 mg/kg EAI045. Data are given as mean ± S.D. (n = 6-7). *, *P* < 0.05; **, *P* < 0.01; ***, *P* < 0.001 compared to WT mice. $^{+}$, *P* < 0.05; $^{++}$, *P* < 0.01; $^{+++}$, *P* < 0.001 compared to *Abcb1a/1b;Abcg2*$^{-/-}$ mice. K-M: data log transformed before applying statistical tests.

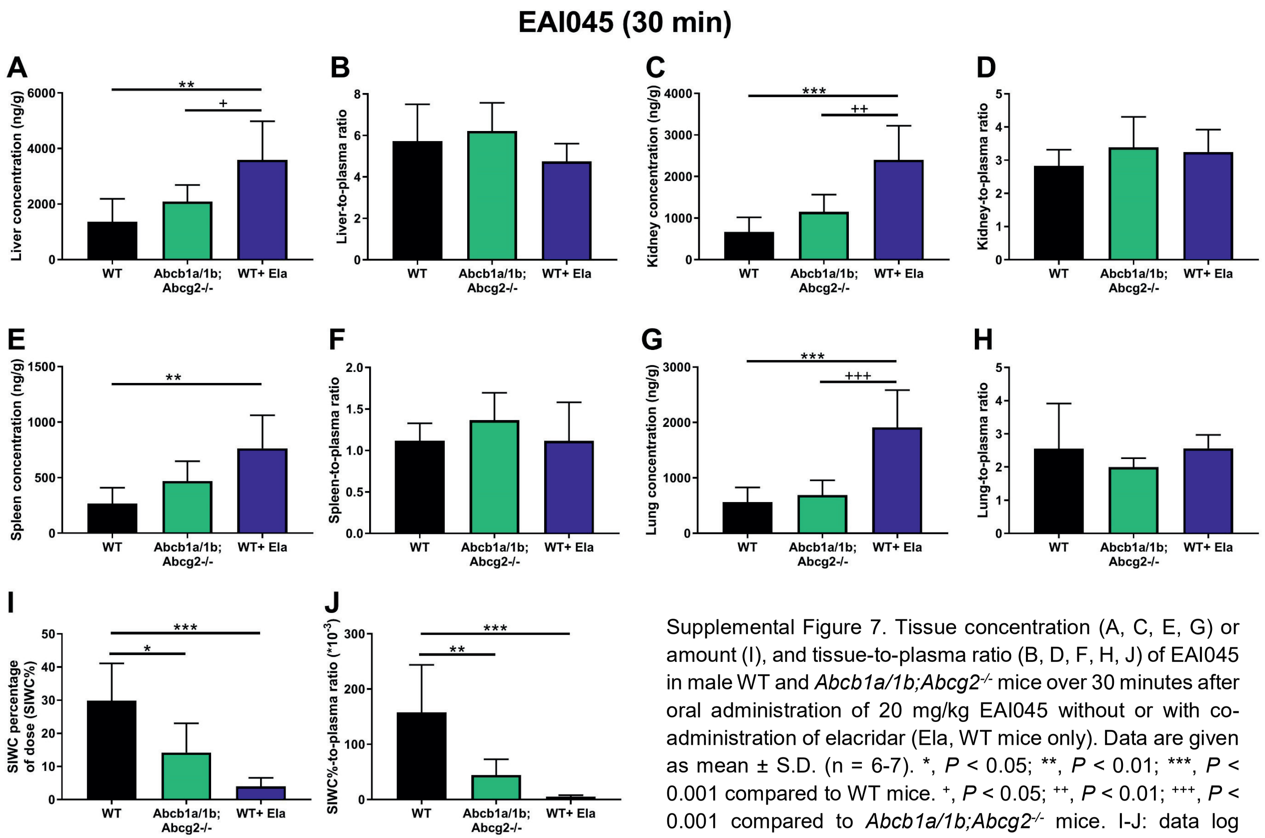

Supplemental Figure 7. Tissue concentration (A, C, E, G) or amount (I), and tissue-to-plasma ratio (B, D, F, H, J) of EAI045 in male WT and *Abcb1a/1b;Abcg2*$^{-/-}$ mice over 30 minutes after oral administration of 20 mg/kg EAI045 without or with co-administration of elacridar (Ela, WT mice only). Data are given as mean ± S.D. (n = 6-7). *, $P < 0.05$; **, $P < 0.01$; ***, $P < 0.001$ compared to WT mice. $^{+}$, $P < 0.05$; $^{++}$, $P < 0.01$; $^{+++}$, $P < 0.001$ compared to *Abcb1a/1b;Abcg2*$^{-/-}$ mice. I-J: data log transformed before applying statistical tests.

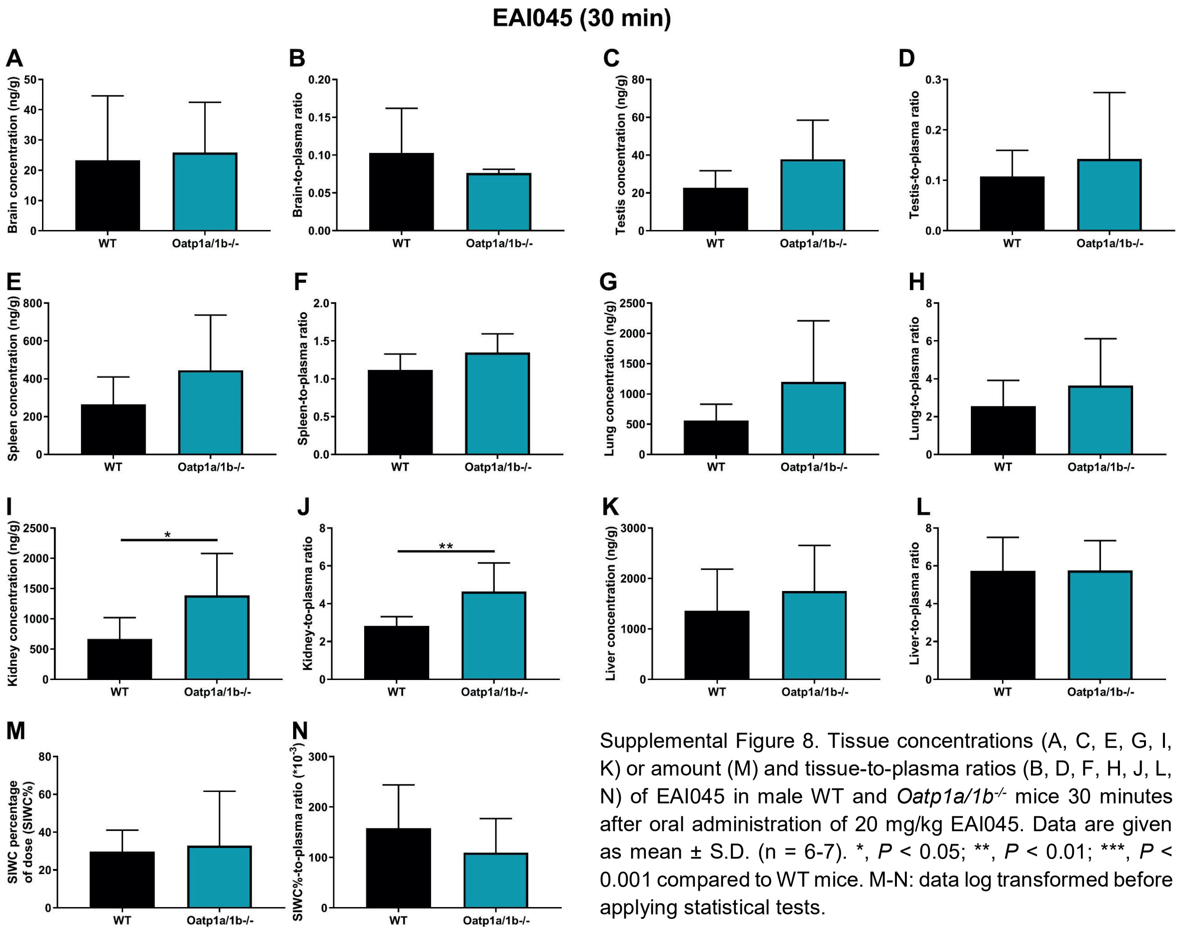

Supplemental Figure 8. Tissue concentrations (A, C, E, G, I, K) or amount (M) and tissue-to-plasma ratios (B, D, F, H, J, L, N) of EAI045 in male WT and *Oatp1a/1b*$^{-/-}$ mice 30 minutes after oral administration of 20 mg/kg EAI045. Data are given as mean ± S.D. (n = 6-7). *, $P < 0.05$; **, $P < 0.01$; ***, $P < 0.001$ compared to WT mice. M-N: data log transformed before applying statistical tests.

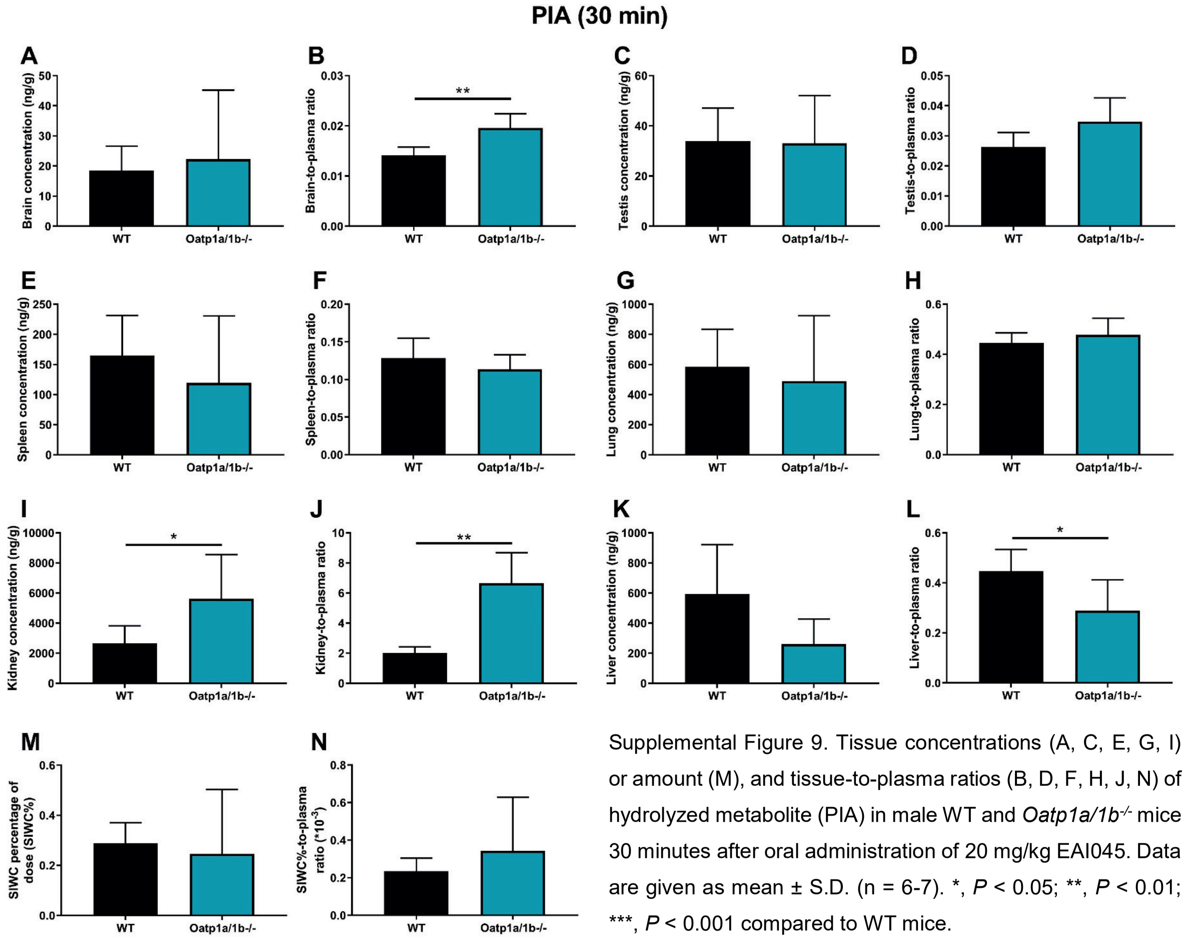

Supplemental Figure 9. Tissue concentrations (A, C, E, G, I) or amount (M), and tissue-to-plasma ratios (B, D, F, H, J, N) of hydrolyzed metabolite (PIA) in male WT and *Oatp1a/1b*$^{-/-}$ mice 30 minutes after oral administration of 20 mg/kg EAI045. Data are given as mean ± S.D. (n = 6-7). *, $P < 0.05$; **, $P < 0.01$; ***, $P < 0.001$ compared to WT mice.

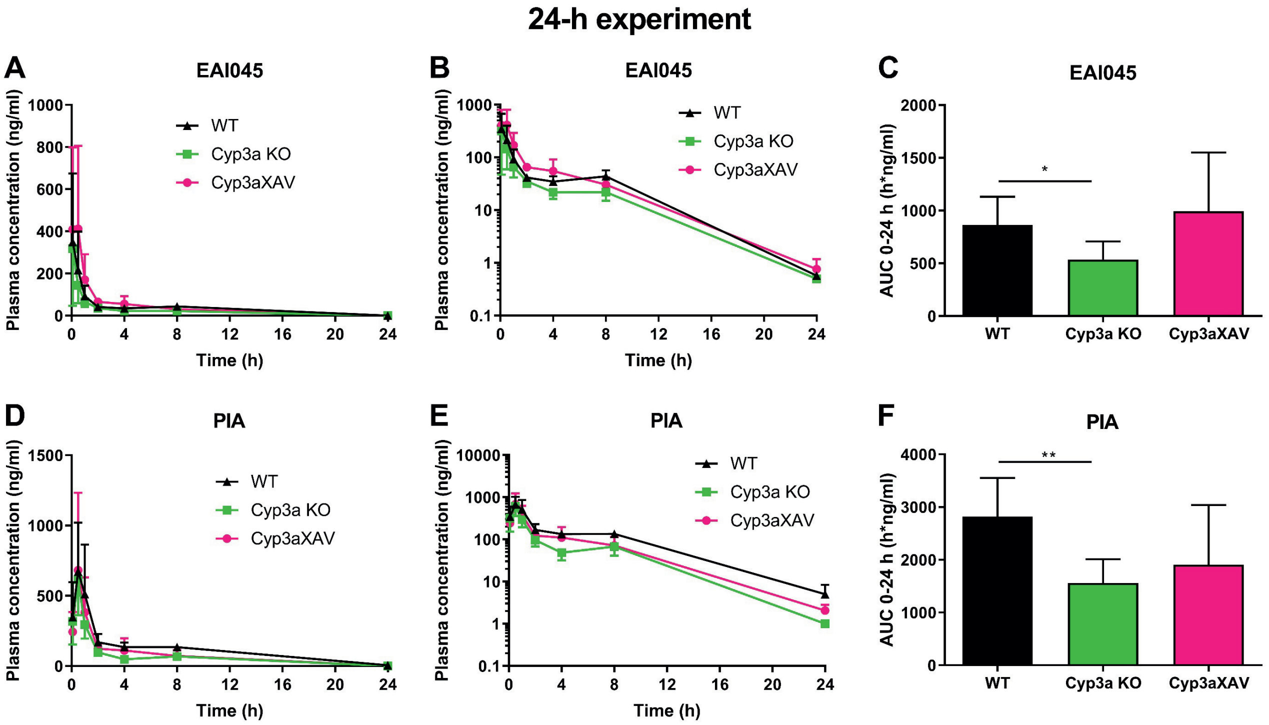

Supplemental Figure 10. Plasma concentration-time curves (A, D), Semi-log plots of plasma concentration-time curves (B, E), and AUC$_{0\text{-}24h}$ (C, F) of EAI045 and PIA in female WT, *Cyp3a*$^{-/-}$, and Cyp3aXAV mice over 24 h after oral administration of 20 mg/kg EAI045. Data are given as mean ± S.D. (n = 6-7). *, *P* < 0.05; **, *P* < 0.01; ***, *P* < 0.001 compared to WT mice.

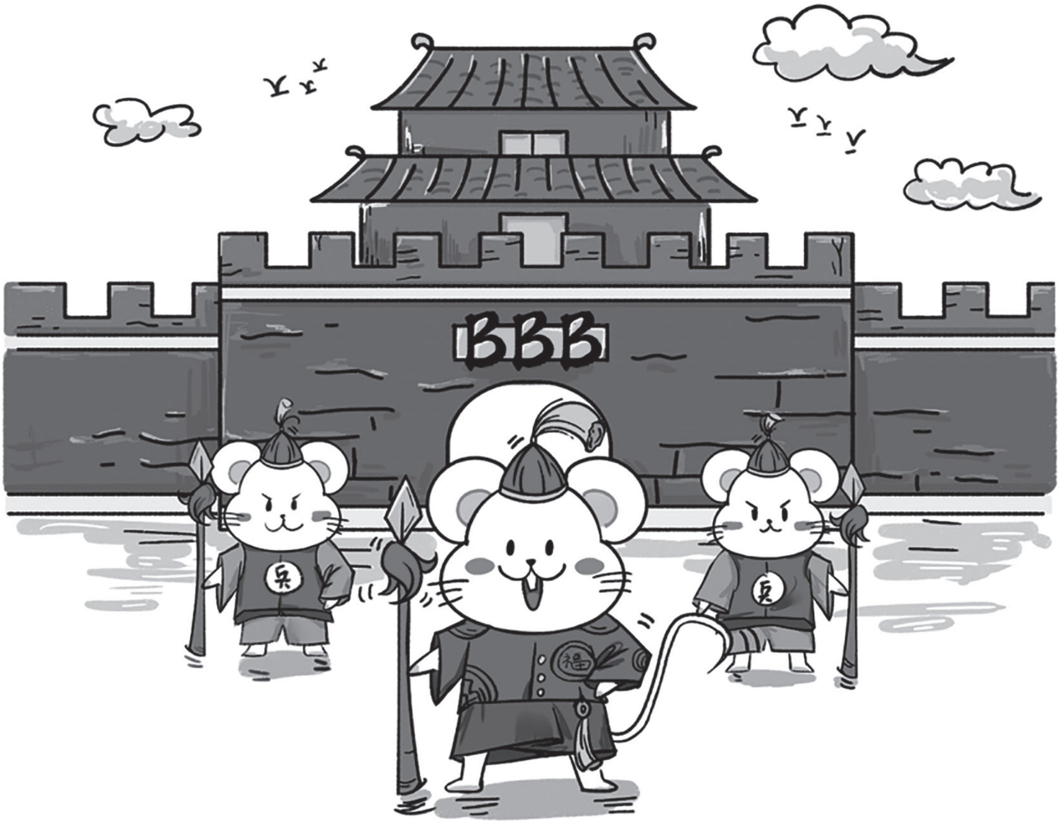

BBB
兵
福
兵

Chapter 6

Human organic anion transporting polypeptide (OATP) 1B3 and mouse Oatp1a/1b affect liver accumulation of Ochratoxin A in mice

Jing Wang
Changpei Gan
Xiaozhe Qi
Maria C. Lebre
Alfred H. Schinkel

Toxicology and Applied Pharmacology, 2020, 401: 115072

Abstract

Ochratoxin A (OTA) is a dietary mycotoxin that can cause nephrotoxicity, hepatotoxicity, neurotoxicity and carcinogenicity. We found that in mice OTA is transported by the drug transporters mouse (m)Abcb1 and/or mAbcg2, mOatp1a/1b, and human (h)OATP1B3. The complete deletion of mAbcb1 and mAbcg2 resulted in ~2-fold higher OTA liver and kidney accumulation upon intravenous injection. Upon oral administration, absence of mOatp1a/1b led to a substantial (>3-fold) decrease in hepatic and small intestinal exposure of OTA. Furthermore, in humanized mouse strains, hepatic expression of transgenic hOATP1B3, but not hOATP1B1, partly reversed the reduced liver concentration of OTA in Oatp1a/1b knockout mice. These data indicate that transgenic hOATP1B3 can significantly transport OTA into the liver, and can at least partly compensate for the loss of the mOatp1a/1b transporters. This study shows that some ABC and OATP transporters can substantially affect the pharmacokinetics of OTA, which might have implications for its toxicity behavior.

Keywords: OTA, liver accumulation, mOatp1a/1b, hOATP1B3, mAbcb1, mAbcg2

Graphical abstract:

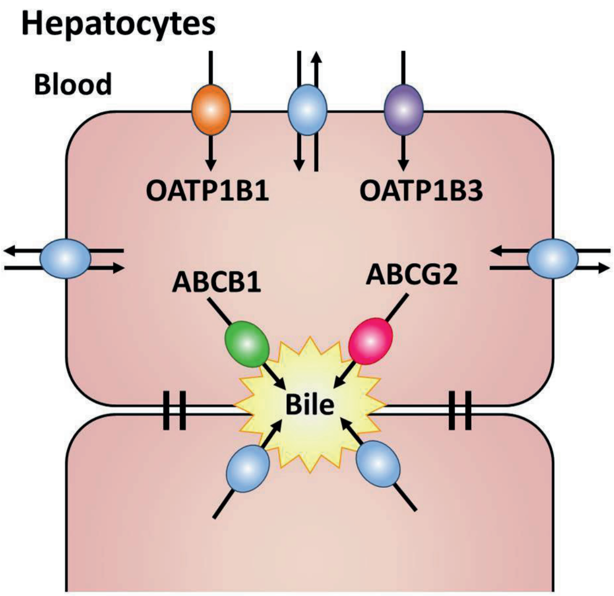

1. Introduction

Ochratoxin A (OTA) is a mycotoxin mainly produced by several species of the fungal genera *Aspergillus* and *Penicillium*. This secondary metabolite can contaminate a great variety of foods, such as cereals, beans, coffee, beer, wine, cocoa, dried fruit, nuts and spices all over the world [1]. OTA is a thermostable compound and it is not destroyed by common food preparation procedures. It can thus enter the food chain through both raw and processed products [2], as well as through animal origin products from livestock fed with contaminated feed [1]. The main route of human exposure to OTA is through intake of contaminated food [3]. High levels of OTA were detected in blood samples in healthy persons from European countries [4]. Since mothers exposed to OTA excrete the ingested mycotoxin also via milk, infant OTA exposure can occur through breast-feeding [5]. Once it reaches the bloodstream, OTA binds strongly to serum proteins (>99%), including albumin [6] and other small proteins [7]. OTA has been classified as a possible human carcinogen (group 2B) by the International Agency for Research on Cancer [8]. Previous studies showed that OTA is a carcinogen in rodent species, inducing tumors in the kidney, mammary gland, and liver [9]. OTA also has genotoxic properties, and it has been found to be a potent renal toxin in all of the animal species tested [1]. It has been suspected as a cause of various human nephropathies since the 1970s, including Balkan Endemic Nephropathy (BEN) [10] and chronic interstitial nephropathy (CIN) [11].

Transmembrane transporters can play important roles in pharmacokinetic pathways (drug and other xenobiotic absorption, distribution, metabolism, and excretion) [12]. P-glycoprotein (MDR1/ABCB1) and Breast Cancer Resistance Protein (BCRP/ABCG2) are important ATP binding cassette (ABC) efflux transporters, with broad substrate specificities including numerous drugs and other xenobiotics [13, 14]. They are localized at apical membranes of liver, intestine, and kidney, where they can pump their substrates into bile, feces and urine, respectively, and at pharmacological sanctuary site barriers such as the blood-brain barrier (BBB) and blood-testis barrier (BTB), where they can protect the tissue by pumping their substrates back into blood. ABCB1 and ABCG2 can thus reduce oral availability, enhance elimination, and limit tissue distribution of substrate xenobiotics.

Organic anion transporting polypeptides (human: OATP, gene SLCO; rodents: Oatp, gene Slco) are primarily transmembrane uptake transporters, which can have profound roles in drug and other xenobiotic disposition and in drug-drug and drug-food interactions, because they are mainly expressed in pharmacokinetically important organs (e.g. liver, small intestine and kidney) and exhibit wide substrate specificities encompassing many drugs [15-17]. For instance, human OATP1B1 (SLCO1B1) and OATP1B3 (SLCO1B3) are both selectively expressed in the liver [18-22], at the basolateral (sinusoidal) plasma membrane of hepatocytes where they can mediate hepatic uptake of compounds [18, 22, 23]. Consequently, the OATP uptake transporters are involved in the uptake of many substrate xenobiotics, modulating their overall body exposure.

Our previous *in vitro* study showed that both mouse Bcrp and human BCRP can mediate extrusion of OTA from cells at pH 6.4, thus reducing OTA toxicity [24]. We also found that human OATP1A2, OATP1B1, and OATP2B1 can mediate cellular uptake of OTA, which might aggravate OTA toxicity [24]. In this study we aimed to assess OTA transport by mouse Abcb1, Abcg2, Oatp1a/1b, and human OATP1B1 and OATP1B3 *in vivo*, and possible effects on oral availability and tissue distribution of OTA, using wild-type and transporter knockout and transgenic mouse strains. Insight into the *in vivo* interactions of OATPs, ABCB1, and ABCG2 with OTA could help us to better understand how OTA enters into and goes out of cells in different tissues such as brain, liver and kidney, and whether this results in aggravation or reduction of OTA toxicity.

2. Material and methods

2.1. Chemicals

OTA was extracted and purified from corn particle medium and then analyzed by HPLC as described previously [24]. [^{3}H]-OTA (26.0 Ci/mmol) was from Campro Scientific (Veenendaal, the Netherlands). Heparin (5000 IU ml^{-1}) was from Leo Pharma (Breda, The Netherlands), and isoflurane was purchased from Pharmachemie (Haarlem, The Netherlands).

2.2. Animals

Mice (*Mus musculus*) were bred in the Netherlands Cancer Institute and housed and handled according to institutional guidelines complying with Dutch and EU legislation. Animals used were male WT, *Abcb1a/1b;Abcg2*$^{-/-}$ [25], and Slco*1a/1b*$^{-/-}$ [17] mice of a >99% FVB/N strain background. Homozygous OATP1B1 and OATP1B3 humanized transgenic mice (Slco1B1, Slco1B3) were generated by cross-breeding of transgenic mice with stable human OATP1B1 or OATP1B3 expression in liver, in a *Slco1a/1b*$^{-/-}$ background [26]. All the mice used were between 9 and 14 weeks of age, and generally between 23 and 35 gram of body weight. Animals were kept in a temperature-controlled environment with a 12 h light/12 h dark cycle and received a standard diet (Transbreed, SDS Diets, Technilab-BMI, Someren, The Netherlands) and acidified water *ad libitum*. Depending on the type of experiment, between 5 and 7 mice were tested in each experimental group. All animal experiments were reviewed and approved by the Institutional Animal Care and Use Committee (IACUC).

2.3. Drug solutions

OTA was administered to mice at a dose of 4 mg/kg, 1 μCi/30 g of body weight for both oral and intravenous (i.v.) injection. OTA stock solution was prepared in methanol at a concentration of 0.1 M and stored at -30˚C. It was then further diluted with 0.1 M $NaHCO_3$ (pH 7.4), and [^{3}H]-OTA was added to reach a final concentration of 8.3 μCi/mL. The final OTA working concentration was 1 mg/mL, and injected volumes were adjusted according to body weight. All working solutions were prepared freshly on the day of the experiment.

2.4. Plasma and tissue pharmacokinetics of OTA

OTA (4 mg/kg, 1 µCi/30 g of body weight) was administered to the mice by oral gavage using a blunt-ended needle, or by i.v. injection into the tail vein using a standard injection syringe. In order to minimize the variation in oral absorption, mice were fasted for about 3 h before OTA was orally administered (n = 5-7). For the 4 h (oral) or 1 h (i.v.) experiments, 50 µl blood samples were collected from the tail vein at 7.5 min, 30 min, 1, and 2 h or 7.5 min, 15 min, and 30 min, respectively, using heparin-coated capillaries (Sarstedt, Nümbrecht, Germany). At 4 or 1 h, mice were anesthetized with isoflurane and blood was collected by cardiac puncture. The mice were then sacrificed by cervical dislocation, and perfused with 10 ml physiological saline. Then the brain, liver and a set of other tissues were rapidly removed, weighed and rapidly frozen at −30˚C. Organs were homogenized on ice in appropriate volumes of 4% (w/v) BSA in water using a FastPrep®-24 device (MP Biomedicals, SA, CA), and then stored at −30°C until analysis. Blood samples were centrifuged at 9,000 *g* for 6 min at 4°C immediately after collection, and plasma was collected and stored at −30°C until analysis.

2.5. Liquid scintillation counting

5 µl plasma samples and 100 µl tissue homogenized samples were used in the measurements. Hydrogen peroxide (30%) was added to decolor both plasma and tissue samples (~100 µl hydrogen peroxide solution per 100 µl sample), and after 1 h at room temperature, 3 or 10 ml Ultima Gold scintillation cocktail (PerkinElmer, Waltham, MA) were added to the samples, respectively. They were then analyzed for the amount of [^{3}H]-OTA by liquid scintillation counting (Beckman Coulter, Brea, CA).

2.6. Pharmacokinetic and statistical calculations

Pharmacokinetic parameters were calculated by the software GraphPad Prism7 (GraphPad Software Inc., La Jolla, CA). Ordinary one-way analysis of variance (ANOVA) was used to determine significance of differences between groups, after which post-hoc tests with Tukey correction were performed for comparison between individual groups. The two-sided unpaired Student's t test was used when treatments or differences between two groups were compared. The area under the plasma concentration-time curve (AUC) was calculated using the trapezoidal rule with the Microsoft Excel plug in PKsolver [27], without extrapolating to infinity. The peak plasma concentration (C_{max}) and the time to reach C_{max} (t_{max}) were estimated from the original (individual mouse) data. Data were first log-transformed before applying statistical analysis, and differences were considered statistically significant when $P < 0.05$. Data are presented as mean ± S.D. with each experimental group containing 6-7 mice.

3. Results

3.1. Abcb1 and/or Abcg2 have limited impact on OTA plasma pharmacokinetics and tissue disposition 1 h after i.v. injection

In order to assess the *in vivo* impact of Abcb1 and Abcg2 on OTA pharmacokinetics at initially high plasma levels of OTA, we first tested intravenous [^{3}H]-OTA pharmacokinetics in male WT and Abcb1 and Abcg2 combination knockout (*Abcb1a/1b;Abcg2$^{-/-}$*) mice, at a dose of 4 mg/kg. After i.v. injection, the plasma exposure of [^{3}H]-OTA over 1 h (AUC$_{0\text{-}1h}$) showed no significant differences between WT and *Abcb1a/1b;Abcg2$^{-/-}$* mice (Figure 1A; Supplemental Table 1). This suggests that mAbcb1 and mAbcg2 have little impact on the plasma clearance of [^{3}H]-OTA after i.v. injection. Interestingly, loss of Abcb1 and Abcg2 resulted in about 2-fold higher liver concentrations and liver-to-plasma ratios, perhaps indicating reduced biliary clearance of [^{3}H]-OTA (Figure 2A, B). However, no significant difference was obtained for the small intestinal content (SIC) percentage of dose or concentrations, or for small intestine (SI) tissue concentrations in the *Abcb1a/1b;Abcg2$^{-/-}$* mice (Figure 2C-H; Supplemental Table 1).

We also measured brain, testis, as well as other tissue (kidney, spleen, lung and heart) concentrations of OTA 1 h after i.v. injection in WT and *Abcb1a/1b;Abcg2$^{-/-}$* mice. Perhaps unsurprisingly for a charged compound like OTA, brain concentration and brain-to-plasma ratio of [^{3}H]-OTA at 1 h in WT and *Abcb1a/1b;Abcg2$^{-/-}$* mice were extremely low (Supplemental Figure 1A, B), and while mean values were somewhat higher in the knockout strain, high experimental variation did not allow an assessment of significance. In contrast, testis, kidney, and spleen did show modest but significant increases in concentrations and tissue-to-plasma ratios in the knockout mice, suggesting a limited impact of mouse Abcb1 and/or Abcg2 on [^{3}H]-OTA distribution in these tissues (Supplemental Figure 1C-H). With respect to testis, possibly the relatively higher intrinsic permeability of the blood-testis barrier (BTB) for [^{3}H]-OTA compared to the blood-brain barrier (BBB) (tissue-to-blood ratios 3.8% vs 0.25%) allowed for detection of a noticeable impact of the ABC transporter(s) in reducing [^{3}H]-OTA uptake. Lung and heart did not shown any change in tissue penetration in the *Abcb1a/1b;Abcg2$^{-/-}$* mice (Supplemental Figure I-L). For all the tissues we measured, the highest tissue-to-plasma ratios were found in SI (15.8%), followed by kidney (9.0%), liver (7.6%), lung (7.2%), heart (6.3%), testis (3.8%), spleen (3.7%), and brain (0.25%) in WT mice (Figure 2 and Supplemental Figure 1).

3.2. Abcb1 and Abcg2 have little impact on OTA plasma pharmacokinetics and tissue disposition 4 h after oral administration

Since OTA reaches the circulation normally through food, we next performed an *in vivo* experiment using oral administration. [^{3}H]-OTA was administered by gavage into the stomach of WT and *Abcb1a/1b;Abcg2$^{-/-}$* mice after about 3 h of fasting, at a dose of 4 mg/kg. Exposure of [^{3}H]-OTA in plasma and tissues (brain, testis, kidney, spleen, stomach plus content, liver, SIC and SI) was tested. As shown in Figure 1B, oral absorption of OTA was quite rapid in both strains, with the highest concentrations in plasma observed around 1 h after dosing. The plasma concentrations were quite high, with a mean C_{max} of 15-18 µg/ml in both strains. Over this short time period, the oral plasma AUC was about 3- to 4-fold lower than upon i.v. OTA administration. Plasma levels of [^{3}H]-OTA ($AUC_{0\text{-}4h}$) did not change upon the loss of Abcb1a/1b and Abcg2 (Figure 1B). As shown in Supplemental Figures 2-3, there were also no significant changes between the strains when considering the tissue-to-plasma ratios between WT and *Abcb1a/1b;Abcg2*$^{-/-}$ mice. The stomach content of [^{3}H]-OTA remaining at this time point, while substantial (~40% of the dose), was not significantly different between the strains. Collectively, the data suggest that there is no substantial role of mAbcb1 and mAbcg2 in relative OTA distribution to these tissues after oral administration (Supplemental Table 2). The contrast between the 1 h i.v. and 4 h oral data could mean that ABC transporters play a substantial role only at high plasma OTA concentrations, and once the plasma levels decrease, other (more high-affinity) transporters may take over OTA disposition.

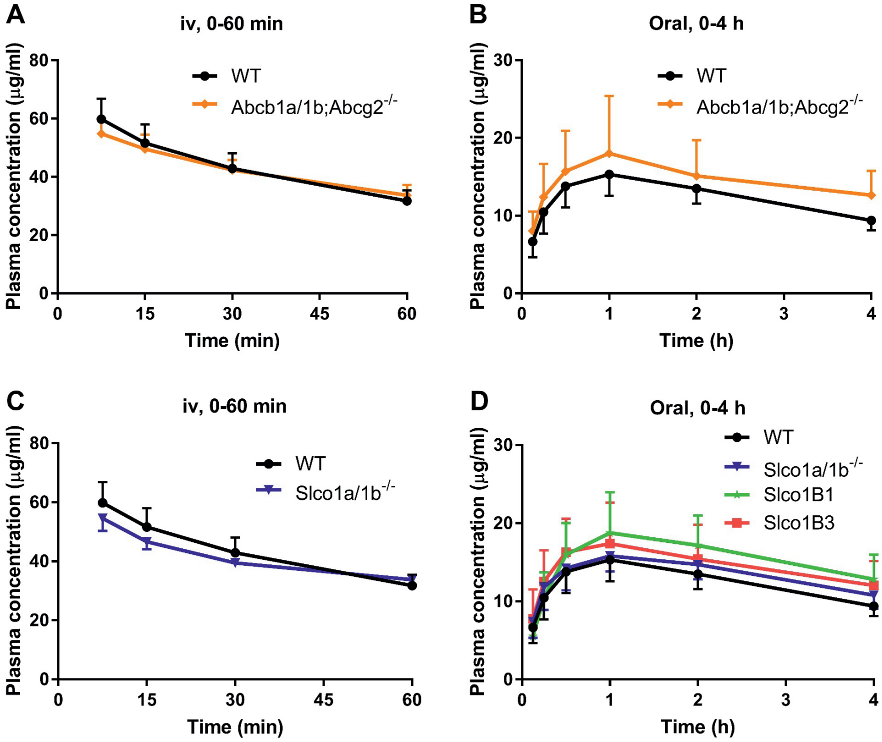

Figure 1. Plasma concentration-time curves of OTA-related radioactivity in male mice after i.v. (A, C) or oral (B, D) administration of 4 mg/kg [^{3}H]-OTA. Data are presented as mean ± S.D. (n = 6-7). A: 0-60 min i.v. experiment in WT and *Abcb1a/1b;Abcg2*$^{-/-}$ mice. B: 0-4 h oral experiment in WT and *Abcb1a/1b;Abcg2*$^{-/-}$ mice. C: 0-60 min i.v. experiment in WT and *Slco1a/1b*$^{-/-}$ mice. D: 0-4 h oral experiment in WT, *Slco1a/1b*$^{-/-}$, Slco1B1 and Slco1B3 mice.

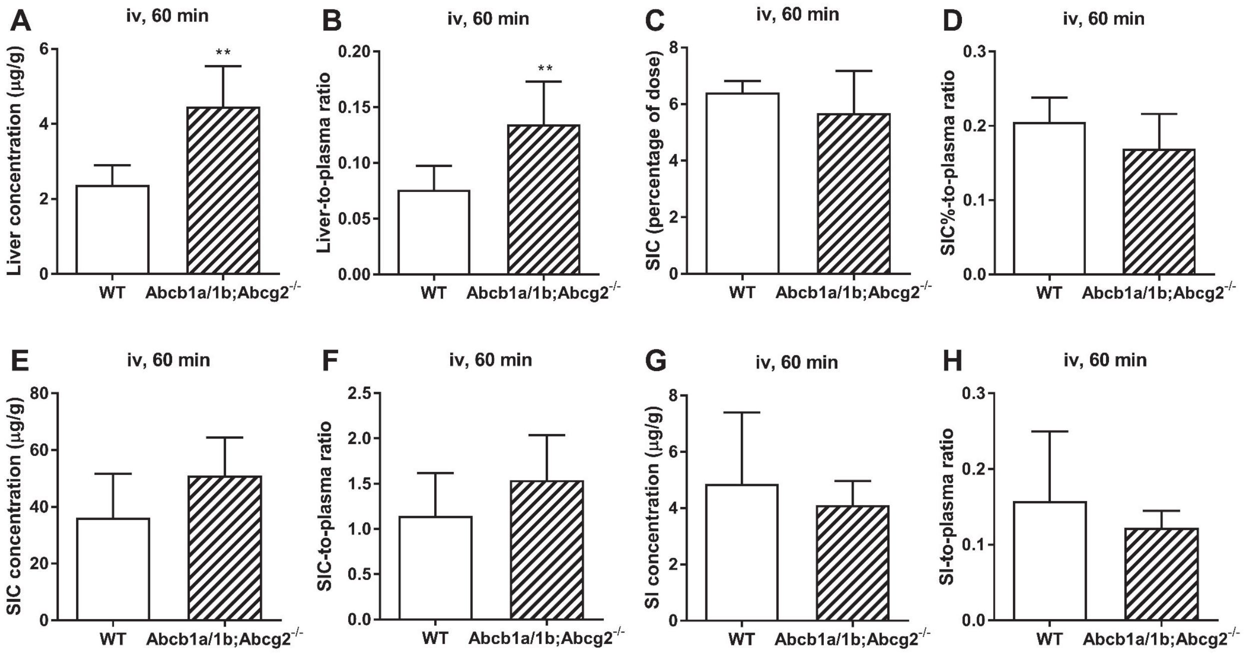

Figure 2. OTA-related radioactivity in WT and *Abcb1a/1b;Abcg2*$^{-/-}$ mice 60 min after i.v. injection of 4 mg/kg [^{3}H]-OTA. Data are presented as mean ± S.D. (n = 6-7). A: Liver concentration. B: Liver-to-plasma ratio. C: Small intestinal content (SIC) percentage of dose (SIC%), which was expressed as total drug (µg) in SIC divided by total drug administered (µg). D: SIC%-to-plasma ratio, expressed as C divided by last time point plasma concentration. E: SIC concentration. F: SIC-to-plasma ratio. G: Small intestinal tissue (SI) concentration. H: SI-to-plasma ratio. Data were first log-transformed before applying statistical analysis. *, $P < 0.05$; **, $P < 0.01$; ***, $P < 0.001$ compared to WT mice.

3.3 mOatp1a/1b transporters have a clear role in the distribution of OTA to the liver 1 h after i.v. administration

To assess the impact of Oatp transporters on OTA disposition, an i.v. pilot experiment with 4 mg/kg OTA over 1 h was performed in WT and *Oatp1a/1b* $^{-/-}$ mice. Plasma exposure of [^{3}H]-OTA (AUC$_{0\text{-}1}$) showed no significant differences between the knockout and WT strain (Figure 1C; Supplemental Table 1). The data suggest that the mouse Oatp1a/1b proteins have little impact on the plasma clearance of [^{3}H]-OTA after i.v. injection. The [^{3}H]-OTA tissue distribution was also determined 1 h after i.v. injection. Although [^{3}H]-OTA concentrations in plasma at 1 h were quite similar, there was a ~3-fold lower liver [^{3}H]-OTA concentration in *Slco1a/1b*$^{-/-}$ compared to WT mice, and the liver-to-plasma ratio was also ~3-fold reduced (Figure 3A, B; Supplemental Table 1). These results suggest an impaired hepatic uptake of OTA in the absence of Oatp1a/1b transporters. The overall amount of hepatic [^{3}H]-OTA was modest, with ~3.7% of the total [^{3}H]-OTA dose recovered in the liver of WT mice and 1.5% in *Slco1a/1b*$^{-/-}$ mice at this time point (data not shown).

In line with the reduced liver [^{3}H]-OTA concentrations, and consequently presumably reduced hepatobiliary OTA excretion, we observed markedly lower [^{3}H]-OTA levels in the small intestinal content (SIC) in the *Slco1a/1b*$^{-/-}$ compared to WT mice. This was on average more than 8-fold reduced in *Slco1a/1b*$^{-/-}$ mice compared to the WT mice, whether expressed as percentage of dose (SIC%) or SIC%-to-plasma ratio (Figure 3C, D; Supplemental Table 1). The total amount of [^{3}H]-OTA retrieved from the SIC in WT mice at 1 h was 6.4% of the dose, vs 0.79% in the *Slco1a/1b*$^{-/-}$ mice. We also examined the amount of [^{3}H]-OTA in the small intestinal tissue (SI). The SI concentrations and SI-to-plasma ratios were also significantly reduced in *Slco1a/1b*$^{-/-}$ mice compared to WT mice, by 3.8-fold and 4.0-fold, respectively ($P < 0.01$, Figure 3G, H; Supplemental Table 1). The SI concentration was 7.3-fold lower than that in SIC (Figure 3E, G; Supplemental Table 1). Overall, the data indicate that mOatp1a/1b can substantially transport [^{3}H]-OTA into the liver *in vivo*. The decreased small intestinal content and tissue levels of [^{3}H]-OTA likely secondarily reflect the lower hepatic uptake of [^{3}H]-OTA in *Slco1a/1b*$^{-/-}$ mice.

We further measured the impact of the mOatp1a/1b transporters on the brain and testis accumulation of [^{3}H]-OTA at 1 h, as well as that of kidney, spleen, lung and heart (Supplemental Figure 4). We observed no significant differences in brain concentration and brain-to-plasma ratio of [^{3}H]-OTA between WT and *Slco1a/1b*$^{-/-}$ mice, suggesting that there was no meaningful impact of mouse Oatp1a/1b transporters on [^{3}H]-OTA brain distribution. The brain-to-plasma ratio of [^{3}H]-OTA was extremely low (0.25% for WT mice), indicating very low penetration of this compound into the brain at this time point (Supplemental Figure 4A, B). However, the testis concentration and testis-to-plasma ratios were 1.3- and 1.4-fold lower in *Slco1a/1b*$^{-/-}$ mice compared to WT mice, respectively ($P < 0.001$, Supplemental Figure 4C, D). This might suggest a minor impact of mOatp1a/1b on facilitating testis accumulation of [^{3}H]-OTA. The testis-to-plasma ratio of OTA was about 3.8% in WT mice, so around 15-fold higher than that for the brain. This suggests that it is relatively easier for OTA to cross the blood-testis barrier (BTB) than the blood-brain barrier (BBB). Next, we analyzed kidney, spleen, lung and heart concentrations of [^{3}H]-OTA at 1 h. We found no statistically significant differences in tissue concentrations or tissue-to-plasma ratios between WT and *Slco1a/1b*$^{-/-}$ mice for spleen, lung and heart (Supplemental Figure 4G-L). However, it is worth noting that while these parameters were somewhat reduced in spleen, lung, and heart (as well as testis and brain), in kidney they were substantially increased by more than 2-fold ($P < 0.01$, Supplemental Figure 4E, F). Perhaps this reflects a partial rerouting of [^{3}H]-OTA that was not distributed to the liver towards renal distribution and elimination in the *Slco1a/1b*$^{-/-}$ mice.

3.4 mOatp1a/1b and hOATP1B3 transporters have a moderate role in the distribution of OTA to the liver 4 h after oral administration

We next investigated the effect of mouse Oatp1a/1b deficiency in mice on OTA disposition over 4 h after oral administration of 4 mg/kg [3H]-OTA. In view of the observed clear role of mouse Oatp1a/1b in the pharmacokinetics of OTA, we also included humanized transgenic mice, specifically expressing human OATP1B1 or OATP1B3 in the liver in a *Slco1a/1b*$^{-/-}$ background (Slco1B1 and Slco1B3, respectively). [^{3}H]-OTA was administered by gavage into the stomach of WT, *Slco1a/1b*$^{-/-}$, Slco1B1, and Slco1B3 mice after about 3 h of fasting. As shown in Figure 1D, oral absorption of OTA was quite rapid in all four strains, with the highest concentrations in plasma observed around 1 h after dosing. The plasma concentrations were quite high, with a mean C_{max} of 15-19 µg/ml in all strains. At t = 4 h, the plasma concentrations in all strains were similar, and the plasma $AUC_{0\text{-}4h}$ revealed no significant differences in [^{3}H]-OTA oral availability between the WT and other mouse strains (Figure 1D; Table 1).

Liver and other tissue concentrations of [^{3}H]-OTA were also determined 4 h after oral administration. Like in the earlier i.v. experiment, we observed markedly decreased liver concentrations (2.8-fold) and liver-to-plasma ratios (3.3-fold) in *Slco1a/1b*$^{-/-}$ mice in comparison with WT mice (Figure 4A, B; Table 1). The hepatic uptake of [^{3}H]-OTA at 4 h was again modest, with ~1.2% of the total dose retrieved from liver in WT mice (data not shown). Even more pronounced effects were obtained for SIC and SI in these strains: the SIC% of dose was on average more than 7-fold reduced in *Slco1a/1b*$^{-/-}$ compared to WT mice, whether expressed as percentage of dose or percentage of dose-to-plasma ratio. The total amount of [^{3}H]-OTA retrieved from SIC was maximal in WT mice, representing ~7% of the total dose, whereas it was only ~1% in the *Slco1a/1b*$^{-/-}$ mice (Figure 4C, D; Table 1). The SI tissue concentrations and SI-to-plasma ratios were also significantly reduced in *Slco1a/1b*$^{-/-}$ mice compared to WT mice, by 2.2-fold ($P < 0.05$) and 2.5-fold ($P < 0.001$), respectively (Figure 4G, H; Table 1).

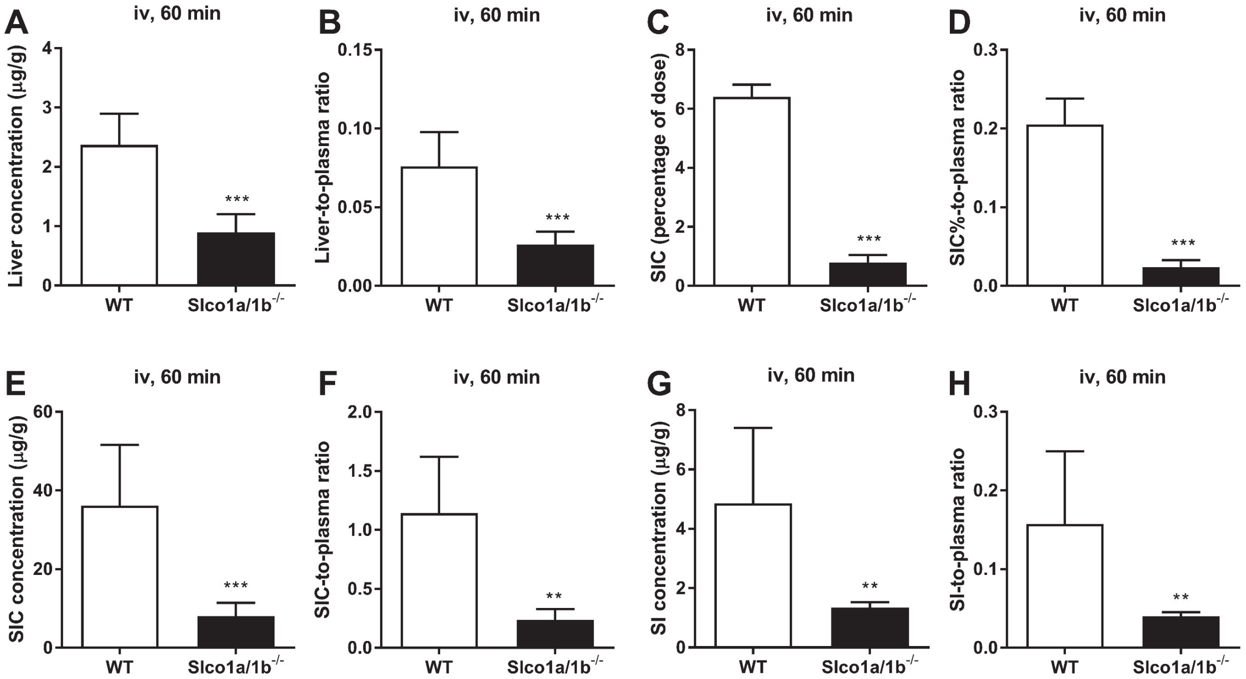

Figure 3. OTA-related radioactivity in WT and *Slco1a/1b*$^{-/-}$ mice 60 min after i.v. injection of 4 mg/kg [^{3}H]-OTA. Data are presented as mean ± S.D. (n = 6-7). A: Liver concentration. B: Liver-to-plasma ratio. C: Small intestinal content (SIC) percentage of dose (SIC%), which was expressed as total drug (µg) in SIC divided by total drug administered (µg). D: SIC%-to-plasma ratio, expressed as C divided by last time point plasma concentration. E: SIC concentration. F: SIC-to-plasma ratio. G: Small intestinal tissue (SI) concentration. H: SI-to-plasma ratio. Data were first log-transformed before applying statistical analysis. *, $P < 0.05$; **, $P < 0.01$; ***, $P < 0.001$ compared to WT mice.

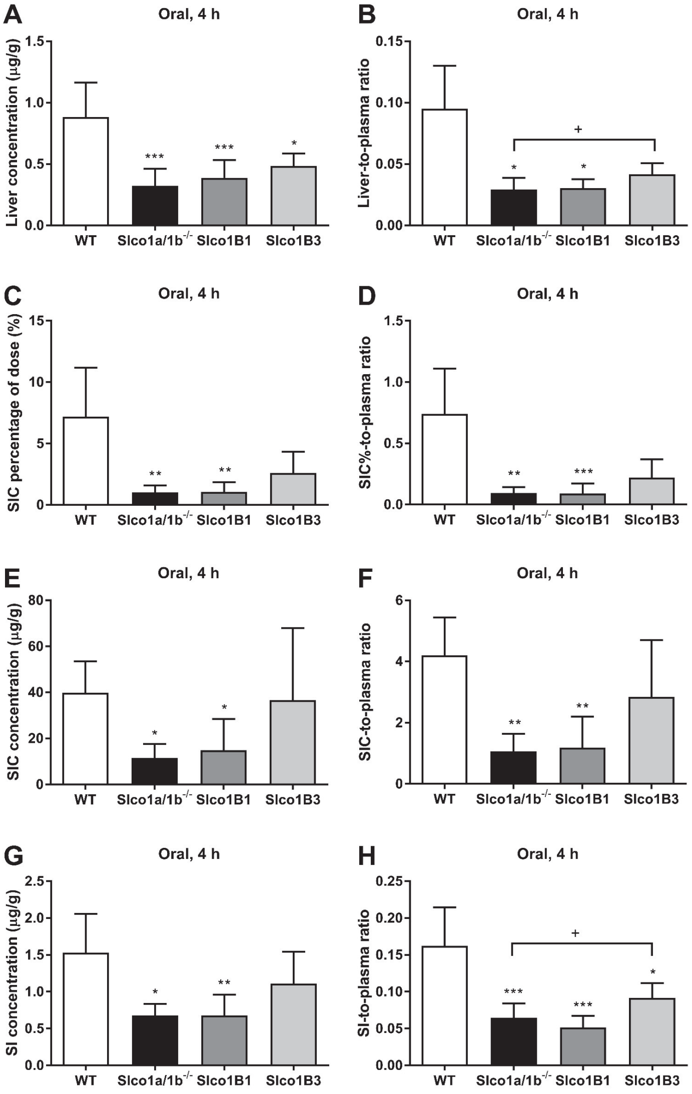

Figure 4. OTA-related radioactivity in WT, *Slco1a/1b*$^{-/-}$, Slco1B1, Slco1B3, and *Abcb1a/1b;Abcg2*$^{-/-}$ mice 4 h after oral administration of 4 mg/kg [^{3}H]-OTA. Data are presented as mean ± S.D. (n = 6-7). A: Liver concentration. B: Liver-to-plasma ratio. C: Small intestinal content (SIC) percentage of dose (SIC%), which was expressed as total drug (μg) in SIC divided by total drug administered (μg). D: SIC%-to-plasma ratio, expressed as C divided by last time point plasma concentration. E: SIC concentration. F: SIC-to-plasma ratio. G: Small intestinal tissue (SI) concentration. H: SI-to-plasma ratio. Data were first log-transformed before applying statistical analysis. *, $P < 0.05$; **, $P < 0.01$; ***, $P < 0.001$ compared to WT mice. $^+$, $P < 0.05$, comparing Slco1B3 to *Slco1a/1b*$^{-/-}$ mice.

Table 1. Plasma pharmacokinetic parameters and tissue concentrations 4 h after oral administration of [^{3}H]-OTA at 4 mg/kg to male WT, *Slco1a/1b*$^{-/-}$, Slco1B1 and Slco1B3 mice.

Parameter	Genotype			
	WT	*Slco 1a/1b*$^{-/-}$	Slco1B1	Slco1B3
Plasma AUC$_{0\text{-}4h}$ (h*µg/ml)	49 ± 7	53 ± 7	61 ± 15	58 ± 16
C$_{max}$ (µg/ml)	16 ± 1	16 ± 2	19 ± 5	17 ± 5
T$_{max}$ (h)	1	1	1	0.5-1
C$_{liver}$ (µg/g)	0.88 ± 0.28	0.32 ± 0.14 ***	0.39 ± 0.14 ***	0.48 ± 0.10 *
Fold change C$_{liver}$	1.0	0.36	1.2[a]	1.5[b]
Liver-to-plasma ratio	0.095 ± 0.034	0.029 ± 0.010 *	0.030 ± 0.007 *	0.042 ± 0.009 $^{+}$
Fold change ratio	1.0	0.31	1.0[a]	1.4[b]
SIC percentage of dose (SIC%)	7.2 ± 4.0	1.0 ± 0.6 **	1.1 ± 0.8 **	2.6 ± 1.7
Fold change SIC%	1.0	0.14	1.0[a]	2.5[b]
SIC%-to-plasma ratio	0.74 ± 0.37	0.094 ± 0.049 *	0.091 ± 0.082 ***	0.22 ± 0.15
Fold change ratio SIC%	1.0	0.13	0.97[a]	2.4[b]
C$_{SIC}$ (µg/g)	39 ± 14	11 ± 6.1 *	15 ± 14 *	37 ± 31
C$_{SI}$ (µg/g)	1.5 ± 0.53	0.68 ± 0.16 *	0.68 ± 0.29 **	1.1 ± 0.43 $^{+}$
Fold change C$_{SI}$	1.0	0.44	1.00[a]	1.6[b]
SI-to-plasma ratio	0.16 ± 0.05	0.065 ± 0.020 ***	0.052 ± 0.015 ***	0.092 ± 0.020 $^{*,+}$
Fold change ratio	1.0	0.40	0.80[a]	1.4[b]
Stomach percentage of dose (stomach%)	36 ± 11	49 ± 10	43 ± 9	31 ± 14
Fold change Stomach %	1.0	1.4	0.88[a]	0.63[b]
Stomach%-to-plasma ratio	4.0 ± 1.5	4.5 ± 1.3	3.7 ± 1.5	3.0 ± 1.7
Fold change ratio Stomach%	1.0	1.1	0.81[a]	0.66[b]

[a] The fold change comparing Slco1B1 to *Slco1a/1b*$^{-/-}$ mice.

[b] The fold change comparing Slco1B3 to *Slco1a/1b*$^{-/-}$ mice.

Data are given as mean ± S.D. (n = 5-7). C$_{tissue}$, tissue concentration. OTA percentage of dose in SIC or stomach, which was expressed as total OTA (µg) in SIC or stomach divided by total OTA administered to mouse (µg). Data were first log-transformed before applying statistical analysis. *, $P < 0.05$; **, $P < 0.01$; ***, $P < 0.001$ compared to WT mice. $^{+}$, $P < 0.05$, comparing Slco1B3 to *Slco1a/1b*$^{-/-}$ mice.

In the liver of the humanized OATP1B1 and OATP1B3 strains, only hepatic expression of OATP1B3 caused significantly higher liver concentrations and liver-to-plasma ratios compared to *Slco1a/1b*$^{-/-}$ mice, by 1.5- and 1.4-fold ($P < 0.05$), respectively (Figure 4A, B; Table 1). However, OATP1B3 could not restore the liver [^{3}H]-OTA parameters back to WT levels, reaching only 55% and 44% compared to WT values, respectively (Figure 4A, B; Table 1). Consistent with a putatively increased hepatobiliary excretion, SIC% of dose and SIC%-to-plasma ratios of [^{3}H]-OTA showed 2.6-fold and 2.3-fold increases in OATP1B3 mice compared to *Slco1a/1b*$^{-/-}$ mice, being no longer significantly reduced compared to WT values (Figure 4C, D; Table 1). Although the increases relative to *Slco1a/1b*$^{-/-}$ values did not reach statistical significance, similar shifts occurred in SIC and SI concentrations, and the increase in SI-to-plasma ratios in the OATP1B3 mice (Figure 4E-H; Table 1) did reach statistical significance. Collectively, the data indicate that transgenic OATP1B3 could partially reverse the effects of the Oatp1a/1b knockout on liver-to-plasma ratios of OTA, whereas transgenic OATP1B1 had no detectable effect on the hepatic uptake of OTA. This suggests that transgenic human OATP1B3, but not OATP1B1, can substantially transport OTA into the liver, and can at least partly compensate for the loss of the mouse Oatp1a/1b transporters.

The modest shifts in concentrations and tissue-to-plasma ratios of [^{3}H]-OTA observed in a range of other tissues (brain, testis, kidney, spleen) in these strains 4 h after oral administration were mostly unremarkable (Supplemental Figure 5A-H), in line with the earlier i.v. data (Supplemental Figure 4A-H): an increase in kidney-to-plasma ratios in *Slco1a/1b*$^{-/-}$ mice was significant in the i.v. experiment, but not in the oral experiment, whereas the opposite applied for a decrease in spleen-to-plasma ratios. Because [^{3}H]-OTA was orally administered into the stomach, we also measured the amount of [^{3}H]-OTA remaining in the stomach plus content at 4 h. Up to ~30-50% of the total dose was still retained in the stomach of the mice, but without significant differences between the strains (Supplemental Figures 5I, J; Table 1). The percentage of dose retrieved in other tissues was comparatively low, for instance, in the WT mice, 7.2% for SIC, 1.2% for liver, 0.7% for SI, 0.4% for kidney, 0.14% for testis, 0.05% for spleen, and 0.03% for brain.

4. Discussion

We show here that loss of Abcb1a/1b and Abcg2 has little influence on the systemic exposure of OTA after either intravenous or oral administration (Figure 1A, B). However, we did find that when Abcb1a/1b and Abcg2 were ablated, there was a significant increase in the accumulation of OTA in liver, testis, kidney and spleen after i.v. injection (Figure 2A, B, Supplemental Figure 1). With respect to liver, it could be that reduced biliary clearance of [^{3}H]-OTA due to the absence of Abcb1a/1b and/or Abcg2 caused the increased accumulation of [^{3}H]-OTA in the hepatocytes. This higher hepatocyte concentration of OTA may have driven an overall biliary OTA excretion that was not too much lower than in the WT mice, resulting in a more or less unchanged flux of OTA into the intestinal lumen, explaining that we observed no marked decrease in the small intestinal content values. Also in the kidney of the knockout mice we observed higher [^{3}H]-OTA tissue-to-plasma ratio (Supplemental Figure 1E, F), suggesting a role of the ABC transporters in excreting OTA from the kidney towards urine, or in reducing its net uptake into the kidney from the pre-urine.

While comparatively modest, the higher tissue-to-plasma ratios of [^{3}H]-OTA we observed in testis and spleen of the ABC transporter knockout mice after i.v. administration suggest that Abcb1a/1b and/or Abcg2 contribute to removing OTA from these tissues (Supplemental Figure 1). Given our earlier demonstration that mouse Abcg2 can transport OTA efficiently *in vitro* [24], Abcg2 is probably the primary ABC efflux transporter responsible for these effects. We note that similar changes in tissue-to-plasma ratios were not observed for liver, kidney, testis, or spleen 4 h after oral OTA administration (Supplemental Figures 2 and 3). These differences between the i.v. and oral experiments may in part relate to the differences in plasma exposure, suggesting a more prominent role of the ABC transporters at higher plasma concentrations (compare Figure 1A and B).

We further found that OATP1A/1B transporters play a moderate role in the *in vivo* disposition of OTA. In mice, absence of the Oatp1a/1b transporters led to a substantial decrease in hepatic (3.3-fold) and small intestinal (7.9-fold) exposure of OTA after oral administration, although OTA plasma levels were not affected (Table 1). Qualitatively similar results were obtained after i.v. administration. Furthermore, using humanized transgenic mice with liver-specific expression of human OATP1B1 or -1B3 in an Oatp1a/1b knockout background, we found that OATP1B3 could partly reverse the reducing effect of the Oatp1a/1b knockout on liver-to-plasma ratios of OTA, raising them from 31% to 44% of the WT levels at 4 h after oral administration of OTA. In line with this, the decreased small intestinal tissue and content concentration of OTA in *Oatp1a/1b*$^{-/-}$ mice as judged by SIC%-to-plasma ratios was also partly rescued by OATP1B3, raising them from 13% to 30% of WT levels (Table 1). Very likely the OATP1B3-mediated improved liver uptake of OTA resulted in partial recovery of the biliary OTA excretion into the small intestinal lumen. In contrast, a contribution of transgenic OATP1B1 was not obvious (Figure 4A, B, Table 1).

To the best of our knowledge, this is the first study demonstrating that the mouse Oatp1a/1b and human OATP1B3 proteins can affect OTA pharmacokinetics *in vivo*. These findings indicate a potentially important role of these transporters in OTA distribution to normal tissues. For most of the other OATP substrate compounds tested in previous studies, an increase in uptake in liver of the hOATP1B1 or hOATP1B3 mice relative to the Oatp1a/1b knockout liver was observed, albeit in most cases not with a full recovery to WT levels [26, 28]. The lack of full recovery for OTA was therefore not unexpected, also considering that five functional mouse Oatp1a/1b proteins were replaced with only one functional OATP1B transporter, OATP1B1 or -1B3, in the humanized mice. It is worth noting that in preceding *in vitro* experiments with human OATPs expressed in the HEK 293 kidney cell line, we found significant uptake of OTA by human OATP1B1, but not OATP1B3, although the absolute differences were small [24]. In contrast, we here found significant activity of human OATP1B3, but not OATP1B1, in *in vivo* uptake of OTA into the mouse liver. It may be that cell-type or local environmental conditions (e.g., local pH, abundance of optimal counter-transport ions in the cellular cytoplasm) can explain in part this discrepancy in the cell-type specific transport behavior (substrate preference) of OATPs. Similar apparent discrepancies have also been described by other research groups [29].

Although both mOatp1a/1b and hOATP1B3 appear to be involved in the hepatic uptake of OTA, it is also clear that there must be additional hepatic OTA uptake mechanisms, as the hepatic uptake was not much more than 3-fold reduced in *Oatp1a/1b*$^{-/-}$ mice (Figures 3A, 3B, 4A, 4B). While speculative, these might encompass passive diffusion, mOatp2b1, given the previously observed noticeable uptake of OTA by (human) OATP2B1 at both pH 7.4 and 6.4 *in vitro* [24], and possibly other hepatic sinusoidal organic anion, cation, or other transporters.

As described previously, OATP transporters often function more effectively at lower pH, also dependent on the probe substrate, and something similar appears to apply to OTA transport by mouse and human ABCG2 (as well as ABCC2). Our earlier *in vitro* study indicated that hABCG2 does not noticeably transport OTA at pH 7.4, whereas mAbcg2 does. In contrast, at pH 6.4 both hABCG2 and mAbcg2 effectively transport OTA [24]. It is worth noting that mildly acidic conditions readily occur *in vivo* in the lumen of renal proximal tubules and proximal small intestine [30], and in the space of Disse, where OATPs mediate uptake of substrates from blood into the liver. At pH 7.4, slightly more than 50% of OTA will be dianionic, and the remainder mostly monoanionic. At pH 6.4, 80-90% of the OTA will be monoanionic, and a smaller fraction dianionic [24]. As mammalian cells are generally negatively charged inside, there is an outward driving force for ionized OTA, countering entry of the cells. Reducing the level of negative charge in OTA by lowering the extracellular pH might thus facilitate net entry of OTA into cells, facilitating the uptake function of OATPs. In addition, it is possible that acidic pH affects the configuration of various OATPs, making them more efficient uptake transporters. It is also worth noting that, although the impact of human OATP1B3 on OTA disposition in the transgenic mice is modest, in human liver both OATP1B3 and OATP1B1 proteins are co-expressed in hepatocytes. If both could contribute to OTA uptake in the liver, this may help with the overall elimination of OTA from blood into the liver for further metabolism, and excretion into the bile, in part by ABCG2, ABCC2, and perhaps ABCB1. Under normal circumstances, the uptake processes will increase liver exposure and toxicity, whereas the efflux processes will decrease liver exposure and toxicity. Given that there are genetic polymorphisms (SNPs) for both OATP1B3 and ABCG2 in humans that reduce their transport functions, as well as more rare full deficiency mutations [31], it is possible that these polymorphisms/mutations to some extent enhance, or alter, the susceptibility of carriers to OTA toxicity. This might particularly apply for the kidney, where we observed increased OTA exposure in both ABC and OATP transporter knockout strains, albeit only after i.v., but not oral, OTA administration.

The kidney is the main target organ for OTA toxicity. Various studies have linked OTA exposure with the nephropathies BEN and CIN in humans [32-35], but an unequivocal causal link has not been completely demonstrated. Still, higher exposure levels to OTA have been confirmed in BEN-affected households than in BEN-free within-village controls and in the controls in BEN-free villages [36]. It is likely that OTA is not the only etiologic factor in all the cases of nephritic syndrome in this study population. It should be noted that a very high level of OTA exposure is not expected in most parts of the world, and therefore the risk of OTA-related nephritic syndrome on a global scale is limited. Nonetheless, the occurrence of OTA in food is unpredictable and not completely avoidable, and carry-over from animal feed to animal products has been confirmed. It has further recently been reported that OTA is also present in airborne dust and spores [37, 38]. Moreover, various drugs have been described that can extensively and sometimes even completely inhibit the activity of one or more of these transporters *in vivo* [39, 40]. It is therefore in theory possible that people with variable activity of these transporters (due to genetic polymorphisms, but also due to inhibitory dietary compounds or other coadministered drugs) may have altered systemic clearance and/or distribution of OTA to tissues. This might contribute to OTA toxicity and/or detoxification processes, and thus to different progression to toxicity and perhaps carcinogenesis.

5. References

1. EFSA, Opinion of the scientific panel on contaminants in the food chain on a request from the commission related to ochratoxin A in food. EFSA J, 2006. 365: p. 1-56.
2. Boudra, H., P. Le Bars, and J. Le Bars, Thermostability of Ochratoxin A in wheat under two moisture conditions. Applied and Environmental Microbiology, 1995. 61(3): p. 1156-1158.
3. Walker, R., Risk assessment of ochratoxin: current views of the European Scientific Committee on Food, the JECFA and the Codex Committee on Food Additives and Contaminants, in Mycotoxins and Food Safety. 2002, Springer. p. 249-255.
4. Pfohl-Leszkowicz, A. and R.A. Manderville, Ochratoxin A: An overview on toxicity and carcinogenicity in animals and humans. Molecular nutrition & food research, 2007. 51(1): p. 61-99.
5. Muñoz, K., et al., Exposure of infants to ochratoxin A with breast milk. Archives of toxicology, 2014. 88(3): p. 837-846.
6. Schwerdt, G., et al., Ochratoxin A-binding proteins in rat organs and plasma and in different cell lines of the kidney. Toxicology, 1999. 135(1): p. 1-10.
7. Stojković, R., et al., High affinity binding of ochratoxin A to plasma constituents. Biochemistry international, 1984. 9(1): p. 33-38.
8. Organization, W.H. and I.A.f.R.o. Cancer, Some naturally occurring substances: food items and constituents, heterocyclic aromatic amines and mycotoxins. IARC Monographs on the Evaluation of the Carcinogenic Risk of Chemicals to Humans, 1993. 56.
9. Kanisawa, M. and S. Suzuki, Induction of renal and hepatic tumors in mice by ochratoxin A, a mycotoxin. GANN Japanese Journal of Cancer Research, 1978. 69(4): p. 599-600.
10. Krogh, P., et al., Balkan (endemic) nephropathy and foodborn ochratoxin A: preliminary results of a survey of foodstuffs. Acta Pathologica Microbiologica Scandinavica Section B Microbiology, 1977. 85(3): p. 238-240.
11. Wafa, E., et al., Human ochratoxicosis and nephropathy in Egypt: a preliminary study. Human & experimental toxicology, 1998. 17(2): p. 124-129.
12. Szakacs, G., et al., The role of ABC transporters in drug absorption, distribution, metabolism, excretion and toxicity (ADME–Tox). Drug discovery today, 2008. 13(9): p. 379-393.
13. Borst, P. and R.O. Elferink, Mammalian ABC transporters in health and disease. Annual review of biochemistry, 2002. 71(1): p. 537-592.
14. Schinkel, A.H. and J.W. Jonker, Mammalian drug efflux transporters of the ATP binding cassette (ABC) family: an overview. Advanced drug delivery reviews, 2003. 55(1): p. 3-29.
15. Cheng, X., et al., Tissue distribution and ontogeny of mouse organic anion transporting polypeptides (Oatps). Drug metabolism and Disposition, 2005. 33(7): p. 1062-1073.
16. Cheng, X. and C.D. Klaassen, Tissue distribution, ontogeny, and hormonal regulation of xenobiotic transporters in mouse kidneys. Drug Metabolism and Disposition, 2009. 37(11): p. 2178-2185.
17. van de Steeg, E., et al., Organic anion transporting polypeptide 1a/1b–knockout mice provide insights into hepatic handling of bilirubin, bile acids, and drugs. The Journal of clinical investigation, 2010. 120(8): p. 2942-2952.
18. Abe, T., et al., Identification of a novel gene family encoding human liver-specific organic anion transporter LST-1. Journal of Biological Chemistry, 1999. 274(24): p. 17159-17163.
19. Abe, T., et al., LST-2, a human liver-specific organic anion transporter, determines methotrexate sensitivity in gastrointestinal cancers. Gastroenterology, 2001. 120(7): p. 1689-1699.
20. Hsiang, B., et al., A novel human hepatic organic anion transporting polypeptide (OATP2) Identification of a liver-specific human organic anion transporting polypeptide and identification of rat and human hydroxymethylglutaryl-CoA reductase inhibitor transporters. Journal of Biological Chemistry, 1999. 274(52): p. 37161-37168.
21. König, J., et al., Localization and genomic organization of a new hepatocellular organic anion transporting polypeptide. Journal of Biological Chemistry, 2000. 275(30): p. 23161-23168.
22. König, J.r., et al., A novel human organic anion transporting polypeptide localized to the basolateral hepatocyte membrane. American Journal of Physiology-Gastrointestinal and Liver Physiology, 2000. 278(1): p. G156-G164.

23. Tamai, I., et al., Molecular identification and characterization of novel members of the human organic anion transporter (OATP) family. Biochemical and biophysical research communications, 2000. 273(1): p. 251-260.
24. Qi, X., et al., Ochratoxin A transport by the human breast cancer resistance protein (BCRP), multidrug resistance protein 2 (MRP2), and organic anion-transporting polypeptides 1A2, 1B1 and 2B1. Toxicology and Applied Pharmacology, 2017. 329: p. 18-25.
25. Jonker, J.W., et al., Contribution of the ABC transporters Bcrp1 and Mdr1a/1b to the side population phenotype in mammary gland and bone marrow of mice. Stem cells, 2005. 23(8): p. 1059-1065.
26. van de Steeg, E., et al., Influence of human OATP1B1, OATP1B3, and OATP1A2 on the pharmacokinetics of methotrexate and paclitaxel in humanized transgenic mice. Clinical cancer research, 2013. 19(4): p. 821-832.
27. Zhang, Y., et al., PKSolver: An add-in program for pharmacokinetic and pharmacodynamic data analysis in Microsoft Excel. Computer methods and programs in biomedicine, 2010. 99(3): p. 306-314.
28. Durmus, S., et al., In vivo disposition of doxorubicin is affected by mouse Oatp1a/1b and human OATP1A/1B transporters. International Journal of Cancer Prevention, 2014. 135(7): p. 1700-1710.
29. de Graan, A.-J.M., et al., Influence of polymorphic OATP1B-type carriers on the disposition of docetaxel. Clinical Cancer Research, 2012. 18(16): p. 4433-4440.
30. DuBose Jr, T.D., et al., Microelectrode determination of pH and PCO2 in rat proximal tubule after benzolamide: evidence for hydrogen ion secretion. Kidney international, 1979. 15(6): p. 624-629.
31. Yee, S.W., et al., Influence of transporter polymorphisms on drug disposition and response: a perspective from the International Transporter Consortium. Clinical Pharmacology & Therapeutics, 2018. 104(5): p. 803-817.
32. Božić, Z., et al., Balkan endemic nephropathy: still a mysterious disease. European Journal of Epidemiology, 1995. 11(2): p. 235-238.
33. Pfohl-Leszkowicz, A., et al., Balkan endemic nephropathy and associated urinary tract tumours: a review on aetiological causes and the potential role of mycotoxins. Food additives & contaminants, 2002. 19(3): p. 282-302.
34. Pfohl-Leszkowicz, A., et al., New molecular and field evidences for the implication of mycotoxins but not aristolochic acid in human nephropathy and urinary tract tumor. Molecular nutrition & food research, 2007. 51(9): p. 1131-1146.
35. Pfohl-Leszkowicz, A., Ochratoxin A and aristolochic acid involvement in nephropathies and associated urothelial tract tumours. Arhiv za higijenu rada i toksikologiju, 2009. 60(4): p. 465-482.
36. Abouzied, M., et al., Ochratoxin A concentrations in food and feed from a region with Balkan Endemic Nephropathy. Food Additives & Contaminants, 2002. 19(8): p. 755-764.
37. Skaug, M.A., W. Eduard, and F.C. Størmer, Ochratoxin A in airborne dust and fungal conidia. Mycopathologia et Mycologia Applicata, 2001. 151(2): p. 93-98.
38. Richard, J.L., et al., The occurrence of ochratoxin A in dust collected from a problem household. Mycopathologia, 1999. 146(2): p. 99-103.
39. Chen, Z., et al., Mammalian drug efflux transporters of the ATP binding cassette (ABC) family in multidrug resistance: A review of the past decade. Cancer letters, 2016. 370(1): p. 153-164.
40. Stieger, B. and B. Hagenbuch, Organic anion-transporting polypeptides, in Current topics in membranes. 2014, Elsevier. p. 205-232.

6. Supplemental materials

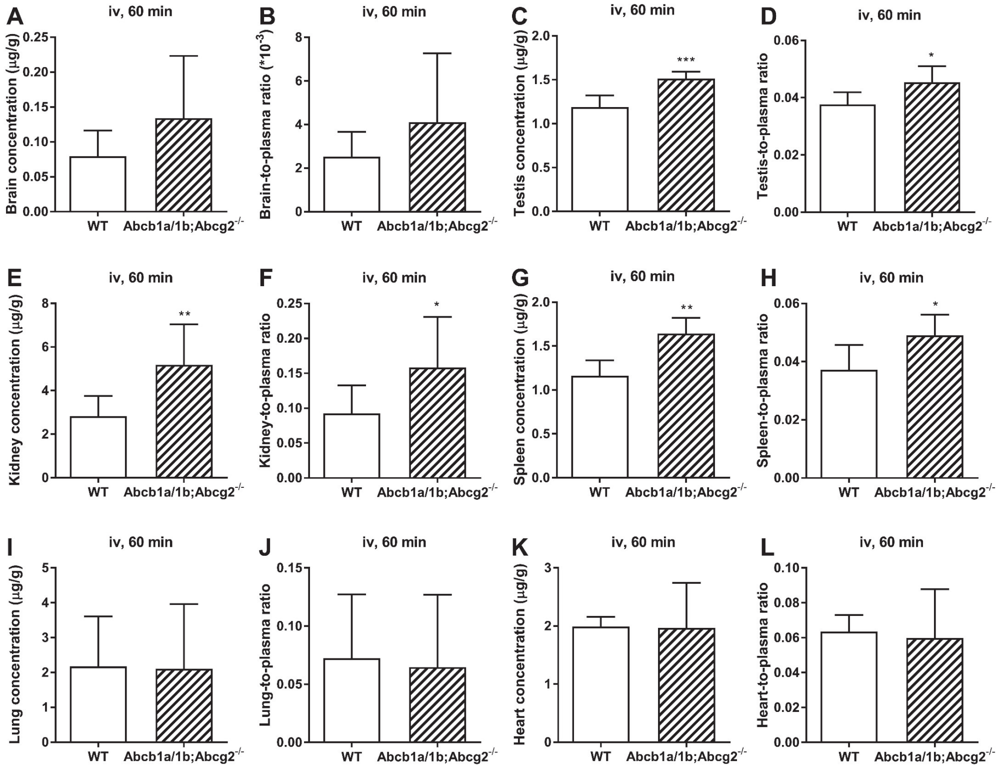

Supplemental Figure 1. Tissue concentration (A, C, E, G, I, K) and tissue-to-plasma ratio (B, D, F, H, J, L) of OTA-related radioactivity in male WT and *Abcb1a/1b;Abcg2*$^{-/-}$ mice 60 min after i.v. injection of 4 mg/kg [^{3}H]-OTA. Data are presented as mean ± S.D. (n = 6-7). Data were first log-transformed before applying statistical analysis. *, $P < 0.05$; **, $P < 0.01$; ***, $P < 0.001$ compared to WT mice.

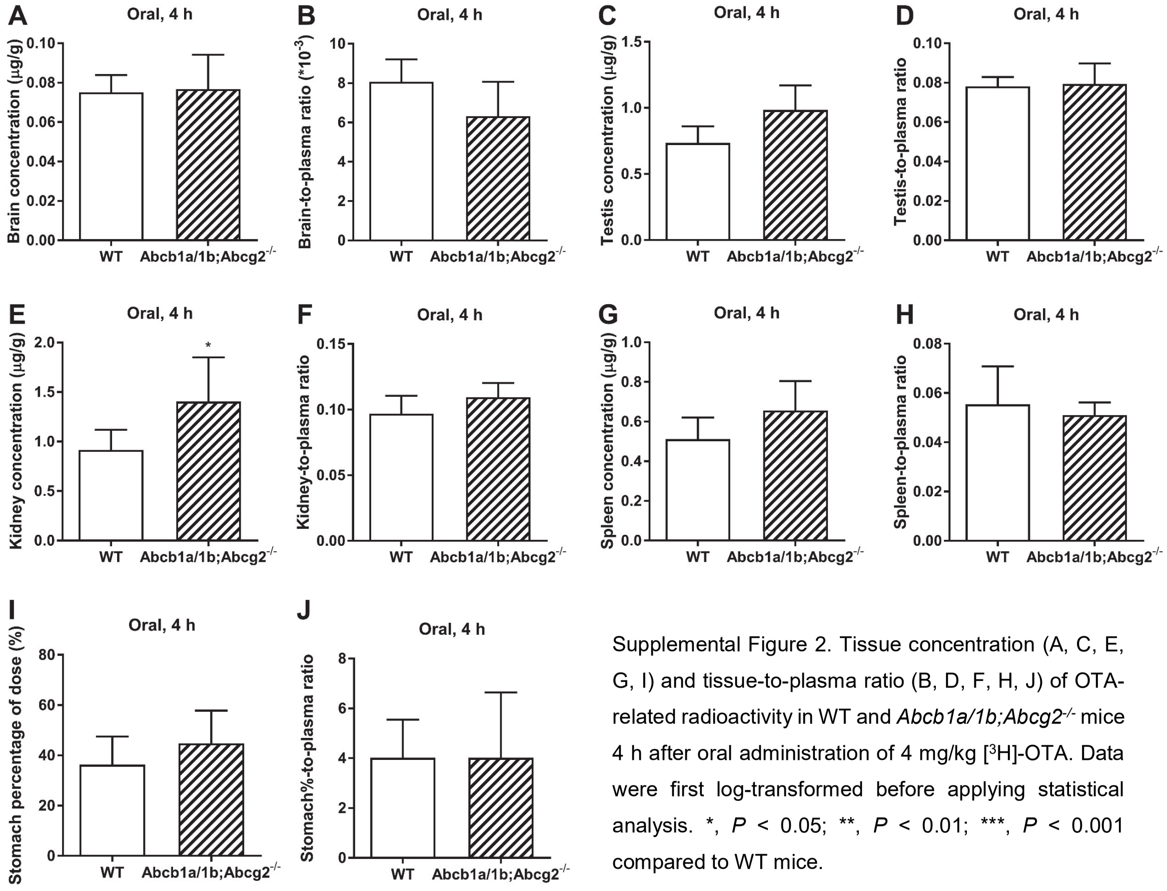

Supplemental Figure 2. Tissue concentration (A, C, E, G, I) and tissue-to-plasma ratio (B, D, F, H, J) of OTA-related radioactivity in WT and *Abcb1a/1b;Abcg2*$^{-/-}$ mice 4 h after oral administration of 4 mg/kg [^{3}H]-OTA. Data were first log-transformed before applying statistical analysis. *, $P < 0.05$; **, $P < 0.01$; ***, $P < 0.001$ compared to WT mice.

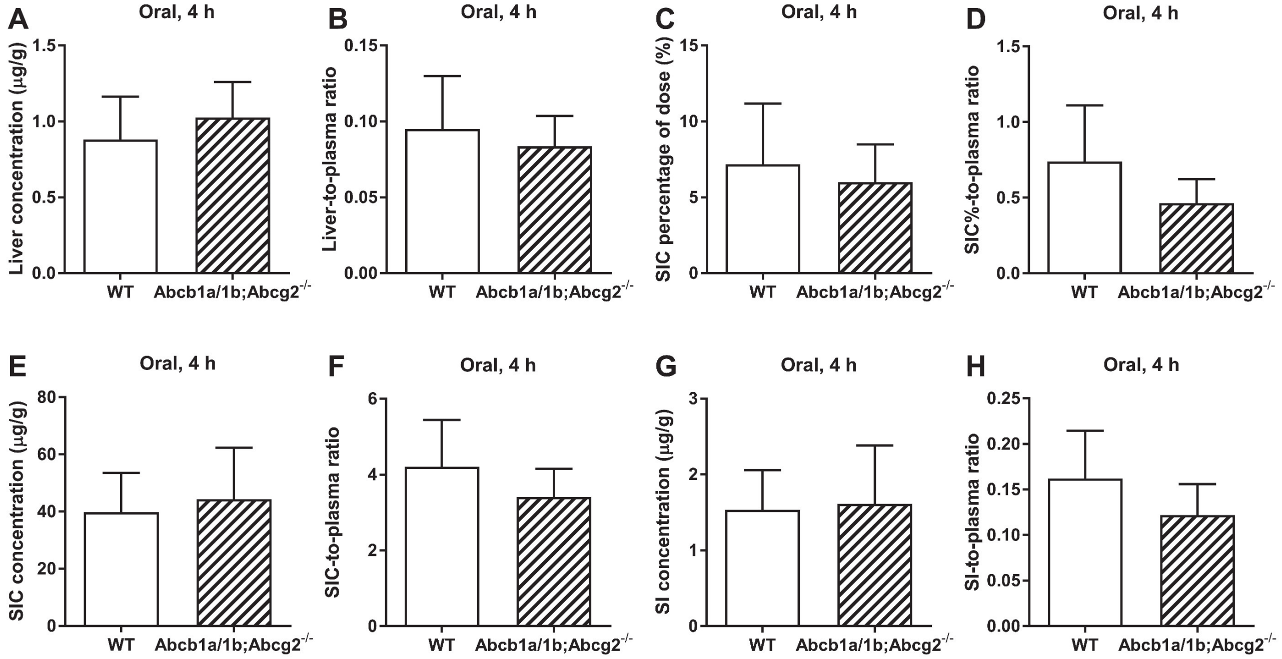

Supplemental Figure 3. OTA-related radioactivity in WT and *Abcb1a/1b;Abcg2*$^{-/-}$ mice 4 h after oral injection of 4 mg/kg [^{3}H]-OTA. Data are presented as mean ± S.D. (n = 6-7). A: Liver concentration. B: Liver-to-plasma ratio. C: Small intestinal content (SIC) percentage of dose (SIC%), which was expressed as total drug (μg) in SIC divided by total drug administered (μg). D: SIC%-to-plasma ratio, expressed as C divided by last time point plasma concentration. E: SIC concentration. F: SIC-to-plasma ratio. G: Small intestinal tissue (SI) concentration. H: SI-to-plasma ratio. Data were first log-transformed before applying statistical analysis. No statistically significant differences compared to WT mice were observed ($P > 0.05$).

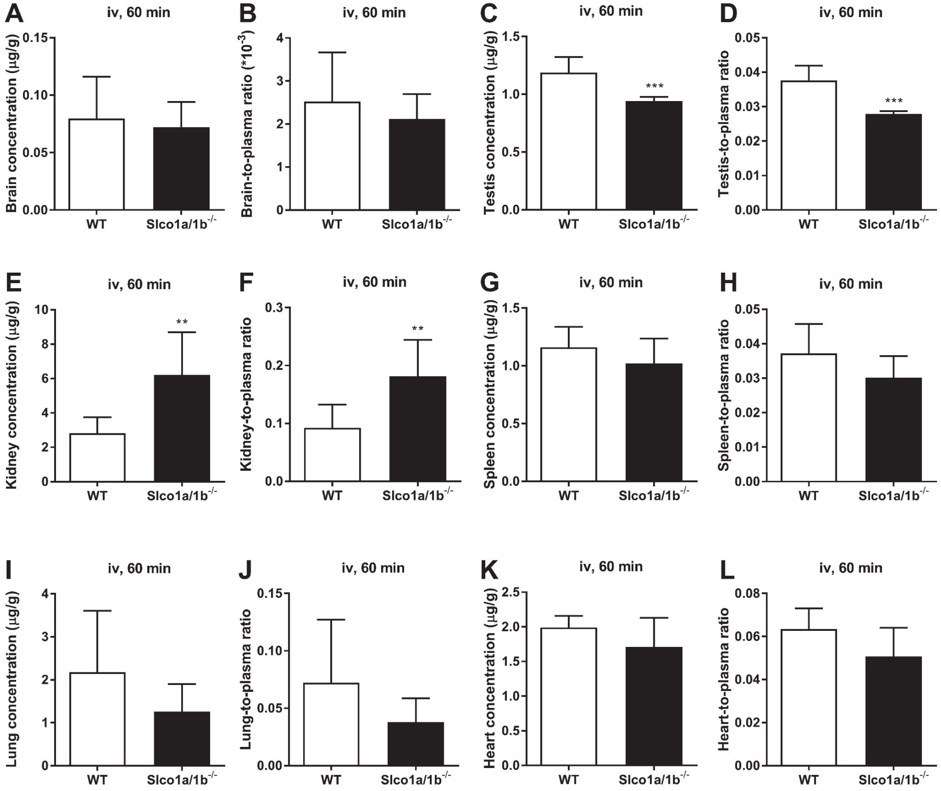

Supplemental Figure 4. Tissue concentration (A, C, E, G, I, K) and tissue-to-plasma ratio (B, D, F, H, J, L) of OTA-related radioactivity in male WT and *Slco1a/1b*$^{-/-}$ mice 60 min after i.v. injection of 4 mg/kg [^{3}H]-OTA. Data are presented as mean ± S.D. (n = 6-7). Data were first log-transformed before applying statistical analysis. *, $P < 0.05$; **, $P < 0.01$; ***, $P < 0.001$ compared to WT mice.

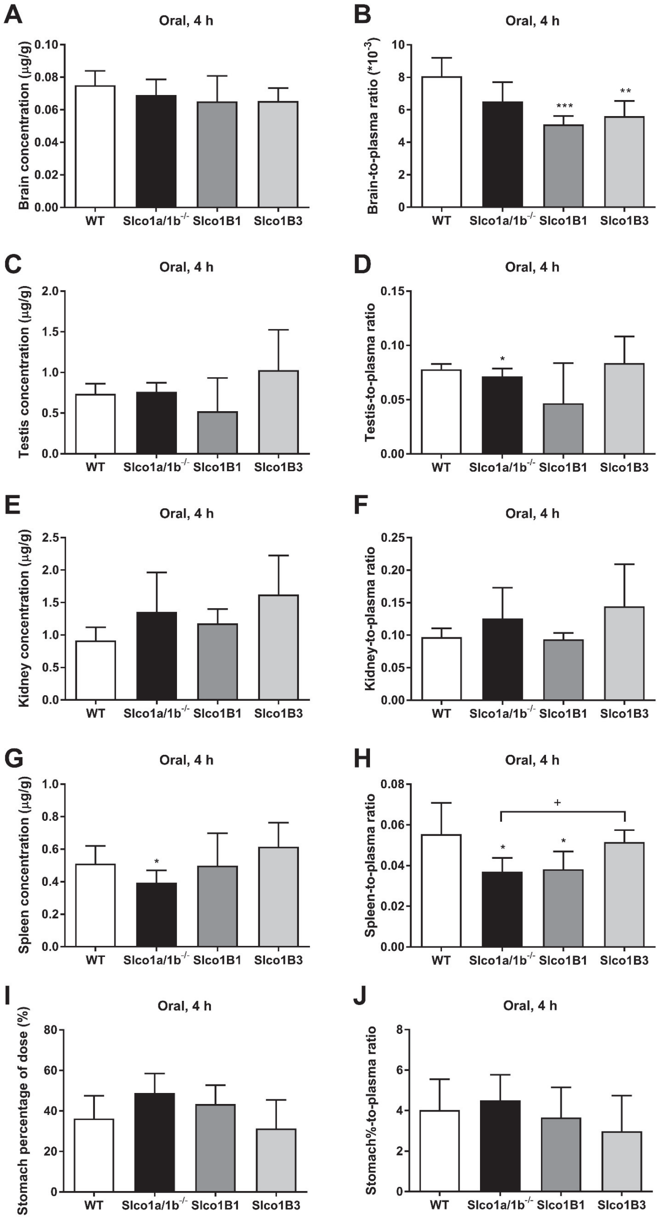

Supplemental Figure 5. Tissue concentration (A, C, E, G, I) and tissue-to-plasma ratio (B, D, F, H, J) of OTA-related radioactivity in male WT, *Slco1a/1b*$^{-/-}$, Slco1B1 and Slco1B3 mice 4 h after oral administration of 4 mg/kg [^{3}H]-OTA. Data are presented as mean ± S.D. (n = 6-7). Data were first log-transformed before applying statistical analysis. *, $P < 0.05$; **, $P < 0.01$; ***, $P < 0.001$ compared to WT mice. $^+$, $P < 0.05$, comparing Slco1B3 to *Slco1a/1b*$^{-/-}$ mice.

Supplemental Table 1. Plasma pharmacokinetic parameters and tissue concentrations 1 h after i.v. injection of 4 mg/kg [^{3}H]-OTA to male WT, *Abcb1a/1b;Abcg2*$^{-/-}$ and *Slco1a/1b*$^{-/-}$ mice.

Parameter	Genotype		
	WT	*Abcb1a/1b;Abcg2*$^{-/-}$	*Slco1a/1b*$^{-/-}$
Plasma $AUC_{0\text{-}1h}$ (h*µg/ml)	46 ± 5.1	44 ± 3.9	43 ± 1.4
C_{liver} (ng/g)	2.4 ± 0.5	4.5 ± 1.1 **	0.89 ± 0.31 ***
Fold change C_{liver}	1.0	1.9	0.38
Liver-to-plasma ratio	0.076 ± 0.022	0.13 ± 0.04 **	0.026 ± 0.008 ***
Fold change ratio	1.0	1.8	0.35
SIC percentage of dose (SIC%)	6.4 ± 0.4	5.7 ± 1.5	0.79 ± 0.26 ***
Fold change SIC%	1.0	0.89	0.12
SIC%-to-plasma ratio	0.21 ± 0.03	0.17 ± 0.05	0.024 ± 0.009 ***
Fold change ratio SIC%	1.0	0.83	0.12
C_{SIC} (µg/g)	36 ± 15	51 ± 13	8.1 ± 3.3 ***
C_{SI} (µg/g)	4.9 ± 2.5	4.1 ± 0.86	1.3 ± 0.18 **
Fold change C_{SI}	1.0	0.85	0.28
SI-to-plasma ratio	0.16 ± 0.09	0.12 ± 0.02	0.040 ± 0.05 **
Fold change ratio	1.0	0.78	0.25

Data are given as mean ± S.D. (n = 5-7). C_{tissue}, tissue concentration. OTA percentage of dose in SIC or stomach, which was expressed as total OTA (µg) in SIC or stomach divided by total OTA administered to mouse (µg). Data were first log-transformed before applying statistical analysis. *, $P < 0.05$; **, $P < 0.01$; ***, $P < 0.001$ compared to WT mice.

Supplemental Table 2. Plasma pharmacokinetic parameters and tissue concentrations 4 h after oral administration of [^{3}H]-OTA at 4 mg/kg to male WT and *Abcb1a/1b;Abcg2$^{-/-}$* mice.

Parameter	Genotype	
	WT	*Abcb1a/1b;Abcg2$^{-/-}$*
Plasma AUC$_{0\text{-}4h}$ (h*µg/ml)	49 ± 7	58 ± 16
C$_{max}$ (µg/ml)	16 ± 1	18 ± 7
T$_{max}$ (h)	1	0.5-1
C$_{liver}$ (µg/g)	0.88 ± 0.28	1.0 ± 0.23
Fold change C$_{liver}$	1.0	1.2
Liver-to-plasma ratio	0.095 ± 0.034	0.084 ± 0.020
Fold change ratio	1.0	0.88
SIC percentage of dose (SIC%)	7.2 ± 4.0	6.0 ± 2.5
Fold change SIC%	1.0	0.83
SIC%-to-plasma ratio	0.74 ± 0.37	0.47 ± 0.16
Fold change ratio SIC%	1.0	0.64
C$_{SIC}$ (µg/g)	39 ± 14	44 ± 18
C$_{SI}$ (µg/g)	1.5 ± 0.5	1.6 ± 0.8
Fold change C$_{SI}$	1.0	1.1
SI-to-plasma ratio	0.16 ± 0.05	0.12 ± 0.03
Fold change ratio	1.0	0.75
Stomach percentage of dose (stomach%)	36 ± 11	45 ± 13
Fold change Stomach %	1.0	1.2
Stomach%-to-plasma ratio	4.0 ± 1.5	4.0 ± 2.6
Fold change ratio Stomach%	1.0	1.0

Data are given as mean ± S.D. (n = 5-7). C$_{tissue}$, tissue concentration. OTA percentage of dose in SIC or stomach, which was expressed as total OTA (µg) in SIC or stomach divided by total OTA administered to mouse (µg).

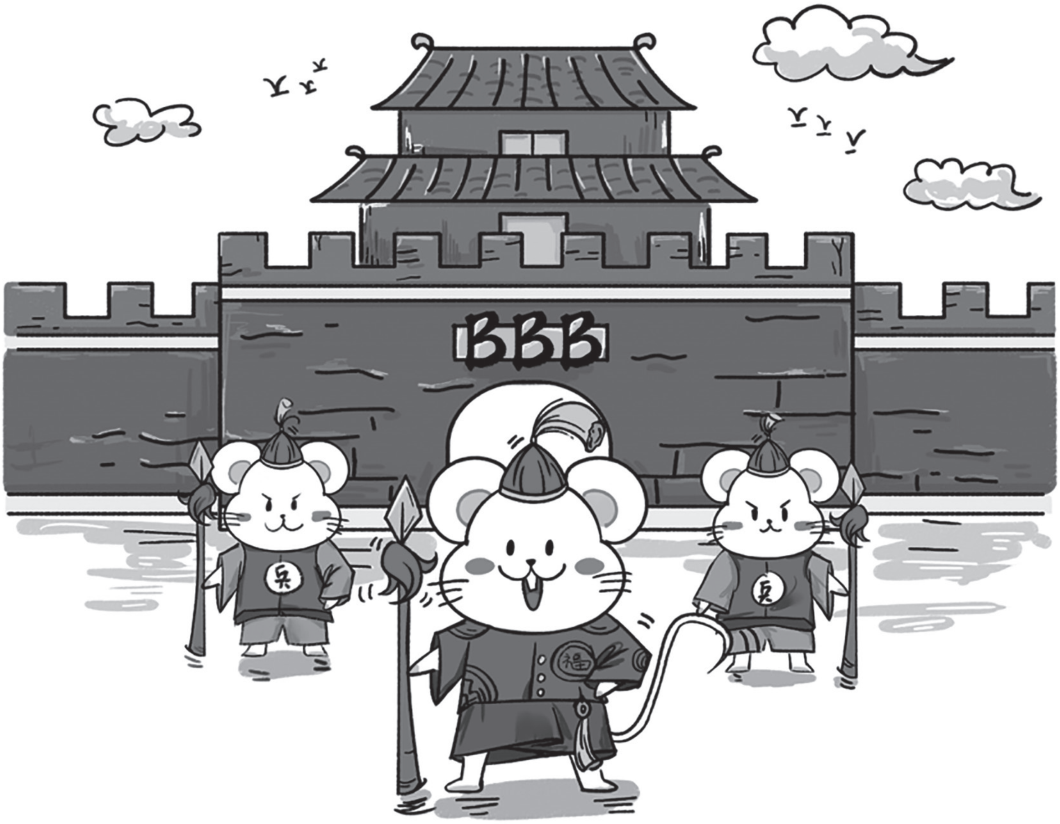
BBB
兵
福
兵

CONCLUSION AND FUTURE PERSPECTIVE

Conclusion and future perspective

In this thesis we investigated the pharmacological functions of ABC efflux transporters *in vitro*, by using transwell transport assays and *in vivo*, by using the single and combination knockout mouse models of ABCB1 and ABCG2. We further used CYP3A knockout and humanized transgenic mouse models to assess the *in vivo* impact of this multispecific drug-metabolizing complex on the study drugs. We also studied OATP uptake transporters *in vivo* using several knockout (lacking all mouse Oatp1a and 1b transporters) and humanized transgenic mouse strains with liver-specific expression of human OATP1B1 or OATP1B3.

Firstly, in this work we have demonstrated the usefulness of single and combination transporter knockout mouse models to study the impact of ABCB1 and ABCG2 on oral availability and brain accumulation of drugs, including several TKIs *in vivo*. We have shown that dual deficiency of ABCB1 and ABCG2 most effectively increases the brain penetration of the studied tyrosine kinase inhibitors (TKIs). The findings in this thesis suggest that tumors expressing ABCB1 and/or ABCG2 may demonstrate resistance to tivozanib-, quizartinib- and EAI045-based cancer therapy. Inhibiting both these ABC transporters during therapy might therefore be beneficial for the response of these tumors. However, for the BRAF^{V600E} inhibitor encorafenib, it is suggested that it may not be the optimal choice for the treatment of melanoma brain metastases when the blood-brain barrier (BBB) is intact. This is because from our studies it appears that the brain concentration of encorafenib is strikingly low, even in the absence of Abcb1a/1b and Abcg2 mice. This suggests that this drug may not have optimal access to malignancies positioned behind a functional -BBB. It will be important to assess whether this also applies in humans. The oral availability of encorafenib, tivozanib, quizartinib and EAI045, however, does not seem to be noticeably affected by the activity of ABCB1 or ABCG2, at least in mice. On the other hand, the high intrinsic oral availability of encorafenib, if replicated in humans, would present a relatively favorable situation for the clinical application of this anticancer drug.

Secondly, characterization of pharmacological functions of human OATPs by using mouse models suggest that mouse Oatp1a/1b has at best a very modest uptake function for tivozanib and EAI045 into liver, without affecting overall plasma kinetics.

Lastly, we use different mouse models to study the possible effects on oral availability and tissue distribution of Ochratoxin A (OTA), a dietary mycotoxin that can cause nephrotoxicity, hepatotoxicity, and neurotoxicity and may be carcinogenic. We found that OTA is transported by the drug transporters mAbcb1 and/or mAbcg2, mOatp1a/1b, and hOATP1B3 in mice. And our data also indicate that transgenic hOATP1B3 can significantly transport OTA into the liver, and can at least partly compensate for the loss of the mOatp1a/1b transporters. This study shows that some ABC and OATP transporters can substantially affect the pharmacokinetics of OTA, which might have implications for its toxicity behavior. It is also worth noting that, although the impact of human OATP1B3 on OTA disposition in the transgenic mice is modest, in human liver both OATP1B3 and OATP1B1 proteins are co-expressed in hepatocytes. If both could contribute to OTA uptake in the liver, this may help with the overall elimination of OTA from blood into the liver for further metabolism, and excretion into the bile, in part by ABCG2, ABCC2, and perhaps ABCB1. Under normal circumstances, the uptake processes will increase liver exposure and toxicity, whereas the efflux processes will decrease liver exposure and toxicity. Given that there are genetic polymorphisms (SNPs) for both OATP1B3 and ABCG2 in humans that reduce their transport functions, as well as more rare full deficiency mutations, it is possible that these polymorphisms/mutations to some extent enhance, or alter, the susceptibility of carrier individuals to OTA toxicity. This might particularly apply for the kidney, where we observed increased OTA exposure in both ABC and OATP transporter knockout strains, albeit only after i.v., but not oral, OTA administration. Collectively, we have gained important insights into the functions of both ABC and OATP drug transporters using various *in vitro* cellular systems and *in vivo* knockout and transgenic mouse strains, which can be used as a solid translational basis for clinical studies in several cases. Furthermore, these transporters may also contribute to OTA toxicity and/or detoxification processes, and thus to different progression to toxicity and perhaps carcinogenesis by this compound.

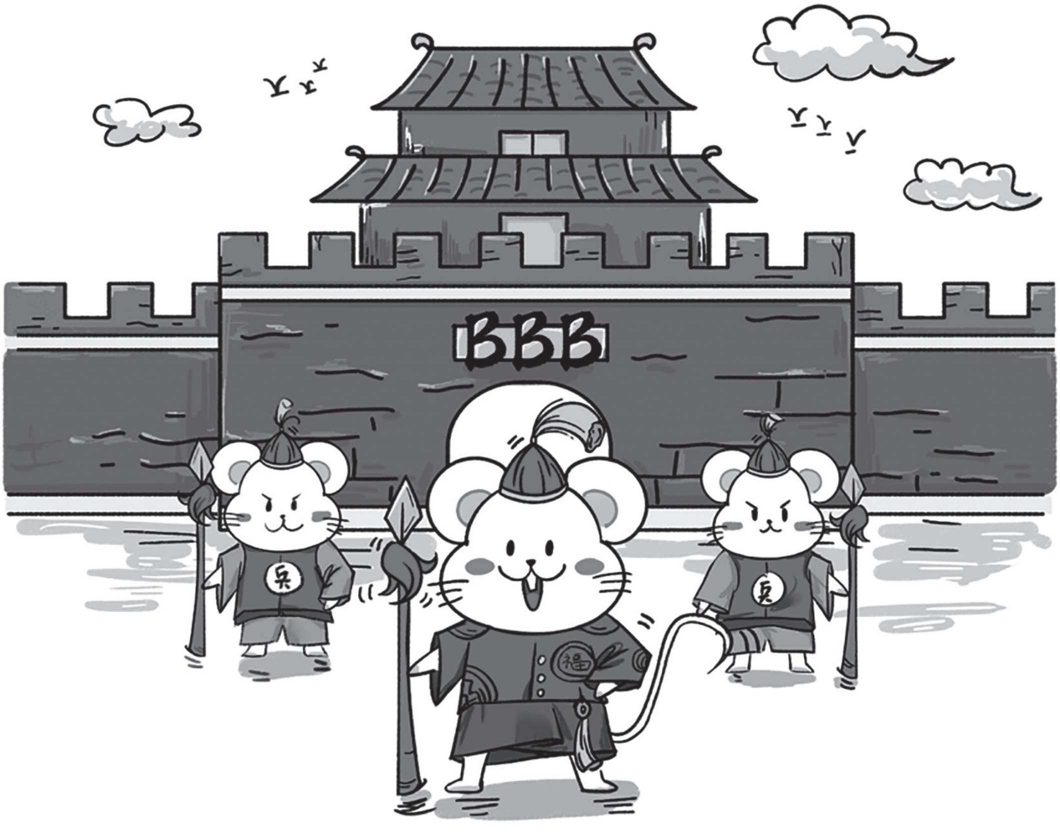
BBB
兵
福
兵

SUMMARY

Summary

Membrane transporters can play important roles in pharmacokinetic pathways (drug absorption, distribution, metabolism, and excretion). Multispecific efflux transporters of the ATP binding cassette (ABC) superfamily can transport many structurally diverse endogenous and exogenous compounds. Especially P-glycoprotein (MDR1/ABCB1) and Breast Cancer Resistance Protein (BCRP/ABCG2) are important ABC efflux transporters. They are localized at apical membranes of liver, kidney and intestine, where they can pump their substrates into bile, urine, and feces, respectively, and at pharmacological sanctuary site barriers such as the BBB and blood-testis barrier, where they can pump their substrates back into blood. Therefore, they can reduce oral availability, enhance elimination, and limit tissue distribution of substrate drugs. Organic anion transporting polypeptides (human: OATP, gene SLCO; rodents: Oatp, gene Slco) are primarily transmembrane uptake transporters, which can have profound roles in drug and other xenobiotic disposition and in drug-drug and drug-food interactions. This is because they are mainly expressed in pharmacokinetically important organs (e.g. liver, small intestine and kidney) and exhibit wide substrate specificities encompassing many drugs. For instance, human OATP1B1 (SLCO1B1) and OATP1B3 (SLCO1B3) are both selectively expressed in the liver, at the basolateral (sinusoidal) plasma membrane of hepatocytes where they can mediate hepatic uptake of compounds, facilitating their elimination. Consequently, the OATP uptake transporters that are involved in the uptake of many substrate xenobiotics will also modulate their overall body exposure. Cytochrome P450-3A (CYP3A) is an abundant multispecific drug-metabolizing enzyme highly expressed in human liver and small intestine, and it plays a significant role in the metabolism of approximately half of the drugs in current clinical use. As CYP3A can display a high degree of inter- and intra-individual activity, it is a major player in variable drug exposure.

In **chapter 1** of this thesis, we provide a brief introduction to the ABC and OATP transporters together with their expression, tissue localization and their pharmacologic role in the distribution of their substrates. We also introduce the Cytochrome P450 enzymes and the tyrosine kinase inhibitors (TKIs). We further review the four generations of EGFR TKIs in EGFR-mutant NSCLC targeted therapy, and provide a commentary on the EAI045 study in the perspective of the blood-brain barrier and other EGFR inhibitors.

Chapter 2 focuses on the role ABCB1 and ABCG2 play in the distribution of the BRAF^{V600E} inhibitor encorafenib. We have shown that encorafenib is efficiently transported by canine and human ABCB1 and ABCG2 and by mouse Abcg2 *in vitro*. *In vivo* data indicate that both Abcb1a/1b and Abcg2 are involved in restricting the net accumulation of encorafenib in the brain, with likely a somewhat more pronounced effect of Abcb1a/1b. Still, especially after oral administration, both transporters appear to be able to largely take over each other's functions at the BBB. The strikingly low brain concentration of encorafenib, even in the absence of Abcb1a/1b and Abcg2, suggests that encorafenib may not have optimal access to malignancies positioned behind a functional BBB. If this would also apply to the human brain, this might perhaps turn out

to be a limitation for encorafenib in targeting malignancies positioned behind a functional BBB. Since a substantial fraction of melanoma patients develop brain metastases, this could be a matter of possible concern in the clinical use of encorafenib. On the other hand, the high oral bioavailability (50%) of encorafenib, if replicated in humans, would present a relatively favorable situation for the clinical application of this anticancer drug. Our experiments on oral encorafenib in *Cyp3a*$^{-/-}$ mice suggest there may be at most a modest limiting effect of mouse Cyp3a on encorafenib oral availability. Cyp3a also does not have a marked impact on the tissue concentrations of encorafenib.

Chapter 3 shows that the second-generation FLT3 inhibitor quizartinib is moderately transported by hABCB1 and slightly by mAbcg2 *in vitro*. Our study is the first to show that the brain penetration of quizartinib, but not its oral availability, can be markedly limited by both mAbcb1 and mAbcg2. The brain penetration of quizartinib in mice was clearly limited by the combined function of mAbcb1 and mAbcg2 (11.8-fold), and by single mAbcb1 activity as well (5.6-fold). Thus, both mAbcb1 and mAbcg2 can restrict brain accumulation of quizartinib in mice. mAbcb1 could fully compensate for the loss of mAbcg2 at the BBB. In contrast, mAbcg2 can only very partly take over the function of mAbcb1 at the BBB when mAbcb1 is absent. This could mean that it may be worthwhile to inhibit ABCB1 and ABCG2 with a pharmacological inhibitor when treating malignant lesions present in part or in whole behind the BBB with quizartinib. Moreover, the reduced AUC in combination (Abcb1a/1b and Abcg2) knockout mice suggests that loss of mouse Abcb1 (but not Abcg2) may perhaps secondarily cause compensatory upregulation of an alternative quizartinib elimination system or decrease of a quizartinib uptake system, resulting in decreased overall quizartinib exposure. It thus appears unlikely that Abcb1 and Abcg2 themselves in the intestine and/or liver can markedly reduce overall systemic uptake of quizartinib after oral administration, as this should have resulted in increased plasma levels upon ablation of these proteins. Furthermore, our *in vivo* experiments do not point to a prominent role of CYP3A in limiting the oral availability or tissue distribution of quizartinib, at least in mice. However, we cannot exclude that there are significant changes in other quizartinib-detoxifying systems. Finally, the oral bioavailability of quizartinib in mice is quite high, in spite of a modest rate of net absorption. If this also applies in humans, this could mean that there is a reduced risk of high CYP3A-related variation in exposure of this drug.

In **chapter 4,** we investigated the involvement of ABCB1 and ABCG2 in transport of tivozanib *in vitro* and *in vivo*. Upon oral administration, tivozanib showed rapid absorption and the plasma concentration-time curves showed secondary peaks in all mouse strains, suggesting enterohepatic recirculation. However, the oral availability was not affected by mAbcb1 and mAbcg2. The brain penetration of tivozanib was only modestly limited by the combined function of mAbcb1 and mAbcg2 (2.6-fold), and by single mAbcb1 activity as well (2.2-fold). Thus, mAbcb1 and perhaps mAbcg2 can modestly restrict brain accumulation of tivozanib in mice. As 9% of renal cell carcinoma (RCC) patients have brain metastases, theoretically, one could therefore consider to try and further improve the brain concentration of tivozanib by co-administration of a strong ABCB1 and ABCG2 inhibitor, such as elacridar. This might help to enhance drug exposure for tumors that are positioned in part or in whole behind the BBB, and thus possibly improve therapeutic efficacy. However, the effect of Abcb1 and Abcg2 on brain penetration of tivozanib was relatively modest. If this would also apply to the human brain, this might perhaps mean that the gain from such a co-administration approach would be relatively limited. We further found that mOatp1a/1b had at best a very modest uptake function for tivozanib into liver, without affecting overall plasma kinetics. Finally, both mCyp3a and human CYP3A4 appear to have little if any direct impact on the *in vivo* oral availability and tissue distribution of tivozanib. Collectively, our data suggest that OATP- and CYP3A-related drug-drug interactions or genetic polymorphisms are probably of minor concern for the clinical application of tivozanib.

We want to point out that the dose we used in mice (1 mg/kg) especially when corrected for physiological weight was substantially higher than the recommended therapeutic dose for tivozanib (1.5 mg/d) in patients. At this relatively high single dose we did not observe any acute toxicity, suggesting that tivozanib was well tolerated in mice under these conditions.

In **chapter 5,** we investigated the roles of the multidrug efflux and uptake transporters ABCB1 (P-gp), ABCG2 (BCRP), and OATP1A/1B, and of the drug-metabolizing enzyme CYP3A in plasma pharmacokinetics and tissue distribution of EAI045. We also assessed concentrations of its hydrolyzed metabolite (PIA), and EAI045 glucuronide response relative to EAI045 in plasma and/or tissue homogenates. *In vitro*, EAI045 was a good transport substrate of human ABCB1, and a moderate transport substrate of the endogenous canine ABCB1. *In vivo*, orally administered EAI045 (20 mg/kg) was very rapidly absorbed, with a t_{max} at or before 5 min. EAI045 brain-to-plasma ratios were increased by 3.9-fold in *Abcb1a/1b*$^{-/-}$ and by 4.8-fold in *Abcb1a/1b;Abcg2*$^{-/-}$ mice compared to wild-type mice, but not in single *Abcg2*$^{-/-}$ mice, whereas EAI045 oral availability was not markedly affected in any of these knockout strains. Since single Abcb1a/1b-deficient mice showed an increase in EAI045 brain penetration almost equal to that in the combination knockout, Abcg2 makes at best a minor contribution in limiting EAI045 penetration across the BBB.

We further found that the dual ABCB1 and ABCG2 inhibitor elacridar could virtually completely reverse the effect of Abcb1a/1b and Abcg2 on limiting brain and testis penetration of EAI045. It also increased net intestinal absorption of EAI045, but likely independent of its effect on the ABC transporters. In elacridar-treated WT (WT+Ela) mice, the EAI045 plasma $AUC_{0\text{-}30min}$ was significantly increased by 4-fold, brain concentration by 17-fold and brain-to-plasma ratios by 5.4-fold compared to WT without elacridar treatment. This might suggest that elacridar coadministration could be considered to enhance the brain (and tumor) penetration of EAI045 in patients suffering from suitable EGFR mutant brain metastases. However, the increased oral exposure might present a toxicity risk of this combination treatment, although we did not observe any acute externally visible toxicity in the mice during this experiment. Nonetheless, coadministration of elacridar with EAI045 in patients should only be considered with extreme caution, and it would be preferable if the alternative EAI045 clearance system affected by elacridar would be first identified.

Interestingly, in the presence of elacridar, the percentage of dose present in the SIWC and the relative SIWC%-to-plasma ratio in WT+Ela mice were significantly decreased by 7.5-fold and 30.8-fold compared to WT mice without elacridar treatment. In conjunction with the disproportionately increased plasma levels of EAI045, this suggests that elacridar can markedly improve the net intestinal uptake of EAI045. It therefore appears that elacridar can not only inhibit Abcb1a/1b and Abcg2 in intestine and liver, but also some other system(s), perhaps another efflux transporter, that can restrict the net intestinal uptake of EAI045.

For EAI045 glucuronide, we observed an increased plasma $AUC_{0\text{-}30min}$ and a markedly decreased accumulation and tissue-to-plasma ratio of EAI045 glucuronide in the SIWC% in the absence of Abcb1a/1b and Abcg2. There was extensive conversion of EAI045 to PIA, however, Abcb1a/1b, Abcg2 and Oatp1a/1b had little impact on the availability, metabolism, or elimination of PIA after oral EAI045 administration. No substantial effects of mouse Cyp3a knockout or transgenic human CYP3A4 overexpression on oral EAI045 pharmacokinetics were observed, perhaps due to a dominant role of mouse Cyp2d or similar enzymes in EAI045 metabolism.

Chapter 6 described that Ochratoxin A (OTA) is transported by the drug transporters mouse (m)Abcb1 and/or mAbcg2, mOatp1a/1b, and human (h)OATP1B3 in mice. Loss of Abcb1a/1b and Abcg2 has little influence on the systemic exposure of OTA after either intravenous or oral administration. However, there appears to be a role of the ABC transporters in excreting OTA from the kidney towards urine, or in reducing its net uptake into the kidney from the pre-urine. We here found significant activity of human OATP1B3, but not OATP1B1, in *in vivo* uptake of OTA into the mouse liver. OATP1B3 could partly reverse the reducing effect of the Oatp1a/1b knockout on liver-to-plasma ratios of OTA. Therefore it is very likely that the OATP1B3-mediated improved liver uptake of OTA resulted in partial recovery of the biliary OTA excretion into the small intestinal lumen. In contrast, a contribution of transgenic OATP1B1 was not obvious.

It is also worth noting that, although the impact of human OATP1B3 on OTA disposition in the transgenic mice is modest, in human liver both OATP1B3 and OATP1B1 proteins are co-expressed in hepatocytes. If both could contribute to OTA uptake into the liver, this may help with the overall elimination of OTA from blood by facilitating hepatic metabolism, and excretion into the bile, in part by ABCG2, ABCC2, and perhaps ABCB1. Under normal circumstances, the uptake processes will increase liver exposure and toxicity, whereas the efflux processes will decrease liver exposure and toxicity.

It should be noted that a very high level of OTA exposure is not expected in most parts of the world, and therefore the risk of OTA-related nephritic syndrome on a global scale is limited. Nonetheless, the occurrence of OTA in food is unpredictable and not completely avoidable, and carry-over from animal feed to animal products has been confirmed. It is therefore in theory possible that people with variable activity of these transporters (due to genetic polymorphisms, but also due to inhibitory dietary compounds or other coadministered drugs) may have altered systemic clearance and/or distribution of OTA to tissues. This might contribute to OTA toxicity and/or detoxification processes, and thus to different progression to toxicity and perhaps carcinogenesis.

In **summary**, the studies described in this thesis demonstrate the value of knockout and transgenic mouse models to investigate the individual and combined impact of drug transporters such as ABCB1, ABCG2 and OATPs, as well as drug-metabolizing enzymes such as CYP3A on the pharmacokinetics of drugs and toxins. In addition, co-administration of elacridar could markedly improve the brain penetration of anticancer drug EAI045 in wild-type mice to the same level as seen in *Abcb1a/1b;Abcg2*$^{-/-}$ mice, which suggests that a strong ABCB1 and ABCG2 inhibitor under some circumstances might increase the efficacy against brain lesions and resistant malignancies. Meanwhile, potential central nervous system toxicity must be taken into consideration when using this approach. We believe there is still much to be discovered in the field of transporter proteins as well as the metabolizing enzymes, in terms of pharmacological, but also physiological functions of these and other families of drug-detoxifying proteins.

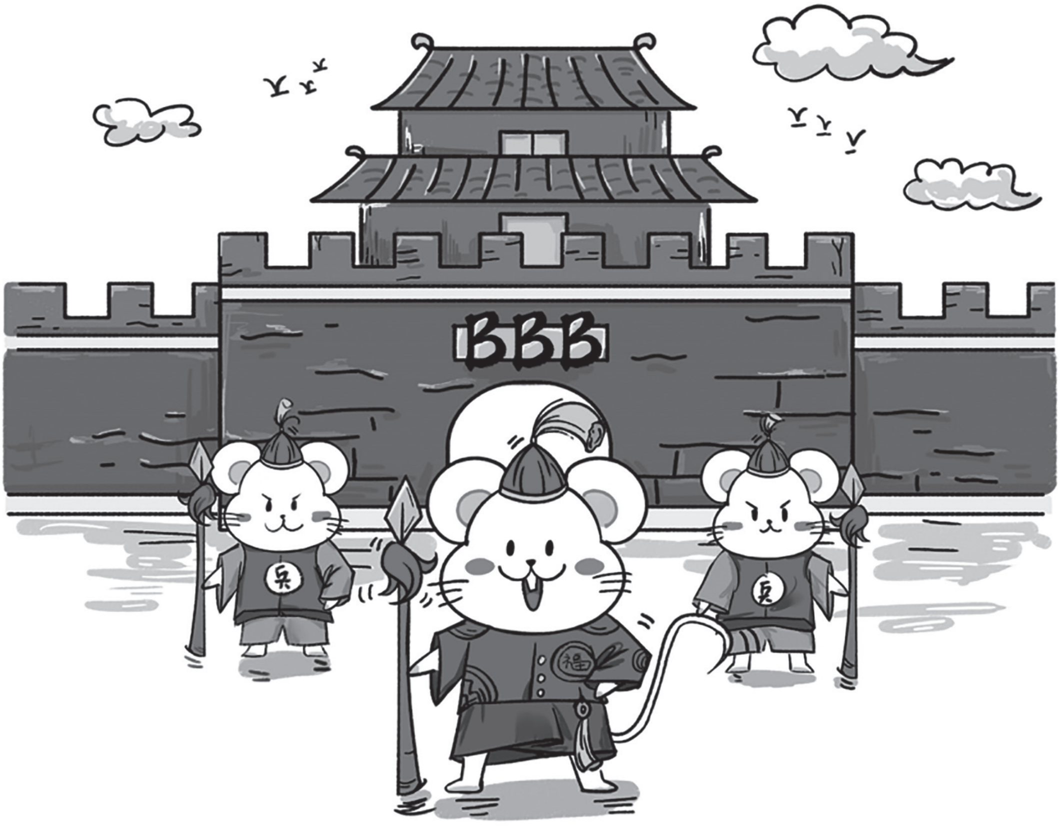
BBB
兵
福
兵

NEDERLANDSE SAMENVATTING

Nederlandse samenvatting

Membraantransporters kunnen een belangrijke rol spelen in farmacokinetische routes (opname, distributie, metabolisme en uitscheiding van geneesmiddelen). Multispecifieke efflux transporters van de ATP-bindingscassette (ABC) superfamilie kunnen veel structureel uiteenlopende endogene en exogene verbindingen transporteren. Vooral P-glycoproteïne (MDR1/ABCB1) en Breast Cancer Resistance Protein (BCRP/ABCG2) zijn belangrijke ABC-efflux transporters. Ze zijn gelokaliseerd in apicale membranen van lever, nier en darm, waar ze hun substraten in respectievelijk gal, urine en feces kunnen pompen, en in farmacologische barrières van ‘sanctuary’ organen zoals de bloed-hersen- en bloed-testisbarrière (BHB en BTB), waar ze hun substraten terug in het bloed pompen. Op deze manier kunnen ze de orale beschikbaarheid en de weefseldistributie van substraatgeneesmiddelen beperken, en hun eliminatie verhogen. Organische anion-transporterende polypeptiden (humaan: OATP, gen SLCO; knaagdieren: Oatp, gen Slco) zijn voornamelijk transmembraanopnametransporters, die een belangrijke rol kunnen spelen bij de dispositie van geneesmiddelen en andere xenobiotica en bij interacties tussen geneesmiddelen. Dit komt omdat ze voornamelijk tot expressie komen in farmacokinetisch belangrijke organen (bijv. lever, dunne darm en nier) en brede substraatspecificiteiten vertonen die veel geneesmiddelen omvatten. Humaan OATP1B1 (SLCO1B1) en OATP1B3 (SLCO1B3) worden bijvoorbeeld beide selectief tot expressie gebracht in de lever, in de basolaterale (sinusoïdale) plasmamembraan van hepatocyten, waar ze de opname van verbindingen door de lever kunnen mediëren, waardoor de eliminatie ervan wordt vergemakkelijkt. Bijgevolg zullen de OATP-opnametransporters die betrokken zijn bij de opname van veel substraatxenobiotica ook hun algehele lichaamsblootstelling beïnvloeden. Cytochroom P450-3A (CYP3A) is een prominent multispecifiek geneesmiddelmetaboliserend enzym dat in hoge mate tot expressie wordt gebracht in de menselijke lever en dunne darm, en dat een belangrijke rol speelt in het metabolisme van ongeveer de helft van de geneesmiddelen die momenteel klinisch worden gebruikt. Aangezien CYP3A een hoge mate van inter- en intra-individuele activiteit kan vertonen, is het een belangrijke speler in variabele blootstelling aan geneesmiddelen.

In **hoofdstuk 1** van dit proefschrift geven we een korte introductie van de ABC- en OATP-transporters samen met hun expressie, weefsellokalisatie en hun farmacologische rol in de distributie van hun substraten. We introduceren ook de Cytochroom P450-enzymen en de tyrosinekinaseremmers (TKI's). Verder presenteren we een review over de verschillende generaties EGFR-TKI's in EGFR-mutant NSCLC-gerichte therapie, en een commentaar op onze EAI045-studie met betrekking tot de bloed-hersenbarrière en de impact daarvan op EGFR-remmers.

Hoofdstuk 2 richt zich op de rol die ABCB1 en ABCG2 spelen in de distributie van de BRAFV600E-remmer encorafenib. We hebben aangetoond dat encorafenib in vitro efficiënt wordt getransporteerd door honden en mensen ABCB1 en ABCG2 en door muizen Abcg2. Uit in-vivo gegevens blijkt dat zowel Abcb1a/1b als

Abcg2 betrokken zijn bij het beperken van de netto-accumulatie van encorafenib in de hersenen, met waarschijnlijk een iets meer uitgesproken effect van Abcb1a/1b. Toch blijken beide transporters, zeker na orale toediening, elkaars functies bij de BHB grotendeels over te kunnen nemen. De opvallend lage hersenconcentratie van encorafenib, zelfs in de afwezigheid van Abcb1a/1b en Abcg2, suggereert dat encorafenib mogelijk geen optimale toegang heeft tot maligniteiten die zich achter een functionele BHB bevinden. Als dit ook zou gelden voor het menselijk brein, kan dit een punt van zorg zijn bij het klinische gebruik van encorafenib, aangezien een aanzienlijk deel van de melanoompatiënten hersenmetastasen ontwikkelt. Aan de andere kant zou de hoge orale biologische beschikbaarheid (50%) van encorafenib, indien gerepliceerd in mensen, een relatief gunstige situatie opleveren voor de klinische toepassing van dit geneesmiddel tegen kanker. Onze experimenten met orale encorafenib bij Cyp3a$^{-/-}$ muizen suggereren dat er hoogstens een bescheiden beperkend effect van muis Cyp3a op de orale beschikbaarheid van encorafenib is. Cyp3a heeft ook geen duidelijke invloed op de weefselconcentraties van encorafenib.

Hoofdstuk 3 laat zien dat de tweede-generatie FLT3-remmer quizartinib in vitro matig wordt getransporteerd door hABCB1 en in geringe mate door mAbcg2. Onze studie is de eerste die aantoont dat de hersenpenetratie van quizartinib, maar niet de orale beschikbaarheid ervan, aanzienlijk kan worden beperkt door zowel mAbcb1 als mAbcg2. De hersenpenetratie van quizartinib bij muizen was duidelijk beperkt door de gecombineerde functie van mAbcb1 en mAbcg2 (11.8-voudig), en ook door enkele mAbcb1-activiteit (5.6-voudig). Dus zowel mAbcb1 als mAbcg2 kunnen de hersenaccumulatie van quizartinib bij muizen beperken. mAbcb1 kon het verlies van mAbcg2 in de BHB vrijwel volledig compenseren. Daarentegen kan mAbcg2 de functie van mAbcb1 in de BHB slechts zeer gedeeltelijk overnemen wanneer mAbcb1 afwezig is. Dit zou kunnen betekenen dat het de moeite waard kan zijn om ABCB1 en ABCG2 te remmen met een farmacologische remmer bij de behandeling met quizartinib van maligne laesies die geheel of gedeeltelijk achter de BHB gesitueerd zijn. Bovendien suggereert de verlaagde AUC in combinatie (Abcb1a/1b en Abcg2) knock-out muizen dat het verlies van Abcb1 (maar niet Abcg2) bij muizen misschien secundaire compensatoire op-regulatie van een alternatief quizartinib-eliminatiesysteem, dan wel een afname van een quizartinib-opnamesysteem, kan veroorzaken, hetgeen resulteert in een verminderde totale blootstelling aan quizartinib. Het lijkt onwaarschijnlijk dat Abcb1 en Abcg2 zelf in de darm en/of lever de algehele systemische opname van quizartinib na orale toediening aanzienlijk kunnen verminderen, aangezien dit had moeten leiden tot verhoogde plasmaspiegels na ablatie van deze eiwitten. Onze in vivo experimenten wijzen verder niet op een prominente rol van CYP3A bij het beperken van de orale beschikbaarheid of weefseldistributie van quizartinib, althans niet bij muizen. We kunnen echter niet uitsluiten dat er significante veranderingen zijn in andere quizartinib-ontgiftende systemen. Ten slotte is de orale biologische beschikbaarheid van quizartinib bij muizen vrij hoog, ondanks een bescheiden snelheid van netto-absorptie. Als dit ook bij mensen van toepassing is, zou dit kunnen betekenen dat er een verminderd risico is op hoge CYP3A-gerelateerde variatie in blootstelling aan dit geneesmiddel.

In **hoofdstuk 4** hebben we de betrokkenheid van het humane ABCB1 en muis Abcg2 bij het transport van tivozanib in vitro onderzocht. Na orale toediening vertoonde tivozanib een snelle absorptie en de plasmaconcentratie-tijdcurves vertoonden secundaire pieken in alle muizenstammen, wat duidt op enterohepatische recirculatie. De orale beschikbaarheid werd echter niet beïnvloed door mAbcb1 en mAbcg2. De hersenpenetratie van tivozanib werd slechts bescheiden beperkt door de gecombineerde functie van mAbcb1 en mAbcg2 (2.6-voudig), en ook door enkelvoudige mAbcb1-activiteit (2.2-voudig). Dus zowel mAbcb1 als, in mindere mate, mAbcg2 kunnen de hersenaccumulatie van tivozanib bij muizen matig beperken. Aangezien 9% van de renal cell carcinoma-patiënten hersenmetastasen heeft, zou men daarom in principe kunnen overwegen om de hersenconcentratie van tivozanib verder te verbeteren door gelijktijdige toediening van een sterke ABCB1- en ABCG2-remmer, zoals elacridar. Dit zou kunnen helpen om de blootstelling aan geneesmiddelen te verhogen voor tumoren die geheel of gedeeltelijk achter de BHB zijn gepositioneerd, en dus mogelijk de therapeutische werkzaamheid ervan verbeteren. Het effect van Abcb1 en Abcg2 op de hersenpenetratie van tivozanib was echter relatief bescheiden. Als dit ook zou gelden voor het menselijk brein, zou dit misschien betekenen dat de winst van een dergelijke co-toedieningsaanpak relatief beperkt zou zijn. We ontdekten verder dat mOatp1a/1b op zijn hoogst een zeer bescheiden opnamefunctie voor tivozanib in de lever had, zonder de algehele plasmakinetiek te beïnvloeden. Ten slotte lijken zowel mCyp3a als humaan CYP3A4 weinig of geen directe invloed te hebben op de in vivo orale beschikbaarheid en weefseldistributie van tivozanib. Gezamenlijk suggereren onze gegevens dat OATP- en CYP3A-gerelateerde geneesmiddelinteracties of genetische polymorfismen waarschijnlijk van ondergeschikt belang zijn voor de klinische toepassing van tivozanib.

We willen erop wijzen dat de toegediende dosis die we gebruikt hebben bij muizen (1 mg/kg) aanzienlijk hoger was dan de aanbevolen therapeutische dosis voor tivozanib (1.5 mg/d) bij patiënten, helemaal wanneer gecorrigeerd voor fysiologisch gewicht. Bij deze relatief hoge enkelvoudige dosis hebben we geen acute toxiciteit waargenomen, wat suggereert dat tivozanib onder deze omstandigheden goed werd verdragen door muizen.

In **hoofdstuk 5** hebben we de rol onderzocht van de multidrug efflux en opname transporters ABCB1 (P-gp), ABCG2 (BCRP), OATP1A/1B, en het geneesmiddelmetaboliserende enzym CYP3A in de plasmafarmacokinetiek en weefseldistributie van EAI045. We hebben verder ook de gehydrolyseerde metaboliet (PIA) concentraties en EAI045-glucuroniderespons ten opzichte van EAI045 in celkweekmedium, plasma en/of weefselhomogenaten gemeten. In vitro is EAI045 een goed transportsubstraat van humaan ABCB1, en een matig transportsubstraat van het endogene hond ABCB1. In vivo wordt oraal toegediend EAI045 (20 mg/kg) zeer snel geabsorbeerd, met een tmax op of vóór 5 minuten. EAI045 hersenen-tot-plasma-ratio's waren 3.9-voudig verhoogd in Abcb1a/1b$^{-/-}$ en 4.8-voudig in Abcb1a/1b;Abcg2$^{-/-}$ muizen vergeleken met wildtype muizen, maar niet in enkelvoudige Abcg2$^{-/-}$ muizen, terwijl de orale beschikbaarheid van EAI045 niet duidelijk werd beïnvloed. Aangezien enkelvoudige Abcb1a/1b-deficiënte muizen een toename in EAI045-hersenpenetratie vertoonden die bijna gelijk was aan die in de combinatie-knock-out, levert Abcg2 voor EAI045 op zijn best een kleine bijdrage aan de BHB.

We ontdekten verder dat de gecombineerde ABCB1- en ABCG2-remmer elacridar het effect van Abcb1a/1b en Abcg2 op het beperken van de penetratie van EAI045 in de hersenen en de testis vrijwel volledig kon blokkeren, evenals het beperken van de netto intestinale absorptie. In met elacridar behandelde wild-type (WT+Ela) muizen was de EAI045 plasma-AUC$_{0\text{-}30min}$ significant verhoogd met een factor 4, de hersenconcentratie met een factor 17 en de hersen-tot-plasma ratio met een factor 5,4 vergeleken met WT muizen zonder behandeling met elacridar. Dit zou erop kunnen wijzen dat gelijktijdige toediening van elacridar kan worden overwogen om de penetratie van EAI045 in de hersenen (en tumoren) te verbeteren bij patiënten die lijden aan geschikte EGFR-mutante hersenmetastasen. De verhoogde orale blootstelling kan echter een toxiciteitsrisico van deze combinatiebehandeling met zich meebrengen, hoewel we tijdens dit experiment geen acute extern zichtbare toxiciteit bij de muizen hebben waargenomen. Desalniettemin dient gelijktijdige toediening van elacridar met EAI045 bij patiënten alleen met uiterste voorzichtigheid te worden overwogen, en het zou de voorkeur hebben als eerst het alternatieve EAI045-klaringssysteem dat door elacridar wordt beïnvloed, wordt geïdentificeerd.

Interessant is dat in de aanwezigheid van elacridar het percentage van de dosis dat aanwezig was in de dunne darm plus inhoud (small intestine with content, SIWC) en de relatieve SIWC%-tot-plasmaverhouding in WT + Ela-muizen significant 7.5-voudig en 30.8-voudig was verlaagd in vergelijking met WT-muizen zonder elacridar-behandeling. In combinatie met de onevenredig verhoogde plasmaspiegels van EAI045, suggereert dit dat elacridar de netto intestinale opname van EAI045 aanzienlijk kan verbeteren. Het lijkt er daarom op dat elacridar niet alleen Abcb1a/1b en Abcg2 in darm en lever kan remmen, maar ook een of meer andere systemen, mogelijk een andere efflux transporter, die de netto intestinale opname van EAI045 kan beperken.

Voor EAI045-glucuronide zagen we een verhoogde plasma-AUC$_{0\text{-}30min}$ en een duidelijk verminderde accumulatie en weefsel-tot-plasmaverhouding van EAI045-glucuronide in het SIWC% in afwezigheid van Abcb1a/1b en Abcg2. Er werd een grote hoeveelheid EAI045 omgezet in PIA, maar Abcb1a/1b, Abcg2 en Oatp1a/1b hebben weinig invloed op de beschikbaarheid, het metabolisme, of de eliminatie van PIA na orale toediening van EAI045. Er werden geen substantiële effecten van muis Cyp3a knock-out of transgene humane CYP3A4-overexpressie op de orale farmacokinetiek van EAI045 waargenomen, vermoedelijk vanwege een dominante rol van Cyp2d-enzymen van muis in het metabolisme van EAI045.

Hoofdstuk 6 beschrijft dat ochratoxine A (OTA) wordt getransporteerd door de geneesmiddeltransporters muis (m)Abcb1 en/of mAbcg2, mOatp1a/1b, en humaan (h)OATP1B3 in muizen. Verlies van Abcb1a/1b en Abcg2 heeft weinig invloed op de systemische blootstelling aan OTA na intraveneuze of orale toediening. Er lijkt echter een rol te zijn voor de ABC-transporters bij het uitscheiden van OTA vanuit de nier naar de urine, dan wel bij het verminderen van de netto-opname in de nier vanuit de pre-urine. We vonden significante activiteit van menselijk OATP1B3, maar niet OATP1B1, bij de in vivo opname van OTA in de muizenlever. OATP1B3 kon het verlagende effect van de Oatp1a/1b-knock-out op de lever-tot-plasmaverhoudingen van OTA gedeeltelijk omkeren. Het is zeer waarschijnlijk dat de door OATP1B3 gemedieerde verbeterde opname van OTA door de lever resulteerde in gedeeltelijk herstel van de uitscheiding van OTA via de gal in het lumen van de dunne darm. Daarentegen waren er geen aanwijzingen voor een functionele bijdrage van transgeen OATP1B1.

Het is ook vermeldenswaard dat, hoewel de impact van menselijk OATP1B3 op OTA-dispositie in de transgene muizen bescheiden is, in de menselijke lever zowel OATP1B3- als OATP1B1-eiwitten samen tot expressie komen in hepatocyten. Als beide zouden kunnen bijdragen aan de opname van OTA in de lever, kan dit helpen bij de algehele eliminatie van OTA uit het bloed door het levermetabolisme en de uitscheiding in de gal te vergemakkelijken, het laatste wellicht gedeeltelijk door ABCG2, ABCC2 en misschien ABCB1. Onder normale omstandigheden zullen de genoemde opnameprocessen de leverblootstelling en -toxiciteit van OTA verhogen, terwijl de efflux processen de leverblootstelling en -toxiciteit juist zullen verminderen.

Opgemerkt moet worden dat in de meeste delen van de wereld geen zeer hoge OTA-blootstelling wordt verwacht, en daarom is het risico op OTA-gerelateerd nefritis syndroom op wereldschaal beperkt. Desalniettemin is het voorkomen van OTA in voedsel onvoorspelbaar en niet volledig te vermijden, en overdracht van OTA via diervoeder naar dierlijke producten (voor humane consumptie) is bevestigd. Het is daarom in theorie mogelijk dat mensen met variabele activiteit van deze transporters (als gevolg van genetische polymorfismen, maar ook vanwege remming door verbindingen in voedsel of andere gelijktijdig toegediende geneesmiddelen) een veranderde systemische klaring en/of distributie van OTA naar weefsels vertonen. Dit zou kunnen bijdragen aan veranderde OTA-toxiciteit en/of ontgiftingsprocessen, en dus aan verschillende progressie naar toxiciteit en mogelijk carcinogenese.

Samenvattend, de studies beschreven in dit proefschrift illustreren de waarde van knock-out en transgene muismodellen om de individuele en gecombineerde impact van geneesmiddeltransporters zoals ABCB1, ABCG2 en OATPs, evenals de geneesmiddelmetaboliserende CYP3A enzymen, op de farmacokinetiek van medicijnen te onderzoeken. Verder zou gelijktijdige toediening van elacridar de hersenpenetratie van het antikankergeneesmiddel EAI045 bij wild-type muizen aanzienlijk kunnen verbeteren tot hetzelfde niveau als waargenomen bij Abcb1a/1b;Abcg2$^{-/-}$ muizen. Dit wijst erop dat een sterke ABCB1- en ABCG2-remmer onder bepaalde omstandigheden de therapeutische werkzaamheid tegen hersenlaesies en resistente maligniteiten zou kunnen vergroten. Ondertussen moet bij het gebruik van deze benadering wel rekening worden gehouden met mogelijke toxiciteit voor het centrale zenuwstelsel. Wij denken dat er nog veel te ontdekken valt op het gebied van geneesmiddel-transporters en -metaboliserende enzymen, in termen van farmacologische, maar ook fysiologische functies van deze en andere families van geneesmiddel-ontgiftende eiwitten.

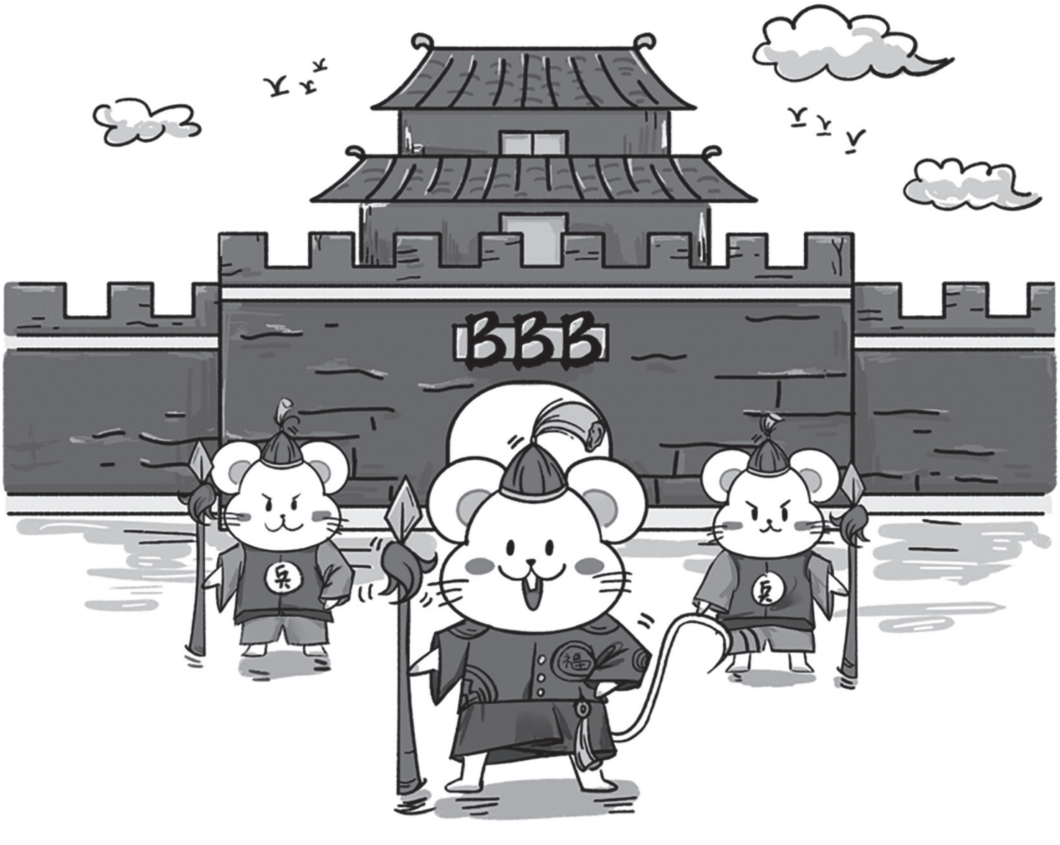
BBB
兵
福
兵

APPENDICS

Chemical structures in this thesis

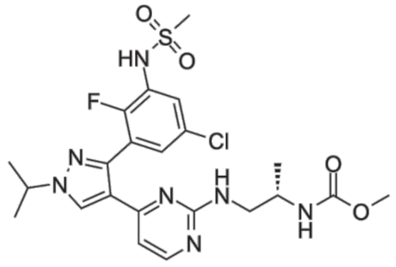

Encorafenib (LGX818)

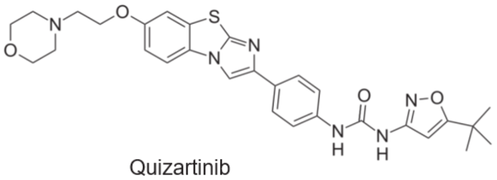

Quizartinib

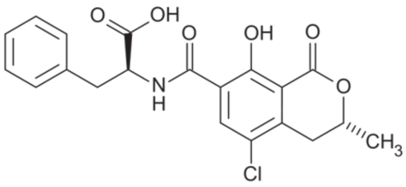

Ochratoxin A (OTA)

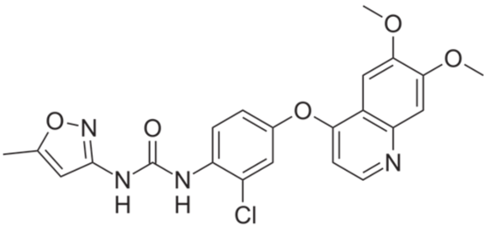

Tivozanib

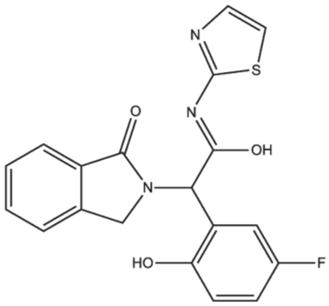

EAI045

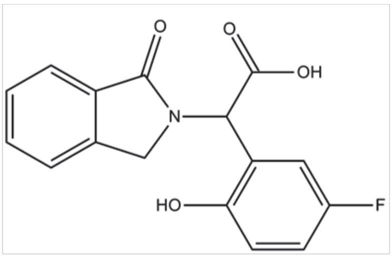

PIA
(EAI045 hydrolysed metabolite)

Author affiliations

Alfred H. Schinkel	The Netherlands Cancer Institute, Division of Pharmacology, Amsterdam, The Netherlands
Changpei Gan	The Netherlands Cancer Institute, Division of Pharmacology, Amsterdam, The Netherlands
Els Wagenaar	The Netherlands Cancer Institute, Division of Pharmacology, Amsterdam, The Netherlands
Hilde Rosing	Department of Pharmacy & Pharmacology, The Netherlands Cancer Institute, Amsterdam, The Netherlands
Irene A. Retmana	Utrecht University, Faculty of Science, Department of Pharmaceutical Sciences, Division of Pharmacoepidemiology & Clinical Pharmacology, Utrecht, The Netherlands
Jing Wang	The Netherlands Cancer Institute, Division of Pharmacology, Amsterdam, The Netherlands
Jos H. Beijnen	The Netherlands Cancer Institute, Division of Pharmacology, Amsterdam, The Netherlands Utrecht University, Faculty of Science, Department of Pharmaceutical Sciences, Division of Pharmacoepidemiology & Clinical Pharmacology, Utrecht, The Netherlands The Netherlands Cancer Institute/Slotervaart Hospital, Department of Pharmacy & Pharmacology, Amsterdam, The Netherlands
Maaike A. C. Bruin	The Netherlands Cancer Institute, Division of Pharmacology, Amsterdam, The Netherlands The Netherlands Cancer Institute, Department of Pharmacy & Pharmacology, Amsterdam, The Netherlands
Maria C. Lebre	The Netherlands Cancer Institute, Division of Pharmacology, Amsterdam, The Netherlands
M. Merve Susam	Utrecht University, Faculty of Science, Department of Pharmaceutical Sciences, Division of Pharmacology, Utrecht, The Netherlands
Rolf W. Sparidans	Utrecht University, Faculty of Science, Department of Pharmaceutical Sciences, Division of Pharmacoepidemiology & Clinical Pharmacology, Utrecht, The Netherlands
Stéphanie van Hoppe	The Netherlands Cancer Institute, Division of Pharmacology, Amsterdam, The Netherlands
Wenlong Li	The Netherlands Cancer Institute, Division of Pharmacology, Amsterdam, The Netherlands
Xiaozhe Qi	Standards and Quality Center of National Food and Strategic Reserves Administration, Beijing, China College of Food Science and Nutritional Engineering, China Agricultural University, Beijing, China

List of publications

1. **Jing Wang**, Changpei Gan, Rolf W. Sparidans, Els Wagenaar, Stéphanie van Hoppe, Jos H. Beijnen, Alfred H. Schinkel. P-glycoprotein (MDR1/ABCB1) and Breast Cancer Resistance Protein (BCRP/ABCG2) affect brain accumulation and intestinal disposition of encorafenib in mice. Pharmacological Research, 2018, 129: 414-423.

2. **Jing Wang**, Changpei Gan, Irene A. Retmana, Rolf W. Sparidans, Wenlong Li, Maria C. Lebre, Jos H. Beijnen, Alfred H. Schinkel. P-glycoprotein (MDR1/ABCB1) and Breast Cancer Resistance Protein (BCRP/ABCG2) limit brain accumulation of the FLT3 inhibitor quizartinib in mice. International Journal of Pharmaceutics, 2019, 556: 172-180.

3. **Jing Wang**, Maaike A. C. Bruin, Changpei Gan, Maria C. Lebre, Hilde Rosing, Jos H. Beijnen, Alfred H. Schinkel. Brain accumulation of tivozanib is restricted by ABCB1 (P-glycoprotein) and ABCG2 (breast cancer resistance protein) in mice. International Journal of Pharmaceutics, 2020, 581: 119277.

4. **Jing Wang**, Changpei Gan, Xiaozhe Qi, Maria C. Lebre, Alfred H. Schinkel. Human organic anion transporting polypeptide (OATP) 1B3 and mouse Oatp1a/1b affect liver accumulation of Ochratoxin A in mice. Toxicology and Applied Pharmacology, 2020, 401: 115072.

5. **Jing Wang**, M. Merve Susam, Changpei Gan, Rolf W. Sparidans, Maria C. Lebre, Jos H. Beijnen, Alfred H. Schinkel. P-glycoprotein (MDR1/ABCB1) restricts brain accumulation of the novel EGFR inhibitor EAI045 and oral elacridar coadministration enhances its brain accumulation and oral exposure. To be submitted.

6. Irene A. Retmana, **Jing Wang**, Alfred H. Schinkel, Jan H.M. Schellens, Jos H. Beijnen, Rolf W. Sparidans. Liquid chromatography-tandem mass spectrometric assay for the quantitative determination of the tyrosine kinase inhibitor quizartinib in mouse plasma using salting-out liquid-liquid extraction. Journal of Chromatography B, 2017, 1061: 300-305.

7. Maaike A. C. Bruin, Hilde Rosing, Luc Lucas, **Jing Wang**, Alwin D.R. Huitema, Alfred H. Schinkel, Jos H. Beijnen. Development and validation of an LC-MS/MS method with a broad linear dynamic range for the quantification of tivozanib in human and mouse plasma, mouse tissue homogenates, and culture medium. Journal of Chromatography B, 2019, 1125: 121723.

8. Changpei Gan, **Jing Wang**, Alejandra Martínez-Chávez, Michel Hillebrand, Niels de Vries, Joke Beukers, Els Wagenaar, Yaogeng Wang, Maria C. Lebre, Hilde Rosing, Sjoerd Klarenbeek, Rahmen Bin Ali, Colin Pritchard, Ivo Huijbers, Jos H. Beijnen, Alfred H. Schinkel. Carboxylesterase 1 family knockout alters drug disposition and lipid metabolism. To be submitted

9. Yaogeng Wang, Rolf W. Sparidans, **Jing Wang**, Maria C. Lebre , Jos H. Beijnen, Alfred H. Schinkel. Rifampin and ritonavir increase oral availability and elacridar enhances overall exposure and brain accumulation of the NTRK inhibitor larotrectinib. European Journal of Pharmaceutics and Biopharmaceutics, submitted.

10. Wenlong Li, Daniela Lehutova, Rolf W. Sparidans, Paniz Heydari, **Jing Wang**, Maria C. Lebre, Jos H. Beijnen, and Alfred H. Schinkel. ABCB1 restricts brain accumulation of the novel RORγ agonist cintirorgon, while OATP1A/1B and CYP3A limit its oral availability. To be submitted.

11. M. Merve Susam, **Jing Wang**, Alfred H. Schinkel, Jos H. Beijnen, Rolf W. Sparidans. Quantitative bioanalytical assay for the tyrosine kinase inhibitor EAI045 and its metabolite in mouse plasma and tissue homogenates using liquid chromatography-tandem mass spectrometry. To be submitted.

12. **Jing Wang**, Alfred H. Schinkel. Four generations of EGFR tyrosine kinase inhibitors in treatment of EGFR-mutant non-small cell lung cancer. To be submitted.

Curriculum vitae

Jing Wang was born on May 18th, 1987 in Chengdu, Sichuan Province, P.R. China. After high school graduation in 2006, she studied Biology at Mianyang Teachers' College. During the Bachelor's programme, she investigated the characteristics and analysis of echolocation calls of bats. In 2010 she received her BSc degree, and was recommended to start her master study of zoology at China West Normal University. Her master program focused on the primate nutritional and foraging strategies of François' langur in Guizhou, China. In 2013, she finished her master program and started teaching Biology in high school for two years. In 2015, Jing started her PhD research at the Department of Pharmacology of the Netherlands Cancer Institute/Antoni van Leeuwenhoek Hospital in Amsterdam, under the supervision of Prof. Jos H. Beijnen and Dr. Alfred H. Schinkel. Her PhD project concerned investigation of the impact of ABC transporters on pharmacokinetics of targeted anticancer drugs and food toxins. The results obtained during this research are described in this thesis.

Acknowledgements

First and foremost I am extremely grateful to my supervisor Dr. Alfred Schinkel and my promotor professor Jos Beijnen. Thank you for giving me the opportunity of being part of your groups and for your supervision during these years. Thank you also for your help and advice with this PhD. Your guidance and critical support taught me how to be an overall better scientist.

Dr. Alfred Schinkel, thank you so much for the continuous support of my PhD study and related research, for your patience, motivation, and extensive knowledge. Your guidance helped me during all the time of my research and writing of this thesis. I could not have imagined having a better advisor and mentor for my PhD study. Although at the beginning my work in the lab seemed challenging and complicated, thanks to your help and support I could successfully finalize all my projects during my PhD journey.

Professor Jos Beijnen, many thanks for your assistance at every stage of my research projects, but also for your insightful comments and suggestions.

Dr. Rolf Sparidans, Maaike, Irene, Paniz, and Merve, thanks a lot for measuring so many samples for me, you are such an efficient collaborator. Without your precious support it would not be possible to conduct this type of research. Your support and encouragement are greatly appreciated.

Dr. Olaf van Tellingen, thank you for your insightful comments and encouragement, and also the hard questions which incentivized me to widen my research from various perspectives.

I would further like to thank all my OIO research committee members for your contributions and support over these years.

My thanks also goes to all the members of the Schinkel lab: Els, Cristina, Changpei, Stéphanie, Yaogeng, Margarida, Alejandra, Wenlong, Nancy, and Xiaozhe,. I am grateful for your support of my studies. I thank you for the stimulating discussions, and for all the fun we have had in the last six years.

My appreciation also goes out to all colleagues from the Pharmacology Division for the nice atmosphere in H3, the animal facility, and all my other friends from the NKI. Thank you for your friendship and encouragement.

And finally, last but by no means least, I would like to thank my family for supporting me spiritually throughout writing this thesis and my life in general.

Thanks for all your encouragement, and for being part of the most challenging experience in my life!

Jing